The biology of variation in anatomical brain asymmetries

Proefschrift
ter verkrijging van de graad van doctor
aan de Radboud Universiteit Nijmegen
op gezag van de rector magnificus prof. dr. J.H.J.M. van Krieken,
volgens besluit van het college van decanen
in het openbaar te verdedigen op donderdag 2 februari 2017
om 12.30 uur precies

door
Tulio Manuel Guadalupe Estrada
geboren op 3 november 1982
te Moskou (Rusland)

Promotor:
Prof. dr. S.E. Fisher

Copromotor:
Dr. C. Francks (MPI)

Manuscriptcommissie:
Prof. dr. C.F. Beckmann
Prof. dr. K.E. Watkins (University of Oxford, Verenigd Koninkrijk)
Dr. S. Ocklenburg (Ruhr-Universität Bochum, Duitsland)

The biology of variation in anatomical brain asymmetries

Doctoral Thesis

to obtain the degree of doctor
from Radboud University Nijmegen
on the authority of the Rector Magnificus prof. dr. J.H.J.M. van Krieken,
according to the decision of the Council of Deans
to be defended in public on Thursday, February 2, 2017
at 12.30 hours
by

Tulio Manuel Guadalupe Estrada
Born on November 3, 1982
in Moscow (Russia)

Supervisor:
Prof. dr. S.E. Fisher

Co-supervisor:
Dr. C. Francks (MPI)

Doctoral Thesis Committee:
Prof. dr. C.F. Beckmann
Prof. dr. K.E. Watkins (University of Oxford, United Kingdom)
Dr. S. Ocklenburg (Ruhr-Universität Bochum, Germany)

Table of Contents

Chapter 1

General introduction

Asymmetries of human brain anatomy

Hidden within an otherwise bilaterally symmetrical body, left-right asymmetries play a key role in the internal plan of the human body. This is notable in the organization and morphology of the viscera, e.g. in the location and disposition of the heart, and also the brain. The brain of a human - or that of any other vertebrate - can be understood as two distinct but interconnected hemispheres, divided along the medial plane by the longitudinal fissure (see Figure 1). In humans, anatomical differences between the two hemispheres are particularly pronounced and have been subject of academic study for well over a century (e.g. Bastian, 1866; Cunningham, 1892).

Detailed assessments of post-mortem brains provided the early foundations towards understanding human brain morphology and its development (e.g. Bastian, 1866; Boyd, 1861). Among these early investigations were already sporadic reports of differences between brain hemispheres (e.g. in terms of weight, Bastian, 1866; or density, Boyd, 1861). However, the conceptual relevance of such differences was initially obscured by the large degree of anatomical similarity and structural correspondence between hemispheres, which led early scholars to favour a view of the brain as a fundamentally symmetric organ, whose function relied on both hemispheres acting in symmetry (e.g. Bichat, 1809). It was not until the seminal discoveries of Broca, Bax and, subsequently, Wernicke (Berker et al., 1986; Finger and Roe, 1999; Wernike, 1874) which brought a paradigm-shift, challenging the notion of a fundamentally symmetric brain. Their examinations of patients who developed aphasia (i.e. an impaired ability to communicate through language following a brain lesion), revealed that these were frequently the result of an insult to the left brain rather than to the right. This led to Broca's famous proposal that humans "speak with the left hemisphere" (Broca, 1865; Berker, 1986).

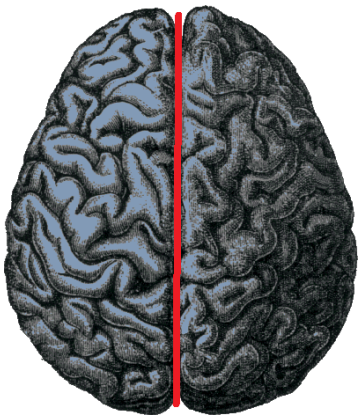

Figure 1. Top down view of the human brain. The red line follows the longitudinal fissure, which divides the brain into a left and right hemisphere.

This raised the question of how the homologous brain hemispheres could be differentially specialized for distinct cognitive functions; in particular, the human language faculty. Subsequently, research efforts focused on anatomical asymmetries between brain hemispheres, to which this functional differentiation might be attributed to. These studies called attention to striking asymmetries linked to the sylvian

fissure, i.e. the junction between the temporal- and frontoparietal lobes (see Figure 2; Cunningham, 1892; Eberstaller, 1884; Heschl, 1878), where lesions leading to aphasia were often located.

Figure 2. Side views of 3-dimensional renderings of left and right hemispheres. The red line traces the classic definition of the sylvian fissure, from its most anterior origin to its posterior end, where it normally bifurcates into an upper and lower ramus (i.e. branch).

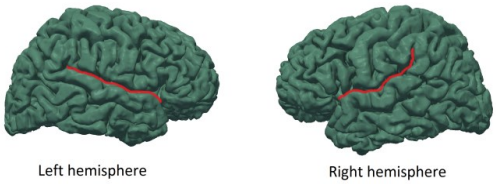

As investigations into brain asymmetry continued, analyses of casts made from inside human skulls revealed a tendency for both hemispheres to be slightly warped and protrude into each other's hemi-space at the occipital and frontal poles (e.g. Hoadley and Pearson, 1929), a phenomenon now referred to as brain torque (see Figure 3; Hadziselimovic and Cus, 1966; LeMay, 1976). Similarly, by studying casts made from the brain's internal cavities, differences were observed in size and shape between the lateral ventricles (Knudsen, 1958; Last and Tompsett, 1953).

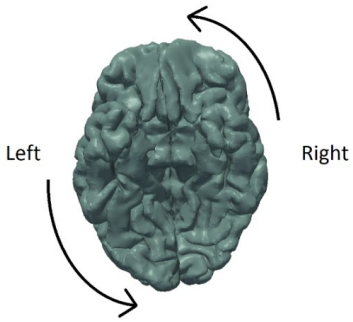

Figure 3. View of the cerebral hemispheres from below, artificially enhanced to show the left-right asymmetries of the frontal and occipital petalias, an overall pattern generally referred to as brain torque.

Individual differences in brain asymmetry

Left-right asymmetries are not exclusive to the salient landmarks of the human brain. The last half of the 20th century saw many advances contributing to a much more complex view of human brain asymmetry. Critical advances have included both methodological developments, based on statistical inference (e.g. Snedecor, 1950), as well as technological ones, including computerized techniques of imaging the brain's anatomy and function (Filler, 2009), and improved post mortem methods such as histological cell characterization (Chance, 2014).

Magnetic resonance imaging (MRI; Lauterbur, 1973) is especially valuable in the current study of brain asymmetries, as it offers a safe and non-invasive way to study the brain in vivo, in increasingly larger samples, from both general, healthy and disorder populations (e.g. Altarelli et al., 2014; Marie et al., 2015; Watkins et al., 2001). Such studies have revealed that brain asymmetries show a large degree of variability in magnitude, and sometimes direction, within and between individuals (e.g. Lyttelton et al., 2009; Watkins et al., 2001). This creates the opportunity to assess the contribution of specific biological factors to naturally occurring differences in brain asymmetries, thus allowing us to learn some aspects of their underlying biology.

Permeating many historical investigations of variability in brain asymmetries lay an assumption that dated back to some of the earliest investigations of aphasia and hemiplegia (impaired motor control of one side of the body): that there is one dominant hemisphere which is anatomically specialized to host 'higher' human cognitive functions including language and hand-motor-control, and which corresponds to the modal pattern of brain asymmetry (e.g. Cunningham, 1902; Smith, 1925). Left-hemisphere-right-hand-control was seen as analogous to the left brain's specialization for language (e.g. Bramwell, 1899; Hughlings-Jackson, 1874), although hand control was then considered a function of the basal ganglia (Hughlings-Jackson, 1873a; Hughlings-Jackson, 1873b). Later theories on the origins of brain asymmetries, proposed in the latter half of the 20th century, still considered left-handedness and atypical language lateralization as closely related manifestations of the same ontogenetic process in most people (e.g. Annett, 1972; Levy and Nagylaki, 1972).

While humans show an overwhelming preference in use towards their right hand, at both individual and population levels; a substantial minority, roughly 10%, prefer to use their left hand (Annett, 1967; Clerke and Clerke, 2001). Moreover, this preference has likely remained stable throughout human history, as well as across cultures and continents (Coren and Porac, 1977; McManus, 2009). However, accounts attempting to link handedness directly to anatomical brain asymmetry or language dominance have been challenged by more recent empirical findings, including one of the studies described in this thesis, which showed only subtle- or no relations (e.g. Amunts et al., 1996; Good et al., 2001a; Herve et al., 2006; Knecht et al., 2000). Indeed it has become apparent (e.g. Good et al., 2001a; Herve et al., 2006),that, while a typical human brain does indeed have anatomical asymmetries, hand motor control, and language functions lateralized consistently with respect to one another, when these traits vary from the average they are largely uncorrelated with one another, and are likely to have more complex relations than previously thought (for more detailed discussions see Badzakova-Trajkov et al., 2010;

Bishop, 2013; Mazoyer et al., 2014; Ooki, 2014). The general conclusion is that left-handedness probably has multifactorial and heterogeneous origins and is consequently related to brain anatomical asymmetries and language lateralization in multiple different ways in different people, depending on the precise nature of the disruption which led to non-typical development (Bukowski et al., 2013; Herve et al., 2013; Mazoyer et al., 2014; Willems et al., 2014). This does not, however, exclude the possibility that different aspects of brain asymmetry share substantially overlap with developmental mechanisms in typically developing people (Francks, 2015).

It is worth noting that the majority of studies of handedness have been hindered by the relatively low incidence of left-handers in unselected population datasets (approximately 10% in western populations), which has likely contributed to a number of inconclusive or contradictory claims based on studies performed in tens or low hundreds of participants (see Bishop, 1990a for an investigation of this).

Another factor long suspected to have an effect on brain asymmetries is sex. Next to the moderating role of sex in overall brain size, males have consistently shown a slightly higher incidence of left-handedness compared to females (Halpern et al., 1998; Peters et al., 2006; Sommer et al., 2008), and were reported initially in post mortem studies to have a more pronounced leftward asymmetry of the planum temporale than females (Harris, 1980). This led to the study of the potential role of sex hormones in shaping the asymmetries of the sylvian fissure, in particular. Notably, Geschwind and colleagues (e.g. Geschwind and Behan, 1982) were the first to propose a theory to account for individual differences, as well as sex differences, in asymmetry around the sylvian fissure by attributing them to varying testosterone levels present in the developing brain. To summarize, it was proposed that during brain development the sex-hormone testosterone exerts a delaying influence on the maturation of the left hemisphere, specific to perisylvian regions (Geschwind and Behan, 1982; Geschwind and Levitsky, 1968). Differential maturation rates between hemispheres would explain the origin of perisylvian brain asymmetries, including left lateralization for language and hand-control. In addition, abnormal asymmetry development, linked to abnormal levels of testosterone during development, would explain left-handedness, as well as the higher incidence of certain deficits that were thought, at the time, to associate with it (e.g. dyslexia or autoimmune disorders; Geschwind and Behan, 1982). Still a highly influential theory, many of its predictions, however, have received mixed support from further investigations (e.g. Bishop, 1990b; London, 1989; McKeever and Rich, 1990; Sommer et al., 2008). Nonetheless, one of the studies described in this thesis investigated sexual dimorphism of anatomical

brain asymmetry and genes involved in sex hormone biology, and thus traces its roots to the work of Geschwind and colleagues.

A much less studied factor than handedness or sex is the possible modulating effect of age on brain asymmetries. Only a relatively small number of studies have addressed age as a factor at all (e.g. Abedelahi et al., 2013; Galaburda and Geschwind, 1981; Good et al., 2001b; Li et al., 2014; Plessen et al., 2014; Yamashita et al., 2011) and these studies reported small effect sizes and contradictory findings, such that any true effects of age on brain asymmetries remained ambiguous prior to one of the studies included in this thesis.

Genetics of brain asymmetries

The genetic origins of human brain asymmetries are virtually unknown. However, converging evidence strongly suggests that genes are responsible for initiating human brain asymmetries in early development, as well as maintaining them through adulthood (Francks, 2015). For example, by means of ultrasound imaging it was shown that at 11 weeks gestational age, the developing brain already shows population-level asymmetries in the size of the choroid plexus, with the left structure being on average larger than the right (Abu-Rustum et al., 2013). At 20 weeks gestation, there is an asymmetry in the size of the lateral ventricles (Hering-Hanit et al., 2001). In turn, this has been suggested to be a potential precursor of cortical perisylvian asymmetries, which can be observed from the 31st week of gestation (Corballis, 2013). Furthermore, these early signs of asymmetric brain development, seen in utero, are possibly preceded by behavioural asymmetries (Hepper, 2013). In an ultrasound scanning study at 10 weeks gestational age, the majority of human foetuses showed preferential movement of their right arms (Hepper et al., 1998). Moreover, hand preference for thumb sucking at 15 weeks gestation was predictive of handedness at 12 years of age (Hepper et al., 2005).

Such early manifestations of brain asymmetry likely reflect differential genetic activity between the left and right sides of the central nervous system in the embryo/foetus. This possibility has been directly assessed in human embryos by measuring subtle differences in gene messenger RNA (mRNA) expression between left and right hemispheres from post-mortem brain tissue (Johnson et al., 2009; Lambert et al., 2011; Sun et al., 2005). An inherent caveat to this approach is that gene expression is not homogeneously distributed across the brain, nor expected to be stable through development. This makes it difficult to detect developmental asymmetries in gene expression that are potentially region-specific and transient in nature. Furthermore, post-mortem brain tissue on which such experiments can

be performed is not easily available (Francks, 2015), and the statistical corrections necessary when analysing large numbers of genes limit such analyses to detecting only relatively strong asymmetries in gene activity, which may be unusual (Lambert et al., 2011; Pletikos et al., 2014). However, a recent study was able to show that genes involved in synaptic transmission and signal transduction were differentially expressed between homologous left and right cerebral cortex in adult post mortem brains (Karlebach and Francks, 2015). The authors focused their analyses on the superior temporal cortex, a critical region in the asymmetrical language network. Their findings, in turn, have suggested specific sets of genes in which polymorphisms should be tested in relation to anatomical asymmetry of this brain region, as well as individual differences in language lateralization.

Molecular mechanisms are known to be involved in setting up brain asymmetries in both vertebrates and non-vertebrates (e.g. Taylor et al., 2010), as well as in determining left-right patterning of the viscera (Tamura et al., 1999). The best characterized vertebrate model of structural brain asymmetry is the zebrafish. In these animals, brain asymmetry originates from left- biased migration of an organ in the embryonic diencephalon, guided by differential levels of signalling proteins between the left and right sides (Colombo et al., 2013; Concha et al., 2009). This, in turn, cascades into further asymmetries of the central nervous system during the zebrafish's subsequent development (Concha et al., 2009). However, the origins of fish brain asymmetry appear to be linked developmentally to visceral asymmetry mechanisms, while it is not clear that the same applies to human brain asymmetry (Kennedy et al., 1999; Tanaka et al., 1999), it further supports the idea of molecularly-programmed human brain asymmetries (Francks, 2015).

These converging lines of evidence place genetic factors in a pivotal position with regards to the development and maintenance of anatomical brain asymmetries. It therefore follows that common genetic variability, i.e. individual differences in DNA between individuals, is a potentially important factor affecting variability in brain asymmetry at the population level. Furthermore, if naturally occurring differences in brain asymmetry can be associated with variability at particular genomic loci through genetic mapping approaches, then specific molecular mechanisms affecting brain asymmetries might be identified, yielding powerful new insights into the biology of brain asymmetries.

Twin-based heritability studies of brain features have already suggested that some differences in brain asymmetry between individuals can be explained by genetic variability. In other words, genetic influences on brain structures have been found to differ between hemispheres for cortical, i.e. in the size of cortical and subcortical structures (Eyler et al., 2014; Hulshoff Pol et al., 2006), including

properties of white-matter fibers (Jahanshad et al., 2010). However encouraging, these initial studies of heritability have indicated that the role of genetic variability on brain asymmetries is relatively subtle compared to other brain morphological features, with heritability estimates usually less than 50% for the asymmetries investigated so far.

Throughout the 20th century several theories were proposed regarding the genetics of variation in cerebral asymmetry (e.g. Annette and Annett, 1981; Chamberlain, 1928; Levy and Nagylaki, 1972; McManus, 1991). Although these theories each varied in the degree of focus on handedness, language-lateralization or anatomical brain asymmetries, all shared the simplifying assumption that variation in these traits is strongly interdependent (see above). The theories also involved distinct versions of mostly monogenic (Mendelian, single-gene) accounts of hand-preference inheritance. While the authors undoubtedly set new standards regarding phenotypic analyses, of handedness in particular, a major caveat of these early studies is that they were attempting to solve a particularly complex inverse problem (see Aster et al., 2011), that is, to infer the unknown genetic architecture of handedness from limited views of its phenotypic distribution.

The true nature of the problem has become evident just in this last decade, due to rapid advances in genotyping and computational technologies. A recent genome-wide association study (GWAS) based on 3940 twins resulted in no individual locus significantly associated to handedness after correction for multiple testing across the genome (Armour, Davison, & McManus, 2014). This GWAS study was adequately powered to detect a major-genetic effect on handedness, if it was due to common variation in the genome. A preliminary report of a GWAS from the ENGAGE Handedness Consortium, based on 23,443 subjects, also did not indicate significant evidence for association (Medland, Lindgren, et al., 2009). The true genetic architecture of left-handedness, and other brain and behavioural asymmetries, is therefore likely to be much more complex than the single-gene accounts allowed for. The 'complex trait' model had important implications for the studies that comprise this thesis, as discussed further below.

Altered anatomical brain asymmetries and cognitive functions

There is much evidence that departures from the typical pattern of brain asymmetries can have clinical relevance (Renteria, 2012). Assessed mostly through MRI, asymmetries of the superior temporal lobe, including that of the planum temporale or of the transverse gyrus (of Heschl) for example, have often been linked to both schizophrenia and language-related disorders (Altarelli et al., 2014; Oertel-Knochel

and Linden, 2011; Richlan et al., 2013), although not always consistently (Deep-Soboslay et al., 2010). Other local abnormalities in anatomical brain asymmetry have been associated to a broad range of cognitive or psychiatric disorders. To highlight a few examples, individuals diagnosed with autism spectrum disorder also display aberrant asymmetries of perisylvian structures (e.g.Floris et al., 2016). Attention-deficit/hyperactivity disorder and its symptoms have been related to abnormal striatal asymmetry (Hynd et al., 1993; Schrimsher et al., 2002), as is also the case for obsessive-compulsive disorders (Hendren et al., 2000; Szeszko et al., 1999). Consequently, atypical asymmetry of brain anatomy is often seen as a potential etiological factor in cognitive pathology (Ocklenburg et al., 2015; Qiu et al., 2009; Renteria, 2012), although cause-effect relations are not yet understood (Bishop, 2013).

Although fewer in number than clinical studies, studies of non-disorder populations have suggested weak links between individual differences in anatomical asymmetries and cognitive performance levels (e.g. Jensen et al., 2015; Woolard and Heckers, 2012). The most commonly investigated domain of cognition has been language, through assessing linguistic auditory processing, or motor speech-production, focusing particularly on distinct asymmetric features of the superior temporal lobe (e.g. Bidula and Kroliczak, 2015; Boles and Barth, 2011; Greve et al., 2013; Jansen et al., 2010; Josse et al., 2009; Tzourio-Mazoyer et al., 2015). The findings obtained by these studies point again to complex and subtle relations between structural asymmetries and cognitive functions, and overall suggest a large degree of plasticity in relation to lateralized functions, by which either hemisphere is often able to become dominant for a given function without major consequences for performance (Francks, 2015).

Identifying biological factors related to anatomical brain asymmetries

The findings discussed so far have illustrated that relationships between biological factors and brain asymmetries are relatively subtle and difficult to establish unambiguously. Underlying the available literature, one can distil two themes of particular importance. (1) Brain asymmetries are qualitatively different from other aspects of brain morphology. They are by definition relative traits, derived from the comparison of bilateral morphological features. As a result, any inconsistency or uncertainty in the anatomical definition of a bilateral trait will have a distorting effect on its asymmetry measurement, making it potentially very sensitive to methodological choices. This issue will inevitably become more severe when analysing slight asymmetries in datasets which are not sufficiently large to yield robust measurements and adequate statistical power to detect or refute effects. (2) Brain asymmetry is a multidimensional trait. The early accounts discussed above suggested a somewhat monolithic view of brain asymmetry: "brain dominance", motivated by the available findings on handedness and language

lateralization (e.g. Annette and Annett, 1981; Crow, 2002). However, the field now favours a more complex view (Ocklenburg et al., 2015; Whitehouse and Bishop, 2009). This reflects accumulating evidence suggesting the presence of both shared and independent asymmetry mechanisms and dimensions in the brain, each with a multifactorial basis (Francks, 2015; Ocklenburg et al., 2015).

The studies presented in this dissertation describe a novel set of investigations of variation in human anatomical brain asymmetries, which build upon the rich and interdisciplinary history summarized above, while overcoming some of the chief limitations that have hitherto been inherent to this line of research, such as variable trait measurement and limited sample size. The main resource used for this dissertation was the Brain Imaging Genetics (BIG) dataset, collected under the Cognomics initiative of the Donders Institute for Brain, Cognition and Behaviour (Radboud University, Nijmegen), and the Max Planck Institute for Psycholinguistics. This dataset consists of thousands of Magnetic Resonance (MR)-derived brain images, as well as genome-wide genotypes of millions of genetic variants which are common in the population. Crucially, my approaches aimed to overcome study heterogeneity and measurement reliability through the use of uniform, automated protocols of image and data analysis in large datasets, including but not limited to BIG. These are unifying aspects across the various chapters of this dissertation, which shared the central goal of reliably identify subtle, biological effects on variability in anatomical brain asymmetries. Such a framework was essential for testing common genetic variation (i.e. genomic polymorphisms that are common in the population) in relation to multifactorial traits like brain asymmetries. Based on previous studies, we can expect the effect of any individual common genetic variant on brain structure to be tiny, explaining less than 1% of overall trait variance (Hibar et al., 2015; Stein et al., 2012), even if many thousands of such genetic effects may sum to have substantial overall influences. My large-dataset approach also proved to be extremely valuable for reliably detecting and measuring the subtle effects of sex and age on brain asymmetries, as will become clear throughout the dissertation, as well as indicating that handedness is of limited relevance for most brain anatomical asymmetries. The studies and findings described in the following chapters are based on the greatest samples sizes ever used to address the biology of variation in human anatomical brain asymmetries; some of them greater than previous studies by orders of magnitude. The large-scale nature of this novel approach also introduced new methodological challenges. Issues related to data reliability for brain phenotypes as well as for genotypes, for example, were carefully assessed and controlled for in each chapter, and tailored to each research question.

To conclude, a robust investigation on the potential influences of sex, handedness, age and genetics on individual differences in brain asymmetry, relied heavily on a faithful representation of the biological diversity which is natural to the human population. This was now possible in light of the recent and rapid growth in data collections, as well as joint international efforts for the study of brain structure. Large datasets are becoming available, internationally, which include brain data from structural MRI and, in some cases, genetic data (Thompson et al., 2014). The timing of this dissertation thus allowed robust investigations at a scale not previously possible. At the same time, the availability of these datasets explains the focus on anatomical rather than functional brain lateralizations, because data on functional asymmetries are much more limited in availability and numbers. Nijmegen's BIG dataset is a case in point: the thousands of structural MRI scans were pooled to create a large resource by numerous investigators, who nonetheless each performed different fMRI experiments in studies of just tens of subjects, with diverse aims across a broad range of cognitive domains.

Summary of research chapters

The relationship between handedness and anatomical brain asymmetries, as well as functional asymmetries in other cognitive domains, is far from clear (e.g. Ooki, 2014; see above). In Chapter 2 I examine the potential relations between anatomy of the cerebral cortex and handedness in the largest study to have been performed of this question to date (1960 right-handed and 106 left-handed subjects). Identifying anatomical brain correlates of handedness could provide clues to its ontogeny. In turn, by postulating specific ontogenetic mechanisms, these could guide further investigations on the overall genetic architecture (Ocklenburg et al., 2013; Willems et al., 2014), as well as clarify the relations of handedness with other forms of lateralized cognition, including the relationship between brain structure and function.

Although sex has often been postulated as one of the driving factors underlying differences in brain asymmetry, there is currently no strong consensus with regards to the morphological specificity of sex effects or their functional implications (see above). In Chapter 3 I set out to map sex differences in gray matter asymmetries over the entire cerebral cortex, initially in more than 2000 healthy adults. Followed by a replication analysis, in collaboration with the University of Greifswald, our conclusions were solidified regarding sexual dimorphisms in the adult brain. At the same time, this collaboration allowed a detailed investigation on the genetic basis of the most sexually dimorphic asymmetry in the brain, leading to the first genome-wide analysis of a cortical brain asymmetry to date. Moreover, further analyses were performed with the goal of identifying gene networks relevant to asymmetry-determining

processes. Through this approach, it was possible to highlight genetic mechanisms and specific candidate genes that can be further probed in relation to human cognitive variation, particularly related to lateralized functions.

In line with evidence suggesting a possible subcortical origin in development for brain asymmetries (as outlined above), in Chapter 4 I investigate volumetric asymmetries in 6 subcortical structures and the hippocampus. Due to the overall strong similarity between the left and right sides of these bilateral structures, the initial focus of this study was to assess the feasibility of automated measurement of subtle differences in volumetric asymmetry, applied to large datasets. This was assessed by two automated methods of segmentation (FSL|FIRST and FreeSurfer). With the use of data from 235 subjects who had undergone MRI twice, I was able to assess both inter-subject agreements between measures obtained at different time points, as well as the agreement between both automated methods. In addition, the analysis included assessments of systematic, asymmetric biases in the automated processes themselves. Such biases could potentially introduce artificial findings regarding directional asymmetries at the population level. This was done by re-analysing the same brain images, after they had been flipped on the left-right axis. The most reliable measurement was further meta-analysed in a genome-wide association scan, in a combined sample of 3,028 adult subjects. Again, this was the first comprehensive genetic association study for a subcortical human brain asymmetry. The insights gained from this study would then be highly valuable for future and on-going consortium projects, as regards the approach to asymmetry measures to be pursued for genome-wide association scan meta-analysis.

Chapter 5 presents the first work by the Lateralization working group within the ENIGMA consortium (Enhancing Neuro Imaging Genetics through Meta-Analysis; (Thompson et al., 2014), for which I am the leading hands-on researcher. ENIGMA is an international collaborative effort with the goal to perform large-scale analysis of brain morphology, assessed with MRI, and to identify genetic variants influencing it (Hibar et al., 2015; Stein et al., 2012). The previous literature on subcortical asymmetries was inconclusive in relation to the roles of age, handedness and sex in affecting subcortical brain asymmetries, thus motivating a large-scale investigation of this issue. In a meta-analysis of more than 15,000 human participants, within the ENIGMA consortium, we established unambiguous effects of sex and age on the asymmetries of some subcortical structures, by pooling data across 52 different datasets recruited worldwide. This was one of the largest studies ever to have been performed in relation to any aspect of human brain variability. In addition, the heritabilities of subcortical volumetric asymmetries

were estimated. This information will prove valuable to support further genetic mapping studies of these brain asymmetries.

Finally, in Chapter 6, my findings are discussed in the context of their overall contributions to our understanding of brain asymmetry and its ontogeny. It also discusses a set of additional studies that I contributed to as a co-author rather than primary author. Although not directly performed in support for this dissertation, the topics investigated do bear upon the themes covered by this dissertation. Finally, Chapter 6 elaborates the new research directions which can now be pursued. Briefly, as the hands-on leader of the ENIGMA-Lateralization working group, and building upon the findings and insights gained from this dissertation, I will continue this line of research on the biological underpinnings of brain asymmetry. Such large scale studies are necessary to disentangle the highly complex biology underlying brain asymmetries, particularly the genetics, as has previously shown in successful investigations of other features of brain morphology (Hibar et al., 2015; Stein et al., 2012). Furthermore, working within the ENIGMA consortium, whose objectives include understanding the biological mechanisms responsible for disease, our investigations will shed light on the relations between brain asymmetries and disorders such as schizophrenia (Hirnstein and Hugdahl, 2014), attention deficit hyperactivity disorder (ADHD; Aylward et al., 1996; Castellanos et al., 1996; Singer et al., 1993; Uhlikova et al., 2007), obsessive compulsive disorder (OCD; Peng et al., 2015; Szeszko et al., 1999) or bipolar disorder (BP; Liao et al., 2008), to name a few. Finally, we are setting up a separate, but complementary, project investigating the relations between brain anatomical asymmetries and hemispheric lateralization of function as assessed indirectly through resting-state fMRI, for which large datasets are now becoming increasingly available. Current evidence suggests a far from clear relationship, in need of empirical investigations.

Chapter 2

Differences in cerebral cortical anatomy of left- and right-handers

Adapted from:

Guadalupe T, Willems RM, Zwiers MP, Arias Vasquez A, Hoogman M, Hagoort P, Fernandez G, Buitelaar J, Franke B, Fisher SE and Francks C. (2014): Differences in cerebral cortical anatomy of left- and right-handers. Front Psychol 5(261).

Abstract

The left and right sides of the human brain are specialized for different kinds of information processing, and much of our cognition is lateralized to an extent towards one side or the other. Handedness is a reflection of nervous system lateralization. Roughly ten percent of people are mixed- or left-handed, and they show an elevated rate of reductions or reversals of some cerebral functional asymmetries compared to right-handers. Brain anatomical correlates of left-handedness have also been suggested. However, the relationships of left-handedness to brain structure and function remain far from clear. We carried out a comprehensive analysis of cortical surface area differences between 106 left-handed subjects and 1960 right-handed subjects, measured using an automated method of regional parcellation (FreeSurfer, Destrieux atlas). This is the largest study sample that has so far been used in relation to this issue. No individual cortical region showed an association with left-handedness that survived statistical correction for multiple testing, although there was a nominally significant association with the surface area of a previously implicated region: the left precentral sulcus. Identifying brain structural correlates of handedness may prove useful for genetic studies of cerebral asymmetries, as well as providing new avenues for the study of relations between handedness, cerebral lateralization and cognition.

Introduction

Handedness is perhaps the most overt reflection of lateralization of the central nervous system in humans. Humans show a strong and population-level bias towards using one hand rather than the other for manual activities, which is unusual among mammals (Vallortigara et al., 2011). Roughly 90% of humans are right-handed, while even other primates (e.g. chimpanzees and macaques) do not show such a strong degree of population-level handedness (Lonsdorf and Hopkins, 2005; Meunier et al., 2013). This motor asymmetry is observable at least as early during human development as 15 weeks of gestation, and is preceded by asymmetries of arm movements even earlier (Hepper, 2013). In addition the tendency towards right handedness has apparently been present throughout human history, and across cultures and continents (Coren and Porac, 1977; Faurie and Raymond, 2004; Hardyck and Petrinovich, 1977; McManus, 1991; McManus, 2009).

Due in part perhaps to its minority status and past cultural stigmatization, left-handedness has often been studied in the context of pathology, for example in relation to Alzheimer´s disease (de Leon et al., 1986), substance use (London, 1989) and autoimmune disorders (Geschwind and Behan, 1982). Handedness has also been investigated in relationship to lateralized cognitive functions, such as visuospatial processing (Gordon and Kravetz, 1991), face recognition (Bukowski et al., 2013; Luh et al., 1994; Willems et al., 2010) and, prominently, language (Knecht et al., 2000b; Tzourio et al., 1998). Knecht and colleagues found an increased incidence of bilateral and right hemisphere language lateralization among left-handers, compared to right-handers, although the majority of left/mixed handers still showed left-hemisphere language dominance (Knecht et al., 2000a; Knecht et al., 2000b). This suggests that developmental mechanisms affecting cerebral language dominance overlap to an extent with those influencing hand motor control. However, it remains poorly understood how these different domains of functional lateralization are related to each other (Badzakova-Trajkov et al., 2010).

Several early attempts to understand human handedness attributed right-handedness to socio-cultural, anatomical, as well as genetic factors (for a review see Hardyck and Petrinovich, 1977; or Corballis et al., 2012 for a more recent one). However, the developmental basis of human brain lateralization remains almost wholly unknown, and likewise the causes of its variation are hardly understood (Willems et al, in press). One robust observation is that males show a slightly higher proportion of left-handedness than females (Halpern et al., 1998; Peters et al., 2006; Sommer et al., 2008). Recent twin studies, based on thousands of families, have indicated that 21%-24% of the liability to left- handedness can be explained by additive genetic effects (Medland et al., 2009; Vuoksimaa et al., 2009). This indicates that genetic

variation plays a role in causing variation in handedness. In contrast to original models of handedness as a monogenic trait (Annett, 1985; McManus, 1985), recent evidence from genome-wide association studies strongly suggest more complex models (Medland, 2009; Armour et al., 2014; McManus et al., 2013). So far, studies aimed at discovering the specific genetic loci involved have yielded tentative associations with the genes AR, APOE, COMT, PCSK6, LRRTM1 (Brandler et al., 2013; Bloss et al., 2010; Francks et al., 2007; Medland et al., 2005; Savitz et al., 2007; Scerri et al., 2011). Although originally discovered in populations affected by dyslexia, PCSK6 has also shown association with degree of handedness in a healthy sample of unrelated adults (Arning et al., 2013). It is not yet known how these genes may influence asymmetrical development of the brain (see Ocklenburg et al., 2011).

Identifying brain anatomical correlates of left-handedness may provide potential endophenotypes for further genetic association studies (Ocklenburg et al;, 2011; Willems et al, in press). Finding anatomical correlates of left-handedness may also inform on the relations between handedness and lateralized cognitive functions, and more broadly on brain structure-function relationships (Ocklenburg et al., 2011; Willems et al, in press). Amunts et al. (1996) found deeper left precentral sulci in right-handers than left-handers using manual segmentations of magnetic resonance (MR) images. Consistent with this, Foundas et al. (1998) examined left-right asymmetries of the precentral gyrus in a sample of 15 left- and 15 right handers based on manual segmentations of their MR images, and found leftward asymmetries in right-handers, but no consistent asymmetry in left-handers (also see Kloppel et al., 2007, and Willems and Hagoort, 2009, for corroborating findings using functional MR imaging). More recently, gray matter volume in the central sulcus was shown to relate to hand motor skill, but to different extents depending on handedness (Herve, et al. 2005). In addition, asymmetry of the planum temporale (PT), the posterior portion of the superior surface of the temporal lobe, has been reported to associate with hand preference (Foundas et al., 1995; Steinmetz et al., 1991; Herve, et al., 2006). However, results regarding the PT have not been consistent throughout the literature (Good et al., 2001; Witelson and Kigar, 1992). Similarly, an association between handedness and cerebral torque, another structural brain asymmetry, has also been assessed with inconclusive results (Narr et al., 2007). More recently, Powell and colleagues (2012) in a study of 40 left-handers and 42 right-handers found differences in sulcal shape of the pars orbitalis (PO) and pars triangularis (PTr), as well as differences of volumetric asymmetry within the PO,. To our knowledge, Good et al. (2001) has studied the largest sample to have been used in examining brain morphological differences related to handedness. Using a voxel-based morphometry analysis with a total sample of 465 subjects (67 lefthanders) they did not find structural correlates of

handedness in the brain. This suggests that any such correlates are subtle and will require larger samples and/or other ways to quantify brain structure, in order to detect them unambiguously.

The goal of the present study was to identify cerebral cortical differences between left and right-handers, by analysing the largest sample used so far for this purpose (106 left-handed subjects and 1960 right-handed subjects), and using recently developed methodology for the automated segmentation and quantification of regional grey matter (Fischl et al., 2004). We analysed the data in three stages. First we examined total cortical surface area in relation to handedness. Then, we tested a set of candidate cortical regions for associations with handedness, based on the previous studies mentioned above. Finally, we carried out a screen over all remaining cortical regions.

Methods

Study dataset

The Brain Imaging Genetics (BIG) study was initiated in 2007 and comprises healthy volunteer subjects, including many university students, who participate in diverse imaging studies at the Donders Centre for Cognitive Neuroimaging (DCCN), Nijmegen, The Netherlands (Franke et al., 2010). At the time of this study the BIG subject-pool consisted of 2337 self-reported healthy individuals (1248 females) who had undergone anatomical (T1-weighted) MRI scans, usually as part of their involvement in diverse smaller-scale studies at the DCCN, and who had given their consent to participate in BIG. Their median age was 23 years. A subset of 235 subjects had undergone a brain MRI scan twice, with at least one day separation between scans. Fifty percent of the 235 re-scans took place within 181 days of the first, with the mean elapsed time being 320 days (SD = 360). At the time of the first scan, the median age of this group was 23 years.

Handedness of the participants was assessed by an item in their enrolment form. This consisted of subjects selecting the appropriate label, either "left-handed / right-handed" (in Dutch). We discuss the validity of this method of assessing handedness further below. Only those subjects who clearly indicated one or the other state were included in our analysis. This resulted in a sample of 1960 right-handed subjects and 106 left-handed subjects, with a median age of 22 years and a standard deviation of 11 years. The proportion of left-handers was substantially lower than in the general population; this was due to left- handedness being used as an exclusion criterion for some of the imaging studies that were pooled into the overall BIG dataset.

Image acquisition

MRI data in BIG were acquired with either a 1.5 Tesla Siemens Sonata or Avanto scanner or a 3 Tesla Siemens Trio or TimTrio scanner (Siemens Medical Systems, Erlangen, Germany). Given that images were acquired during several smaller scale studies, the parameters used were slight variations of a standard T1-weighted three-dimensional magnetization prepared rapid gradient echo sequence (MPRAGE; 1.0×1.0×1.0 mm voxel size). The most common variations in the TR/TI/TE/sagittal-slices parameters were the following: 2300/1100/3.03/192, 2730/1000/2.95/176, 2250/850/2.95/176, 2250/850/3.93/176, 2250/850/3.68/176, 2300/1100/3.03/192, 2300/1100/2.92/192, 2300/1100/2.96/192, 2300/1100/2.99/192, 1940/1100/3.93/176 and 1960/1100/4.58/176. There was also variation in the number of headcoils used across BIG scans, however, no systematic differences were observed in their use between left- and right-handed subjects. The following arrays were employed (and their frequencies) in the right-handed population: 32-channel (24%), 12-channel (4%), 8-channel (38%) arrays and single headcoil (33%). In the left-handed population, this distribution was 32-channel (27%), 12-channel (0%), 8-channel (33%) arrays and single headcoil (40%).

Image processing

Automated parcellation of cerebral cortical regions from T1-weighted images was done in FreeSurfer v5.1 (Fischl et al., 2004) according to the Destrieux atlas (Destrieux et al., 2010) within the '-recon-all' processing pipeline, and using default parameters. Measures of surface area (in mm^2) were produced for the total cortical surface and for each of 74 cortical parcellations, in each hemisphere. Outlier values (more extreme than 3.5 SD from the mean) were excluded for each measure. The scan-rescan correlation of each measure was then calculated in the sample of 235 subjects who had undergone two MRI scans, after correcting for the potential covariate effects of age, sex, total cortical surface area and scanner field strength (IBM SPSS v.20).

Out of the 74 covariate-corrected bilateral cortical measures, 23 were excluded from subsequent analyses, due to low scan-rescan correlation in either left, right or both structures (Pearson´s $r < 0.7$; i.e. corresponding to shared proportion of variance between scan and re-scan measures of < 0.49). Regional measures of cortical thickness were also generated. There is evidence that cortical surface and thickness have independent sources of variation (Panizzon et al., 2009). However, we discarded the thickness measures because the majority (81%) showed scan-rescan correlations below 0.7.

Cortical correlates of handedness

We tested for associations between handedness and cortical surface areas using repeated-measures ANOVA, implemented in SPSS (IBM SPSS v.20). Hemisphere (left vs right) was factored as a within-subjects variable and handedness group as a between-subject variable in a full factorial design. This allowed the detection of bilateral associations of handedness with cortical surface areas, as well as asymmetrical associations (by means of the interaction between handedness and hemisphere). We first tested the total hemispheric surface areas, and then we tested the regional surface areas. In addition, the following covariates were entered into the analyses: sex, age, scanner field strength, and total (i.e. left plus right) hemispheric surface area (the latter only for the analyses of regional surfaces).

We tested candidate cortical regions motivated by previous findings in the literature (specifically by the studies reviewed in the introduction). We separated these candidate regions into three domains; language, motor control and visual processing. Language-related candidate regions were the inferior frontal gyrus and superior temporal gyrus. These corresponded most closely to the following parcellations within the Destrieux atlas, that had also showed a robust scan-rescan correlation: Opercular part of the inferior frontal gyrus, triangular part of the inferior frontal gyrus, anterior transverse temporal gyrus (of Heschl), lateral aspect of the superior temporal gyrus, and planum temporale. The motor control candidate regions were the superior and inferior parts of the precentral sulcus (as defined in the Destrieux atlas). The visual-related candidate regions comprised inferior and ventral areas of the temporal lobe. In the Destrieux atlas these corresponded most closely to the following regions: inferior temporal gyrus, lateral occipito-temporal gyrus (fusiform gyrus) and lingual part of the medial occipito-temporal gyrus. We applied Bonferroni corrections for the comparisons done within each of these domains.

After the analysis of candidate regions, we then tested all of the remaining cortical regions for differences between left- and right-handers, again using Bonferroni adjustment to correct for multiple testing.

Power analysis

We used G*Power v3.1.9 (Faul et al., 2009) to estimate the necessary effect sizes to be detected given our study design. We considered our sample size, a required power (1- β) of 80%, a correlation between bilateral volumes of r ~0.8, and an α level corrected for multiple testing. This resulted in estimates of partial $\eta^2 \sim 0.07$ [$F_{(1,2055)} \sim 5.7$] for analyses within each of the candidate domains, and a partial $\eta^2 \sim 0.09$ [$F_{(1,2055)} \sim 10$] for the analysis of the remaining cortical surfaces. In other words we had 80% power to

detect an association explaining 9% of the residual variance in a regional cortical surface area after having removed the effects of covariates and after considering the multiple comparisons, for the screening analysis of non-candidate regions.

Results

The proportion of left-handers in our sample differed significantly between males and females. Of the 942 males, 59 were left-handed (6.3%), and of the 1077 females, 47 were left-handed (4.4%); $\chi^2_{(1)} = 4.56$, p = 0.02, phi = 0.047.

Table 1. Mean surface areas (and SDs) for the left and right hemispheres, by handedness.

	Left-handers	Right-handers
Left hemisphere surface area	87855.1 (7717.6)	87984.5 (8469.9)
Right hemisphere surface area	87817.2 (8133.5)	88295.6 (8487.4)

Table 2. Repeated-measures ANOVA results from testing for an association between handedness and total hemispheric cortical surface areas.

	Repeated-measures ANOVA		
	P	F	Partial η^2
Handedness	0.114	2.501	0.001
Handedness*Hemisphere	0.132	2.266	0.001
Sex	< 0.001	1193.7	0.367
Age	< 0.001	90.1	0.042
Scanner field strength	< 0.001	12.48	0.006

Handedness did not show a significant association with bilateral hemispheric surface area, nor with overall hemispheric surface asymmetry (see Table 1 & 2). None of the candidate regions, related to either language, visual processing, or motor control showed significant evidence for association with handedness after correction for multiple testing within each of these domains (see Table 3). The only regions showing main effects of handedness with $p < 0.05$ before correction for multiple testing were the superior precentral sulcus and the inferior temporal gyrus. Means (and SDs) for these regions, by hemisphere and handedness group, are shown in Table 4.

Table 3. Summarized results for the candidate cortical regions. Reported are p-values before correction for multiple testing (none survived this correction).

	Repeated-measures ANOVA		
Language-related	P	F	partial η^2

Opercular part of the interiorfrontal gyrus	Handedness	0.73	0.12	< 0.001
	Handedness*Hemisphere	0.63	0.23	< 0.001
Triangular part of the inferior frontal gyrus	Handedness	0.88	0.02	< 0.001
	Handedness*Hemisphere	0.17	1.8	0.001
Anterior transverse temporal gyrus (of Heschl)	Handedness	0.86	0.03	< 0.001
	Handedness*Hemisphere	0.06	3.4	0.002
Lateral aspect of the superior temporal gyrus	Handedness	0.57	0.33	< 0.001
	Handedness*Hemisphere	0.36	0.85	< 0.001
Planum temporale	Handedness	0.42	0.64	< 0.001
	Handedness*Hemisphere	0.94	0.01	< 0.001
Motor control-related		P	F	partial η^2
Superior part of the precentral sulcus	Handedness	0.044	4.07	0.002
	Handedness*Hemisphere	0.6	0.28	< 0.001
Inferior part of the precentral sulcus	Handedness	0.76	0.09	< 0.001
	Handedness*Hemisphere	0.85	0.03	< 0.001
Visual-related		P	F	partial η^2
Inferior temporal gyrus	Handedness	0.037	4.36	0.002
	Handedness*Hemisphere	0.58	0.3	< 0.001
Lateral occipito-temporal gyrus (fusiform gyrus)	Handedness	0.17	1.87	0.001
	Handedness*Hemisphere	0.53	0.4	< 0.001
Lingual part of the medial occipito-temporal gyrus	Handedness	0.26	1.27	0.001
	Handedness*Hemisphere	0.1	2.67	0.001

Table 4. Means (and SDs) for the superior part of the precentral sulcus, and inferior temporal gyrus, by hemisphere and handedness group.

	Left hemisphere		Right hemisphere	
	Left-handers	Right-handers	Left-handers	Right-handers
Superior part of the precentral sulcus	914.9 (207.5)	952.7 (200.9)	965.1 (201.9)	990.4 (214.8)
Inferior temporal gyrus	1853.2 (328.6)	1911.7 (311.3)	1744.8 (319.6)	1787.6 (281.8)

Tables 5 & 6 show results for the remaining (non-candidate) regional surface areas that reached nominal significance (i.e. uncorrected $p < 0.05$) for an association with handedness, either as a main effect on bilateral surface or as an interaction with hemisphere. None of these associations survived correction

for multiple testing. The results for all cortical regions and covariates, regardless of nominal significance, can be found in the supplementary material, together with descriptive statistics of all metrics, per handedness group.

Table 5. Summary results for non-candidate cortical regions that achieved nominal significance in ANOVA. (None of these results survived correction for multiple testing). Complete results for all regions and covariates are provided in the supplementary material.

		Repeated-measures ANOVA		
Regional surface areas		P	F	partial η^2
Anterior part of the cingulate gyrus and sulcus (ACC)	Handedness	0.139	2.19	0.001
	Handedness*Hemisphere	0.023	5.18	0.003
Middle-anterior part of the cingulate gyrus and sulcus (aMCC)	Handedness	0.67	0.18	< 0.001
	Handedness*Hemisphere	0.003	8.99	0.005
Superior occipital gyrus (O1)	Handedness	0.04	4.23	0.002
	Handedness*Hemisphere	0.255	1.3	< 0.001
Posterior transverse collateral sulcus	Handedness	0.648	0.21	< 0.001
	Handedness*Hemisphere	0.048	3.92	0.002
Superior frontal sulcus	Handedness	0.038	4.31	0.002
	Handedness*Hemisphere	0.221	1.5	< 0.001
Sulcus intermedius primus (of Jensen)	Handedness	0.743	0.14	< 0.001
	Handedness*Hemisphere	0.037	4.37	0.002
Parieto-occipital sulcus (or fissure)	Handedness	0.029	4.8	0.002
	Handedness*Hemisphere	0.25	1.32	< 0.001

Table 6. Means (and SDs) for non-candidate cortical regions that achieved nominal significance in ANOVA, by hemisphere and handedness group.

	Left hemisphere		Right hemisphere	
	Left-handers	Right-handers	Left-handers	Right-handers
Anterior part of the cingulate gyrus and sulcus (ACC)	1648.0 (223.2)	1707.4 (264.5)	1998.8 (251.3)	2016.7 (271.1)
Middle-anterior part of the cingulate gyrus and sulcus	974.6 (144.7)	1014.5 (170.3)	1144.0 (162.7)	1114.1 (169.8)
Superior occipital gyrus (O1)	1131.5 (166.2)	1101.1 (167.7)	1251.1 (177.8)	1239.6 (186.7)
Posterior transverse collateral sulcus	300.7 (70.9)	294.2 (66.4)	373.0 (98.8)	386.9 (98.8)
Superior frontal sulcus	2004.9 (286.8)	2077.1 (302.7)	1867.6 (271.7)	1906.7 (296.1)
Sulcus intermedius primus (of Jensen)	280.2 (145.6)	257.6 (127.3)	350.1 (150.3)	364.0 (151.7)
Parieto-occipital sulcus (or fissure)	1445.9 (225.9)	1429.0 (239.3)	1584.5 (265.8)	1544.2 (255.8)

Discussion

In a large sample of primarily young adult and healthy individuals, we tested for associations of handedness with total and regional measures of hemispheric cerebral cortical surface area. We report on the largest sample to have been analysed to date in relation to this question. The proportion of left-handers in our sample was lower than in the general population, due to an exclusion of left-handers from some of the smaller studies that were pooled to create our Brain Imaging Genetics dataset. This exclusion bias, however, did not affect the heterogeneity of scan parameters present in both handedness groups, as reflected in the similar usage of headcoils between them. Nonetheless, we observed a sex difference in the incidence of left-handedness that was consistent with previous literature (with left-handedness occurring at an elevated rate in males; Sommer et al., 2008).

We did not observe any difference in bilateral cortical surface area in left-handers compared to right-handers. Nor did we find significant evidence for associations of handedness with region-specific bilateral surface areas, or their asymmetries, for regions related to language, hand motor control, or visual processing (Foundas et al., 1998; Foundas et al., 1995; Willems et al., 2010). Our data therefore provide little support for previously reported region-specific associations with handedness, although the Destrieux atlas' definitions of regions might not be identical to the definitions used in these previous studies. For example, the planum temporale in the Destrieux atlas extends parietally (Destrieux et al., 2010), which is not a classic neuroanatomical definition (Geschwind and Levitsky, 1968; Steinmetz et al.,1991).

A limitation of our study was that, due to our large sample size and the number of cortical regions analysed, systematic manual checking and adjustment of the automated parcellations was not feasible. Visual checks were made for only a small minority of images and not targeted to specific regions. However we exploited our subset of twice-scanned subjects in order to exclude regions that were not consistently parcellated from scan to re-scan, and also used outlier exclusion, as two forms of quality control. Clearly there is a need for improved methods of automated parcellation that capture some of the more variable and anatomically complex cortical regions better, in order to carry out future studies based on thousands of images. Another caveat is that the left and right definitions of cortical regions can only be considered 'homologous' on the basis of information that was used in constructing the Destrieux atlas (that included information on cytoarchitecture), but this does not necessarily imply strict homology in genetic/developmental terms.

We found a suggestive association of handedness with the bilateral surface area of the superior part of the precentral sulcus, a region overlapping primary motor cortex. However, this association did not survive correction for multiple testing. Left-handers showed reduced surface areas compared to right handers in our sample (Table 4), which is at least consistent with the findings reported by Amunts et al. (1996) and Foundas et al (1998). Males tend to have larger brains than females, which was also the case in our dataset, but this observed trend of decreased cerebral cortical surface area in left-handers was independent of this sex effect, and in the opposite direction to what might be predicted by it. Another suggestive association was found bilaterally with the inferior temporal gyrus. Again, left-handers in our sample showed reduced surface areas bilaterally (Table 4).

Our broader screen of non-candidate regional surface area and asymmetry differences between left- and right-handers did not identify significant novel associations. While relatively large, our sample size allowed us to detect standardized effect sizes regarded as medium (http://imaging.mrc-cbu.cam.ac.uk/statswiki/FAQ/effectSize), both before and after adjustment for multiple comparisons.

Although our dataset included a degree of heterogeneity in terms of scanning parameters used, there was no systematic difference in parameters applied for left- and right-handers, and we only analysed measurements that showed a high scan-rescan correlation in twice-scanned subjects, despite this heterogeneity. Future studies based on even larger datasets will likely be affected by the same issue of heterogeneity, since large datasets are typically achieved through data pooling from multiple sources. It is therefore encouraging that most of our measurements showed high scan-rescan correlations regardless of scanning heterogeneity.

An important issue in research on handedness is how exactly to define the trait. Many approaches have been taken to measure hand preference, ranging from motor performance measurements (e.g. relative hand skill, relative grip-strength; see Clerke and Clerke, 2001, for a brief overview); to self-report inventories assessing hand choice across various manual activities (Annett, 1967; Crovitz and Zener, 1962; Oldfield, 1971). Handedness inventories that account for preference across a range of tasks yield a rich assessment of (the degree of) handedness, and a detailed picture of its inter-subject variability. However, the resulting data are usually bimodal and are often subsequently dichotomized. For example, (Tan, 1993) showed that hand preference, when assessed by a very detailed questionnaire (Waterloo handedness questionnaire; Steenhuis and Bryden, 1989), shows a clear distinction between left-handed and right-handed populations. Further evidence for an intrinsic dichotomy in handedness was also provided by McManus (1991) who observed the same proportion of left-handers regardless of the

questionnaire used. Accordingly, simple self-assessments of overall handedness, such as that used in the present study (asking subjects only to categorize themselves as left- or right-handed) show close agreement with dichotomous scoring of handedness as derived from multi-item inventories, as well as robust test-retest repeatability (Bryden et al., 1991; Ransil and Schachter, 1994; Tan, 1993). We are therefore confident of the validity of the binary, self-reported assessment of handedness that was used in our study.

Identifying cortical regional correlates of handedness may prove particularly useful in providing endophenotypes for future genetic studies of this trait, as well as clarifying the relationships between this and other forms of cerebral lateralization (Ocklenburg et al., 2011; Willems et al; in press). We note that an association between handedness and cerebral cortical anatomy does not necessarily imply a simple causative relationship between the two. While it is conceivable that hand preference may arise due to hemispheric differences in cortical anatomy and function, it is equally conceivable that hand preference exerts developmental effects on cerebral cortical anatomy and function. As noted in the Introduction, there is strong evidence indicating that motor asymmetry of the arms and hands is initiated very early during human embryonic development, possibly even before the cerebral cortex exerts significant influence (Hepper, 2013). These early motor asymmetries, potentially under spino-muscular control, could therefore contribute to the determination of both handedness and regional cortical development.

Left-handed people show increased rates of reductions or reversals of lateralized brain functions, compared to right-handers (reviewed by Willems et al. in press). Functional imaging studies of left-handers allow the possibility to study not only basic lateralization of brain function (e.g. of face perception), but also embodied cognition, and the extent of co-lateralization of different cognitive functions (Willems et al; in press). Our survey of cerebral anatomical correlates of handedness may serve to inform these investigations, as it can suggest a prioritization of specific regions and cognitive processes to focus on with functional imaging techniques.

It is clear from our results, and those of previous studies, that any changes in brain structure associated with left-handedness are subtle. As noted earlier, it is likely that the genetic contributions to left-handedness are heterogeneous in nature, with multiple different genes being involved, and the same may be true of environmental influences (which also remain poorly understood). Etiologic heterogeneity suggests that there will be different forms of left-handedness which may manifest differently in terms of how striking any brain structural and functional correlates may be, and also differently in how, and to

what extent, other lateralized cognitive systems are re-organized. A promising approach for studying the relations between lateralization and cognition will therefore be to specifically recruit left-handers, in order to recruit sufficient numbers for characterising their heterogeneity, followed by assessments of brain structure and function in addition to neuropsychological testing, and genetic analysis (Marie et al., 2013; Mellet et al., 2013)

Acknowledgements

We wish to thank Han Brunner for his involvement in the creation and growth of the BIG (Brain Imaging Genetics) dataset and to all persons who kindly participated in the BIG research. This work makes use of the BIG (Brain Imaging Genetics) database, first established in Nijmegen, The Netherlands, in 2007. This resource is now part of Cognomics (www.cognomics.nl), a joint initiative by researchers of the Donders Centre for Cognitive Neuroimaging, the Human Genetics and Cognitive Neuroscience departments of the Radboud university medical centre and the Max Planck Institute for Psycholinguistics in Nijmegen. The Cognomics Initiative is supported by the participating departments and centres and by external grants, i.e. the Biobanking and Biomolecular Resources Research Infrastructure (Netherlands) (BBMRI-NL), the Hersenstichting Nederland, and the Netherlands Organisation for Scientific Research (NWO).

Appendix

Supplementary material

Supplementary Table S1: Complete list of repeated-measures ANOVA results.

		Repeated-measures ANOVA		
Region		P	F	partial η2
Inferior occipital gyrus (O3) and sulcus	Hand	0.19	1.70	<0.001
	Hand*hemisphere	0.40	0.71	<0.001
	Age	0.79	0.07	<0.001
	sex	0.50	0.46	<0.001
	TBS	0.00	627.50	0.2344
	Scanner	0.79	0.07	<0.001
Subcentral gyrus (central operculum) and sulci	Hand	0.80	0.06	<0.001
	Hand*hemisphere	0.51	0.43	<0.001
	Age	0.39	0.72	<0.001
	sex	0.05	3.77	0.0018
	TBS	0.00	1192.80	0.3682
	Scanner	0.27	1.21	<0.001
Anterior part of the cingulate gyrus and sulcus (ACC)	Hand	0.14	2.19	0.0011
	Hand*hemisphere	0.02	5.18	0.0025
	Age	0.53	0.40	<0.001
	sex	0.00	49.72	0.0236
	TBS	0.00	3313.52	0.6172
	Scanner	0.03	4.72	0.0023
Middle-anterior part of the cingulate gyrus and sulcus (aMCC)	Hand	0.67	0.18	<0.001
	Hand*hemisphere	0.00	8.99	0.0044
	Age	0.86	0.03	<0.001
	sex	0.00	61.10	0.0289
	TBS	0.00	2147.33	0.5115
	Scanner	0.00	27.41	0.0132
Middle-posterior part of the cingulate gyrus and sulcus (pMCC)	Hand	0.54	0.37	<0.001
	Hand*hemisphere	0.98	0.00	<0.001
	Age	0.04	4.38	0.0021
	sex	0.00	33.94	0.0163
	TBS	0.00	2055.81	0.5007
	Scanner	0.00	24.06	0.0116
Posterior-dorsal part of the cingulate gyrus (dPCC)	Hand	0.85	0.04	<0.001
	Hand*hemisphere	0.70	0.15	<0.001
	Age	0.83	0.04	<0.001
	sex	0.10	2.77	0.0014
	TBS	0.00	1439.66	0.4131
	Scanner	0.48	0.51	<0.001
Opercular part of the inferior frontal gyrus	Hand	0.73	0.12	<0.001

	Hand*hemisphere	0.63	0.23	<0.001
	Age	0.46	0.54	<0.001
	Sex	0.37	0.81	<0.001
	TBS	0.00	855.75	0.2953
	Scanner	0.15	2.03	0.0010
Triangular part of the inferior frontal gyrus	Hand	0.88	0.02	<0.001
	Hand*hemisphere	0.17	1.84	<0.001
	Age	0.00	12.72	0.0062
	Sex	0.04	4.21	0.0020
	TBS	0.00	345.28	0.1441
	Scanner	0.79	0.07	<0.001
Middle frontal gyrus (F2)	Hand	0.88	0.02	<0.001
	Hand*hemisphere	0.88	0.02	<0.001
	Age	0.01	6.30	0.0031
	Sex	0.00	35.94	0.0172
	TBS	0.00	2583.83	0.5571
	Scanner	0.84	0.04	<0.001
Superior frontal gyrus (F1)	Hand	0.66	0.19	<0.001
	Hand*hemisphere	0.31	1.03	<0.001
	Age	0.00	10.67	0.0052
	Sex	0.05	3.73	0.0018
	TBS	0.00	3304.86	0.6166
	Scanner	0.53	0.39	<0.001
Middle occipital gyrus (O2, lateral occipital gyrus)	Hand	0.75	0.10	<0.001
	Hand*hemisphere	0.35	0.86	<0.001
	Age	0.98	0.00	<0.001
	Sex	0.26	1.25	<0.001
	TBS	0.00	1471.02	0.4177
	Scanner	0.00	12.96	0.0063
Superior occipital gyrus (O1)	Hand	0.04	4.24	0.0021
	Hand*hemisphere	0.25	1.30	<0.001
	Age	0.01	6.07	0.0030
	Sex	0.00	14.51	0.0070
	TBS	0.00	761.37	0.2713
	Scanner	0.36	0.84	<0.001
Lateral occipito-temporal gyrus (fusiform gyrus, O4-T4)	Hand	0.17	1.87	<0.001
	Hand*hemisphere	0.53	0.40	<0.001
	Age	0.04	4.06	0.0020
	Sex	0.03	4.69	0.0023
	TBS	0.00	701.18	0.2545
	Scanner	0.20	1.63	<0.001
Lingual gyrus, ligual part of the medial occipito-	Hand	0.26	1.27	<0.001

temporal gyrus, (O5)	Hand*hemisphere	0.10	2.67	0.0013
	Age	0.18	1.77	<0.001
	sex	0.43	0.63	<0.001
	TBS	0.00	944.86	0.3156
	Scanner	0.00	19.91	0.0096
Angular gyrus	Hand	0.94	0.01	<0.001
	Hand*hemisphere	0.77	0.09	<0.001
	Age	0.13	2.34	0.0011
	sex	0.04	4.23	0.0021
	TBS	0.00	857.14	0.2947
	Scanner	0.77	0.08	<0.001
Supramarginal gyrus	Hand	0.20	1.66	<0.001
	Hand*hemisphere	0.78	0.08	<0.001
	Age	0.00	9.68	0.0047
	sex	0.36	0.84	<0.001
	TBS	0.00	1466.62	0.4171
	Scanner	0.55	0.36	<0.001
Superior parietal lobule (lateral part of P1)	Hand	0.65	0.21	<0.001
	Hand*hemisphere	0.81	0.06	<0.001
	Age	0.36	0.82	<0.001
	sex	0.04	4.15	0.0020
	TBS	0.00	1090.63	0.3476
	Scanner	0.23	1.42	<0.001
Precuneus (medial part of P1)	Hand	0.17	1.88	<0.001
	Hand*hemisphere	0.78	0.08	<0.001
	Age	0.00	11.25	0.0055
	sex	0.11	2.63	0.0013
	TBS	0.00	1033.27	0.3358
	Scanner	0.21	1.55	<0.001
Anterior transverse collateral sulcus	Hand	0.86	0.03	<0.001
	Hand*hemisphere	0.06	3.44	0.0017
	Age	0.32	1.00	<0.001
	sex	0.98	0.00	<0.001
	TBS	0.00	722.57	0.2603
	Scanner	0.98	0.00	<0.001
Lateral aspect of the superior temporal gyrus	Hand	0.57	0.33	<0.001
	Hand*hemisphere	0.36	0.85	<0.001
	Age	0.00	9.06	0.0044
	sex	0.17	1.90	<0.001
	TBS	0.00	1634.83	0.4438
	Scanner	0.00	9.82	0.0048
Planum temporale or temporal plane of the	Hand	0.42	0.64	<0.001

superior temporal gyrus	Hand*hemisphere	0.94	0.01	<0.001
	Age	0.63	0.23	<0.001
	Sex	0.00	14.39	0.0070
	TBS	0.00	753.83	0.2695
	Scanner	0.91	0.01	<0.001
Inferior temporal gyrus (T3)	Hand	0.04	4.36	0.0021
	Hand*hemisphere	0.58	0.30	<0.001
	Age	0.50	0.46	<0.001
	Sex	0.14	2.15	0.0010
	TBS	0.00	1366.81	0.3994
	Scanner	0.39	0.75	<0.001
Middle temporal gyrus (T2)	Hand	0.61	0.27	<0.001
	Hand*hemisphere	0.91	0.01	<0.001
	Age	0.01	6.24	0.0030
	Sex	0.97	0.00	<0.001
	TBS	0.00	2080.20	0.5034
	Scanner	0.55	0.35	<0.001
Horizontal ramus of the anterior segment of the lateral sulcus (or fissure)	Hand	0.22	1.49	<0.001
	Hand*hemisphere	0.38	0.77	<0.001
	Age	0.21	1.58	<0.001
	Sex	0.00	8.25	0.0040
	TBS	0.00	247.20	0.1079
	Scanner	0.59	0.29	<0.001
Vertical ramus of the anterior segment of the lateral sulcus (or fissure)	Hand	0.77	0.08	<0.001
	Hand*hemisphere	0.76	0.09	<0.001
	Age	0.11	2.55	0.0012
	Sex	0.60	0.28	<0.001
	TBS	0.00	160.09	0.0725
	Scanner	0.98	0.00	<0.001
Posterior ramus (or segment) of the lateral sulcus (or fissure)	Hand	0.80	0.06	<0.001
	Hand*hemisphere	0.62	0.24	<0.001
	Age	0.45	0.57	<0.001
	Sex	0.00	12.12	0.0059
	TBS	0.00	605.27	0.2285
	Scanner	0.51	0.44	<0.001
Calcarine sulcus	Hand	0.16	1.99	<0.001
	Hand*hemisphere	0.12	2.36	0.0011
	Age	0.01	7.31	0.0035
	Sex	0.00	8.37	0.0041
	TBS	0.00	814.71	0.2839
	Scanner	0.00	8.45	0.0041
Anterior segment of the circular sulcus of the	Hand	0.61	0.26	<0.001

insula	Hand*hemisphere	0.91	0.01	<0.001
	Age	0.20	1.65	<0.001
	sex	0.01	6.31	0.0031
	TBS	0.00	522.18	0.2031
	Scanner	0.62	0.24	<0.001
Superior segment of the circular sulcus of the insula	Hand	0.38	0.79	<0.001
	Hand*hemisphere	0.66	0.19	<0.001
	Age	0.21	1.55	<0.001
	sex	0.00	9.02	0.0044
	TBS	0.00	1215.05	0.3719
	Scanner	0.00	9.06	0.0044
Anterior transverse collateral sulcus	Hand	0.85	0.04	<0.001
	Hand*hemisphere	0.56	0.35	<0.001
	Age	0.00	8.43	0.0041
	sex	0.00	12.39	0.0060
	TBS	0.00	448.10	0.1792
	Scanner	0.19	1.70	<0.001
Posterior transverse collateral sulcus	Hand	0.65	0.21	<0.001
	Hand*hemisphere	0.05	3.92	0.0019
	Age	0.13	2.30	0.0011
	sex	0.04	4.23	0.0021
	TBS	0.00	181.55	0.0812
	Scanner	0.05	3.95	0.0019
Inferior frontal sulcus	Hand	0.62	0.25	<0.001
	Hand*hemisphere	0.57	0.31	<0.001
	Age	0.04	4.15	0.0020
	Sex	0.00	29.75	0.0143
	TBS	0.00	1546.64	0.4299
	Scanner	0.55	0.36	<0.001
Middle frontal sulcus	Hand	0.78	0.08	<0.001
	Hand*hemisphere	0.61	0.26	<0.001
	Age	0.67	0.18	<0.001
	Sex	0.30	1.07	<0.001
	TBS	0.00	896.02	0.3037
	Scanner	0.24	1.38	<0.001
Superior frontal sulcus	Hand	0.04	4.31	0.0021
	Hand*hemisphere	0.22	1.50	<0.001
	Age	0.00	15.57	0.0075
	Sex	0.00	12.82	0.0062
	TBS	0.00	1491.50	0.4208
	Scanner	0.64	0.22	<0.001
Sulcus intermedius primus (of Jensen)	Hand	0.71	0.14	<0.001

	Hand*hemisphere	0.04	4.37	0.0021
	Age	0.64	0.22	<0.001
	Sex	0.00	12.28	0.0060
	TBS	0.00	86.72	0.0407
	Scanner	0.58	0.31	<0.001
Intraparietal sulcus (interparietal sulcus) and transverse parietal sulci	Hand	0.92	0.01	<0.001
	Hand*hemisphere	0.52	0.40	<0.001
	Age	0.32	1.00	<0.001
	Sex	0.77	0.09	<0.001
	TBS	0.00	1088.35	0.3468
	Scanner	0.64	0.22	<0.001
Middle occipital sulcus and lunatus sulcus	Hand	0.71	0.14	<0.001
	Hand*hemisphere	0.75	0.11	<0.001
	Age	0.30	1.07	<0.001
	Sex	0.04	4.27	0.0021
	TBS	0.00	474.74	0.1877
	Scanner	0.00	15.57	0.0075
Superior occipital sulcus and transverse occipital sulcus	Hand	0.27	1.21	<0.001
	Hand*hemisphere	0.81	0.06	<0.001
	Age	0.76	0.09	<0.001
	Sex	0.60	0.28	<0.001
	TBS	0.00	701.28	0.2544
	Scanner	0.01	7.05	0.0034
Anterior occipital sulcus and preoccipital notch (temporo-occipital incisure)	Hand	0.78	0.08	<0.001
	Hand*hemisphere	0.68	0.17	<0.001
	Age	0.01	6.69	0.0033
	Sex	0.85	0.03	<0.001
	TBS	0.00	246.08	0.1072
	Scanner	0.39	0.75	<0.001
Lateral occipito-temporal sulcus	Hand	0.35	0.86	<0.001
	Hand*hemisphere	0.91	0.01	<0.001
	Age	0.00	13.32	0.0064
	Sex	0.00	17.07	0.0082
	TBS	0.00	573.48	0.2182
	Scanner	0.55	0.35	<0.001
Medial occipito-temporal sulcus (collateral sulcus) and lingual sulcus	Hand	0.96	0.00	<0.001
	Hand*hemisphere	0.15	2.06	0.0010
	Age	0.02	5.28	0.0026
	Sex	0.00	24.28	0.0117
	TBS	0.00	641.15	0.2382
	Scanner	0.00	15.86	0.0077
Lateral orbital sulcus	Hand	0.79	0.07	<0.001

	Hand*hemisphere	0.73	0.12	<0.001
	Age	0.13	2.30	0.0011
	Sex	0.09	2.82	0.0014
	TBS	0.00	456.96	0.1823
	Scanner	0.11	2.52	0.0012
Parieto-occipital sulcus (or fissure)	Hand	0.03	4.80	0.0023
	Hand*hemisphere	0.25	1.32	<0.001
	Age	0.48	0.49	<0.001
	Sex	0.33	0.95	<0.001
	TBS	0.00	868.76	0.2975
	Scanner	0.00	8.90	0.0043
Pericallosal sulcus (S of corpus callosum)	Hand	0.57	0.32	<0.001
	Hand*hemisphere	0.84	0.04	<0.001
	Age	0.00	18.26	0.0088
	Sex	0.81	0.06	<0.001
	TBS	0.00	1124.37	0.3544
	Scanner	0.00	12.17	0.0059
Postcentral sulcus	Hand	0.45	0.56	<0.001
	Hand*hemisphere	0.77	0.08	<0.001
	Age	0.00	15.44	0.0075
	Sex	0.25	1.34	<0.001
	TBS	0.00	1091.54	0.3476
	Scanner	0.56	0.33	<0.001
Inferior part of the precentral sulcus	Hand	0.76	0.09	<0.001
	Hand*hemisphere	0.85	0.04	<0.001
	Age	0.42	0.65	<0.001
	Sex	0.00	12.26	0.0059
	TBS	0.00	790.43	0.2783
	Scanner	0.18	1.78	<0.001
Superior part of the precentral sulcus	Hand	0.04	4.07	0.0020
	Hand*hemisphere	0.60	0.28	<0.001
	Age	0.08	2.99	0.0015
	Sex	0.00	21.10	0.0102
	TBS	0.00	396.44	0.1625
	Scanner	0.37	0.82	<0.001
Subparietal sulcus	Hand	0.07	3.40	0.0017
	Hand*hemisphere	0.21	1.59	<0.001
	Age	0.00	8.62	0.0042
	sex	0.67	0.18	<0.001
	TBS	0.00	583.58	0.2221
	Scanner	0.00	9.44	0.0046
Inferior temporal sulcus	Hand	0.52	0.42	<0.001

	Hand*hemisphere	0.40	0.71	<0.001
	Age	0.03	4.90	0.0024
	sex	0.03	4.71	0.0023
	TBS	0.00	914.62	0.3080
	Scanner	0.00	16.09	0.0078
Superior temporal sulcus (parallel sulcus)	Hand	0.45	0.56	<0.001
	Hand*hemisphere	0.90	0.02	<0.001
	Age	0.04	4.42	0.0022
	sex	0.09	2.94	0.0014
	TBS	0.00	1737.24	0.4588
	Scanner	0.93	0.01	<0.001
Transverse temporal sulcus	Hand	0.84	0.04	<0.001
	Hand*hemisphere	0.45	0.57	<0.001
	Age	0.82	0.05	<0.001
	sex	0.42	0.64	<0.001
	TBS	0.00	439.54	0.1766
	Scanner	0.44	0.60	<0.001

Supplementary Table S2: Means and SDs for all cortical regions, by hemisphere and handedness group.

	Left hemisphere				Right hemisphere			
	Righthanders		Lefthanders		Righthanders		Lefthanders	
	Mean	Standard Deviation	Mean	Standard Deviation	Mean	Standard Deviation	Mean	Standard Deviation
Inferior occipital gyrus (O3) and sulcus	1137.2	202.79	1162.34	206.42	921.82	178.69	924.04	160.17
Subcentral gyrus (central operculum) and sulci	1039.72	169.11	1027.19	151.92	946.8	161.05	944.39	156.9
Anterior part of the cingulate gyrus and sulcus (ACC)	1707.41	264.52	1648	223.25	2016.75	271.05	1998.77	251.29
Middle-anterior part of the cingulate gyrus and sulcus (aMCC)	1014.45	170.26	974.63	144.66	1114.09	169.76	1122.02	162.75
Middle-posterior part of the cingulate gyrus and sulcus (pMCC)	945.9	126.09	934.8	128.56	1043.41	155.18	1026.1	135.02
Posterior-dorsal part of the cingulate gyrus (dPCC)	397.35	87.3	393.2	93.02	375.4	81.73	374.67	80.68
Opercular part of the inferior frontal gyrus	1014.87	162.05	999.85	142.84	900.96	154.42	896.73	135.3
Triangular part of the inferior frontal gyrus	800.31	150.68	809.84	152.82	785.73	170.98	773.11	175.4
Middle frontal gyrus (F2)	3211.03	507.53	3183.17	467.43	2927.62	472.32	2897.2	482.66
Superior frontal gyrus (F1)	5013.14	603.73	4986.29	555.95	4749.46	567.49	4687.52	537.41
Middle occipital gyrus (O2, lateral occipital gyrus)	1480.77	246.44	1463.92	235.04	1587.71	267.51	1598.36	272.15

	Left hemisphere				Right hemisphere			
	Righthanders		Lefthanders		Righthanders		Lefthanders	
	Mean	SD	Mean	SD	Mean	SD	Mean	SD
Superior occipital gyrus (O1)	1101.09	167.73	1131.45	166.24	1239.58	186.67	1251.14	177.79
Lateral occipito-temporal gyrus (fusiform gyrus, O4-T4)	1348.41	241.17	1372.33	248.25	1311.04	248.93	1320.72	261.33
Lingual gyrus, ligual part of the medial occipito-temporal gyrus, (O5)	2103	328.95	2142.25	356.76	2008.1	286.43	1996.52	325.12
Angular gyrus	1714.58	278.22	1701.25	282.77	2074.69	344.06	2067.43	340.04
Supramarginal gyrus	2103.44	340.95	2127.71	352.52	1924.38	307.98	1930.42	272.81
lh_G_parietal_sup_area	2091.5	328.85	2088.86	343.75	1712.15	279.01	1707.27	294.14
lh_G_precuneus_area	1863.42	287.73	1828.92	287.89	1849.88	278.47	1815.72	248.13
Superior parietal lobule (lateral part of P1)	358.77	78.14	349.34	70.48	278.14	58.92	281.85	59.26
Lateral aspect of the superior temporal gyrus	1456.86	186.05	1466.91	175.07	1274.63	168.94	1267.28	162.88
Planum temporale or temporal plane of the superior temporal gyrus	683.35	154.87	691.1	157.56	555.83	109.3	559.35	106.24
Inferior temporal gyrus (T3)	1911.66	311.34	1853.15	328.58	1787.62	281.76	1744.8	319.6
Middle temporal gyrus (T2)	2029.02	300.93	2024.9	310.95	2128.28	291.58	2133.33	324.04
Horizontal ramus of the anterior segment of the lateral sulcus (or fissure)	234.27	43.37	232.04	37.38	288.28	55.88	281.03	56.46
Vertical ramus of the anterior segment of the lateral sulcus (or fissure)	208.72	60.82	205.89	61.66	154.22	46.92	153.2	48.08

	Left hemisphere				Right hemisphere			
	Righthanders		Lefthanders		Righthanders		Lefthanders	
	Mean	SD	Mean	SD	Mean	SD	Mean	SD
Posterior ramus (or segment) of the lateral sulcus (or fissure)	839.61	136.54	838.57	134.45	995.48	110.39	998.1	104.69
Calcarine sulcus	1763.54	308.79	1797.71	324.43	1691.94	296.65	1696.94	303.44
Anterior segment of the circular sulcus of the insula	372.02	63.86	373.01	64.04	425.19	79.96	427.32	72.91
Superior segment of the circular sulcus of the insula	1259.87	134.4	1250.75	133.62	986.18	121.1	974.08	121.06
Anterior transverse collateral sulcus	713.82	182.13	698.27	179.42	737.34	165.56	729.97	168.17
Posterior transverse collateral sulcus	294.23	66.4	300.74	70.88	386.9	98.8	373.01	98.78
Inferior frontal sulcus	1679.15	284.16	1663.48	256.61	1543.08	256.64	1509.46	263.13
Middle frontal sulcus	1136.41	230.89	1117.36	232.76	1576.87	301.52	1566.79	276.07
Superior frontal sulcus	2077.1	302.72	2004.92	286.84	1906.66	296.12	1867.58	271.67
Sulcus intermedius primus (of Jensen)	257.6	127.33	280.16	145.57	363.98	151.67	350.14	150.34
Intraparietal sulcus (interparietal sulcus) and transverse parietal sulci	2201.93	314.74	2195.7	357.47	2289.58	333.47	2275.45	337.06
Middle occipital sulcus and lunatus sulcus	803.55	192.92	797.9	197.2	745.37	195.68	732.94	203.21
Superior occipital sulcus and transverse occipital sulcus	907.87	168.6	913.75	159.34	1077.04	208.71	1089.03	199.94
Anterior occipital sulcus and preoccipital notch (temporo-occipital incisure)	575.01	152.98	571.27	154.42	557.58	145.81	560.32	155.92

	Left hemisphere				Right hemisphere			
	Righthanders		Lefthanders		Righthanders		lefthanders	
	Mean	SD	Mean	SD	Mean	SD	Mean	SD
Lateral occipito-temporal sulcus	682.69	156.2	668.5	152.16	713.25	158.52	702.25	176.95
Medial occipito-temporal sulcus (collateral sulcus) and lingual sulcus	1483.23	243.14	1497.21	250.24	1380.02	210.86	1369.28	218.22
Lateral orbital sulcus	288.07	64.9	287.16	70	324.7	81.61	325.39	77.07
Parieto-occipital sulcus (or fissure)	1428.97	239.29	1445.91	225.88	1544.17	255.76	1584.46	265.83
Pericallosal sulcus (S of corpus callosum)	782.94	147.05	773.28	139.56	1046.12	187.98	1033.8	173.13
Postcentral sulcus	2111.17	343.64	2113.72	367.47	1786.79	330.98	1795.69	368.98
Inferior part of the precentral sulcus	1079.92	193.18	1074.39	212.45	1181.15	203.31	1178.31	182.64
Superior part of the precentral sulcus	952.67	200.9	914.87	207.54	990.44	214.78	965.08	201.89
Subparietal sulcus	790.95	175.17	768.86	168.68	881.42	208.55	838.87	206.23
Inferior temporal sulcus	987.2	232.3	976.31	243.09	921.54	211.05	893.53	214.27
Superior temporal sulcus (parallel sulcus)	3955.2	500.88	3922.28	501.44	4353.06	559.69	4311.56	639.29
Transverse temporal sulcus	265.52	52.76	261.74	42.2	213.6	48.17	214.58	43.68

Chapter 3

Asymmetry within and around the human planum temporale is sexually dimorphic and influenced by genes involved in steroid hormone receptor activity

Adapted from:

Guadalupe T, Zwiers MP, Wittfeld K, Teumer A, Vasquez AA, Hoogman M, Hagoort P, Fernandez G, Buitelaar J, van Bokhoven H, Hegenscheid K, Voelzke H, Franke B, Fisher SE, Grabe HJ and Francks C. (2015): Asymmetry within and around the human planum temporale is sexually dimorphic and influenced by genes involved in steroid hormone receptor activity. Cortex 62:41-55.

Abstract

The genetic determinants of cerebral asymmetries are unknown. Sex differences in asymmetry of the planum temporale, that overlaps Wernicke's classical language area, have been inconsistently reported. Meta-analysis of previous studies has suggested that publication bias established this sex difference in the literature. We screened with voxel-based-morphometry over the cerebral cortex for sexual dimorphisms of asymmetry in 2337 healthy subjects, and found the planum temporale to show the strongest sex-linked asymmetry of all regions, which was supported by two further datasets, and also by analysis with the Freesurfer package that performs automated parcellation of cerebral cortical regions. We performed a genome-wide association scan meta-analysis of planum temporale asymmetry in a pooled sample of 3095 subjects, followed by a candidate-driven approach which measured a significant enrichment of association in genes of the ´steroid hormone receptor activity´ pathway. We also found suggestive association on chromosome 2q32.2 (rs785248, $p=2.1*10^{-7}$). Variants in the genes and pathways identified may affect the role of the planum temporale in language cognition.

Introduction

The planum temporale (PT), a triangular shaped area on the superior surface of the posterior temporal lobe, has long been recognized as one of the most anatomically asymmetrical regions of the human cerebral cortex (Geschwind and Levitsky, 1968). In most people the PT on the left side is larger than the right (Galaburda, 1993; Steinmetz, 1996), although varying definitions of the precise structure have resulted in different estimates of its asymmetry (Galaburda, 1993; Shapleske et al., 1999; Shapleske et al., 1999b). The left PT overlaps with Wernicke's classically defined language region (Geschwind and Levitsky, 1968), which is part of the broadly left-lateralised speech and language network present in the majority of people. At least some of the PT is regarded as secondary auditory cortex in terms of cyto-architecture (Shapleske et al., 1999). The PT has been characterized as a computational hub for processing spectrotemporal variation in auditory perception (Griffiths and Warren, 2002), as well as having a role in mapping acoustic speech signals to frontal lobe articulatory networks (Hickok and Poeppel, 2007), and in auditory attention (Hirnstein et al., 2013).

Given these important roles of the PT in speech and language, and its asymmetrical nature in the typically developed brain, there has been much interest in whether individual differences in PT asymmetry are associated with traits that involve changes in language cognition, including dyslexia, reduced verbal ability, and schizophrenia (Eckert et al., 2008; Frank and Pavlakis, 2001; Hasan et al.; Kawasaki et al., 2008; McCarley et al., 2002; Oertel et al.; Shapleske et al., 1999; Sommer et al., 2001). These studies have shown that alterations in PT asymmetry may be relevant to some etiological subtypes of these complex traits, although are not necessarily a universal feature of them (Bishop, 2013). It also remains unclear to what extent associations between PT asymmetry and language-related cognitive disorders may arise from shared genetic, versus environmental, influences.

In fact the molecular and developmental basis of human brain asymmetry is almost completely unknown, as are the causes of variation in cerebral asymmetries within the population. Although present to a degree in other primates (Gannon et al., 1998; Lyn et al., 2011), a population-level bias towards leftward PT asymmetry is pronounced in the human brain and is already visible in third trimester fetuses (Bossy et al., 1976). Various other studies have shown fetal and infant asymmetries in the perisylvian region, sylvian fissure, and superior temporal sulcus (Dubois et al., 2008; Dubois et al., 2010; Habas et al., 2012; Kasprian et al., 2011; Li et al., 2013). These early developmental asymmetries clearly indicate a role for genetic mechanisms, but very few individual genes have so far been implicated in any aspect of lateralization of the human brain (Francks et al., 2007; Ocklenburg et al., 2013; Scerri et

al., 2011; Sun et al., 2005; Sun and Walsh, 2006). Language lateralization appears to develop largely independently of early embryonic mechanisms that pattern left-right asymmetry of the viscera (heart, lungs etc.; Tanaka et al., 1999). Genetic studies of PT asymmetry therefore offer a potential route to discovering novel, fundamental mechanisms that underlie lateralization of the human brain, which provides a basic organizing principle for much of human cognition (Gunturkun, 2003).

Males have sometimes been reported to show a subtle mean increase in leftward lateralization of the PT relative to females (de Courten-Myers, 1999; Good et al., 2001; Shapleske et al., 1999). Consistent with this, fetal testosterone levels have been linked to gray matter volumes within some putatively, sexually dimorphic regions of the human brain, including the PT (Lombardo et al., 2012). Prenatal testosterone levels have also been implicated in language delay in males (Whitehouse et al., 2012). However, some studies have not found an effect of sex on PT asymmetry (Watkins et al., 2001), and a meta-analysis of thirteen earlier studies did not find significant evidence for sexual dimorphism of PT asymmetry (Sommer et al., 2008). Publication bias was suggested to have established a sex difference of PT asymmetry in the literature (Sommer et al., 2008; Watkins et al., 2001). Furthermore, a recent review concluded that overall results from studies on regional grey matter distribution, using voxel-based morphometry (VBM), indicate no consistent differences between males and females in language-related cortical regions (Wallentin, 2009).

In this study we used region-of-interest probability masks derived from the Harvard-Oxford atlas (distributed with the FSL software package; http://fsl.fmrib.ox.ac.uk/fsl/), to perform a large-scale analysis of sex differences for human cerebral asymmetries, mapped over the entire cerebral cortex, in 2337 healthy human subjects. We refer to this method hereafter as HO. We unambiguously confirmed asymmetry within and around the PT as a subtly, sexually dimorphic trait, and this pattern replicated in two additional population samples. We then performed genome-wide association scanning (GWAS) for PT regional asymmetry in three datasets derived from a total of 3095 subjects from the Netherlands and Germany, and used the results to test for an enrichment of association in genes involved in steroid hormone biology, motivated by the sexual dimorphism of the trait. We also explored the brain-wide effects on grey matter volume of an individual polymorphism that was suggestively associated with PT asymmetry (rs785248, p=2.1*10-7, see below), since we do not necessarily expect genetic effects to localize solely to cortical regions as defined in specific brain atlases.

Methods

Study datasets

The Brain Imaging Genetics (BIG) study was initiated in 2007 and comprises healthy volunteer subjects, including many university students, who participate in studies at the Donders Centre for Cognitive Neuroimaging, Nijmegen, The Netherlands (Franke et al., 2010). At the time of this study the BIG subject-pool consisted of 2337 self-reported healthy individuals (1248 females) who had undergone anatomical (T1-weighted) MRI scans, usually as part of their involvement in diverse smaller-scale studies at the Donders Centre, and who had given their consent to participate in BIG. Their mean age was 27.2 years (SD = 12.6; range 18-83). Furthermore, a subset of 242 subjects had undergone a brain MRI scan at least twice. Fifty percent of the rescans took place within 181 days of the first, with the mean elapsed time being 320 days (SD = 360). At the time of the first scan, their mean age was 24.2 (SD = 7.7; range = 18-72).

For the genetic analysis, genome-wide SNP genotype data were available from 1276 of BIG subjects (see below for genotyping details). Their mean age was 22.9 (SD = 3.8; range = 18-35) years, and 748 of these subjects were female.

The Study of Health in Pomerania (SHIP) is an on-going, longitudinal, population-based study in north-east Germany, aimed at describing the prevalence of common diseases, and their risk factors. Subjects from the two independent surveys SHIP-2 (the second follow-up of the baseline study SHIP-0) and SHIP-TREND (baseline of the second survey) had undergone a whole-body MRI scan, as well as genotyping for common polymorphisms. For more detailed information about the dataset, see (Volzke et al., 2011). For our analysis we were able to include 935 subjects from SHIP-2 (497 females) with a mean age of 56.7 years (SD = 12.8; range = 31-89 years) and 888 subjects from SHIP-TREND (495 females) with a mean age of 50.3 years (SD =13.6; range = 21-81).

Image acquisition

MRI data in BIG were acquired with either a 1.5 Tesla Siemens Sonata or Avanto scanner or a 3 Tesla Siemens Trio or TimTrio scanner (Siemens Medical Systems, Erlangen, Germany). Given that images were acquired during several smaller scale studies, the parameters used were slight variations of a standard T1-weighted three-dimensional magnetization prepared rapid gradient echo sequence (MPRAGE; 1.0×1.0×1.0 mm voxel size). See table 1 for an overview of scanning parameters used in BIG. For the SHIP datasets, all MRI images were obtained on a 1.5 Tesla scanner (Magnetom Avanto; Siemens

Medical Systems, Erlangen, Germany). using a standard T1-weighted MPRAGE sequence (TE 1900.0, TR 3.4, Flip angle 15°, 1.0×1.0×1.0 mm voxel size; Hegenscheid et al., 2009).

Table 1. Overview of the different scanning parameters used in the BIG sample

Study sample	TR/T1/TE/saggital-slices parameters	Scanners	Field strength
BIG	2300/1100/3.03/192; 2730/1000/2.95/176; 2250/850/2.95/176; 2250/850/3.93/176; 2250/850/3.68/176; 2300/1100/3.03/192; 2300/1100/2.92/192; 2300/1100/2.96/192; 2300/1100/2.99/192; 1940/1100/3.93/176 & 1960/1100/4.58/176	Sonata/Avanto, Trio/TrioTim	1.5 Tesla (N=634) 3 Tesla (N=642)

Image processing

Pre-processing of MR images in BIG, SHIP-2 and SHIP-TREND was done in SPM8 (http://www.fil.ion.ucl.ac.uk/spm/) using 'Segment' with the default settings to obtain the bias field corrected, normalised and warped tissue class images for the grey matter.

Volumetric measures were then extracted by the application of the probabilistic Harvard-Oxford (HO) Cortical Structural Atlas that defines 48 cortical regions on a normalized brain (as distributed with the FSL software package http://www.cma.mgh.harvard.edu/fsl_atlas.html). The cortical parcellations for this atlas were originally described in (Goldstein et al., 1999; Goldstein et al., 2007). We created two subsets by splitting the original atlas at the centre of the left-right axis, to produce 48 regions for each cerebral hemisphere. No other manipulation of the atlas or of its probabilistic regions was applied. For each region, we then performed a voxel-wise sum of grey matter volumes, weighted by the probability of each voxel belonging to that specific cortical region.

For each cerebral cortical region, volumetric differences between the left and right were expressed as an Asymmetry Index (AI), calculated by the formula (L-R)/(L+R), where L and R were the left and right regional grey matter volumes respectively. The values of the AI could range theoretically from -1 to +1, with negative values denoting a rightward asymmetry, positive values a leftward asymmetry and zero in the case of perfect volume symmetry. Note that regional asymmetries present in the HO atlas would necessarily influence the mean AIs that we measured in our datasets (see below). However, our focus was on individual and group differences in AIs rather than the grand mean, as the left and right perisylvian regions were already known to differ systematically in their anatomy on average. For measuring individual and group differences we needed our left and right atlas definitions to be as closely

anatomically matched as possible to our subject data, and therefore we did not create a left-right averaged template to define the PT, as this fails to adequately capture the systematic anatomical differences between the two sides. In addition we intended to follow up significant genetic associations with individual differences in PT asymmetry, as defined by the asymmetrical HO atlas, by testing the effects of the associated polymorphisms in a brain-wide grey matter voxel-based-morphometry (VBM) analysis without use of atlas-based regional definitions, since we do not necessarily expect genetic effects to be limited to one anatomical region as defined in a particular atlas. Thus the PT AI derived from the HO atlas is a useful initial probe for genetic analysis, but individual genetic effects on this AI then require further analysis to better understand their localization. We return to this issue in more detail in the Discussion.

Exclusion of outlier values (more extreme than 3.5 SD from the mean), correction for covariates (sex, age, total brain volume and scanner field strength), and residual extraction, was done using Microsoft Excel (2010), by Visual Basic for Applications (VBA) scripting. We did not include handedness as a covariate because handedness itself is a partly heritable trait (Medland et al., 2009), and it was therefore important to retain any shared variance of handedness with PT asymmetry, for the purposes of genetic analysis of PT asymmetry.

Voxel-based morphometry analysis (VBM; Ashburner and Friston, 2000) was performed within the VBM8 pipeline and toolbox (http://dbm.neuro.uni-jena.de/vbm/), implemented in SPM8 (http://www.fil.ion.ucl.ac.uk/spm/). All sites followed VBM8's default procedures and the segmented images were normalized to standard space (as defined by the Montreal Neurological Institute; MNI) by high-dimensional DARTEL warping (Ashburner, 2007) and bias field corrected. The resulting images were modulated by the non-linear part of their DARTEL warp field and smoothed with an 8mm FWHM Gaussian smoothing kernel, providing for an analysis of relative differences in regional GM volume, corrected for individual brain size.

Parcellation of cortical regions

For a methodological validation we also performed automated parcellation of cerebral cortical regions using the FreeSurfer package (Fischl et al., 2002) and according to the Destrieux atlas (Destrieux et al., 2010), within the '-recon-all' processing pipeline, and using default parameters. This yielded volumetric measures for 74 cortical regions in each hemisphere, for which we also derived AIs and adjusted for covariates as above.

Regional asymmetry mapping by sex

Within the BIG population we used independent sample t-tests to assess sex differences in regional AIs (IBM SPSS v. 20). Significance levels were conservatively Bonferroni-corrected for all AIs. We did not test for sex differences on bilateral volumes of cerebral cortical regions, as it is well known that males have larger brains on average than females, and this was broadly reflected over the cerebral cortex in our datasets (data not shown).

Total brain volume and asymmetry in the PT region

This analysis was performed in the BIG dataset. We estimated total brain volume (TBV) as the voxel-wise sum of the grey matter and white matter probabilities, produced by the segmentation done by SPM8. We then assessed the correlations of sex and TBV with the HO PT AI using Pearson correlation analysis (IBM SPSS v. 20). We also assessed the correlation of TBV with the HO PT AI after removing the effect of sex as a linear covariate, and the correlation of sex with the HO PT AI after removing the linear effect of TBV.

As a second approach, we re-assessed the sexual dimorphism of the PT AI on modulated GM images from the VBM8 pipeline. These are images that are corrected for overall differences in brain size.

Genotyping

Genotyping of BIG was performed using the Affymetrix Genome-Wide Human SNP Array 6.0 (Affymetrix Inc., Santa Clara, CA, USA). Genotype calls were made using the Birdseed algorithm (Rabbee and Speed 2006). Samples were excluded that had call rates lower than 90% and that showed deviant values of genome-wide heterozygosity (Purcell, Neale et al. 2007), as this can indicate the presence of genotyping artifacts. Single nucleotide polymorphisms (SNPs) with a minor allele frequency below 1% or that failed the Hardy-Weinberg equilibrium test at a threshold of $p \leq 10\text{-}6$ were also excluded (Purcell, Neale et al. 2007). The resulting markers were then adjusted to the forward strand, as to avoid any ambiguity problems in subsequent steps. A 2-step imputation protocol was followed, in order to use the genotyped set of markers to infer the genotypes at millions of additional positions in the human genome. We used the software MACH for haplotype phasing and minimac for the final imputation (Li, Willer et al. 2010; Howie, Fuchsberger et al. 2012), with the 1000 Genomes Phase 1.v3 EUR reference panel (The 1000 Genomes Consortium, 2010). All monomorphic markers were removed from the reference dataset. Individual genotype calls that had an imputation certainty lower than 90% were removed, as were markers with an overall quality score below 0.3 R2. As a final quality filter, only

markers with no more than 5% missing data were selected. At the end of these procedures, genotypes were available for 1276 subjects from BIG, for 6,131,824 SNPs spanning the genome.

Genotyping of the SHIP-2 and SHIP-TREND samples was done on two different platforms, the Affymetrix Genome-Wide Human SNP Array 6.0 and Illumina Human Omni 2.5, respectively. In SHIP-2 the genotype calling was performed with the Birdseed algorithm and samples were excluded with call rates lower than 86%. For SHIP-TREND, calls were done on the GenomeStudio Genotyping Module v1.0, and excluded samples had a call rate lower than 94%. For both samples, markers that failed Hardy-Weinberg equilibrium ($p < 10\text{-}4$) were removed, as well as markers that had more than 20% and 10% missing data in SHIP-2 and SHIP-TREND, respectively. Imputation of non-observed genotypes was performed on both samples separately, but with the same protocol. The reference panel used, as for the BIG sample, was an all polymorphic 1000 Genomes Phase 1.v3 EUR panel (The 1000 Genomes Consortium, 2010). A two-step approach was used, performed with the software IMPUTE v2.1.2.3 (Howie, Donnelly et al. 2009). This resulted in genotypes for 17,533,349 markers in 932 subjects for SHIP-2 and 17,585,496 markers in 829 subjects for SHIP-TREND.

Genome-wide association scans

We carried out GWAS using the HO PT AI as a quantitative phenotype, in each of the three datasets, and for males and females separately. In each dataset, only markers that had a minor allele frequency higher than 1%, that were in Hardy-Weinberg equilibrium ($p > 5*10\text{-}6$), and had a missing genotype rate lower than 5%, entered the analysis. The association tests were done by linear regression of the HO PT AI on the genotype status separately at each SNP, in an additive genetic model, as implemented in PLINK v1.07 (Purcell et al., 2007).

Genome-wide association scan meta-analysis

The six sets of GWAS results (i.e. for each of the 3 datasets, and separately for males and females) were meta-analysed per SNP using the 'sample size' approach in the software METAL, described in (Willer et al., 2010). Put briefly, the meta-analysis pools the probabilities of a genetic effect at each SNP, across each contributing dataset, and weighted by each dataset's sample size, while considering the direction of the allelic effect on the quantitative trait. We chose this method because our six GWAS differed in terms of sex, mean subject age, and other aspects of subject recruitment, so that we wished to avoid assuming an equivalence of estimated genetic effect sizes across datasets and genders. Finally, we considered only results from SNPs that were present in each of the datasets, resulting in 5,285,490 SNPs genome-wide.

GWAS candidate pathway enrichment analysis

We tested for an enrichment of association with PT asymmetry, of genes involved in steroid hormone biology, using the software INRICH (Lee et al., 2012). Briefly, this approach identifies distinct regions of linkage disequilibrium (LD) in the genome that show association with a trait of interest, below a threshold of nominal significance (we used p = 0.001). The regions of LD are mapped to genes, which are assigned to defined gene sets that represent biological pathways, processes or groups according to prior gene-functional data. Then, regions of LD are shuffled across the genome by permutation (10,000 permutations), to arrive at an empirical measurement of how often the real-data pattern of association within pathways would be observed by chance alone. This approach is robust to the effect that a gene's or gene set's genomic size has on its probability of containing nominally significant associations. The parameters and options we used were as follows; flanking regions +/- 100kb; minimum number of genes in pathway 10; maximum 200.

As input we used the results from each of the six GWAS separately, before merging the statistical evidence for each pathway using the 'sample-size' approach described earlier (Willer et al., 2010). The P value for each pathway was then adjusted by Bonferroni correction to compensate for multiple testing over 17 gene sets (see below). A practical constraint that arose from this approach was that we needed to use the LD structure from only one of the datasets (we chose BIG), but there is no reason to expect substantial differences in the genomic distribution of LD between the Dutch and North German populations. We used the Gene Ontology (GO; Ashburner et al., 2000) as our source of assignments of genes to biological pathways. We searched the GO annotation file provided with INRICH for all pathways containing the search terms 'androgen', 'estrogen', 'progesterone', 'steroid'. 72 pathways were found, of which 16 fulfilled the criteria for association enrichment testing. These pathways were 'Steroid hormone receptor activity', 'Steroid binding', 'Steroid biosynthetic process', 'Androgen biosynthetic process', 'Steroid metabolic process', 'Androgen metabolic process', 'Estrogen metabolic process', 'Steroid hydroxylase activity', 'Estrogen receptor binding', 'Steroid hormone receptor signaling pathway', 'Estrogen receptor signaling pathway', 'Androgen receptor signaling pathway', 'Response to progesterone stimulus', 'Response to estrogen stimulus', 'Response to steroid hormone stimulus' and 'Androgen receptor binding'.

We also created one additional, custom gene set that comprised the genes listed by (Chakrabarti et al., 2009). This was a manually created gene set containing key genes involved in androgen and estrogen biology.

Meta-VBM analysis of the rs785248 polymorphism

We performed a whole-brain VBM analysis of grey matter volume using the genotypes of the SNP rs785248 within a multiple regression, separately for each of the three datasets and the two sexes. Genotypes were coded as 0, 1 or 2 (i.e. under an additive genetic model) and age and sex were used as covariates. In BIG, regressors for scanner field strength were also included as covariates. The resulting statistics were then merged across datasets, separately for each sex and voxel, using the "sample-size" approach described above (Willer et al., 2010). The same approach was then used to meta-analyse both sexes together. To correct for multiple testing across voxels, a false discovery rate (FDR) correction was applied to maintain the family-wise error rate (FWE) at 0.05 (Genovese et al., 2002). We did not account for multiple testing across males, females, and the sexes combined, since this did not affect the results or interpretation (see below).

Results

Sex and cerebral cortical asymmetry

Table 1 shows descriptive statistics of the HO left and right grey matter volumes, and AIs, for regions of the cerebral cortex at which the AI showed a significant mean difference between the sexes. (Data for all regions, regardless of an effect of sex on the AI, are given in Supplementary Table S1). The PT showed the strongest sexually dimorphic asymmetry out of all 48 cortical regions (Table 1). The probabilistic definition of the PT by the HO atlas is illustrated in Figure 1. The voxels with high probability for mapping to the PT correspond closely with post mortem, neuroanatomical definitions of this structure (Geschwind and Levitsky, 1968; Shapleske et al., 1999; Tzourio-Mazoyer et al., 2010b). The scan-rescan correlation for the PT AI was high, r=0.91, despite the heterogeneity of scanner and scanning parameters in the BIG dataset, indicating that this heterogeneity had a negligible impact on the measured trait variance. Males had a more pronounced leftward PT asymmetry than females (Figure 2). Twelve additional cortical regions also showed significant mean differences of their AIs between the sexes (Table 1). These regions were widely distributed over the cerebral cortex, although they included several temporal regions close to the PT (and for which the regional probability maps sometimes overlapped with that of the PT), such as the anterior divisions of the middle and superior temporal gyri (Table 1). The two population datasets, SHIP-2 (935 subjects) and SHIP-TREND (888 subjects), also supported the PT as having a sexually dimorphic asymmetry, and the magnitudes of the effects of sex in these datasets were consistent with the effect in BIG (Table 2).

SHIP-2 and SHIP-TREND showed decreased PT volumes compared with the BIG dataset (Table 2), but these decreases were consistent with the effect of age on PT volume. Within BIG, we observed linear decreases of PT GM volume with increased age (Supplementary Figure S1) that resulted in a volumetric reduction of 13% between the ages of 27 and 53, which are the mean ages of the BIG and SHIP datasets, respectively.

Cortical parcellation with FreeSurfer

With FreeSurfer, the PT showed the third most sexually dimorphic mean AI out of 74 regions defined in the Destrieux atlas, and the neighbouring posterior ramus of the lateral sulcus showed the most significantly sex-linked mean AI (Supplementary Table S2). However, the FreeSurfer-Destrieux definition of the PT deviates substantially from the classical neuroanatomical definition of this region. Due to cytoarchitectonic similarities, FreeSurfer's PTextends beyond the horizontal plane to include the vertically-oriented planum parietale (PP; see Supplementary Figure S2), for which the asymmetry was previously found to be independent of that of the horizontally-oriented PT (Jancke et al., 1994). In addition, the sexual dimorphism of PT asymmetry was weaker for FreeSurfer-Destrieux than for HO, and only one of the SHIP datasets showed a significant effect of sex on PT asymmetry using the FreeSurfer-Destrieux definition (Supplementary Table S2). We therefore focussed on the VBM HO measure of PT asymmetry for subsequent analysis.

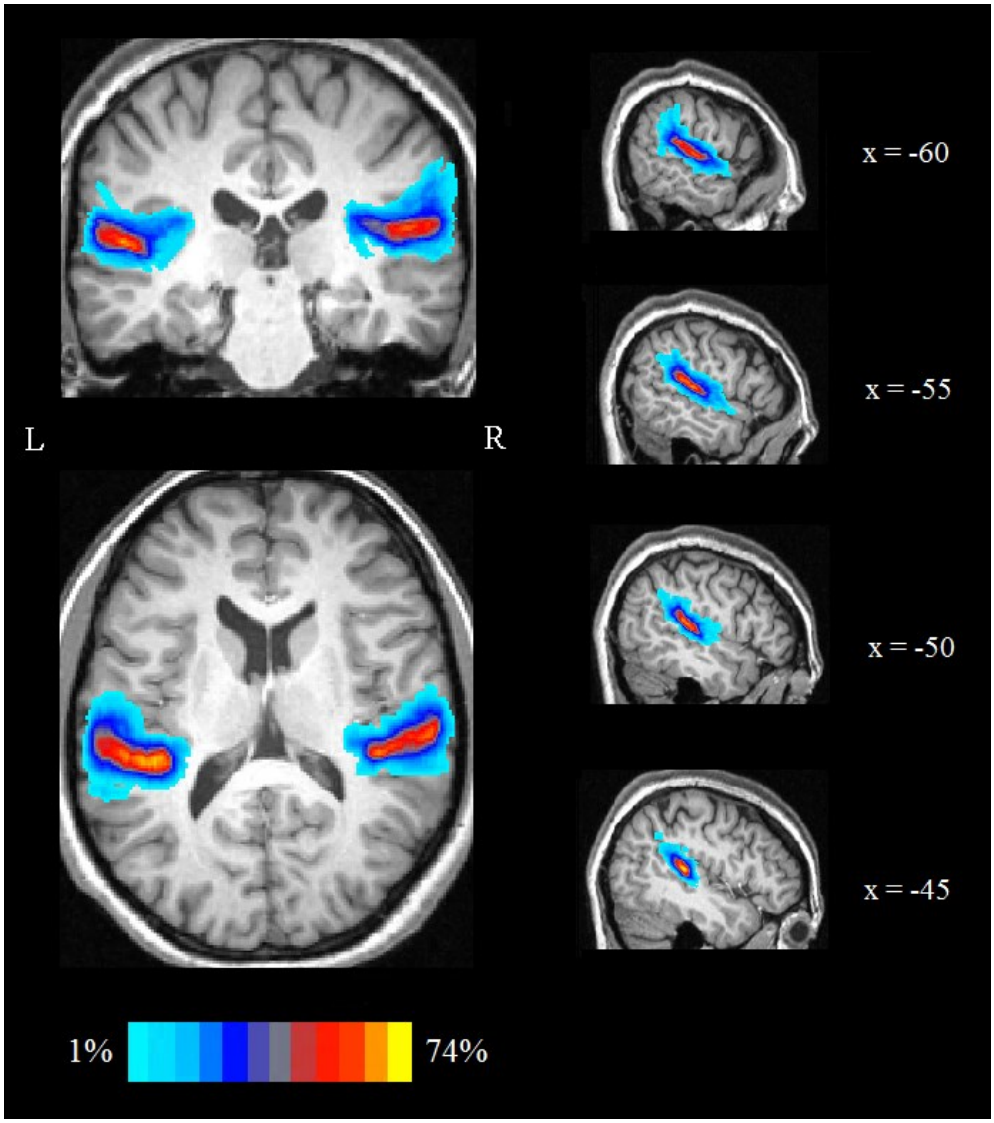

Figure 1. The planum temporale as defined with the HO probability mask, from coronal (top left), axial (bottom left), and sagittal (right) views. The sagittal views show the left PT in 4 different slices. The different colors of the mask indicate the voxel probability of belonging to the PT. The image is of a BIG subject for whom the PT AI was 0.137 (i.e. close to the BIG average AI of 0.130).

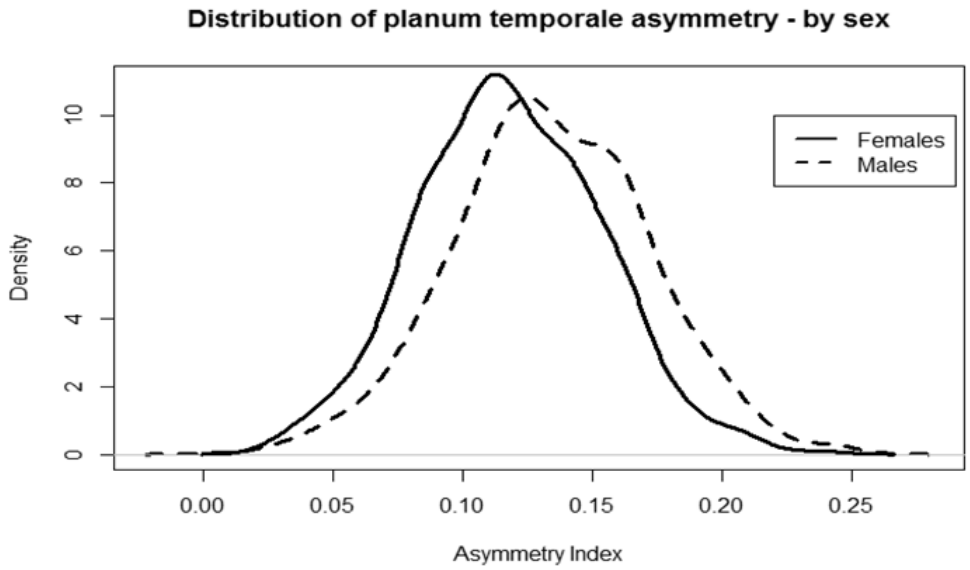

Figure 2. Density plot of the HO planum temporale asymmetry index (PT AI), in the BIG dataset, separately by sex.

Total brain volume and PT asymmetry

Men's brains are well known to be larger on average than women's, and we therefore analysed the link between sex and the HO PT AI in relation to the potentially confounding effect of Total Brain Volume (TBV), using the BIG dataset. Males had a mean TBV of 1315.6 ml, SD 104.6. The female mean TBV was 1171.6 ml, SD 90.0. There was a slight correlation between TBV and PT AI ($r=0.129$, $P < 0.001$). The correlation between PT AI and sex was $r=-0.184$, $P<0.001$ (negative r because males were coded as 1, females as 2). After regressing TBV out of the PT AI, the correlation with sex was slightly decreased, at $r=-0.108$, though still highly significant, $P<0.001$. After regressing sex out of the PT AI, then TBV and the PT AI were no longer significantly correlated ($r=0.020$, $P=0.34$). Congruent with the previous analysis, the correlation between sex and PT AI from the modulated GM images was $r=-0.111$, $P<0.001$. These analyses showed that TBV could not explain the majority of the effect of sex on PT asymmetry.

Table 2. Means and standard deviations of grey matter volumes (mm3), and Asymmetry Indexes (AI), for Harvard-Oxford atlas regions in the BIG dataset that showed a significant effect of sex on the AI after correction for multiple comparisons. See Supplementary Table S1 for a description of all regions.

HO	Males			Females			t-test of AI by sex		
	Left	Right	AI	Left	Right	AI	t-score	P-value	adj. P-value
Planum Temporale	2035 (278)	1543 (208)	0.137 (0.036)	1807 (242)	1406 (178)	0.124 (0.038)	9.05	< 0.001	< 0.001
Subcallosal cortex	1759 (194)	2063 (246)	-0.079 (0.021)	1587 (177)	1889 (222)	-0.087 (0.021)	8.36	< 0.001	< 0.001
Cingulate gyrus, posterior division	3851 (408)	5223 (606)	-0.151 (0.017)	3448 (367)	4727 (543)	-0.156 (0.017)	7.57	< 0.001	< 0.001
Superior temporal gyrus, anterior division	1002 (125)	1020 (124)	-0.009 (0.032)	882 (107)	915 (104)	-0.018 (0.032)	6.95	< 0.001	< 0.001
Parietal operculum cortex	2071 (269)	1851 (246)	0.056 (0.034)	1872 (236)	1704 (214)	0.047 (0.030)	6.82	< 0.001	< 0.001
Lateral occipital cortex, inferior division	6393 (714)	6036 (645)	0.028 (0.025)	5848 (623)	5463 (568)	0.034 (0.024)	-5.52	< 0.001	< 0.001
Frontal medial cortex	1765 (219)	2123 (286)	-0.092 (0.021)	1637 (198)	1990 (267)	-0.096 (0.020)	5.49	< 0.001	< 0.001
Occipital pole	5254 (695)	5433 (734)	-0.017 (0.028)	4779 (585)	4890 (647)	-0.011 (0.031)	-4.77	< 0.001	< 0.001
Middle temporal gyrus, anterior division	1596 (185)	1528 (179)	0.021 (0.031)	1416 (155)	1370 (149)	0.016 (0.029)	4.11	< 0.001	0.002
Paracingulate Gyrus	4782 (598)	5301 (761)	-0.050 (0.022)	4420 (505)	4926 (634)	-0.053 (0.021)	3.77	< 0.001	0.008
Supracalcarine cortex	791 (107)	1372 (189)	-0.268 (0.029)	708 (91)	1216 (154)	-0.264 (0.028)	-3.75	< 0.001	0.009
Cuneal cortex	1628 (220)	2466 (354)	-0.204 (0.028)	1465 (183)	2196 (290)	-0.199 (0.030)	-3.69	< 0.001	0.011
Cingulate gyrus, anterior division	4138 (473)	5863 (769)	-0.171 (0.022)	3781 (407)	5389 (655)	-0.175 (0.021)	3.64	< 0.001	0.013

Genetic analysis

The gene set STEROID HORMONE RECEPTOR ACTIVITY (GO:0003707) showed a significant enrichment of association in the GWAS results, p = 0.007 after adjusting for multiple comparisons across all of the tested pathways. The specific genes in this pathway that contributed to the measured enrichment were: ESR1, ESR2, ESRRA, ESRRG, NROB1, NR1D2, NR1H3, NR2C1, NR2C2, NR2E1, NR2F1, NR3C2, NR4A3, NR5A2, PGR, PGRMC2, PPARA, PPARD, PPARG, RORA, RORB, RXRB, RXRG, THRB and VDR.

The GWAS meta-analysis did not identify any individual SNP that surpassed the commonly agreed threshold for calling genome-wide significance of an individual association (threshold $P=5*10^{-8}$; Figure 3). There were 3 SNPs that showed suggestive association at a significance level below 1*10-6: rs79760216 ($p = 1.59*10^{-7}$), rs785248 ($p=2.1*10^{-7}$) and rs17074257 ($p=5.37*10^{-7}$).

Table 3. Comparison of Planum Temporale (PT) measures, obtained with HO, across the 3 study datasets. Mean lateral volumes (in mm^3), and Asymmetry Index (AI) means, are given by sex. The P value is shown for testing the effect of sex on the AI.

		BIG	SHIP-2	SHIP-TREND
Left PT	Males	2035 (278)	1686 (275)	1751 (270)
	Females	1807 (242)	1525 (224)	1574 (234)
Right PT	Males	1543 (208)	1290 (201)	1334 (196)
	Females	1406 (178)	1187 (162)	1226 (174)
PT AI	Males	0.137 (0.036)	0.132 (0.034)	0.135 (0.035)
	Females	0.124 (0.034)	0.124 (0.036)	0.124 (0.33)
P value		<0.001	<0.001	0.002

Table 4. Standardized regression coefficients and p-values, within each dataset and separately by sex, for the 3 SNPs that showed $P < 10^{-6}$ in the GWAS meta-analysis. Highlighted are the nominally significant statistics.

		rs74462483		rs785248		rs1971444		rs17074257	
		beta	P	beta	P	beta	p	Beta	p
BIG	females	**-0.343**	**0.001**	-0.03	0.593	-0.105	0.064	**-0.198**	**> 0.001**
	males	-0.248	0.073	**-0.209**	**0.002**	-0.089	0.196	**-0.186**	**0.008**
SHIP-2	females	**-0.396**	**0.006**	**-0.145**	**0.041**	**-0.247**	**0.001**	-0.087	0.226
	males	-0.276	0.06	**-0.21**	**0.004**	**-0.158**	**0.036**	-0.096	0.189
SHIP-T	females	-0.235	0.092	**-0.189**	**0.006**	-0.08	0.25	-0.091	0.186
	males	-0.205	0.138	-0.136	0.067	**-0.195**	**0.009**	-0.122	0.095

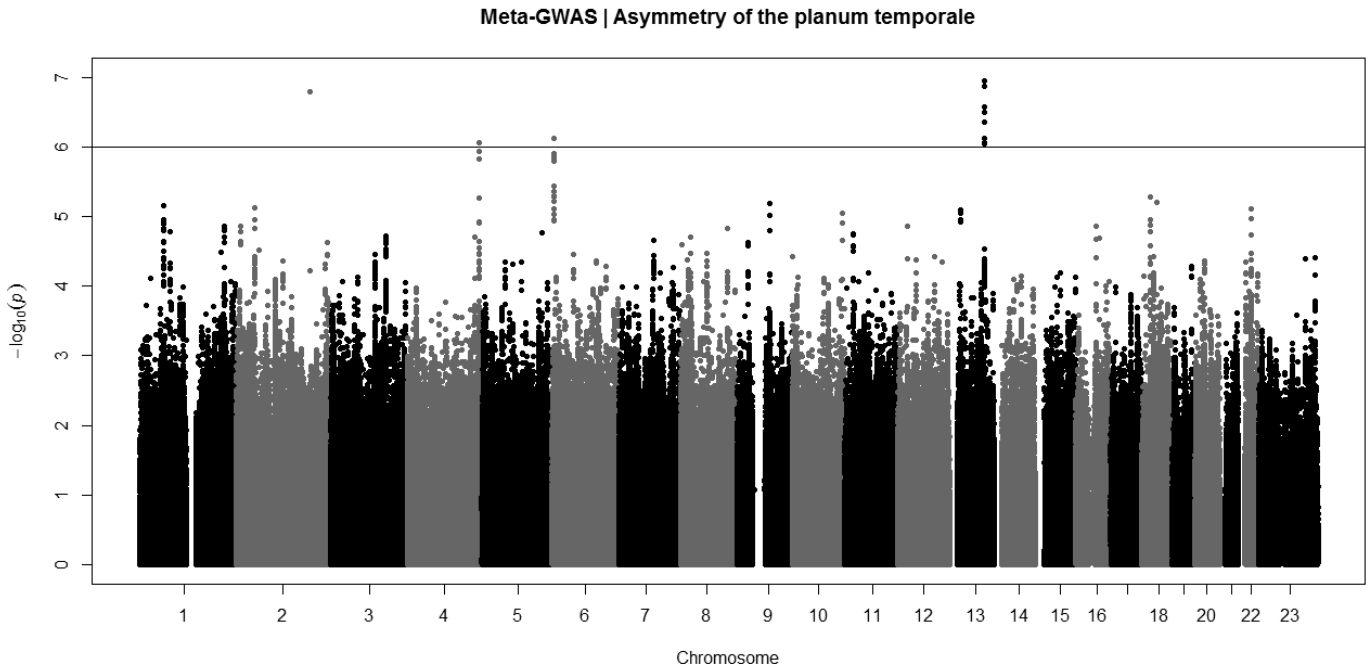

Figure 3. Manhattan plot of GWAS meta-analysis for the HO planum temporale asymmetry index (PT AI). The X-axis represents the chromosomes laid end-to-end, from short to long arms, in ascending numerical order from left to right. The Y-axis shows the pointwise significance of association. Shading represents the different chromosomes.

The SNP rs79760216 is an intergenic variant on chromosome 13, ~50kb away from LINC00559 (long intergenic non-protein coding RNA 559) and mir-622 (microRNA 622), with a minor allele frequency (MAF) of 0.053 (imputation r-square 0.92 in BIG). rs785248 is located on chromosome 2 within an intron of C2orf88 (MGC13057) and has a MAF of 0.29 (imputation r-square >0.99 in BIG). The messenger RNA of C2orf88 has been shown to be up-regulated in response to knockdown of the progesterone receptor gene in decidualizing endometrial tissue (Cloke et al., 2008), but otherwise little is known of the potential biological functions of C2orf88. rs17074257 is an intergenic variant located on chromosome 4, and is ~2kb downstream of DCTD and has a MAF of 0.27 (imputation r-square 0.97 in BIG). The protein encoded by DCTD catalyzes the deamination of dCMP to dUMP, the nucleotide substrate for thymidylate synthase (Weiner et al., 1995). Table 3 shows the magnitudes of the putative effects for these 3 SNPs in each of the datasets, separately by sex. Each of these 3 SNPs showed a negative direction of effect in each dataset and sex, meaning that the minor allele was associated with a decrease in leftward PT asymmetry. However, the effects were not always statistically significant across all of the datasets and sexes. Of the 3 SNPs, rs785248 showed the most consistency in evidence for association across datasets and sexes, with a significant, negative effect of the minor allele in 4 of the 6 analyses (see Table 3).

Meta-VBM analysis of rs785248

This SNP (the second most significant arising from the GWAS meta-analysis) was selected for brain-wide grey matter VBM association analysis due to the relative consistency of its effect on the PT AI across datasets and sexes, and in light of the link between C2orf88 and the progesterone receptor (Cloke et al., 2008). This analysis revealed that the effect of this SNP on the PT AI stemmed from a right-sided superior temporal effect that was present in both genders and mapped fairly consistently with the HO definition of PT (Figure 4). In addition, a cluster of significant voxels was also found in the right inferior frontal lobe, and left hippocampus and amygdala (Figure 5).

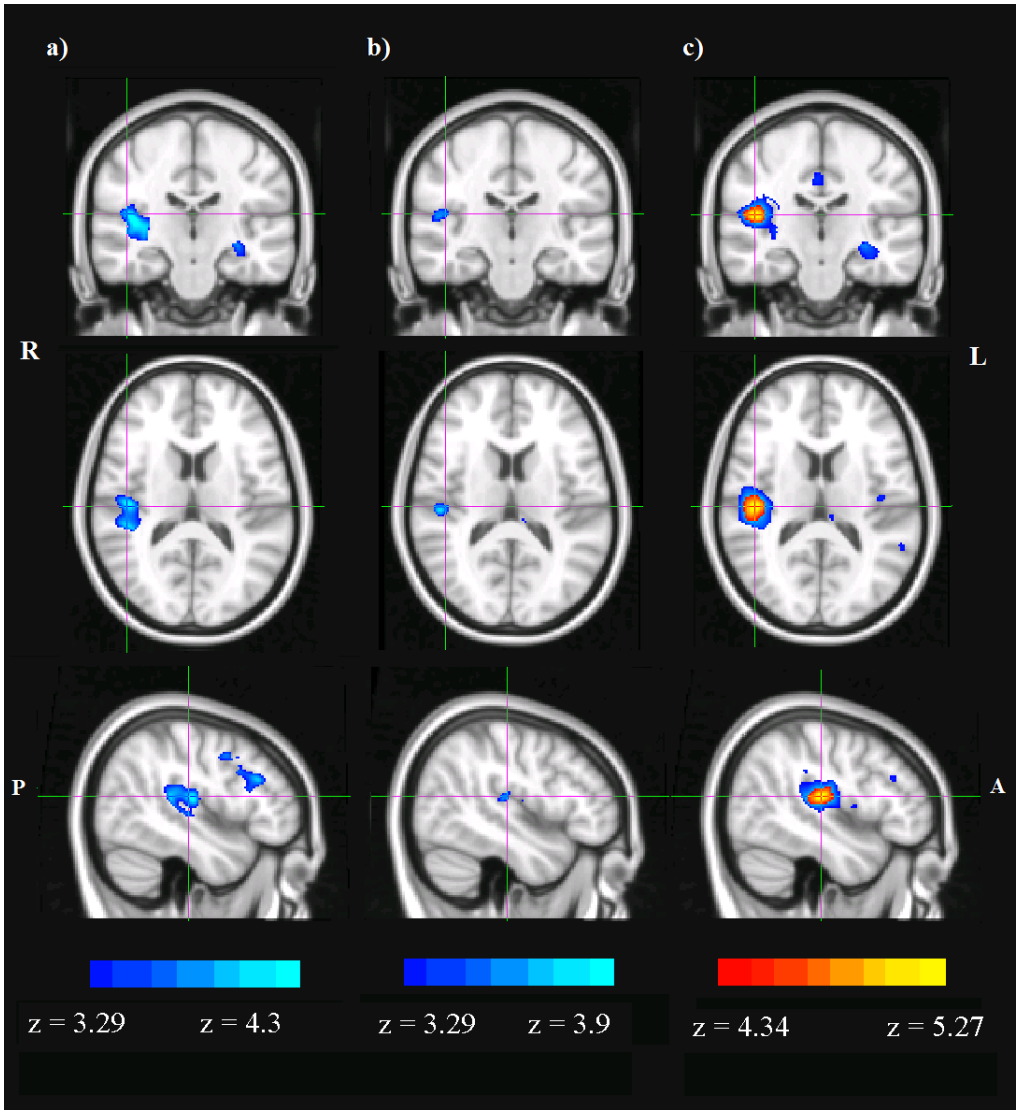

Figure 4. Results of the grey matter VBM analysis of rs785248. Images are shown from 3 different slices, centered on the posterior part of the superior temporal lobe. Depicted in red-orange-yellow (according to their meta-analysed z-score) are the significant voxels after FDR correction brain-wide, while blue shades indicate voxel-wise P values less than 0.0001 but which did not remain significant after FDR correction. Column (a) depicts the results from males only, column (b) from females and column (c) the results from males and females meta-analysed.

Discussion

GWAS for asymmetry of the PT offers the potential to identify novel molecular and developmental mechanisms that are involved in lateralizing the human brain, for aspects of function that include language. Sexual dimorphism of PT asymmetry has been reported (de Courten-Myers, 1999; Good et al., 2001; Shapleske et al., 1999), but also not found by some studies (Sommer et al., 2008; Wallentin, 2009; Watkins et al., 2001). A sex difference in PT asymmetry would suggest steroid hormone-related genes and pathways as specific candidates for involvement in this asymmetry.

Asymmetry of the planum temporale is sexually dimorphic

In the BIG dataset we screened over the cerebral cortex for regions that showed a mean difference in asymmetry between males and females, using probabilistic definitions for regions of interest. We found that the PT as defined by the Harvard-Oxford atlas showed the strongest sexually dimorphic asymmetry of any cortical region, which remained significant when adjusted conservatively for multiple testing over all cortical regions. Males showed stronger leftward PT regional lateralisation than females, which was consistent with some of the larger, previous studies where a sex difference has been reported (de Courten-Myers, 1999; Good et al., 2001; Shapleske et al., 1999). Another consistent finding has been recently reported. Ruigrok et al. (2014) in a meta-analysis showed females to have larger volumes in the right PT than males. The same sexual dimorphism in PT AI observed in BIG was also found in the two SHIP datasets, comprised primarily of older adults from north Germany, which totalled 1823 subjects. Sexual dimorphism was also supported, to a lesser extent and with less consistency, by the FreeSurfer parcellation of cortical regions as defined in the Destrieux atlas. However, its definition of PT also included the vertically-oriented planum parietale, whose asymmetry has been found to be independent of the PT's (Jancke et al., 1994). This would therefore create a measure that confounds two different asymmetry mechanisms.

Handedness was not associated with PT asymmetry; we report elsewhere the results of screening over the entire cerebral cortex in relation to handedness (Guadalupe et al., 2014).

The largest previous study that did not identify a significant sex effect on PT asymmetry (Sommer et al., 2008) was based on meta-analysis of data from 13 separate studies, representing 807 subjects in total. Publication bias was suggested to have established a sex effect on PT asymmetry in the literature (Sommer et al., 2008). Ours is the first study of cerebral cortical asymmetry to have included data from thousands of subjects, while also using relatively uniform methods, and across individually large

datasets. The SHIP datasets were population-based samples, thus with minimal selection bias for, or against, potentially confounding factors such as handedness or psychiatric disease. We therefore conclude that a subtle sexual dimorphism of asymmetry within and around the PT is a true feature of the general human population.

Men's brains are well known to be slightly larger on average than women's (Good et al., 2001; Stein et al., 2012), and we also observed this in our datasets. The question arises whether larger brains tend to be more asymmetrical for some regions, independently of sex, which could be a potential confound in measuring sexual dimorphisms of asymmetry (Josse et al., 2006; Tzourio-Mazoyer et al., 2010a). While we found evidence that total brain volume was weakly correlated with PT regional asymmetry, this correlation could not account for the majority of the effect of sex on the asymmetry, and was no longer significant after the effect of sex was removed. We therefore conclude that sex affects asymmetry of the PT via mechanisms that are largely distinct from those determining overall brain size.

There also remains the possibility that systematic differences caused by the segmentation pipeline or by the application of the H-O probabilistic map may have influenced the sex difference we observed. However, the segmentation and normalization steps relied on priors derived equally from male and female subjects. Similarly, the H-O atlas was derived from a sample of 21 males and 16 females. Another possibility would be that males show substantially greater variation than females in the location and size of the PT. This would have as a consequence that an atlas derived from both sexes would be more accurate at capturing the male PT volumes than it would the females'

Because of the reasons mentioned earlier and given that the effect we measure agrees with a considerable number of previous studies, we do not believe that such artifacts are the main drivers of the sex effect.

HO probability map measures individual differences in PT regional asymmetry

The HO atlas was derived from manual segmentations of sets of reference brain images (Destrieux et al., 2010; Goldstein et al., 1999; Goldstein et al., 2007). It therefore contained asymmetrical definitions for structures that showed different sizes or locations between the left and right hemispheres in the reference dataset (including the planum temporale; Figure 1). Accordingly, the measurement of average regional asymmetries in our samples would reflect left-right differences present in the atlas. For detecting cerebral asymmetries with automated methods, some groups have chosen to work from artificially created, left-right symmetrical atlases, e.g. (Kawasaki et al., 2008). However, our study was

focused on comparing relative degrees of asymmetry between subjects and groups, i.e. using the individual and group-level differences in the AI, regardless of the mean population level of asymmetry. The use of a 'real-world' asymmetrical atlas, rather than an artificially symmetrical atlas, was therefore appropriate for our study, as it had the advantage that regional identification was likely to be more accurate for structures that were asymmetrical both in the atlas and, on average, in our datasets. We did not aim to measure absolute levels of asymmetry, nor confirm a mean population-level asymmetry of any of the regions under study. In addition, we followed up an interesting SNP association with the HO PT AI by performing brain-wide grey matter VBM association analysis without use of atlas-defined regions of interest (see below). Thus the PT AI derived from an asymmetrical atlas acted as a useful probe for GWAS, but one which necessarily required following up with an atlas-free approach for association signals of interest.

The HO regional probability masks were not constrained in their application by local anatomical features specific to each subject, hence we considered the resulting measures of grey matter volume and asymmetry to reflect regions that were somewhat more inclusive than the target anatomical structures as named in the HO atlas. This expectation was consistent with our observation of no subjects having greater right than left PT volumes, in contrast to classical neuroanatomical studies of the PT which have reported larger right PTs in a minority of subjects (Shapleske et al., 1999). The complete PT region as defined by HO is larger and more inclusive than the classically defined structure, and therefore indexes a slightly broader regional asymmetry around the posterior sylvian fissure (Figure 1). However, much of the broader region in the HO atlas was defined at relatively low probability for inclusion in the region, and had correspondingly reduced weight in calculating our volumetric estimates, while the 'higher probability' voxels corresponded closely with classical, neuroanatomical definitions of the PT (Figure 1; Shapleske et al., 1999). The maximum voxel-wise probability for mapping to the PT was 74% in the HO atlas (Figure 1), illustrating the anatomical variability of the region in the reference brains used for this atlas.

In twice-scanned subjects, for the HO PT AI, we found that the proportion of shared variance between first and second scans (r-squared) was 81%. This was encouraging for subsequent genetic mapping with this trait, because the repeatability of a measure sets an upper limit on the proportion of trait variance that can be attributed to genetic factors, and has direct implications for the power to detect the effects of polymorphisms in GWAS. Large scale genetic studies depend on automated methods of image analysis for processing data from very large subject collections, for which manual checking is not an

option (Stein et al., 2012). The high repeatability of the HO PT AI, and the consistency of the effect of sex across the datasets that we analysed, indicated that this measure is largely robust to heterogeneity of scanners and scanning parameters, and therefore would be appropriate for even larger GWAS meta-analyses incorporating further datasets.

A practical approach in future genetic mapping may involve the use of multivariate approaches (Ferreira and Purcell, 2009) for analyzing asymmetries across multiple, neighbouring regions that are defined within a given atlas, or across multiple atlases as implemented in different automated image analysis methods. However, multivariate approaches are not necessarily straightforward to apply in the context of meta-analysis across multiple datasets.

Genes involved in steroid hormone biology influence population variance in PT asymmetry

Genes in the Gene Ontology (GO) set "Steroid Hormone Receptor Activity" were significantly enriched for SNPs showing association with the PT AI, after meta-analysing the results from males and females in the BIG and SHIP datasets. We hypothesise that variants in genes involved in steroid hormone pathways are likely to be downstream modifiers of PT asymmetrical development, rather than directly implicating early embryonic mechanisms that 'break symmetry' in the human CNS. Such mechanisms are currently unknown, but are apparently somewhat distinct from those that initiate embryonic left-right patterning of the viscera (heart, lungs etc.; Tanaka et al., 1999). People with left-right situs inversus of the viscera are reported to have similar rates of left-lateralised language dominance to people with normally patterned viscera (Tanaka et al., 1999). Visceral asymmetry appears to arise as a consequence of the homochirality (biased handedness) of amino acid molecules in living systems, that together create 'handed' cilia leading to a unidirectional, leftward fluid flow within the embryonic node (Shinohara et al., 2012; Takaoka et al., 2007; Yoshiba et al., 2012), and ultimately to different gene expression cascades on the two sides of the body. Human CNS asymmetries may also arise from analogous molecular/biophysical asymmetries, but the core mechanism is unknown. Steroid hormone pathways do not present an obvious 'symmetry breaking' mechanism. Furthermore, sex clearly has only a modifying effect on the population-level asymmetry within and around the PT, that is nonetheless present and pronounced in both sexes. Therefore, insofar as steroid hormone biology may contribute to the effect of sex on these asymmetries, we conceive of the influence in terms of developmental modulation, rather than a core mechanism that triggers directional CNS asymmetry.

The GWAS meta-analysis also yielded three suggestively associated individual SNPs. The one which showed the most consistent effect across samples and sexes was rs785248, located within an intron of

the uncharacterised gene transcript C2orf88 which has been shown to be affected by manipulation of the progesterone receptor in decidualizing endometrial tissue (Cloke et al., 2008). This additional, potential link to steroid hormone biology is intriguing in the context of our other genetic findings. The C2orf88 gene is not contained within the GO set of steroid hormone receptor activity genes, and therefore the association at C2orf88 and the enrichment of association within this GO set are independent findings that arose from our data.

As there is little reason to expect that a genetic effect will be limited only to one brain region as defined by a particular atlas, we followed up the association within C2orf88 with brain-wide grey matter VBM-based meta-analysis. This approach allowed a detailed examination of the putative effect of this locus which was free from considerations relating to HO regional definitions and atlas asymmetries. Nonetheless, the results corroborated the HO-based findings and showed rs785248 was associated with the PT AI by affecting GM volume within the right superior temporal region (Figure 4). While this effect was more significant within females than males, this appears to have reflected a difference in sample sizes between the sexes, rather than a difference in the magnitude of effects between sexes. When the data from males and females were merged by meta-analysis, the putative effect within C2orf88 was seen for a set of voxels across the right superior temporal gyrus, matching closely the HO definition of PT, as well as within the right medial inferior frontal gyrus, and in a region overlapping with the left amygdala/hippocampus.

The proportion of variance in HO PT AI attributable to rs785248 was roughly 0.8%, a figure which was largely stable across each of the meta-analysed datasets and both sexes. The concordance of effect size across the datasets supports validity of this potential association, and 0.8% of trait variance is a realistic size of effect on what is presumably a multifactorial trait that has many contributing genetic and environmental influences (Singleton et al., 2010; Stein et al., 2012). Our results clearly rule out the possibility that there exist individual genetic influences on PT regional asymmetry that account for more than a tiny fraction of overall trait variance. This finding is particularly discordant with single-gene theories of human cerebral asymmetry and language (Berlim et al., 2003). Given the PTs central role in language cognition, variants in the individual genes and steroid-related gene set that we have identified should now be investigated as modifying effects on language and reading performance in clinical and population samples. We recommend the use of gene-set-based approaches for such follow-up investigations, such as that we have used here (Lee et al., 2012) in which subtle effects of individual

variants may be detected in combination. Our data also indicate that larger-scale GWAS meta-analysis of PT regional asymmetry should be pursued, incorporating additional study populations.

An important possibility, for future study, is that sex-linked structural asymmetries in younger females might be dynamically linked to the menstrual cycle, and/or the use of oral contraception which often contains progesterone. Cycle phase-dependent changes in steroid serum levels have been correlated, using functional MRI, with the volume and lateralization of brain activations related to a semantic task, including within the superior temporal cortex (Fernandez et al., 2003). Increased progesterone was linked to more bilateral activation for this task (Fernandez et al., 2003). Menstrual cycle-linked changes in amygdala morphology have also been observed (Ossewaarde et al., 2011). PT leftward asymmetry was slightly reduced in the females of the BIG dataset (many students) as compared to the SHIP datasets (many of whom will have been post-menopausal), which we speculate is consistent with a progesterone-mediated reduction in superior temporal asymmetry.

Additional sexually dimorphic cerebral asymmetries

Our screen over the entire cerebral cortex for sexually dimorphic asymmetries also identified other sex-linked regions, additional to the PT, some of which have not previously been highlighted in this context (such as the cingulate gyrus). These sex-linked asymmetries were widely distributed over the cortex, and individual differences in these asymmetries, across subjects, were not strikingly correlated with one another (data not shown). The discovery of these additional, sexually dimorphic asymmetries illustrates the power of systematic studies in thousands of subjects to pinpoint subtle group differences. With further validation of their relation to sex, these regional asymmetries may also be considered as candidates for the kinds of genetic analysis that we have performed here in relation to the PT region.

Acknowledgements

Many thanks to Nathalie Tzourio-Mazoyer and Fabrice Crivello for advice and critical comments on this manuscript, and to Han Brunner for his involvement in the creation and growth of the BIG (Brain Imaging Genetics) dataset.

The BIG database was established in Nijmegen in 2007. This resource is now part of Cognomics, a joint initiative by researchers of the Donders Centre for Cognitive Neuroimaging, the Human Genetics and Cognitive Neuroscience departments of the Radboud University Medical Centre and the Max Planck Institute for Psycholinguistics. The Cognomics Initiative is supported by the participating departments and centres and by external grants, i.e. the Biobanking and Biomolecular Resources Research

Infrastructure (Netherlands) (BBMRI-NL), the Hersenstichting Nederland and the Netherlands Organisation for Scientific Research (NWO). We wish to thank all persons who kindly participated in this research.

The SHIP datasets are part of the Community Medicine Research net (CMR) of the University of Greifswald, which is funded by the German Federal Ministry of Education and Research and the German Ministry of Cultural Affairs, as well as by the Social Ministry of the Federal State of Mecklenburg–West Pomerania (grants no. 01ZZ9603, 01ZZ0103, and 01ZZ0403), and the network 'Greifswald Approach to Individualized Medicine (GANI_MED)' funded by the Federal Ministry of Education and Research (grant 03IS2061A). Genome-wide data and MRI scans were supported by the Federal Ministry of Education and Research (grant no. 03ZIK012) and a joint grant from Siemens Healthcare, Erlangen, Germany, and the Federal State of Mecklenburg–West Pomerania. The University of Greifswald is a member of the Center of Knowledge Interchange program of the Siemens AG and the Caché Campus Program of the InterSystems GmbH. The SHIP authors are grateful to Mario Stanke for the opportunity to use his Server Cluster for the SNP imputation as well as to Holger Prokisch and Thomas Meitinger (Helmholtz Zentrum München) for the genotyping of the SHIP-TREND cohort.

Appendix

Supplementary material

Supplementary Table S1. Mean volumes (in mm3), Asymmetry Index (AI) and standard deviations (SD's) for both genders in the 48 cortical regions defined in the HO atlas (BIG sample) and corresponding t-test for equality of mean AIs. P-values are Bonferroni corrected for the number of regions in the atlas. Regions are ranked by their significance.

Brain region	Males			Females			t-test of AI by gender		
	Left	Right	AI	left	Right	AI	t-score	P-value	adj. P-value
Planum Temporale	203.52 (27.77)	154.32 (20.81)	0.14 (0.04)	180.73 (24.16)	140.61 (17.78)	0.12 (0.03)	9.05	< 0.001	< 0.001
Subcallosal Cortex	175.87 (19.41)	206.29 (24.62)	-0.08 (0.02)	158.68 (17.73)	188.91 (22.25)	-0.09 (0.02)	8.36	< 0.001	< 0.001
Cingulate Gyrus, posterior division	385.05 (40.82)	522.3 (60.55)	-0.15 (0.02)	344.77 (36.66)	472.68 (54.28)	-0.16 (0.02)	7.57	< 0.001	< 0.001
Superior Temporal Gyrus, anterior division	100.19 (12.46)	102 (12.36)	-0.01 (0.03)	88.22 (10.65)	91.46 (10.45)	-0.02 (0.03)	6.95	< 0.001	< 0.001
Parietal Operculum Cortex	207.13 (26.89)	185.12 (24.59)	0.06 (0.03)	187.2 (23.62)	170.4 (21.36)	0.05 (0.03)	6.82	< 0.001	< 0.001
Lateral Occipital Cortex, inferior division	639.28 (71.36)	603.61 (64.49)	0.03 (0.02)	584.76 (62.25)	546.27 (56.8)	0.03 (0.02)	-5.52	< 0.001	< 0.001
Frontal Medial Cortex	176.46 (21.85)	212.3 (28.59)	-0.09 (0.02)	163.72 (19.8)	198.95 (26.7)	-0.1 (0.02)	5.49	< 0.001	< 0.001
Occipital Pole	525.39 (69.47)	543.31 (73.38)	-0.02 (0.03)	477.87 (58.48)	488.98 (64.69)	-0.01 (0.03)	-4.77	< 0.001	< 0.001
Middle Temporal Gyrus, anterior division	159.57 (18.52)	152.8 (17.95)	0.02 (0.03)	141.55 (15.46)	136.98 (14.92)	0.02 (0.03)	4.11	< 0.001	0.002
Paracingulate Gyrus	478.15 (59.75)	530.11 (76.12)	-0.05 (0.02)	442.03 (50.53)	492.6 (63.37)	-0.05 (0.02)	3.77	< 0.001	0.008
Supracalcarine Cortex	79.08 (10.72)	137.17 (18.9)	-0.27 (0.03)	70.78 (9.05)	121.57 (15.42)	-0.26 (0.03)	-3.75	< 0.001	0.009
Cuneal Cortex	162.78 (21.98)	246.63 (35.43)	-0.2 (0.03)	146.45 (18.31)	219.64 (29.03)	-0.2 (0.03)	-3.69	< 0.001	0.011
Cingulate Gyrus, anterior division	413.75 (47.28)	586.28 (76.91)	-0.17 (0.02)	378.09 (40.74)	538.94 (65.49)	-0.17 (0.02)	3.64	< 0.001	0.013
Planum Polare	123.78 (15.68)	122.9 (16.72)	0 (0.03)	111.68 (13.3)	111.56 (13.84)	0 (0.03)	3.24	0.001	0.056
Lateral Occipital Cortex, superoir division	1189.61 (155.35)	1127.05 (139.54)	0.03 (0.02)	1082.32 (131.33)	1020.38 (119.47)	0.03 (0.02)	-3.19	0.001	0.066
Superior Temporal Gyrus, posterior division	172.76 (21.16)	179.84 (22.27)	-0.02 (0.03)	156.24 (18.19)	163.76 (18.82)	-0.02 (0.03)	3.17	0.002	0.072

Postcentral Gyrus	799.91 (113.83)	735.1 (102.88)	0.04 (0.02)	731.28 (87.32)	676 (80.41)	0.04 (0.02)	3.13	0.002	0.083
Inferior Frontal Gyrus, pars triangularis	200.13 (26.79)	185.04 (23.21)	0.04 (0.02)	187.23 (22.31)	172.43 (19.31)	0.04 (0.02)	-2.87	0.004	0.18
Frontal Orbital Cortex	537.65 (55.97)	508.76 (50.95)	0.03 (0.02)	493.18 (49.19)	468.42 (44.51)	0.03 (0.02)	2.69	0.007	0.292
Middle Temporal Gyrus, posterior division	421.34 (46.71)	423.76 (47.72)	0 (0.02)	381.38 (39.32)	385.57 (40.49)	-0.01 (0.02)	2.59	0.01	0.374
Intracalcarine Cortex	200.99 (27.57)	246.15 (33.46)	-0.1 (0.02)	180.72 (23.5)	222.18 (28.41)	-0.1 (0.02)	2.32	0.02	0.625
Inferior Temporal Gyrus, anterior division	136.75 (15.52)	130.51 (14.45)	0.02 (0.03)	121.82 (13.1)	117.01 (12.32)	0.02 (0.03)	2.24	0.025	0.708
Heschl's Gyrus (includes H1 and H2)	115.29 (16.18)	100.13 (14.83)	0.07 (0.03)	104.11 (13.54)	90.87 (11.94)	0.07 (0.03)	2.19	0.029	0.754
Juxtapositional Lobule Cortex (formerly Supplementary Motor Cortex)	196.19 (25.79)	224.48 (34.11)	-0.07 (0.03)	180.99 (21.44)	208.17 (28.72)	-0.07 (0.03)	2.11	0.035	0.815
Temporal Pole	658.17 (76.82)	664.4 (78.84)	0 (0.03)	588.2 (66.6)	596.27 (66.78)	-0.01 (0.03)	2.08	0.037	0.839
Inferior Temporal Gyrus, temporooccipital part	241.32 (26.41)	275.84 (28.18)	-0.07 (0.03)	221.26 (23.19)	251.63 (24.51)	-0.06 (0.03)	-2.01	0.044	0.887
Lingual Gyrus	505.27 (53.95)	584.25 (64.39)	-0.07 (0.02)	459.44 (45.47)	530.12 (54.99)	-0.07 (0.01)	-1.78	0.076	0.977
Inferior Temporal Gyrus, posterior division	322.27 (34.45)	287.59 (31.66)	0.06 (0.03)	292.57 (29.5)	262.04 (27.32)	0.06 (0.03)	1.63	0.103	0.994
Supramarginal Gyrus, anterior division	294.22 (38.76)	249.03 (31.51)	0.08 (0.03)	269.56 (31.33)	229.1 (25.61)	0.08 (0.03)	1.62	0.105	0.995
Middle Frontal Gyrus	727.71 (100.72)	684.98 (90.88)	0.03 (0.02)	672.57 (82.08)	632.94 (76.1)	0.03 (0.02)	-1.43	0.152	1
Angular Gyrus	355.05 (43)	480.89 (54.49)	-0.15 (0.02)	327.26 (36.74)	442.21 (47.78)	-0.15 (0.02)	-1.35	0.176	1
Superior Frontal Gyrus	700.93 (102.65)	702.84 (109.26)	0 (0.02)	646.28 (81.85)	646.79 (86.2)	0 (0.02)	-1.08	0.281	1
Middle Temporal Gyrus, temporooccipital part	282.94 (31.15)	377.06 (40.73)	-0.14 (0.02)	260.38 (27.32)	346.48 (35.65)	-0.14 (0.02)	-0.92	0.36	1
Occipital Fusiform Gyrus	324.19 (34.06)	295.68 (31.07)	0.05 (0.02)	295.21 (29.47)	269.84 (26.93)	0.05 (0.02)	0.89	0.376	1
Frontal Operculum Cortex	120.04 (14.75)	112.9 (13.58)	0.03 (0.03)	110.83 (12.57)	104.07 (11.53)	0.03 (0.03)	-0.86	0.388	1
Frontal Pole	1865.18 (252.27)	2146.93 (293.46)	-0.07 (0.02)	1733.48 (215.3)	1991.69 (248.61)	-0.07 (0.02)	-0.84	0.398	1
Inferior Frontal Gyrus, pars opercularis	240.04 (31.79)	217.28 (26.77)	0.05 (0.02)	223.68 (25.97)	202.21 (22.36)	0.05 (0.02)	-0.75	0.453	1

Central Opercular Cortex	328.96 (40.86)	299.92 (38.84)	0.05 (0.03)	299 (34.56)	272.97 (31.79)	0.05 (0.02)	0.75	0.456	1
Supramarginal Gyrus, posterior division	365.22 (44.65)	391.24 (46.07)	-0.03 (0.02)	335.84 (37.4)	360.1 (38.73)	-0.03 (0.02)	0.71	0.479	1
Precentral Gyrus	963.53 (129.85)	980.1 (130.52)	-0.01 (0.02)	884.75 (99.75)	899.35 (101.54)	-0.01 (0.01)	-0.68	0.495	1
Parahippocampal Gyrus, anterior division	241.83 (23.12)	266.73 (25.61)	-0.05 (0.02)	216.96 (20.85)	239.05 (23.05)	-0.05 (0.02)	-0.45	0.651	1
Insular Cortex	510.35 (56.99)	519.11 (54.27)	-0.01 (0.02)	467.72 (47.12)	475.54 (45.92)	-0.01 (0.02)	-0.44	0.661	1
Temporal Occipital Fusiform Cortex	267.47 (26.15)	319.72 (29.83)	-0.09 (0.02)	244.7 (23.67)	292.44 (27.18)	-0.09 (0.02)	-0.29	0.773	1
Temporal Fusiform Cortex, anterior division	138.03 (13.76)	129.62 (13)	0.03 (0.03)	122.3 (11.85)	114.91 (11.11)	0.03 (0.03)	0.26	0.794	1
Parahippocampal Gyrus, posterior division	149.25 (14.37)	120.19 (12.18)	0.11 (0.02)	136.97 (12.95)	110.23 (11.05)	0.11 (0.02)	-0.22	0.829	1
Temporal Fusiform Cortex, posterior division	355.57 (31.95)	299.72 (28.17)	0.09 (0.02)	325.91 (29.55)	274.45 (25.28)	0.09 (0.02)	-0.18	0.858	1
Superior Parietal Lobule	342.92 (52.18)	329.7 (50.28)	0.02 (0.03)	314.09 (41.09)	301.93 (39.38)	0.02 (0.02)	0.12	0.907	1
Precuneous Cortex	770.62 (93.17)	927.24 (123.03)	-0.09 (0.02)	693.75 (76.42)	834.8 (101.95)	-0.09 (0.02)	-0.07	0.948	1

Supplementary Table S2. Mean volumes (in mm3), Asymmetry Index (AI) and standard deviations (SD's) for both genders in the 74 cortical regions produced by FreeSurfer's Destrieux atlas (BIG sample) and corresponding t-test for equality of mean AIs. P-values are Bonferroni corrected for the number of regions in the atlas. Regions are ranked by their significance.

Brain region	males			Females			t-test of AI by gender		
	left	right	AI	Left	right	AI	t-score	P-value	adj. P-value
Posterior ramus (or segment) of the lateral sulcus (or fissure)	1812 (327)	2187 (291)	-0.098 (0.082)	1601 (280)	2071 (264)	-0.131 (0.073)	10.35	<0.001	<0.001
Posterior-ventral part of the cingulate gyrus (vPCC, isthmus of the cingulate gyrus)	654 (170)	733 (182)	-0.058 (0.137)	543 (138)	652 (158)	-0.091 (0.131)	5.98	<0.001	<0.001
Planum temporale or temporal plane of the superior temporal gyrus	2196 (490)	1728 (354)	0.117 (0.114)	1875 (431)	1549 (308)	0.091 (0.115)	5.36	<0.001	<0.001
Orbital sulci (H-shaped sulci)	2774 (420)	2841 (453)	-0.011 (0.06)	2605 (379)	2604 (414)	0.001 (0.063)	-4.73	<0.001	<0.001
Long insular gyrus and central sulcus of the insula	1341 (226)	1423 (236)	-0.03 (0.081)	1251 (215)	1292 (210)	-0.016 (0.077)	-4.2	<0.001	0.002

Planum polare of the superior temporal gyrus	1891 (403)	2030 (418)	-0.036 (0.106)	1632 (351)	1807 (365)	-0.052 (0.102)	3.6	<0.001	0.024
Lateral occipito-temporal gyrus (fusiform gyrus, O4-T4)	5284 (954)	5231 (987)	0.006 (0.093)	4708 (844)	4540 (860)	0.019 (0.089)	-3.56	<0.001	0.028
Straight gyrus, Gyrus rectus	2723 (378)	1983 (308)	0.157 (0.074)	2493 (353)	1853 (277)	0.147 (0.072)	3.23	0.001	0.088
Temporal pole	6561 (903)	6318 (863)	0.019 (0.065)	6078 (748)	5947 (743)	0.01 (0.059)	3.21	0.001	0.096
Lateral aspect of the superior temporal gyrus	6880 (1002)	6039 (892)	0.065 (0.06)	6292 (831)	5613 (781)	0.057 (0.056)	3.16	0.002	0.11
Anterior transverse temporal gyrus (of Heschl)	1143 (248)	913 (200)	0.112 (0.109)	1071 (242)	830 (182)	0.125 (0.107)	-3.01	0.003	0.18
Middle-posterior part of the cingulate gyrus and sulcus (pMCC)	2759 (428)	3087 (493)	-0.055 (0.066)	2564 (391)	2821 (448)	-0.047 (0.068)	-2.99	0.003	0.189
Vertical ramus of the anterior segment of the lateral sulcus (or fissure)	514 (158)	392 (125)	0.131 (0.192)	465 (143)	370 (114)	0.11 (0.189)	2.66	0.008	0.444
Middle-anterior part of the cingulate gyrus and sulcus (aMCC)	3096 (576)	3501 (565)	-0.063 (0.075)	2893 (515)	3220 (488)	-0.056 (0.070)	-2.49	0.013	0.62
Transverse temporal sulcus	568 (121)	501 (104)	0.061 (0.127)	545 (111)	473 (109)	0.074 (0.131)	-2.39	0.017	0.717
Supramarginal gyrus	7946 (1307)	7381 (1265)	0.037 (0.072)	7198 (1097)	6789 (1094)	0.03 (0.069)	2.32	0.02	0.781
Superior frontal sulcus	5380 (883)	4927 (816)	0.043 (0.073)	5007 (817)	4517 (744)	0.05 (0.076)	-2.31	0.021	0.796
Medial orbital sulcus (olfactory sulcus)	1483 (272)	1436 (211)	0.013 (0.087)	1387 (258)	1320 (193)	0.022 (0.09)	-2.26	0.024	0.835
Triangular part of the inferior frontal gyrus	3110 (641)	3098 (677)	0.003 (0.109)	2917 (562)	2853 (622)	0.013 (0.110)	-2.23	0.026	0.854
Anterior segment of the circular sulcus of the insula	1046 (179)	1208 (225)	-0.07 (0.095)	935 (159)	1095 (189)	-0.078 (0.093)	2.2	0.028	0.876
Subcentral gyrus (central operculum) and sulci	3624 (611)	3205 (560)	0.061 (0.082)	3247 (516)	2918 (504)	0.054 (0.080)	2.14	0.033	0.915
Posterior-dorsal part of the cingulate gyrus (dPCC)	1692 (358)	1576 (337)	0.035 (0.102)	1454 (303)	1380 (284)	0.026 (0.098)	2.12	0.034	0.925
Precuneus (medial part of P1)	6507 (1016)	6368 (931)	0.011 (0.06)	6045 (906)	5852 (826)	0.016 (0.056)	-2.02	0.044	0.964
Inferior part of the precentral sulcus	2612 (503)	2855 (552)	-0.043 (0.107)	2399 (467)	2653 (495)	-0.051 (0.096)	1.91	0.056	0.986
Parahippocampal gyrus, parahippocampal part of the medial occipito-temporal gyrus, (TS)	4064 (785)	4613 (851)	-0.064 (0.085)	3717 (664)	4280 (731)	-0.07 (0.078)	1.91	0.056	0.986
Transverse frontopolar gyri and sulci	1884 (365)	2850 (508)	-0.204 (0.098)	1749 (326)	2607 (443)	-0.196 (0.095)	-1.88	0.06	0.99
Middle temporal gyrus (T2)	9453 (1546)	10147 (1492)	-0.037 (0.06)	8467 (1239)	9197 (1268)	-0.042 (0.057)	1.87	0.061	0.991
Subcallosal area, subcallosal gyrus	1085 (405)	919 (255)	0.065 (0.186)	869 (338)	754 (217)	0.05 (0.195)	1.8	0.072	0.996
Inferior segment of the circular sulcus of the insula	2598 (389)	2171 (328)	0.089 (0.071)	2408 (309)	1998 (295)	0.094 (0.067)	-1.66	0.096	0.999
Subparietal sulcus	1975 (470)	2230 (538)	-0.058 (0.119)	1771 (418)	2025 (482)	-0.066 (0.114)	1.56	0.119	1
Pericallosal sulcus (S of corpus callosum)	1639 (303)	2064 (381)	-0.114 (0.112)	1510 (282)	1869 (327)	-0.107 (0.111)	-1.48	0.139	1
Orbital part of the inferior frontal gyrus	973 (223)	1088 (253)	-0.055 (0.145)	889 (219)	1009 (233)	-0.064 (0.151)	1.46	0.146	1

Suborbital sulcus (sulcus rostrales, supraorbital sulcus)	1173 (253)	610 (202)	0.32 (0.17)	1100 (236)	563 (201)	0.33 (0.179)	-1.45	0.146	1
Marginal branch (or part) of the cingulate sulcus	1739 (299)	2091 (363)	-0.091 (0.092)	1647 (260)	1964 (337)	-0.086 (0.089)	-1.44	0.149	1
Middle occipital gyrus (O2, lateral occipital gyrus)	5506 (922)	6082 (1041)	-0.049 (0.08)	4985 (862)	5454 (941)	-0.045 (0.08)	-1.44	0.149	1
Superior occipital sulcus and transverse occipital sulcus	1935 (380)	2331 (480)	-0.092 (0.111)	1754 (346)	2087 (421)	-0.085 (0.105)	-1.42	0.156	1
Lateral orbital sulcus	666 (154)	730 (196)	-0.04 (0.158)	590 (144)	660 (188)	-0.05 (0.161)	1.39	0.165	1
Sulcus intermedius primus (of Jensen)	617 (283)	817 (333)	-0.137 (0.275)	539 (241)	697 (300)	-0.121 (0.285)	-1.35	0.176	1
Lateral occipito-temporal sulcus	1690 (384)	1804 (380)	-0.034 (0.123)	1479 (350)	1552 (328)	-0.027 (0.129)	-1.35	0.179	1
Occipital pole	3558 (569)	5299 (781)	-0.196 (0.076)	3183 (519)	4699 (688)	-0.192 (0.072)	-1.32	0.187	1
Calcarine sulcus	3167 (560)	3075 (585)	0.016 (0.06)	2854 (504)	2784 (531)	0.013 (0.057)	1.28	0.201	1
Anterior occipital sulcus and preoccipital notch (temporo-occipital incisure)	1262 (365)	1373 (386)	-0.043 (0.182)	1161 (337)	1243 (365)	-0.033 (0.178)	-1.28	0.202	1
Middle frontal sulcus	2734 (608)	3763 (758)	-0.158 (0.118)	2481 (548)	3381 (727)	-0.152 (0.119)	-1.27	0.204	1
Medial occipito-temporal sulcus (collateral sulcus) and lingual sulcus	3480 (620)	3189 (535)	0.042 (0.072)	3177 (524)	2886 (452)	0.046 (0.071)	-1.24	0.214	1
Opercular part of the inferior frontal gyrus	4053 (710)	3632 (647)	0.054 (0.081)	3766 (585)	3360 (574)	0.058 (0.075)	-1.12	0.263	1
Parieto-occipital sulcus (or fissure)	3094 (574)	3377 (624)	-0.043 (0.077)	2824 (499)	3045 (529)	-0.04 (0.077)	-1.04	0.297	1
Posterior transverse collateral sulcus	580 (140)	788 (227)	-0.141 (0.16)	527 (134)	721 (206)	-0.148 (0.162)	1.02	0.307	1
Lingual gyrus, ligual part of the medial occipito-temporal gyrus, (O5)	5106 (885)	5082 (777)	0 (0.067)	4622 (793)	4632 (725)	-0.003 (0.067)	1.02	0.309	1
Central sulcus (Rolando's fissure)	3916 (549)	3789 (534)	0.017 (0.056)	3575 (469)	3479 (483)	0.014 (0.054)	1.01	0.311	1
Paracentral lobule and sulcus	2846 (505)	2428 (446)	0.079 (0.089)	2698 (471)	2320 (401)	0.075 (0.083)	1.01	0.314	1
Superior segment of the circular sulcus of the insula	3041 (374)	2413 (334)	0.116 (0.056)	2783 (324)	2203 (309)	0.118 (0.055)	-0.92	0.357	1
Inferior frontal sulcus	3998 (776)	3625 (675)	0.048 (0.093)	3607 (646)	3302 (593)	0.045 (0.088)	0.9	0.368	1
Orbital gyri	7112 (896)	7747 (987)	-0.043 (0.04)	6562 (798)	7176 (882)	-0.044 (0.043)	0.88	0.378	1
Inferior occipital gyrus (O3) and sulcus	3480 (684)	3047 (634)	0.066 (0.116)	3076 (617)	2714 (561)	0.062 (0.116)	0.79	0.432	1
Inferior temporal gyrus	8780 (1559)	8347 (1394)	0.024 (0.077)	7848 (1358)	7434 (1282)	0.026 (0.077)	-0.78	0.436	1
Superior part of the precentral sulcus	2219 (501)	2320 (519)	-0.022 (0.114)	1976 (429)	2053 (454)	-0.019 (0.116)	-0.69	0.491	1
Short insular gyri	2485 (334)	2296 (329)	0.04 (0.056)	2230 (303)	2057 (315)	0.041 (0.054)	-0.65	0.518	1
Middle frontal gyrus (F2)	12338 (2065)	11348 (1977)	0.042 (0.058)	11297 (1774)	10420 (1723)	0.041 (0.057)	0.58	0.565	1
Horizontal ramus of the anterior segment of the lateral sulcus (or fissure)	557 (136)	675 (172)	-0.093 (0.149)	508 (124)	619 (154)	-0.096 (0.146)	0.57	0.567	1

Superior occipital gyrus (O1)	3173 (559)	3745 (648)	-0.082 (0.079)	2887 (478)	3427 (595)	-0.084 (0.076)	0.54	0.587	1
Angular gyrus	6607 (1244)	8175 (1519)	-0.106 (0.089)	6184 (1091)	7630 (1310)	-0.104 (0.081)	-0.49	0.623	1
Superior temporal sulcus (parallel sulcus)	10129 (1417)	11413 (1670)	-0.059 (0.058)	9193 (1254)	10323 (1412)	-0.058 (0.054)	-0.44	0.663	1
Superior frontal gyrus (F1)	19835 (2545)	18750 (2418)	0.028 (0.035)	18396 (2113)	17427 (2027)	0.027 (0.034)	0.41	0.685	1
Cuneus (O6)	3094 (513)	3219 (545)	-0.021 (0.073)	2765 (457)	2869 (449)	-0.020 (0.070)	-0.33	0.742	1
Superior parietal lobule (lateral part of P1)	6842 (1204)	5492 (1004)	0.11 (0.073)	6454 (1064)	5160 (855)	0.111 (0.07)	-0.28	0.779	1
Precentral gyrus	6974 (1023)	6883 (1051)	0.008 (0.052)	6431 (884)	6340 (881)	0.007 (0.05)	0.25	0.801	1
Inferior temporal sulcus	2396 (565)	2251 (524)	0.03 (0.128)	2116 (516)	1992 (477)	0.029 (0.131)	0.25	0.804	1
Intraparietal sulcus (interparietal sulcus) and transverse parietal sulci	4803 (777)	4958 (775)	-0.016 (0.082)	4435 (661)	4592 (682)	-0.017 (0.079)	0.22	0.823	1
Postcentral sulcus	4561 (783)	3778 (765)	0.095 (0.094)	4120 (663)	3425 (667)	0.095 (0.086)	-0.19	0.847	1
Middle occipital sulcus and lunatus sulcus	1672 (415)	1621 (417)	0.016 (0.138)	1447 (371)	1407 (377)	0.017 (0.14)	-0.18	0.855	1
Postcentral gyrus	4685 (835)	4236 (746)	0.05 (0.077)	4309 (714)	3909 (667)	0.049 (0.073)	0.11	0.915	1
Fronto-marginal gyrus (of Wernicke) and sulcus	2518 (421)	2237 (380)	0.058 (0.085)	2274 (380)	2022 (344)	0.059 (0.089)	-0.1	0.917	1
Anterior part of the cingulate gyrus and sulcus (ACC)	5539 (809)	6190 (874)	-0.056 (0.051)	5034 (721)	5622 (766)	-0.056 (0.50)	-0.06	0.952	1
Anterior transverse collateral sulcus	2013 (477)	2009 (434)	-0.001 (0.111)	1824 (440)	1816 (385)	-0.001 (0.11)	-0.01	0.993	1

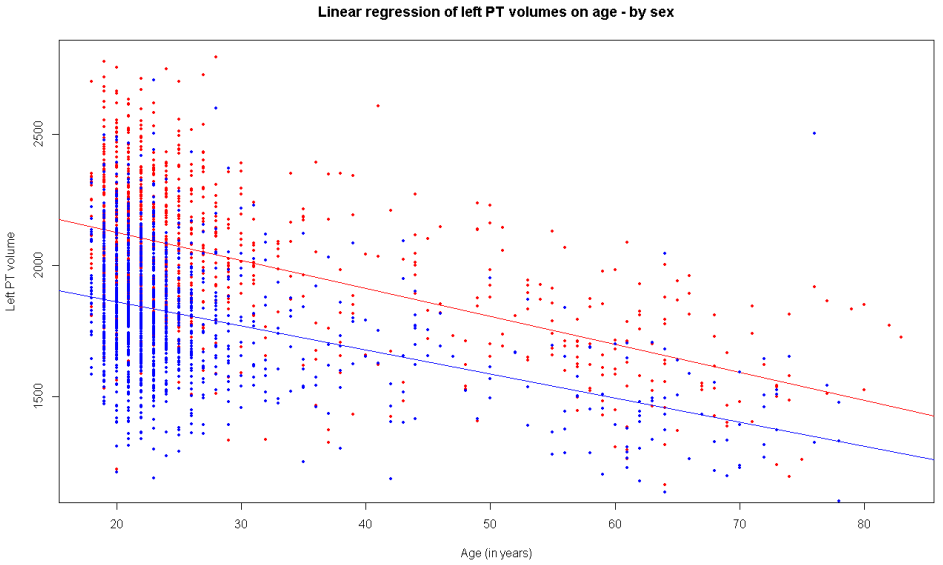

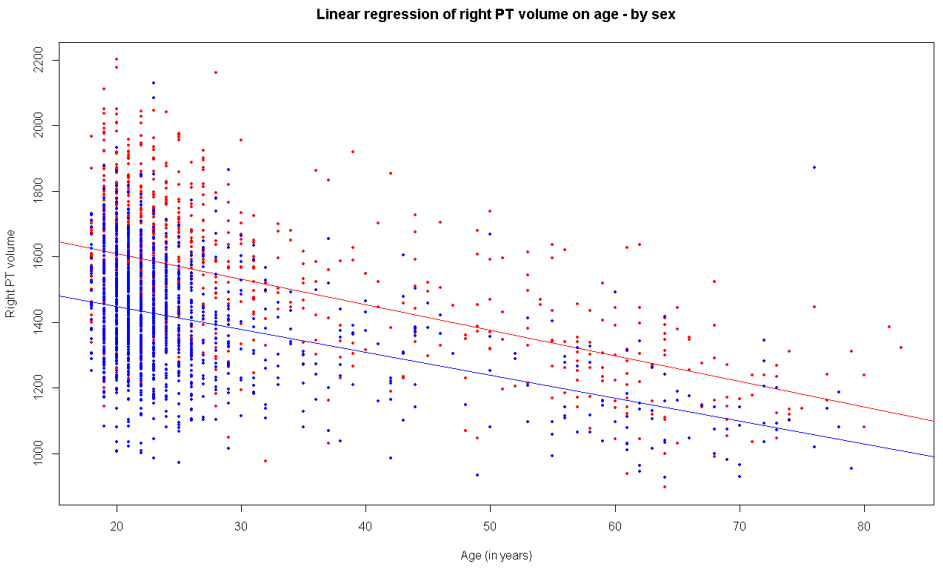

Supplementary Figure S1. Linear regression of age on HO PT volumes (left and right) within the BIG dataset, by sex (males in red, females in blue).

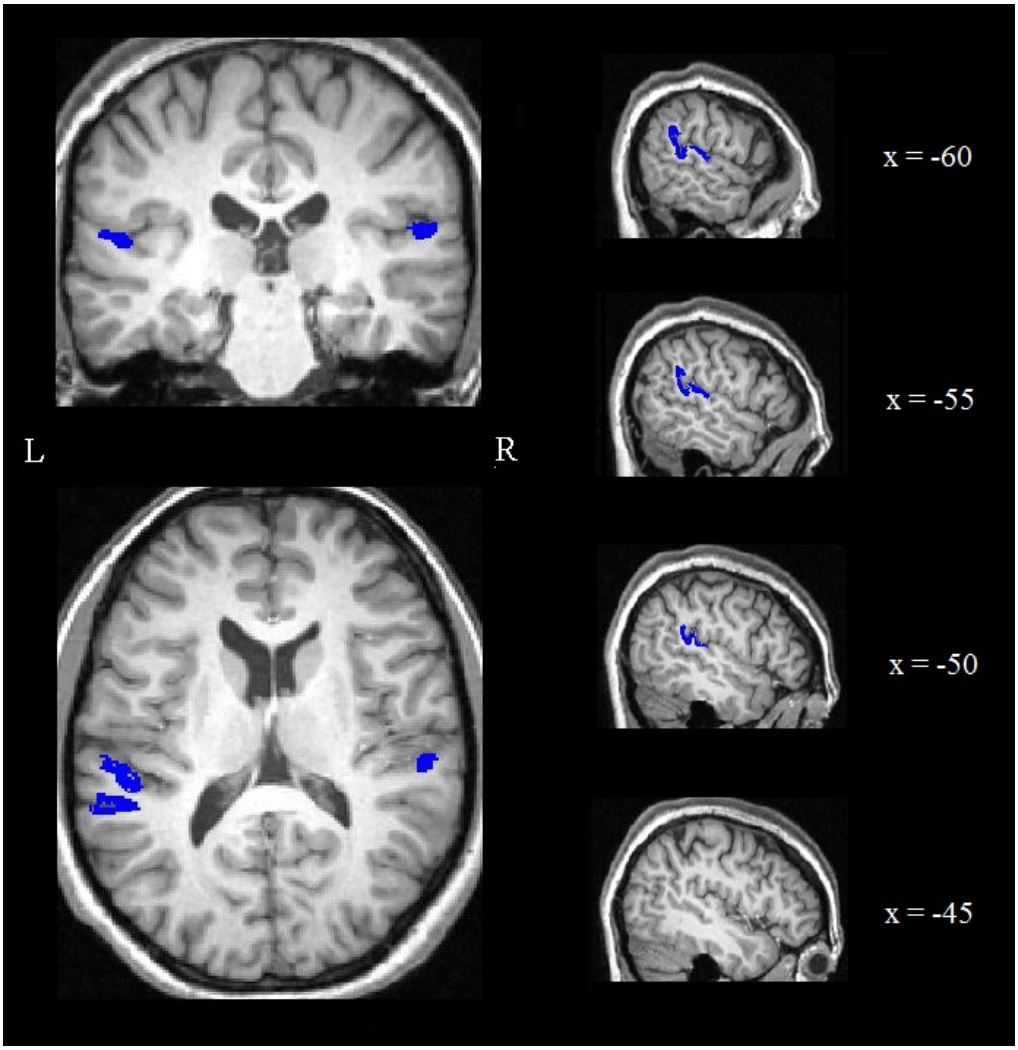

Supplementary Figure S2. The planum temporale as defined with FreeSurfer-Destrieux cortical parcellation, from coronal (top left), axial (bottom left), and sagittal (right) views. The sagittal views show the left hemisphere in 4 different slices. The image is of the same BIG subject as in Figure 1, for whom the FreeSurfer PT AI was 0.0.98 (i.e. close to the BIG average AI of 0.103). The sagittal views make clear the inclusion of the posterior ascending parietal region that is not classically included in neuroanatomical definitions of the PT (see Discussion).

Chapter 4

Measurement and genetics of human subcortical and hippocampal asymmetries in large datasets

Adapted from:

Guadalupe T, Zwiers MP, Teumer A, Wittfeld K, Vasquez AA, Hoogman M, Hagoort P, Fernandez G, Buitelaar J, Hegenscheid K, Voelzke H, Franke B, Fisher SE, Grabe HJ and Francks C. (2014): Measurement and genetics of human subcortical and hippocampal asymmetries in large datasets. Hum Brain Mapp 35(7):3277-89.

Abstract

Functional and anatomical asymmetries are prevalent features of the human brain, linked to gender, handedness and cognition. However, little is known about the neurodevelopmental processes involved. In zebrafish, asymmetries arise in the diencephalon before extending within the central nervous system. We aimed to identify genes involved in the development of subtle, left-right volumetric asymmetries of human subcortical structures using large datasets. We first tested the feasibility of measuring left-right volume differences in such large-scale samples, as assessed by two automated methods of subcortical segmentation (FSL|FIRST and FreeSurfer), using data from 235 subjects who had undergone MRI twice. We tested the agreement between the first and second scan, and the agreement between the segmentation methods, for measures of bilateral volumes of six subcortical structures and the hippocampus, and their volumetric asymmetries. We also tested whether there were biases introduced by left-right differences in the regional atlases used by the methods, by analyzing left-right flipped images. While many bilateral volumes were measured well (scan-rescan r = 0.6 to 0.8), most asymmetries, with the exception of the caudate nucleus, showed lower repeatabilites. We meta-analysed genome-wide association scan results for caudate nucleus asymmetry in a combined sample of 3028 adult subjects but did not detect associations at genome-wide significance ($p < 5*10^{-8}$). There was no enrichment of genetic association in genes involved in left-right patterning of the viscera. Our results provide important information for researchers who are currently aiming to carry out large-scale genome-wide studies of subcortical and hippocampal volumes, and their asymmetries.

Introduction

A bilateral central nervous system (CNS) provides organisms with a basic organizing dimension that has resulted in differences between brain hemispheres in both function and anatomy (Ocklenburg and Gunturkun, 2012). Although CNS asymmetries are found to different extents in arguably all vertebrates, and many invertebrates (Frasnelli et al., 2012), they seem to be pronounced in humans, where evidence points to subtle lateralization being a ubiquitous feature of brain structure and function (Toga and Thompson, 2003).

There has been much research linking neurodevelopmental disorders to departures from normal brain asymmetry, although such links have not been found in all clinical populations. Schizophrenia has been associated with patterns of reduced asymmetry (Berlim et al., 2003; Clark et al., 2010; DeLisi et al., 1997; Hayashi et al., 2012). Language Impairment and Attention Deficit Hyperactivity Disorder can also involve changes in asymmetric development of the brain (Boles and Barth, 2011; de Guibert et al., 2011; Schrimsher et al., 2002; Shaw et al., 2009). While this evidence indicates an important role of lateralization in cognitive development, we still lack knowledge of the genetic mechanisms involved in patterning the normal asymmetries of the human brain, let alone the genetic variants that influence population variability in brain asymmetry.

The best studied animal model of CNS asymmetrical development is the zebrafish, in which early embryonic asymmetries within the diencephalon appear to act as precursors of broader brain asymmetries in subsequent development (Concha et al., 2009). In particular, asymmetric formation of the zebrafish's epithalamus results in differential innervation of the two brain hemispheres, and contributes to their subsequent structural and functional divergence (Concha et al., 2009). This process is linked to genetic and developmental mechanisms that give rise to left-right asymmetry of the viscera (e.g. heart forming to the left side; Concha et al., 2000). Furthermore, molecular asymmetries have been reported in the mouse hippocampus (Hou et al., 2013; Kawakami et al., 2003). In humans, population-level volumetric asymmetries have been reported for the hippocampus, caudate nucleus and thalamus (Alkonyi et al., 2010; Hou et al., 2013; Shi et al., 2009; Watkins et al., 2001; Yamashita et al., 2011). Asymmetries in human subcortical structures and/or hippocampus may therefore play an important role as precursor to broader asymmetrical development of the human brain.

The goal of this study was to identify genetic loci that affect individual differences in subcortical and hippocampal asymmetries in humans, to shed light on the molecular mechanisms involved. We aimed to

use genome-wide association scanning (GWAS) to link common polymorphisms to asymmetries of these structures in adult population samples. GWAS provides a relatively agnostic approach to finding novel genetic effects, and can thus generate new biological insights (Pearson and Manolio, 2008; Visscher et al., 2012). In this study our primary focus was on volumetric asymmetry, the relative difference in volume between the left (L) and right (R) sides of these bilateral structures in the CNS, quantified as an Asymmetry Index (AI) according to the formula AI = 100(L-R)/(L+R). We were particularly interested in structures that showed a population-level asymmetry (i.e. mean AI significantly different from zero), as this would indicate genetically regulated mechanisms of asymmetrical development.

However, GWAS usually requires thousands of study participants pooled from multiple, heterogeneous sources, in order to yield sufficient statistical power to detect the effects of common DNA variants, in the context of massive multiple testing across the genome, and individual genetic effects that are anticipated to be small. This presents the challenge of assessing human brain asymmetry in large datasets from healthy, living subjects. Currently, this can only be achieved indirectly, through sophisticated imaging techniques, and automated methods of quantifying brain structure. Magnetic resonance imaging (MRI) and genome-wide genotyping of common single nucleotide polymorphisms (SNPs) are currently being used for such large-scale genetic studies of human brain structure (Stein et al., 2012).

Moreover, since we were interested in relatively small differences between left and right volumes, we anticipated the stability of individual difference measurement of AIs to be lower than for the absolute left or right volumes. For the purposes of genetic analysis, the repeatability of individual difference measurement in a quantitative phenotype sets an upper limit on the proportion of trait variance that can be attributed to heritable factors. If a large proportion of trait variance is likely to be due to measurement error, or other uncontrolled and non-reproducible factors that differ between MRI scans of the same subject, then the required sample sizes for genetic mapping must be accordingly larger. Therefore, we began by selecting candidate subcortical asymmetry traits for genetic analysis through detailed investigation of the measures produced by two widely-used subcortical segmentation algorithms, FSL|FIRST and FreeSurfer (Fischl et al., 2002; Patenaude et al., 2011). This analysis consisted of testing the robustness of measured asymmetries against methodological biases in left-right flipped brain images, and by analysing the repeatability of variance in these measures across two MRI scans, taken at different time-points from the same set of subjects. In addition, we assessed the repeatability of the measures' residual variance, after correcting for covariates that are typically regressed out of

brain imaging traits prior to GWAS. This would yield a more accurate representation of how repeatable the 'variance of interest' is for genetic studies. In carrying out these analyses we therefore extend the work done by Morey and colleagues on bilateral volumes (Morey et al., 2009; Morey et al., 2010), by testing the ability of the methods to measure variance in subtle left-right differences. Furthermore, we assessed the repeatability of individual difference measurement, which ultimately is the target of genetic analyses, for the bilateral volumes as well as their asymmetries.

We selected the most reliable asymmetry phenotype, that of the caudate nucleus, for genome-wide association scanning with common polymorphisms in three large datasets, followed by genome-wide meta-analysis of association based on the data from all 3028 subjects from the three datasets combined. Anatomically, each caudate nucleus (together with the putamen), receives several projections from the cortex. In turn, these project back to the cortex indirectly via the globus pallidus and thalamus (Draganski et al., 2008; Lehericy et al., 2004). One role of the caudate nucleus has been hypothesized as gating information from the cortex, thus playing a role in cognitive control and behaviour selection (Gil Robles et al., 2005; Grahn et al., 2008). Consistent with this, there is functional evidence showing that the caudate nucleus subserves language processes such as bilingual lexical access (Crinion et al., 2006; Friederici, 2006). Many language functions are relatively left-lateralised in the brains of most people (Knecht et al., 2000; Zatorre et al., 1992). Previous studies have pointed to a rightward volume asymmetry of the caudate nucleus in humans, while reversed patterns of this asymmetry have been reported to associate with attention deficit symptoms in ADHD patients and healthy subjects, pre-natal alcohol exposure, and schizophrenia (Qiu et al., 2009; Schrimsher et al., 2002; Uhlikova et al., 2007; Willford et al., 2010). Therefore, identifying genetic effects on caudate nucleus asymmetry might provide insights into the aetiology of certain subtypes of common neuropsychiatric disorders.

Methods

Participant populations

The Brain Imaging Genetics (BIG) study started in 2007 and is a collection of healthy volunteers, including many university students, who participated in studies at the Donders Centre for Cognitive Neuroimaging (DCCN), Nijmegen, The Netherlands (Franke et al., 2010). At the time of this study, the BIG subject-pool consisted of 2337 self-reported healthy individuals (1248 females), mean age 27.2 years (SD = 12.6), who had undergone anatomical (T1-weighted) MRI scans, usually as part of their

involvement in diverse smaller-scale studies at the DCCN, and who had given their consent to participate in BIG. A subset of 235 subjects had undergone a brain MRI scan at least twice, with at least one day separation between scans. Fifty percent of the 235 re-scans took place within 181 days of the first, with the mean elapsed time being 320 days (SD = 360). At the time of the first scan, their mean age was 24.2 (SD = 7.7). For the genetic analysis, genome-wide SNP genotype data were available from 1276 BIG subjects (see below for genotyping details). Their mean age was 22.9 (SD = 3.8) years, and 748 of these subjects were females.

The Study of Health in Pomerania (SHIP) is an on-going, population-based study in north-east Germany, aimed at describing the prevalence of common diseases and their risk factors. It now consists of two independent datasets: SHIP, and the more recently initiated SHIP-TREND. Participants had undergone a whole-body MRI scan, as well as genotyping for common polymorphisms. For more detailed information about the datasets, see Volzke et al., 2011. For our genetic analyses we were able to include 932 subjects from SHIP (491 females) with a mean age of 56.3 years (SD = 12.4) and 829 subjects from SHIP-TREND (461 females) with a mean age of 49.9 years (SD =13.4).

Image acquisition

MRI data in BIG were acquired with either a 1.5 Tesla Siemens Sonata or Avanto scanner or a 3 Tesla Siemens Trio or TimTrio scanner (Siemens Medical Systems, Erlangen, Germany). Given that images were acquired during several smaller scale studies, the parameters used were slight variations of a standard T1-weighted three-dimensional magnetization prepared rapid gradient echo sequence (MPRAGE; 1.0×1.0×1.0 mm voxel size). The most common variations in the TR/TI/TE/saggital-slices parameters were the following: 2300/1100/3.03/192; 2730/1000/2.95/176; 2250/850/2.95/176; 2250/850/3.93/176; 2250/850/3.68/176; 2300/1100/3.03/192; 2300/1100/2.92/192; 2300/1100/2.96/192; 2300/1100/2.99/192; 1940/1100/3.93/176 and 1960/1100/4.58/176. There was also variation in the number of headcoils used across BIG scans, with the following arrays being employed (and their frequencies): 32-channel (26%), 12-channel (5%), 8-channel arrays (32%) and single headcoil (37%).

For the GWAS sample 634 subjects were scanned at 1.5 Tesla, and 642 subjects at 3 Tesla. Of the 235 double-scanned subjects, 30 were scanned twice at 1.5 Tesla, 70 subjects twice at 3 Tesla, and 135 subjects were scanned at both field strengths.

For the SHIP datasets, all MRI images were obtained on a 1.5 Tesla scanner (Magnetom Avanto; Siemens Medical Systems, Erlangen, Germany). using a standard T1-weighted MPRAGE sequence (TE 1900.0, TR 3.4, Flip angle 15°, 1.0×1.0×1.0 mm voxel size; Hegenscheid et al., 2009).

Segmentation and derivation of measures

A default correction was applied against field inhomogeneities, implemented in the Siemens scanners we employed. In addition, segmentation with FreeSurfer included a bias field correction step. The orientation of the images was extracted directly from the DICOM files which were then converted into nifti format using SPM5's 'spm_dicom_convert' function. To preserve the correct left-right orientation for all subsequent steps, all images were first reoriented to the MNI152 standard using FSL's (version 4.1) 'fslreorient2std' function. FSL|FIRST (version 1.2) segmentation parameters were set according to the ENIGMA (Enhancing Neuro-Imaging Genetics Through Meta-Analysis) protocol, (http://enigma.loni.ucla.edu/protocols/imaging-protocols/), and are listed in Supplementary Table S1. FreeSurfer subcortical segmentations were produced with the standard '-recon-all' processing pipeline and default parameters. From these analyses we extracted left (L) and right (R) volumes of seven paired, bilateral structures; amygdala, nucleus accumbens, caudate nucleus, globus pallidus, putamen, thalamus and hippocampus (see Figure 1 for an example comparison of both segmentation procedures). For each structure, percentage differences between the left and right volumes were expressed as an Asymmetry Index (AI), calculated by the formula AI = 100*(L-R)/(L+R), whose values could range theoretically from -100 to +100, with positive values denoting a larger left structure, negative values a larger right structure, and zero in the case of perfect volume symmetry. Estimates of total brain volume (TBV) were calculated as the voxel-wise sum of the grey matter and white matter probability maps produced by the VBM5.1 toolbox, version 1.19 (http://dbm.neuro.uni-jena.de/vbm/), in SPM5 and with default settings. Exclusion of outlier values (more extreme than 3.5 SD from the mean), correction for covariates and residual extraction, was done with MS Excel (2010) using VBA scripting. In line with imaging genetic association studies (Stein et al., 2012; http://enigma.loni.ucla.edu/protocols/genetics-protocols/), the following covariates were controlled for in subsequent analyses: gender, age, TBV, and field strength (the latter only in BIG). Note that we did not include handedness as a covariate effect on AIs because handedness itself is a partly heritable trait (Medland et al., 2009). Therefore any shared variance of AIs with handedness was important to retain for genetic analysis.

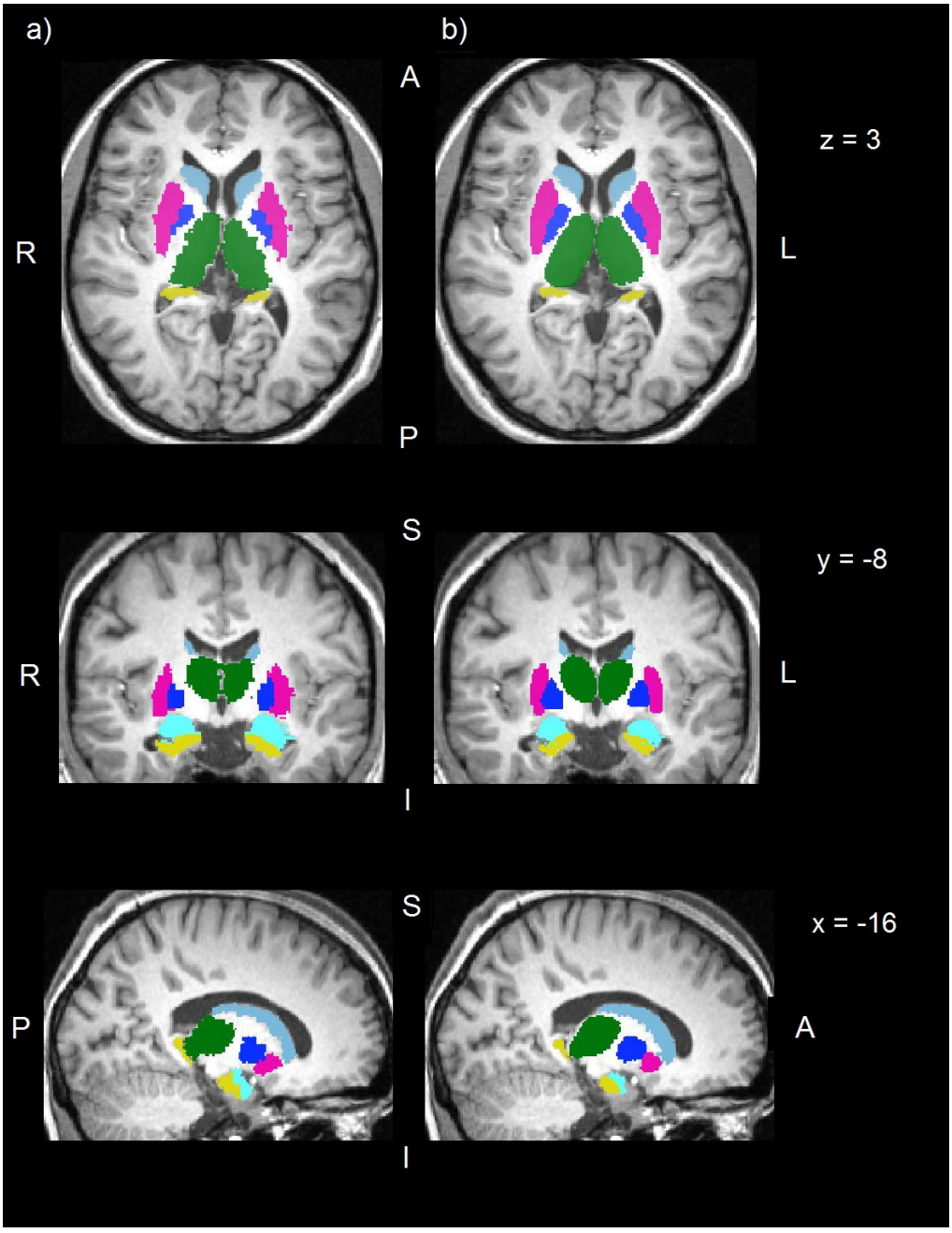
a)
b)
A
P
R
L
z = 3
S
I
R
L
y = -8
S
I
P
A
x = -16

Figure 1. Example segmentation of subcortical structures. The two columns show the segmentation results of the same subject by a) FreeSurfer and b) FSL|FIRST in three different slices.

Left-right flipped image analysis

In simple terms, segmentations done by both FSL|FIRST and FreeSurfer rely on defining structures in the brain while using prior knowledge (probability maps) from sets of manually segmented reference images. To test for possible influences of asymmetries in these probability maps, we randomly selected a subset of 44 BIG subjects and flipped their image data on the left-right axis (without changing the image header), so that the left sided structures would then be segmented according to the software's definition of the right side, and vice versa.

Repeatability analysis

For each structure, we used data from 235 twice-scanned subjects to assess the scan-rescan correlations for the measures of bilateral, summed volumes (L+R), and the AIs. We also analysed the agreement between FSL|FIRST and FreeSurfer outputs for these measures. We employed Pearson correlations to measure the amount of phenotypic variance common to both scan sessions/segmentation methods. In addition, we also included calculations of intra-class correlations using two-way mixed effects models (McGraw and Wong, 1996; Shrout and Fleiss, 1979), to allow a more direct comparison of our results with previous work on segmentation accuracy. These analyses were done in IBM SPSS (v. 20).

Genotyping

Genotyping of BIG was performed using the Affymetrix Genome-Wide Human SNP Array 6.0 (Affymetrix Inc., Santa Clara, CA, USA). Genotype calls were made using the Birdseed algorithm (Rabbee and Speed, 2006). Samples were excluded that had call rates lower than 90% and that showed deviant values of genome-wide heterozygosity (Purcell et al., 2007), as this can indicate the presence of genotyping artifacts. Single nucleotide polymorphisms (SNPs) with a minor allele frequency below 1% or that failed the Hardy-Weinberg equilibrium test at a threshold of $p \leq 10\text{-}6$ were also excluded (Purcell et al., 2007). The resulting markers were then adjusted to the forward strand, as to avoid any ambiguity problems in subsequent steps. A 2-step imputation protocol was followed, in order to use the genotyped set of markers to infer the genotypes at millions of additional positions in the human genome. We used the software MACH for haplotype phasing and minimac for the final imputation (Howie et al., 2012; Li et al., 2010), with the 1000 Genomes Phase 1.v3 EUR reference panel (The 1000 Genomes Project Consortium, 2010). All monomorphic markers were removed from the reference dataset. Individual genotype calls that had an imputation certainty lower than 90% were removed, as were markers with an overall quality

score below 0.3 R2. As a final quality filter, only markers with no more than 5% missing data were selected. At the end of these procedures, genotypes were available for 1276 subjects from BIG, for 6,131,824 SNPs spanning the genome.

Genotyping of the SHIP and SHIP-TREND samples was done on two different platforms, the Affymetrix Genome-Wide Human SNP Array 6.0 and Illumina Human Omni 2.5, respectively. In SHIP the genotype calling was performed with the Birdseed algorithm and samples were excluded with call rates lower than 86%. For SHIP-TREND, calls were done on the GenomeStudio Genotyping Module v1.0, and excluded samples had a call rate lower than 94%. For both samples, markers that failed Hardy-Weinberg equilibrium ($p < 10\text{-}4$) were removed, as well as markers that had more than 20% and 10% missing data in SHIP and SHIP-TREND, respectively. Imputation of non-observed genotypes was performed on both samples separately, but with the same protocol. The reference panel used, as for the BIG sample, was an all polymorphic 1000 Genomes Phase 1.v3 EUR panel (The 1000 Genomes Project Consortium, 2010). A two-step approach was used, performed with the software IMPUTE v2.1.2.3 (Howie et al., 2009). This resulted in genotypes for 17,533,349 markers in 932 subjects for SHIP and 17,585,496 markers in 829 subjects for SHIP-TREND.

GWAS for asymmetry of the caudate nucleus

We carried out GWAS using the Caudate Nucleus AI as a quantitative phenotype, in each of the three datasets separately. The following covariates were controlled for in all three datasets: age, gender and TBV. In addition, scanner field strength was controlled for in BIG (at either 1.5 or 3 Tesla). The association tests were performed using linear regression, as implemented in PLINK v1.07 (Purcell et al., 2007).

GWAS meta-analysis

The GWAS results from the 3 datasets were merged using the 'sample size' approach in the software METAL (Willer et al., 2010). Put briefly, this approach pools the probabilities of a genetic effect at each SNP, across the three contributing studies, and weighted by each study's sample size, while considering the direction of the allelic effect on the quantitative trait. We chose this method because our three populations differed in terms of mean age and other aspects of their recruitment, so that we wished to avoid assuming an equivalence of genetic effect sizes across them. Finally, we considered only results from SNPs that were present in each of the three datasets, resulting in 4,187,195 markers genome-wide.

Genetic candidate pathway analysis

We tested for an enrichment of association between asymmetry of the caudate nucleus and genes involved in left-right visceral determination, using the software INRICH (Lee et al., 2012). Briefly, this approach identifies distinct regions of linkage disequilibrium (LD) in the genome that show association with a trait of interest, below a certain threshold of nominal significance. The regions of LD are mapped to genes, which are assigned to defined biological pathways, processes or groups according to prior gene-functional data. Then, regions of LD are shuffled across genes by permutation, to arrive at an empirical measurement of how often the real-data pattern of association within pathways would be observed by chance alone. This approach is robust to the effect that a gene's or pathway's genomic size has on its probability of containing nominally significant associations. We used the default parameters, with the exception of the following: the flanking regions, for a gene to be considered hit by an interval, were +/- 100 kb, and pathways had to consist of 10 or more genes to enter the analysis.

We used the GWAS meta-analysis as our source of nominal P values ($P \leq 0.001$), in order that our analysis would be maximally powered. A practical constraint that arose from this approach was that we needed to use the LD structure from only one of the datasets (we chose BIG), but there is no reason to expect substantial differences in the genomic distribution of LD between the Dutch and Northern German populations. We used the Gene Ontology (GO; Ashburner et al., 2000) as our source of assignments of genes to biological pathways. We searched the GO annotation file provided with INRICH for pathways involved in visceral left-right asymmetry determination, using the search terms 'symmetry', 'asymmetry', 'left', 'right' and 'left/right'. Six relevant pathways were found, of which one fulfilled the size criterion for association enrichment testing. This pathway was 'Determination of left/right symmetry'.

Results

Volume measures

Table 1 shows the volume measurements and AIs in the three studies, before adjustment for the covariate effects of age, gender, TBV, and field strength (the latter only in BIG). The segmentations of the BIG sample resulted in volumes that were larger than those observed in the SHIP datasets (Table 1). Taken across all structures together, BIG volumes were 10.6% larger for FSL|FIRST segmentations, and 13.3% larger for FreeSurfer, than in SHIP and SHIP-TREND. To investigate whether the differences in age between BIG and SHIP could explain this observed difference in volumes, we modelled the effect of age

on GM and TBV within the BIG sample. We observed linear decreases of GM and TBV with increased age, that resulted in a volumetric reduction of 15% (GM) and 8% (TBV) between the ages of 27 and 53, which are the mean ages of the BIG and SHIP datasets, respectively.

There were notable differences between FSL|FIRST and FreeSurfer in the mean measurements of volumes of some structures. FreeSurfer measures, relative to FSL|FIRST, were greater for the amygdala (19% larger), nucleus accumbens (9% larger), hippocampus (7% larger) and putamen (5% larger). FSL|FIRST yielded greater measures for the globus pallidus (8% larger) and thalamus (7% larger), relative to FreeSurfer.

Almost all structures showed mean AIs that were significantly different from zero for both segmentation methods, with the exception of the amygdala, as segmented by FSL-FIRST, in SHIP and SHIP-TREND (Table 1). The most pronounced deviations from mean AI=0 were observed for the thalamus and nucleus accumbens for the FSL|FIRST segmentations, and for the putamen and globus pallidus for FreeSurfer. These asymmetries were particularly striking, with the mean AI's roughly 1 standard deviation from zero. In the case of the FSL|FIRST measurement of the thalamus, for example, this corresponded to the left structure being assessed 2.5% larger on average than the right.

For each separate structure and method, the direction of the mean shift from AI=0 was largely concordant across the three datasets, with the exception of the FreeSurfer measurements of the nucleus accumbens. For this measure the BIG sample showed the opposite mean shift of AI, relative to SHIP and SHIP-TREND. Discordances between FSL|FIRST and FreeSurfer, in terms of the direction of mean shifts from AI=0, were seen for the thalamus (positive AI with FSL|FIRST in all three studies, and negative AI with FreeSurfer in all three studies), and globus pallidus (negative AI with FSL|FIRST in all three studies, and positive AI with FreeSurfer in all three datasets; Table 1).

Table 1. Means and standard deviations for L and R volumes (in mm^3) and AIs, derived from FSL|FIRST and FreeSurfer in the three study datasets, before correction for covariate effects and standardization.

		FSL|FIRST			FreeSurfer		
		BIG	SHIP	SHIP-T	BIG	SHIP	SHIP-T
Nucleus Accumbens	L	572.5 (117.4)	493.1 (116.5)	516.6 (109.2)	582.4 (120.0)	488.1 (82.2)	498.9 (83.5)
	R	486.1 (109.1)	395 (101)	424.6 (93.1)	622.8 (117.5)	432.9 (80.1)	445.2 (85.4)
	AI	8.4** (8.7)	11.2** (10.2)	9.8** (8.5)	-3.4** (8.7)	6.1** (7.6)	5.9** (7.8)
Amygdala	L	1377.2 (245.8)	1208.3 (215)	1222.3 (202.4)	1581.5 (222.6)	1441.6 (183.4)	1457.9 (183.6)
	R	1375.5 (283.1)	1212.8 (237)	1225.8 (226.5)	1608.0 (212.9)	1518.9 (193.6)	1534.6 (193.7)
	AI	-0.6* (9.7)	0.0 (8.9)	0.1 (8.2)	-0.9** (4.4)	-2.6** (4.2)	-2.6** (4.2)
Caudate Nucleus	L	3786.0 (457.0)	3343.7 (405.5)	3383.7 (407.7)	3881.6 (515.8)	3547.5 (470.5)	3582.3 (468.7)
	R	3879.1 (485.0)	3403.1 (408.9)	3441.7 (412.8)	3926.1 (526.3)	3593.3 (487.1)	3622.6 (481.2)
	AI	-1.3** (2.3)	-0.9** (2.7)	-0.9** (2.4)	-0.6** (2.2)	-0.6** (2.4)	-0.6** (2.3)
Hippocampus	L	3936.8 (446.7)	3681.3 (436.7	3715.2 (438.2)	4338.4 (457.3)	3834.0 (445.4)	3892.3 (437.7)
	R	3971.5 (460.9)	3807.3 (440.1)	3818.6 (422.5)	4380.5 (467.6)	3930.1 (465.1)	3977.0 (445.1)
	AI	-0.5** (4.8)	-1.7** (4.4)	-1.4** (4.3)	-0.5** (2.8)	-1.2** (3.0)	-1.1** (2.9)
Globus pallidus	L	1821.6 (191.6)	1708.4 (223.3)	1709.5 (202.4)	1844.0 (261.9)	1614.5 (232.8)	1643.5 (234.1)
	R	1847.4 (188.4)	1744.3 (219.4)	1743.5 (202.1)	1658.2 (235.4)	1465.2 (220.3)	1496.9 (225.0)
	AI	-0.7** (3.4)	-1.1** (3.9)	-1.0** (3.9)	5.2** (4.6)	4.9** (4.5)	4.7** (4.6)
Putamen	L	5276.2 (583.6)	4816 (599.66)	4876.9 (588.2)	5812.1 (720.0)	4932.3 (652.1)	4993.9 (671.8)
	R	5286.8 (585.4)	4748.2 (578.3)	4796.8 (575.3)	5538.5 (694.1)	4766.2 (636.9)	4824.5 (652.3)
	AI	-0.1* (2.6)	0.7** (2.9)	0.8** (2.8)	2.4** (2.1)	1.7** (2.6)	1.7** (2.7)
Thalamus	L	8437.3 (779.8)	7554.2 (802.1)	7680.5 (836.5)	7607.2 (933.2)	6990.5 (887.9)	7139.2 (942.1)
	R	8242.5 (772.4)	7357 (803.8)	7478.0 (818.3)	7718.7 (942.2)	7205.7 (936.9)	7369.8 (981.2)
	AI	1.2 **(1.6)	1.3** (1.7)	1.3** (1.7)	-0.8** (2.8)	-1.5** (2.7)	-1.6** (2.8)
N		2330	1057	1905	2330	1120	2092

Mean AI is significantly different from 0 ($p<0.05$; ** $p<0.005$)

Flipped image analysis

Forty-four subjects randomly drawn from BIG were analysed both before and after left-right flipping of their input images into segmentation. As expected, the 'un-flipped' AI means for these 44 subjects (Table 2) were representative of those for the whole BIG dataset (2337 subjects; Table 1), although not all AIs showed a statistically significant mean shift from 0 in this relatively small subset (Table 2). The mean shift from zero of the AI was reversed or cancelled in the flipped images, compared to non-flipped images, for the caudate nucleus as segmented by FSL|FIRST, and for the amygdala, caudate nucleus, globus pallidus and thalamus as segmented by FreeSurfer (Table 2). Other structures including the nucleus accumbens (for the FSL|FIRST and FreeSurfer segmentations) and the thalamus (for the FSL|FIRST segmentation) failed to reverse the direction of their mean AI shift from zero in flipped images, as compared to non-flipped images (Table 2).

Table 2. Means and standard deviations of AIs in a subset of 44 BIG subjects, for both the original and left-right flipped images. In bold are the values that show an appropriate sign change when input images were flipped.

	FSL|FIRST		FreeSurfer	
	Original	Mirrored	Original	Mirrored
Nucleus Accumbens	8.0 (9.5)*	5.8 (10.4)*	-2.4 (6.5)*	-7.7 (6.0)*
Amygdala	0.2 (9.0)	-0.7 (13.0)	***-1.8 (3.9)****	***1.9 (4.6)****
Caudate Nucleus	***-0.9 (2.1)****	***2.0 (2.9)****	***-0.8 (2.3)****	***0.2 (2.1)***
Hippocampus	0.5 (3.9)	-1.6 (4.3)*	0.1 (2.6)	1.0 (2.6)*
Globus pallidus	-0.4 (3.5)	-1.6 (2.9)*	***5.4 (4.1)****	***-0.2 (5.2)***
Putamen	-0.0 (2.4)	1.0 (2.6)*	2.6 (1.9)*	2.0 (1.9)*
Thalamus	1.3 (1.4)*	2.3 (1.7)*	***-1.0 (2.4)****	***1.9 (2.2)****

*Mean AI is significantly different from 0 at $p<0.05$

Repeatability analysis

Within the 235 BIG subjects who had been scanned twice, we used Pearson correlations to assess the agreement between the first and second scans for bilateral volumes (L+R), as well as the residual bilateral volumes after correcting for the covariate effects (Table 3). These covariate effects are typically regressed out prior to genetic analysis of brain volumetric measures (Stein et al., 2012) and results of these regressions can be found in Supplementary Table S2. Overall, there was a decrease in scan-rescan correlations for the residuals, as compared to the unadjusted volumes, for both FSL|FIRST and FreeSurfer (Table 3). This was particularly pronounced for the thalamus as segmented by FSL|FIRST, for which the scan-rescan correlation dropped from 0.907 (unadjusted bilateral volume) to 0.664 (adjusted bilateral volume), meaning that 44% of the variance in this residualized measure was shared between first and second scan. For FreeSurfer measures of bilateral volumes, four of the structures (nucleus accumbens, amygdala, globus pallidus and thalamus) showed scan-rescan correlations that were lower than 0.6, after adjustment for covariate effects. This means that less than 36% of the variance in these residualized measures was shared between first and second scans. When subjects were scanned twice using the same scanner (either 1.5T or 3T) the repeatabilities were slightly higher than when subjects were scanned once at 1.5T and once at 3T. However, we did not have sufficient power to test the significance of these subtle differences in within-scanner and between-scanner correlation coefficients (see Supplementary Table S3).

Table 3. Repeatability (Pearson r between first and second MRI scan measures), based on 235 BIG subjects, for summed bilateral volumes (L+R), before and after adjustment for covariate effects of gender, age, total brain volume, and field strength.

	FSL|FIRST		FreeSurfer	
	Raw volumes	Adjusted volumes	Raw volumes	Adjusted volumes
Nucleus Accumbens	.685**	.670**	.639**	.546**
Amygdala	.574**	.650**	.714**	.559**
Caudate Nucleus	.944**	.798**	.926**	.810**
Hippocampus	.873**	.795**	.775**	.645**
Globus pallidus	.862**	.693**	.717**	.589**
Putamen	.898**	.774**	.873**	.717**
Thalamus	.907**	.664**	.774**	.555**

** Significance of the correlation p<0.005

We also used the 235 twice-scanned BIG subjects to correlate the AIs between the first and second scans for each structure, as well as the residual, standardized AIs after adjusting for the covariate effects (Table 4). Overall, the scan-rescan correlations for AIs (Table 4) were lower than those for the bilateral volumes. Nonetheless, the AIs of the caudate nucleus, hippocampus, and thalamus, as segmented with FSL|FIRST, showed scan-rescan correlations higher than 0.6 (Table 4). None of the FreeSurfer AIs showed scan-rescan correlations greater than 0.5 (Table 4). In addition, we also tested the absolute agreement of bilateral volumes (L+R) and AI's, between the first and second scans, using intra-class correlations (ICC), results of this analysis can be seen in Supplementary Table S4.

Table 4. Repeatability (Pearson r between first and second MRI scan measures), based on 235 BIG subjects, for AIs, before and after adjustment for covariate effects of gender, age, total brain volume, and field strength.

	FSL|FIRST		FreeSurfer	
	Raw AI	Adjusted AI	Raw AI	Adjusted AI
Nucleus Accumbens	.570**	.570**	.260**	.350**
Amygdala	.570**	.542**	.370**	.398**
Caudate Nucleus	.647**	.652**	.441**	.454**
Hippocampus	.632**	.626**	.507**	.482**
Globus pallidus	.562**	.560**	.088	.091
Putamen	.446**	.528**	.291**	.313**
Thalamus	.614**	.609**	.183**	.188**

** Significance of the correlation p<0.005

Correlations between measures derived from FSL|FIRST and FreeSurfer

Using only data from the first scan of the 235 twice-scanned BIG subjects, we assessed the agreement between FSL|FIRST and FreeSurfer in terms of measuring individual differences in bilateral volumes and

AIs for each structure, both before and after adjustment for covariate effects (Table 5). The bilateral volume of the caudate nucleus stood out as being reliably measured across the two methods (r=0.855 after adjustment for covariates), while the bilateral volumes of the hippocampus and putamen also showed inter-method correlations greater than 0.6 after adjustment for covariate effects (Table 5). The AIs generally showed low agreement between FSL|FIRST and FreeSurfer (Table 5), with the caudate nucleus AI proving to be the most consistent between the two methods (r=0.392 after adjustment for covariates). The same pattern of results is also found when assessing intra-class correlations of consistency, between FSL|FIRST and FreeSurfer, for measures of bilateral volumes and AI's (see Supplementary Table S5).

Table 5. Agreement between FSL-FIRST and FreeSurfer (Pearson r), based on 235 BIG subjects, for summed bilateral volumes (L+R), and AIs (100(L-R)/(L*R)), before and after adjustment for covariate effects of gender, age, total brain volume, and field strength.

	FSL|FIRST and FreeSurfer			
	Raw Volumes	Adjusted volumes	Raw AI	Adjusted AI
Nucleus Accumbens	.377**	.327**	.090	.165*
Amygdala	.177**	.125	.094	.113
Caudate Nucleus	.894**	.855**	.357**	.392**
Hippocampus	.692**	.609**	.217**	.210**
Globus pallidus	.688**	.529**	.119	.127
Putamen	.785**	.668**	.094	.122
Thalamus	.764**	.501**	-.011	.009

* Significance of the correlation p<0.05; ** Significance of the correlation p<0.005

Genetic analysis

GWAS meta-analysis of the caudate nucleus AI (FSL|FIRST), for which we merged genetic association data across the three study datasets for each of 4,187,195 SNPs spanning the genome, did not identify an individual association that surpassed the commonly applied significance threshold for GWAS of P=5*10-8 (Figure 2). The most significant individual locus was rs75553296 (P = 1.4* 10-6) on chromosome 16q32.1, which is 80 kilobases upstream of the gene NUDT7. This gene encodes a protein member of the Nudix hydrolase family which eliminates potentially toxic nucleotide metabolites from the cell, and regulates the concentrations and availability of many different nucleotide substrates, cofactors, and signaling molecules [RefSeq; http://www.ncbi.nlm.nih.gov/nuccore/343887371].

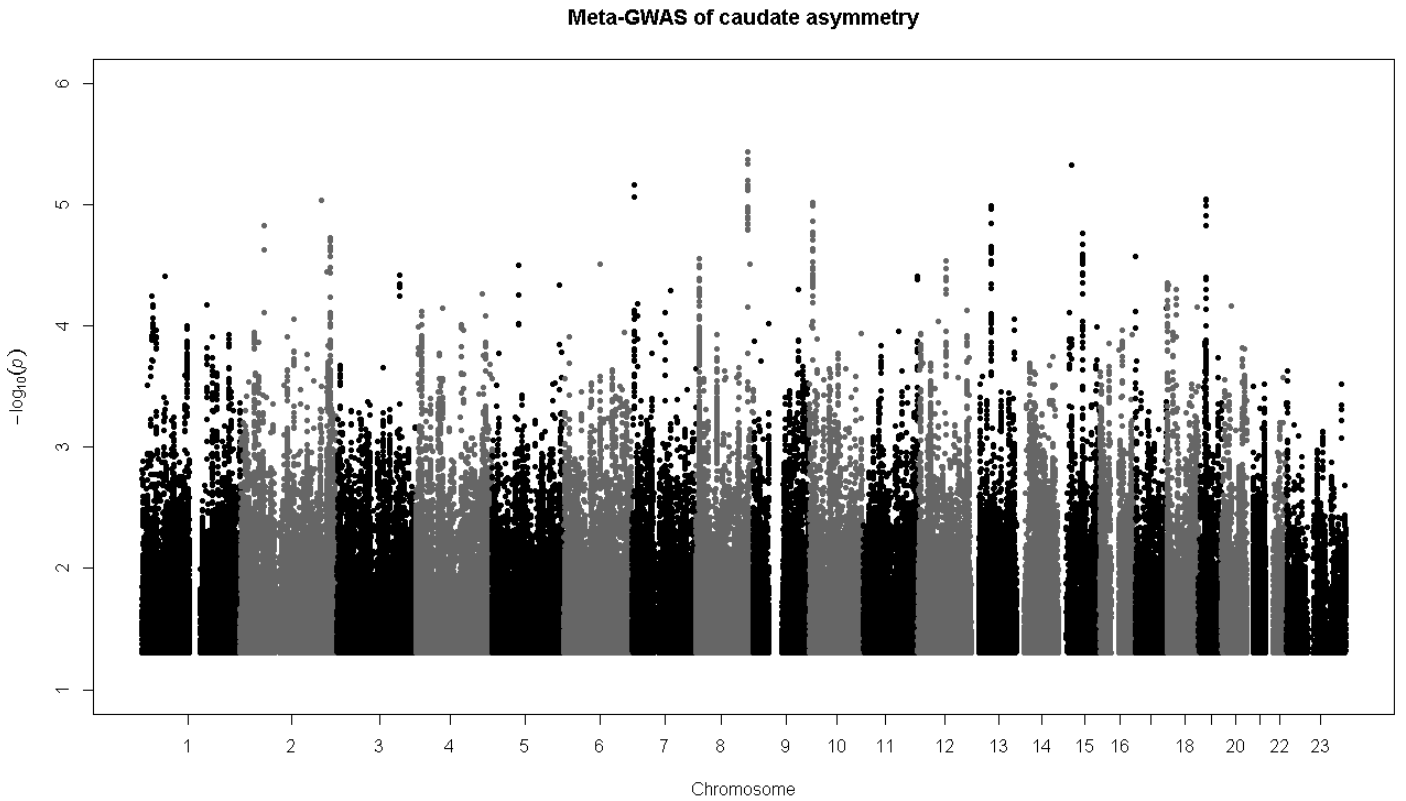

Figure 1: Meta-GWAS of caudate nucleus asymmetry (FSL|FIRST). The X-axis represents each of the chromosomes arranged from end-to-end, from p arm to q arm, in ascending numerical order from left to right. The Y-axis represents the pointwise significance of association with caudate AI (Plotted only nominal $p < 0.05$). Colours and shades distinguish SNPs from different chromosomes.

There was no significant enrichment of association within genes involved in visceral left-right axis determination. Of the 36 genes assigned to this Gene Ontology pathway, none individually contained SNPs that showed association with the caudate nucleus AI at nominal P<0.001.

Discussion

Automated methods of segmenting brain structures from T1-weighted MRI images are currently the most feasible option for performing large scale, genome-wide association analysis of human brain morphology. Such analysis requires thousands of participants and in practice must usually be based on pooled data, or meta-analysed data, from multiple, separate sources. GWAS studies of subcortical and hippocampal volumes, and their volumetric asymmetries, are already underway (Bis et al., 2012; Renteria et al., 2011; Renteria et al., 2012; Sleiman et al., 2012; Stein et al., 2012). In this study we performed an investigation of candidate phenotypes for large-scale genetic studies of subcortical and hippocampal volumes and their asymmetries, evaluating results from two widely used segmentation software packages. Our results can contribute to on-going, consortium-based genetic studies, as regards the choices of measures to be pursued for genetic analysis, and/or the interpretation of genetic findings that arise for particular measures.

The mean volume measurements for various structures differed between our study datasets, and between segmentation methods. We showed that the larger volumes measured in the BIG dataset, as compared to the SHIP datasets, were as expected given the average ages of the different collections (Good et al., 2001; Sherwood et al., 2011). However, we cannot exclude the possibility that other, uncontrolled differences in study protocol or image acquisition may also have had minor contributions to the differences in mean volumes between the datasets.

The mean volume differences between the two segmentation methods, for example for the hippocampus (larger with FreeSurfer) and thalamus (larger with FSL), are likely to have arisen from differences in the anatomical definitions of the regions in the probability maps used by the two programs, as well as from differences in the segmentation algorithms, including differences in the weighting of the prior probability maps (Fischl et al., 2002; Patenaude et al., 2011).

Regardless of systematic differences in mean volume measurements between studies and segmentation methods, it is important to note that, for the purposes of genetic analysis, the focus is on the relative individual differences between subjects, and how accurately these can be determined. Therefore our focus for repeatability analysis, either using double-scanned subjects to evaluate the segmentation

methods, or for comparing the two segmentation methods against each other, was on the correlation of measured variance, and not on the accuracy of mean volume measurement.

For bilateral volumes (L+R), which are currently the focus of consortium GWAS in tens of thousands of subjects (Bis et al., 2012; Ikram et al., 2012; Stein et al., 2012), our data showed good repeatability across scans for the larger volumes in the uncorrected analysis, although repeatability was somewhat reduced after adjustment for the covariate effects of gender, age, total brain volume and scanner field strength. For many structures, with either segmentation method, scan-rescan correlations of covariate-adjusted bilateral volumes were less than 0.7, which corresponds to 49% of trait variance being shared from first to second scan. The heritable proportion of variance in these measures is likely to be lower. Our results clearly underscore the necessity of meta-analyzing data from thousands of individuals to obtain sufficient power for GWAS studies of these traits. Before correction for covariate effects, the repeatabilities of bilateral volume measurements were comparable, but slightly lower, than those reported previously in smaller samples (Morey et al., 2009; Morey et al., 2010). This is likely to be due to our use of a more heterogeneous sample in terms of scanning parameters, which have been previously found to have a subtle effect on the repeatability of volumetric measurements (Wonderlick et al., 2009). Our finding of a greater reliability for segmentation of larger structures compared to smaller ones is in agreement with a previous report (Nugent et al., 2012; Wonderlick et al., 2009).

For AIs, which are also now beginning to be investigated in the context of genetic mapping (Renteria et al., 2011), the first step was to identify structures for which we could reliably detect a population-level bias in the direction of their asymmetry, as this would suggest the presence of regulated genetic/developmental mechanisms in generating such a bias. While several structures seemed to show population-level asymmetry at face value (i.e. having a mean AI that differed significantly from zero), not all structures were consistent between the two segmentation methods in the direction of this mean shift, and some failed to show a reversed mean shift after left-right flipping of the T1 images. Together, these observations indicate that, for some structures, the methods were affected by different asymmetries that existed in their prior probability maps. One possibility is that there was not always enough tissue contrast in the input images to define some structures clearly (Nugent et al., 2012). Another possibility, that has not been investigated to our knowledge, is that subtle differences in shape between the left- and right-sided structures did not allow proper segmentation of left-right flipped images. In either case, the segmentations would ultimately be weighted more on the algorithms' prior information. The algorithms both rely on atlases constructed from manual segmentations (considered

the gold standard), and there is in fact evidence of systematic left-right bias also in manual segmentations (Maltbie et al., 2012). The caudate nucleus stood out as the only structure showing a reversed mean shift of AI in the flipped images for both segmentation methods, as well as a close agreement between methods in the direction and magnitude of mean AI. This made us confident that the mean left-right asymmetry of the caudate nucleus was driven mostly by the images, and not by the prior probability maps for this structure, and that the caudate nucleus therefore showed a real population-level asymmetry in our study datasets.

For all structures, the scan-rescan correlations of AIs were lower than those for summed, bilateral volumes (L+R). This was not surprising, as the volumetric differences between left and right sides were equivalent to only small proportions of the structures' overall volumes. Clearly the repeatability of AI individual difference measurement is dependent on the presence of true and variable asymmetries in the images. Poor repeatability of AIs may arise when individual differences are very subtle, in which case the AIs will predominantly reflect error variance. The scan-rescan analysis again supported the caudate nucleus as showing the most robustly assessed asymmetry. This structure had the highest scan-rescan correlations for raw and covariate-adjusted volumes, regardless of the segmentation method. Furthermore, in the correlation analysis of measures produced by FSL|FIRST with those produced by FreeSurfer, it was again the caudate nucleus that showed the best agreement between the two methods, for bilateral volumes and AIs. This is in agreement with the results of (Wonderlick et al., 2009), where the measures of caudate volume also showed robustness against variability in image acquisition. This is likely due to the caudate showing clear tissue contrasts with the neighbouring white matter and cerebrospinal fluid.

In general, FSL|FIRST showed slightly higher scan-rescan correlations than FreeSurfer, both for bilateral volumes and AIs (and the covariate-adjusted residuals derived from them). It is difficult to draw general conclusions from our study on the relative merits of FSL|FIRST and FreeSurfer for supporting genetic analysis of subcortical structures, as the heterogeneity of scan acquisition parameters in the 235 twice-scanned subjects from BIG may have affected the two methods' performance in different ways. However, this heterogeneity was a valid representation of the reality that is commonly encountered in pooled datasets for large-scale genetic association studies, which require thousands of participants from multiple sources (Stein et al., 2012). Our data are therefore informative in this 'real-world' context.

We are already contributing data from the BIG and SHIP datasets to consortium GWAS analysis of bilateral subcortical volumes, which will be reported elsewhere. Here we focussed on genetic analysis of

the most reliably measured subcortical asymmetry in our datasets, that of the caudate nucleus. The fact that the caudate nucleus showed a consistent, population-level asymmetry in all studies, and with both segmentation algorithms, which also reversed correctly in flipped images, suggests strongly that caudate nucleus asymmetry is real and that at least part of this trait is genetically regulated. Our GWAS meta-analysis of caudate nucleus AI (FSL-FIRST), based on 3028 subjects, resulted in no marker reaching statistical significance. We conclude that GWAS meta-analysis of more datasets will be required to detect individually significant genetic effects on this trait. We found no evidence from our genetic pathway analysis that genes involved in left-right visceral axis determination affect caudate nucleus asymmetry. However, although the caudate nucleus AI was the most reliably measured asymmetry, there was only a modest agreement between FSL-FIRST and FreeSurfer in terms of measuring the individual differences between subjects. This suggests that disagreements in the exact neuroanatomical definitions of the structure exist within the atlases used by the two methods, which can only be resolved through detailed neuroanatomical investigation.

To conclude, GWAS studies of quantitative traits in the general population usually assume that many common genetic variants will each have small individual contributions. The statistical correction needed, to account for multiple testing across the whole genome, results in having to gather large numbers of subjects (in the thousands) to achieve reasonable statistical power. Brain imaging genetics is a growing field that will depend crucially on automated methods of image segmentation and analysis. In this paper we highlight the importance of careful, prior assessment of trait properties and reproducibility for such large scale studies. Our findings can contribute to future research on subcortical and hippocampal volumes and their asymmetries, and indicate in particular that the caudate nucleus is a promising structure to investigate further in this context, with larger sample sizes.

Acknowledgements

This work makes use of the BIG (Brain Imaging Genetics) database, first established in Nijmegen in 2007. This resource is now part of Cognomics, a joint initiative by researchers of the Donders Centre for Cognitive Neuroimaging, the Human Genetics and Cognitive Neuroscience departments of the Radboud University Medical Centre and the Max Planck Institute for Psycholinguistics. The Cognomics Initiative is supported by the participating departments and centres and by external grants, i.e. the Biobanking and Biomolecular Resources Research Infrastructure (Netherlands) (BBMRI-NL), the Hersenstichting Nederland and the Netherlands Organisation for Scientific Research (NWO). We wish to thank all persons who kindly participated in this research.

The SHIP datasets are part of the Community Medicine Research net (CMR) of the University of Greifswald, which is funded by the German Federal Ministry of Education and Research and the German Ministry of Cultural Affairs, as well as by the Social Ministry of the Federal State of Mecklenburg–West Pomerania. Genome-wide data and MRI scans were supported by the Federal Ministry of Education and Research and a joint grant from Siemens Healthcare, Erlangen, Germany, and the Federal State of Mecklenburg–West Pomerania. The University of Greifswald is a member of the Center of Knowledge Interchange program of the Siemens AG and the Caché Campus Program of the InterSystems GmbH. The SHIP authors are grateful to Mario Stanke for the opportunity to use his Server Cluster for the SNP imputation.

Appendix

Supplementary material

Supplementary Table S1**.** Changes to the default parameters in FSL|FIRST used to comply with the ENIGMA protocol

-cost normmi
-searchrx -180 180
-searchry -180 180
-searchrz -180 180

Supplementary Table S2. Table of coefficients from covariate regression analysis. Scanner and Gender were treated as dichotomous variables and the coefficients indicate the relative effect of 3T (compared to 1.5T) and females (compared to males) in measures of volume (in mm^3) and AI. Age and TBV were scalar variables and their effect on volumes and AI is expressed in standardized coefficients.

Vols	**FSL**				**FreeSurfer**			
	Scanner	Gender	Age	TBV	Scanner	Gender	Age	TBV
Nucleus Accumbens	-126.7**	-2.0	-0.178**	0.446**	38.5**	-47.1**	-0.274**	0.320**
Amygdala	-242.1**	-10.6	0.193**	0.339**	261.7**	-137.6**	-0.017	0.500**
Caudate Nucleus	50.8	-43.4	-0.203**	0.515**	-140.2**	-100.3*	-0.145**	0.516**
Hippocampus	63.6*	-13.9	0.023	0.507**	267.6**	24.9	-0.006	0.577**
Globus Pallidus	7.6	-142.9**	0.079**	0.501**	-74.1**	-197.3**	-0.211**	0.441**
Putamen	-102.9**	-467.2**	-0.125**	0.511**	19.5	-637.1**	-0.304**	0.422**
Thalamus	-297.5**	-77.6*	-0.060**	0.729**	-554.8**	-592.8**	-0.115**	0.603**
Asy	**FSL**				**FreeSurfer**			
	Scanner	Gender	Age	TBV	Scanner	Gender	Age	TBV
Nucleus Accumbens	1.5**	-0.5	0.100**	-0.012	-6.7**	-2.0**	0.089**	0.013
Amygdala	-1.4**	0.2	0.038	0.063*	1.0**	-0.4	-0.093**	-0.022
Caudate Nucleus	-0.2	0.2	0.033	-0.012	0.5**	0.3*	-0.013	-0.030
Hippocampus	0.3	0.0	-0.033	-0.002	-0.4**	-0.5**	-0.076**	-0.057*
Globus Pallidus	0.6**	0.0	0.055*	-0.028	1.7**	-0.3	-0.005	-0.002
Putamen	-1.3**	0.2	0.041	0.022	0.5**	0.3*	0.050*	0.097**
Thalamus	-0.1	0.0	0.032	-0.025	0.3*	0.1	-0.060*	-0.035

Supplementary Table S3. Scan re-scan correlations for bilateral volume residuals per scanner field strength and method

	FSL|FIRST			**FreeSurfer**		
	1.5T	3T	across	1.5T	3T	across
Nucleus Accumbens	.627**	.673**	.688**	.357	.688**	.480**

Amygdala	.751**	.578**	.662**	.728**	.578**	.516**
Caudate Nucleus	.855**	.860**	.740**	.851**	.857**	.775**
Globus Pallidus	.794**	.722**	.651**	.611**	.634**	.582**
Hippocampus	.810**	.866**	.747**	.637**	.754**	.584**
Putamen	.859**	.832**	.727**	.682**	.783**	.694**
Thalamus	.741**	.714**	.613**	.683**	.620**	.511**

Supplementary Table S4. ICCs for measures of volume. Scan-rescan ICCs are calculated based on absolute agreement. ICCs for between method comparison are based on consistency.

	Scan-rescan		**Between-method**
	FSL|FIRST	FreeSurfer	FSL and FS
Nucleus Accumbens	0.68	0.61	0.375
Amygdala	0.575	0.715	0.173
Caudate Nucleus	0.944	0.91	0.888
Hippocampus	0.873	0.736	0.69
Globus Pallidus	0.862	0.707	0.67
Putamen	0.898	0.873	0.78
Thalamus	0.907	0.764	0.752

Supplementary Table S5. ICCs for measures of AI. Scan-rescan ICCs are calculated based on absolute agreement. ICCs for between method comparison are based on consistency.

	Scan-rescan		**Between-method**
	FSL|FIRST	FreeSurfer	FSL and FS
Nucleus Accumbens	0.571	0.251	0.089
Amygdala	0.566	0.37	0.061
Caudate Nucleus	0.648	0.442	0.354
Hippocampus	0.633	0.501	0.185
Globus Pallidus	0.56	0.088	0.114
Putamen	0.447	0.288	0.092
Thalamus	0.615	0.183	-0.009

Chapter 5

Subcortical human brain asymmetries in 15,847 people worldwide reveal effects of age and sex

A revised version has been published as:
Guadalupe T, Mathias SR, van Erp TGM, Whelan CD, Zwiers MP, Abe Y, Abramovic L, Agartz I, Andreassen OA, Aribisala BS and 150 others. (2016): Subcortical human brain asymmetries in 15,847 people worldwide reveal effects of age and sex. Brain Imaging and Behavior. doi: 10.1007/s11682-016-9629-z

Abstract

The two hemispheres of the human brain differ functionally and structurally. Despite over a century of research, the extent to which brain asymmetry is influenced by sex, handedness, age, and genetic factors is still controversial. Here we present the largest ever meta-analysis of subcortical brain asymmetries. Volumetric asymmetry of seven subcortical structures was assessed in 15,847 MRI scans from 52 datasets worldwide. There were sex differences in the asymmetry of the globus pallidus, putamen, and thalamus. Heritability estimates, derived from 1170 subjects belonging to 71 extended pedigrees, revealed that additive genetic factors influenced the asymmetry of these three structures, and hippocampus. Handedness had no detectable effect on subcortical asymmetries, even in this unprecedented sample size, but the asymmetry of the nucleus accumbens, amygdala, and putamen varied with age. Genetic drivers of asymmetry in the hippocampus, basal ganglia, and thalamus may affect variability in human cognition, including susceptibility to psychiatric disorders.

Introduction

Left–right differentiation of the central nervous system (CNS) results in anatomical, functional, and behavioral asymmetries in many organisms (Ocklenburg and Gunturkun, 2012). Humans are no exception: functions including language, visuospatial cognition, and hand–motor control are asymmetrically organized between hemispheres in a typical human brain (Haaland and Harrington, 1996; Mellet et al., 2014). At the population level, these asymmetries show clear directional biases, or lateralizations (Bryden, 1982). Handedness is the most overt example: around 90% of people have a right-hand preference, a strong bias not seen in other species including our closest evolutionary relatives, the apes (Hopkins et al., 2011).

Functional and structural lateralization of the human brain may be influenced by left-right differences in gene expression (Francks, 2015), as recently demonstrated in language-related regions of the adult superior temporal cortex (Karlebach and Francks, 2015). Even so, lateralization varies markedly across individuals. Women and men show average differences in asymmetry, as well. Men show, on average, more pronounced asymmetries in superior temporal language regions of the cerebral cortex than women, based on brain magnetic resonance imaging (MRI) data from over 3,000 people (Guadalupe et al., 2015). Genes involved in steroid hormone biology may affect the degree of lateralization in both men and women (Guadalupe et al., 2015). Another trait linked to cerebral lateralization is handedness (Willems et al., 2014): the largest study of cerebral cortical structural differences by handedness showed weak associations with changes in surface area of the left precentral sulcus (Guadalupe et al., 2014a), consistent with prior reports (Amunts et al., 1996; Foundas et al., 1998). Left-handers have a slightly higher incidence of atypical functional hemispheric language dominance (Mazoyer et al., 2014). Alterations of cerebral cortical lateralization have also been linked to cognitive and psychiatric disorders, including language-related impairments (Altarelli et al., 2014; Herbert et al., 2005), autism (Eyler et al., 2012; Herbert et al., 2005), schizophrenia (SCZ; Oertel-Knochel et al., 2012), and substance-use disorders (Balconi and Finocchiaro, 2015).

In contrast to the cerebral cortex, lateralizations of human subcortical structures and the hippocampus have not been well studied, nor the factors that might affect their individual differences or roles in lateralized cognition. Most investigations have been in clinical contexts, where differences between cases and controls in asymmetry patterns of subcortical structures have been linked to various neuropsychiatric disorders. For example, abnormal asymmetries in the basal ganglia, particularly of the globus pallidus and caudate nucleus, have been observed in cases of attention-deficit/hyperactivity

disorder (ADHD; Hynd et al., 1993), and in developmental stuttering and Tourette's syndrome (TS; Foundas et al., 2013; Singer et al., 1993). Abnormal asymmetry of the striatum has been linked to prenatal alcohol or methamphetamine exposure (Roos et al., 2014; Willford et al., 2010). Changes in thalamic asymmetry have been found in cases of TS (Lee et al., 2006) and SCZ (Zhou et al., 2003). Regarding limbic system structures, studies of major depression (Xia et al., 2004), obsessive-compulsive disorder (Szeszko et al., 1999), SCZ (Niemann et al., 2000), anorexia nervosa (Titova et al., 2013), and age-related memory impairment (Soininen et al., 1994) have shown abnormal asymmetries of the hippocampus, which in patients with temporal lobe epilepsy also included the amygdala (Cendes et al., 1993). Abnormal asymmetries of the amygdala have also been reported in SCZ (Niu et al., 2004) and in cocaine addiction (Makris et al., 2004). Some of these disorders differ in their prevalence between sexes and by handedness (Castellanos et al., 2001; DeLisi et al., 2002; Niemann et al., 2000). Interestingly, sex differences in subcortical asymmetries have been suggested to have an etiological role in TS (Zimmerman et al., 2000) and SCZ (Niu et al., 2004). These findings suggest that, in addition to the more salient cerebral cortical asymmetries, asymmetries of the subcortical nuclei also play a role in brain health and disease.

Despite these intriguing initial findings with respect to disease states, decades of research have failed to answer definitively how brain asymmetries in the healthy population are linked to basic biological factors such as age, sex, and handedness. This is partly because many brain asymmetries and their normal variability are subtle, and difficult to measure reliably in small studies (tens to low hundreds of subjects are typical). Regarding sexual dimorphisms, a sex difference in asymmetry of the amygdala has been reported (Niu et al., 2004), while no sex difference was detected in another study (Szabo et al., 2001). For striatal asymmetry, no significant sex differences were observed by three studies (Abedelahi et al., 2013; Giedd et al., 1996; Wyciszkiewicz and Pawlak, 2014), although a sex difference in putamen asymmetry was suggested to affect TS etiology (Zimmerman et al., 2000). Sexual dimorphism in thalamic asymmetry has been recently reported (Kang et al., 2015) but not replicated. Asymmetry of striatal nuclei changes with age (Abedelahi et al., 2013; Yamashita et al., 2011), but prior studies of subcortical structures have tended to look at age and asymmetry as separate aspects of study (Caviness et al., 1996; Giedd et al., 1996). Left-handedness has not been robustly investigated in relation to subcortical asymmetries, as there are so few left-handers in most datasets (Foundas et al., 1998; Kloppel et al., 2007). Likewise, in clinical studies, possible effects of sex, age, and handedness have not often been investigated, either as a result of restricted inclusion criteria, or otherwise not considering these factors in their analyses (e.g. Kang et al., 2015; Yamashita et al., 2011).

The present study was the first by the Lateralization working-group embedded within the ENIGMA (Enhancing Imaging Genetics through Meta-Analysis) Consortium (Thompson et al., 2014). Our goal was to detect effects of sex, handedness, and age on the normal variability in subcortical asymmetries, by testing and meta-analyzing these in a large number (n = 52) of healthy control and population-based datasets, for a total pool of 15,847. All brain magnetic resonance (MR) images were analysed using a single, uniform protocol, despite inevitable heterogeneity in image acquisition (Hibar et al., 2015; Stein et al., 2012). This study was by two orders of magnitude the largest ever of asymmetry with respect to subcortical structures of the human brain, and factors affecting its variability. This allowed us to establish subtle but definitive findings of sex and age-related effects on some of the structures, where previously the literature has been inconsistent and contradictory (see Discussion). We also measured the heritabilities of subcortical and hippocampal asymmetries in a large family dataset, as previous studies have suggested these to be partially heritable (Eyler et al., 2014; Hulshoff Pol et al., 2006; Renteria, 2013). This heritability screen is a valuable precursor to future genome-wide association studies of laterality in brain traits, as well as identifying genetic overlap between asymmetries and cognitive or psychiatric disorders.

Methods

Datasets

The participating sites were members of the Lateralization working-group within the ENIGMA Consortium (Thompson et al., 2014), who contributed data from 52 independent samples to this study comprising a total of 15,847 healthy participants (7524 males and 8323 females). Samples were drawn from the general population or comprised healthy controls from clinical studies. Table 1 and Supplementary Figure S1 summarize the datasets' sample sizes and age distributions. Each dataset and its image acquisition protocols are described in Supplementary Table S1.

Handedness of participants was known for a subset of the overall sample. The method of assessment varied per dataset (see Supplementary Table S3). An ambidextrous category was not included and only datasets with enough left-handers to perform statistical comparisons were considered. In total, 959 and 11,236 subjects were left- and right-handed, respectively.

The final numbers of subjects and datasets that were used for meta-analyses differed per test and structure according to the availability of covariate and structure-specific volumetric information, and the minimum sample-size criteria. Details are given below per analysis.

Table 1. List of contributing datasets (arranged alphabetically in two columns), their sample sizes split by sex, and their median ages. Each dataset is also given a suffix number code for reference to Figure 2, 3 and Supplementary Figure S2.

Dataset	N		Median age (years)	Dataset	N		Median age (years)
	Males	Females			Males	Females	
BIG 1.5T [1]	733	728	23	**OCD-Kunming 3T** [27]	27	68	25
BIG 3T [2]	579	729	22	**OCD-Kyoto 1.5T** [28]	25	23	30
BIL & GIN [3]	221	232	24	**OCD-Kyoto 3T** [29]	20	22	30
BP-Houston [4]	79	94	19	**OCD-London** [30]	12	21	32
CIAM [5]	16	14	27	**OCD-Shangai** [31]	21	17	25
CLiNG [6]	132	191	24	**OCD-SNU A** [32]	53	26	25
FBIRN [7]	129	54	37	**OCD-SNU B** [33]	97	59	24
HMS [8]	21	34	41	**OCD-SNU C** [34]	115	72	24
HUBIN [9]	69	33	46	**OCD-SU** [35]	11	18	29
IMAGEN [10]	735	847	15	**OCD-VUmc Amsterdam 1.5T** [36]	16	38	34
IMpACT [11]	61	80	32	**OCD-VUmc Amsterdam 3T** [37]	20	22	38
LBC-1936 [12]	282	274	73	**OCD-Zürich** [38]	15	23	17
MAS [13]	224	280	78	**Osaka 1.5T** [39]	206	231	33
MCIC [14]	103	60	28	**Osaka 3T** [40]	131	106	24
Meth-CT [15]	50	13	25	**PAFIP-IDIVAL1** [41]	51	30	26
MüNC [16]	327	420	32	**PAFIP-IDIVAL2** [42]	69	45	29
NCNG [17]	105	222	54	**PAFIP-IDIVAL3** [43]	13	21	69
NESDA [18]	23	43	41	**QTIM** [44]	169	422	22
NeuroIMAGE [19]	180	208	17	**SHIP-2** [45]	538	572	56
OATS [20]	87	153	69	**SHIP-Trend** [46]	994	1046	52
OCD-AMC [21]	9	18	14	**STROKEMRI** [47]	19	33	45
OCD-Barcelona [22]	30	36	33	**TCD|NUIG** [48]	116	145	28
OCD-Fukuoka [23]	16	25	37	**TOP** [49]	159	144	34
OCD-India 1.5T [24]	34	12	26	**UCLA|NL BP** [50]	82	84	46
OCD-India 3T [25]	95	60	26	**UMCU** [51]	166	121	29
OCD-Kunming 1.5T [26]	13	27	31	**Würzburg|Tübingen** [52]	24	29	44

Image acquisition and subcortical segmentation

Image acquisition and subcortical volume measurement has been described in previous reports from the ENIGMA Consortium (e.g. Hibar et al., 2015; Stein et al., 2012) , and is consistent enough to detect SNP effects at a genome-wide significant level, which individually account for less than 1% of the variance in structure volumes. To summarize, T1-weighted brain structural MRI scans were acquired at multiple different sites using scanners of mostly 1.5 or 3 Tesla field strengths. One dataset (QTIM) was acquired with a 4 Tesla field strength scanner. See Supplementary Table S1 for detailed information on manufacturers and image acquisition parameters per dataset. All sites followed the same protocol for automated segmentation of subcortical structures, volume computation, and quality control. The protocol is downloadable from the ENIGMA website (http://enigma.ini.usc.edu/protocols/imaging-protocols/). For the present study, all subcortical measurements were derived from FreeSurfer (versions 4.3 through to 5.3; Fischl et al., 2002). See Supplementary Table S1 for details. This resulted in volume estimates for the following seven bilaterally paired structures: nucleus accumbens, amygdala, caudate nucleus, globus pallidus, hippocampus, putamen, and thalamus, and estimates of total intracranial volume (ICV). In addition, a number of checks were performed to assess potential errors in the left-right orientation of the data (see Supplementary Information S4 for details).

Within-dataset analyses

For each dataset and each of the seven bilaterally paired structures, volumetric asymmetries, descriptive and statistical analyses were computed at each participating site using a single script in R (R Development Core Team; 2012), on table-formatted data. Asymmetry Indices (AI) were defined as the relative volume difference between the left and right structure in relation to its total bilateral volume: (Left-Right)/(Left+Right). To exclude possible outliers in volumes or AIs we used an adaptive SD threshold (SD_{Thresh}) depending on each dataset's sample size ($N < 150 \Rightarrow SD_{Thresh} = 2.5$; $150 \geq N \geq 1000 \Rightarrow SD_{Thresh} = 3$; $N > 1000 \Rightarrow SD_{Thresh} = 3.5$). Statistical tests were run on the seven subcortical AIs separately. Differences between sexes or handedness groups were assessed by Welch's two-sample t-test, to avoid assuming balanced group sizes and equal variances (Ruxton, 2006). Tests were performed on residualised AIs, after removing effects of age and ICV (and sex for the handedness tests) by linear regression. The effects of age on AIs were estimated by ANCOVAs, modelled together with sex and ICV as covariate factors.

This approach supported the subsequent meta-analyses by using within-site summary statistics without sites needing to share primary data.

AI heterogeneity between datasets

We assessed the heterogeneity in AIs across datasets through analysis of variance, treating 'dataset' as the main factor. This analysis partitioned the total AI variance for a given structure into its between- and within-dataset contributions, to calculate estimates of R^2, i.e., the percentage of the total variance explained by differences between datasets.

Meta-analysis approach

The chosen method for all of our meta-analyses was to combine probabilities (p-values) across datasets, rather than average their effects. We used a signed and weighted Z-test (Liptak-Stouffer test; Liptak, 1958). This approach to meta-analysis is agnostic to the kind of underlying effect across datasets. It tests the null hypothesis that there is no pooled evidence for an effect, in either direction. This effect-agnostic approach seemed appropriate given the observed heterogeneity in the AI distributions (see Table 2 and Supplementary Figure S2), and the demographic and ethnic diversity included in our analyses (Byrd et al., 2015).

Formally, each p-value was halved and converted to a Z-score given by the inverse of the standard normal cumulative distribution, $\Phi^{-1}(1-P/2)$, and signed by the direction of the observed effect. This resulted in either positive or negative Z-scores, thus allowing for a two-tailed test. Each dataset's Z-score was assigned a weight and combined according to the following formula:

$Z_{meta} = \frac{\sum_i^k w_i Z_i}{\sqrt{\sum_i^k {w_i}^2}}$, where k is the total number of datasets, w_i is the weight assigned to the i^{th} dataset, and Z_i is the corresponding signed Z-score.

In line with our agnostic approach regarding underlying effects, the weights were set proportional to the square root of the corresponding sample size (Liptak, 1958; Zaykin, 2011). The resulting statistic was then tested for significance on the standard normal distribution N(0,1). This method is also implemented in the METAL software (Willer et al., 2010), as the "sample-size approach".

Population-level lateralization

T-scores and corresponding p-values were calculated for the difference between the mean AI and zero for each structure and dataset, separately by sex. These were meta-analysed for population-level lateralizations for each structure, separately for each sex.

Meta-analysis of group differences by sex and handedness

For meta-analyses of sex and handedness effects, we used the mean group differences in residualised AIs and p-values generated by the Welch's two sample t-tests (μ_{males} - $\mu_{females}$; $\mu_{lefthanders}$ - $\mu_{righthanders}$). As we could not expect all test statistics to come from well-balanced group sizes (especially for handedness comparisons), we did not define each dataset's weight as a function of its total sample size, but we calculated the "effective" sample size based on the harmonic mean of the two groups:

$$N_{eff} = 2 * \left(\frac{2}{\frac{1}{N_{group1}} + \frac{1}{N_{group2}}} \right).$$

Including results based on low numbers of observations is likely to reduce reliability, however there is no a priori method to choose a threshold for the minimum number of observations. We chose to initially test with a cut-off of 15 and then check the robustness of our results by repeating this under more strict inclusion thresholds, of 50 or 100 minimum observations per group, and once without any threshold. For the sex group comparisons, a 15-observation minimum threshold resulted in totals between 6867 and 6962 males versus 7708 to 7897 females, depending on the specific structure. For handedness, the totals were from 644 to 668 left handers versus 7298 to 7667 right handers.

Meta-analysis of age effects on AIs

These analyses were based on the coefficients from the ANCOVA regression of AIs on age and their corresponding p-values (see section above on within-dataset analyses). We applied the threshold of at least 15 observations per sex group and included an extra criterion based on the age-range of each dataset. Only results from datasets with a minimum 5-year range between their 1st and 3rd quartile (50% of the dataset) were included.

The meta-analyses were also repeated with no threshold on age-range or sample size to check that these had not affected the results substantially.

Heterogeneity of effects

We assessed heterogeneity in sex and handedness effects directly on the mean, residualised, AI group differences, and their corresponding error estimates, by weighted F-tests. Likewise, heterogeneity in age effects was assessed directly from the age coefficients and their error estimates by weighted F-tests.

We summed the weighted squared deviations between each dataset's effect and the pooled mean effect to obtain its variance, then divided it by the pooled error variance. Each dataset's contribution to

the overall F-statistic was weighted in the same way as the previous analyses. The resulting F-statistic provided an accurate assessment of heterogeneity, which was more robust against violations of distributional assumptions than, for example, Cochran's Q test (Higgins and Thompson, 2002). The probability of this value was then assessed on the F-distribution, with the number of datasets minus 1 as the denominator degrees of freedom.

Heritability of AIs

We estimated the heritability of volumetric asymmetries using the Genetics of Brain Structure (GOBS) dataset (McKay et al., 2014; Mitchell et al., 1996). This analysis included data from 1170 subjects of Mexican-American ancestry, belonging to 71 extended pedigrees. Heritability estimates were derived from variance-component analysis (Almasy and Blangero, 1998). The method partitions the observed phenotypic variance into sub-components based on the relationship structures within the families, in order to estimate the proportion of overall phenotypic variance due to additive genetic effects. To calculate this family-based heritability estimate, the method requires large pedigrees and accurate kinship estimates between family members. For a more detailed description of the approach, applied to brain imaging measures, see (Chouinard-Decorte et al., 2014; Koran et al., 2014). These analyses were performed using SOLAR (Almasy and Blangero, 1998) including age, sex, and ICV as covariates. For each of the seven structures we estimated the heritability of the AI, as well as the heritability of the phenotypic correlation between left and right volumes considered separately.

Results

Means and variances of AIs

We observed notable heterogeneity in the AI distributions across datasets (Table 2 and Supplementary Figure S2). Except for the amygdala, hippocampus, and putamen, dataset heterogeneity explained over 25% of the total pooled variance per structure.

Independent of dataset mean differences, the nucleus accumbens showed the most variable AI estimates, and the caudate nucleus was the least variable (see Table 2). The average variability around AI means as a proportion of bilateral volume (σ_{within}*100) was 7.8% for the nucleus accumbens and 2.5% for the caudate nucleus. All structures showed highly significant mean lateralization (see Table 2 and Figure 1), as well as consistency in mean direction of lateralization between the sexes (See Supplementary Table S2).

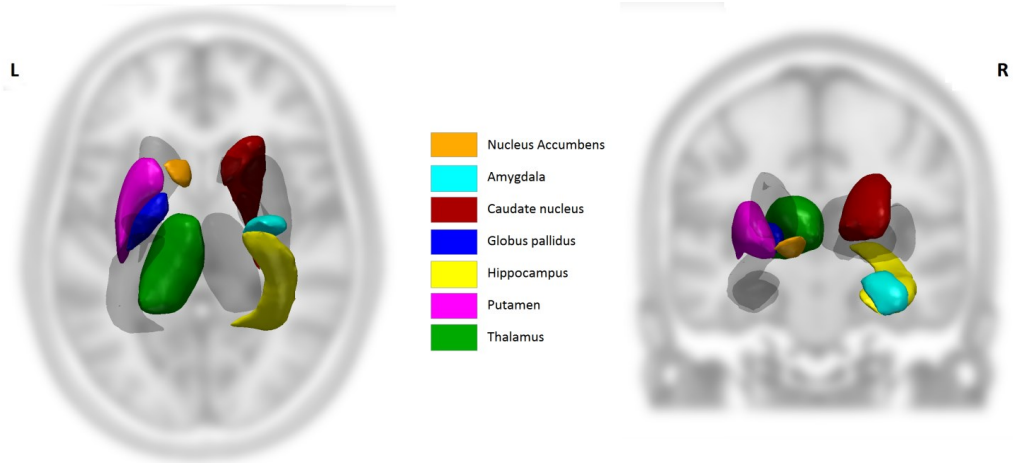

Figure 1. Visual representation of the 7 bilaterally paired structures, colored on the side of the relatively larger volume.

Table 2. AI heterogeneity across datasets assessed by analysis of variance (ANOVA). The R^2 statistic gives the proportion of the total variability attributed to dataset mean differences. In the last two columns are the pooled estimates of between- and within-dataset variance. All mean AI's were significantly different from zero.

Regions	Mean AI	N (observed)	R^2 - Site	$\sigma^2_{between}$	σ^2_{within}
Nucleus accumbens	-0.0072	15010	0.32	0.849	0.0061
Amygdala	-0.0205	15167	0.10	0.093	0.0027
Caudate nucleus	-0.0095	15105	0.29	0.075	0.0006
Globus pallidus	0.0180	14932	0.31	0.360	0.0027
Hippocampus	-0.0066	15046	0.08	0.020	0.0008
Putamen	0.0194	14961	0.07	0.020	0.0008
Thalamus	0.0211	15158	0.52	0.278	0.0009

Meta-analyses of sex and handedness effects on AIs

Meta-analyses showed significant differences in AIs between males and females for the globus pallidus, putamen, and thalamus (Table 3 and Figure 2), corrected for covariate effects of age and intracranial volume (ICV) within datasets. The direction of the sex difference was the same for the putamen and thalamus (see Table 3), where a negative pooled Z-score indicated a lower AI in males versus females, i.e. a rightwards shift in asymmetry in males regardless of the sign of the population mean. The opposite

was found for the globus pallidus, where a leftward shift in AI was observed in males relative to females. We observed no significant heterogeneity in sex effects across datasets for these three structures (see Table 3). Meta-analyses of handedness effects on AIs showed no significant group differences (results not shown). The same pattern of results was observed after repeating the analyses under different sample inclusion criteria (results not shown).

Table 3. Meta-analyses results of AI differences by sex, corrected for possible covariate effects of age and ICV. F-het and P(F) are the statistics for the heterogeneity of effects. The significance threshold was Bonferroni-adjusted to 0.007 for the seven comparisons. Highlighted in bold are the statistically significant results. For the globus pallidus, putamen, and hippocampus, post-hoc pooled sex effects across datasets are also given, with their respective standard errors.

Structure	Z-score	P-value	F-Het	P(F)	Effective N (N datasets)	Pooled effect	SE
Nucleus accumbens	2.37	0.02	1.27	($F_{1,41}$): 0.27	14261 (42)		
Amygdala	0.03	0.97	1.00	($F_{1,42}$): 0.32	14451(43)		
Caudate nucleus	-1.48	0.14	1.25	($F_{1,40}$): 0.27	14335 (41)		
Globus pallidus	**4.58**	**$5*10^{-6}$**	**0.94**	**($F_{1,39}$): 0.34**	**14194 (40)**	**0.0046**	**0.0012**
Hippocampus	2.26	0.02	0.40	($F_{1,42}$): 0.53	14367 (43)		
Putamen	**-4.06**	**$5*10^{-5}$**	**0.63**	**($F_{1,40}$): 0.43**	**14224 (41)**	**-0.0018**	**0.0007**
Thalamus	**-3.83**	**$1*10^{-4}$**	**1.15**	**($F_{1,40}$): 0.29**	**14383 (41)**	**-0.0012**	**0.0007**

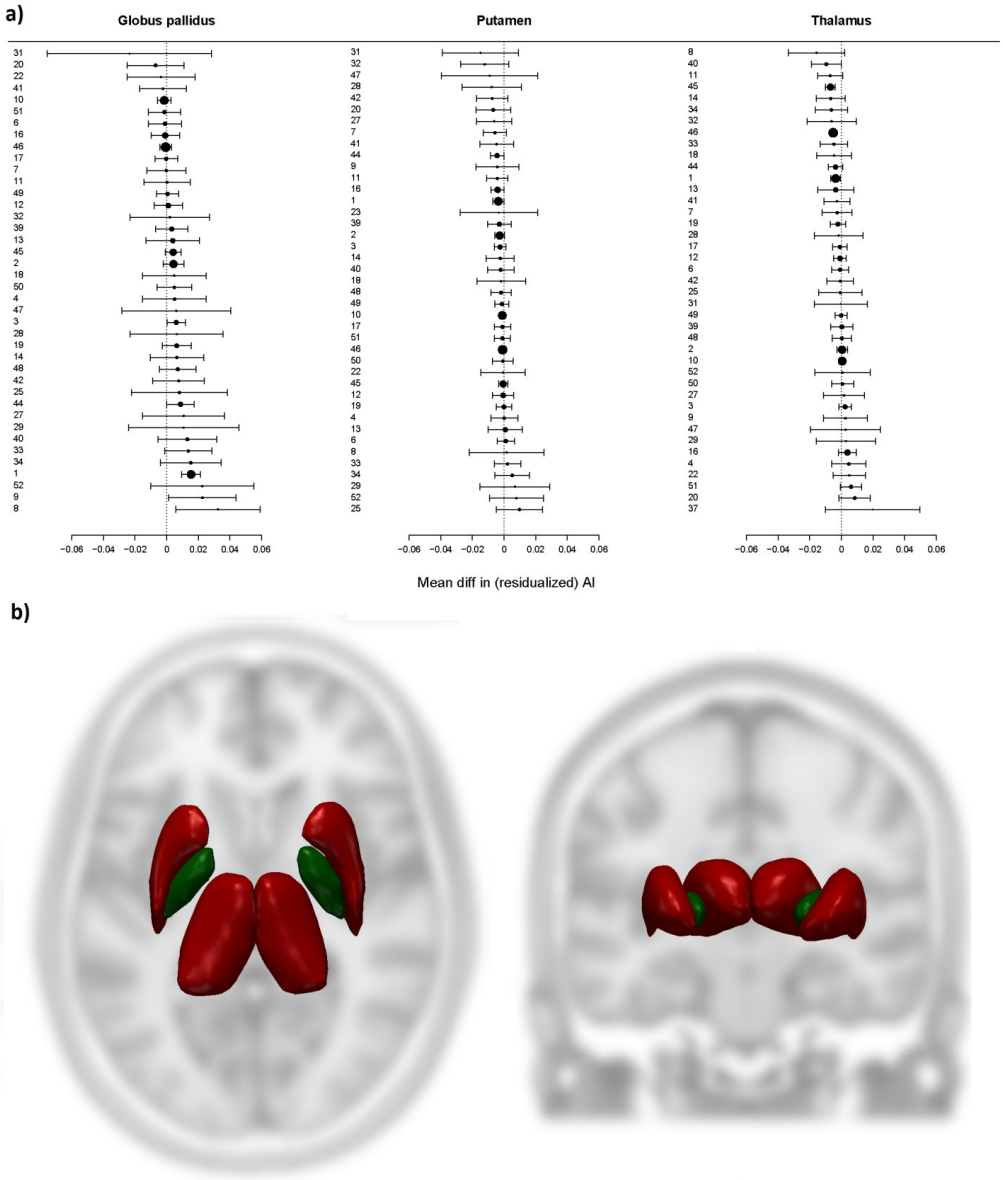

Figure 2. Results from meta-analysis of sex effects. a) Forest plots of the mean sex differences in AIs per dataset, for the structures that showed significant sex effects in meta-analysis. For each structure, the datasets are ordered top-to-bottom by their estimated sex difference. The identities of the datasets are given by the numbers in the left-hand columns, with reference to Table 1. The size of a point is proportional to the square root of the dataset's effective sample size. The confidence intervals are shown, as well as dashed vertical lines to

indicate the point of no mean sex difference. b) Visual representation of the 3 structures that showed significant sex effects in meta-analysis, colored by the sign of the overall effect, in either green (females' AI is more rightward lateralized relative to males) or red (females' AI is more leftward lateralized relative to males).

Meta-analysis of age effects on AIs

After adjusting the significance threshold to p=0.007 for seven structures, meta-analysis revealed significant effects of age on the AIs of the nucleus accumbens, amygdala, hippocampus and putamen (see Table 4 and Figure 3), corrected for covariate effects of sex and ICV within datasets. Positive Z-scores for the nucleus accumbens and putamen indicated increasingly leftward shifts in asymmetry with increasing age. Negative Z-scores for the amygdala and hippocampus indicated rightward shifts in asymmetry with increasing age. Only the association between age and hippocampus asymmetry was not robust to altering the sample inclusion criteria (results not shown).

Table 4. Meta-analyses results for the effects of age on AIs, after correcting for sex and ICV. F-het and P(F) are the statistics for heterogeneity of effects across datasets. The statistically significant results are highlighted in bold.

Structure	Z-score	P-value	F-Het	P(F)	Total N (N datasets)
Nucleus accumbens	**5.67**	**$1*10^{-8}$**	**3.76**	**($F_{1,36}$): 0.06**	**12073 (37)**
Amygdala	**-7.15**	**$9*10^{-13}$**	**1.84**	**($F_{1,37}$): 0.18**	**12287 (38)**
Caudate nucleus	1.36	0.14	2.44	($F_{1,35}$): 0.13	12150 (36)
Globus pallidus	-0.96	0.34	6.28	($F_{1,34}$): 0.02	12026 (35)
Hippocampus	**-2.95**	**$3*10^{-3}$**	**0.87**	**($F_{1,37}$): 0.36**	**12212 (38)**
Putamen	**6.11**	**$1*10^{-9}$**	**1.24**	**($F_{1,35}$): 0.27**	**12042 (36)**
Thalamus	-0.31	0.76	4.12	($F_{1,35}$): 0.05	12202 (36)

Heritabilities of AIs

AIs of the globus pallidus, hippocampus, putamen, and thalamus showed modest but statistically significant heritabilities, ranging from h2 = 0.15 to 0.27 (using a corrected alpha of p = 0.007; Table 5). For each subcortical region, we also estimated the genetic correlation (the proportion of variance that two traits share due to the additive effects of genes) between the absolute volumes of the left and right structures. While these correlations were all high (indicating partial pleiotropy), they all were significantly different from 1 (i.e., complete pleiotropy; see Table 5). In other words, most genetic effects on volume variation are shared between the left and right hemispheres and therefore affect bilateral volumes of these structures, but some independent or quantitatively different genetic effects may operate uniquely on each hemisphere, thus constituting heritable effects on asymmetry. The

caudate nucleus and nucleus accumbens also showed suggestively significant heritabilities of their AIs using an uncorrected alpha of 0.05 (see Table 5).

Table 5. Heritability estimates for the AIs, their corresponding standard errors and p-values, based on a large family dataset. In the middle part of the table are the genetic correlations between left and right volumes (heritabilities of their phenotypic correlations), and test p-values for whether the genetic correlations differ significantly from 0 and 1. In the right-hand part of the table are the environmental and phenotypic correlation estimates between left and right volumes.

Structure	AI heritability		Genetic correlation (ρ) between Left and Right			Phenotypic (ρ-phen) and environmental (ρ-env) correlation between Left and Right	
	h^2 (se)	**P-value**	**ρ (se)**	**P (ρ = 0)**	**P (ρ = 1)**	**ρ-phen**	**ρ-env**
Nucleus accumbens	0.114 (0.06)	0.010	0.841 (0.07)	$4*10^{-10}$	0.003	0.54	0.34
Amygdala	0.040 (0.05)	0.222	0.995 (0.03)	$8*10^{-24}$	0.424	0.71	0.39
Caudate nucleus	0.096 (0.06)	0.053	0.974 (0.01)	$2*10^{-32}$	0.021	0.85	0.56
Globus pallidus	0.148 (0.06)	0.002	0.823 (0.08)	$8*10^{-8}$	0.005	0.57	0.45
Hippocampus	0.180 (0.06)	$4*10^{-4}$	0.939 (0.02)	$2*10^{-25}$	$7*10^{-4}$	0.78	0.53
Putamen	0.270 (0.07)	$8*10^{-7}$	0.899 (0.03)	$5*10^{-23}$	$4*10^{-7}$	0.78	0.58
Thalamus	0.228 (0.06)	$2*10^{-5}$	0.824 (0.05)	$1*10^{-13}$	$4*10^{-6}$	0.68	0.56

Discussion

Establishing effects of age, sex, and genetics

There is an inconsistent literature regarding basic biological factors that may affect subcortical and hippocampal asymmetries, including age, handedness, and sex. Subcortical asymmetries are subtle compared to some cerebral cortical asymmetries, and have so far only been assessed in small sample sizes, often with different analysis methods across studies (see Introduction). Compared to prior reports on subcortical asymmetries, our study analysed a large number of datasets worldwide using a harmonized protocol. To our knowledge, this has been by far the largest ever study of healthy variation in any aspect of human brain asymmetry. The 52 component datasets also had technical and demographic differences, allowing us to survey the level of asymmetry that would be found in cohorts worldwide. Given the scale of our study, and in contrast to literature-based meta-analyses, ours was not affected by publication bias nor by spurious results from underpowered studies. The scale of our study also allowed us to see how much difference it made to apply either a strict or inclusive criterion regarding minimum sample sizes of contributing datasets, and the results were consistent. For future genome-wide screens, we also revealed significant heritabilities of asymmetries in a large family sample.

We found reliable sex differences in asymmetries of the globus pallidus, putamen, and thalamus, which, together with the hippocampus, were also the most strongly heritable asymmetries among the seven structures analysed. With increasing age, there were changes in the mean asymmetry of the nucleus accumbens, amygdala, putamen and hippocampus, although the latter effect was dependent on the inclusion criterion that was used. Handedness was not detectably related to any subcortical asymmetry. The ENIGMA Consortium (Thompson et al., 2014) plans future genome-wide association studies in sample sizes comparable to, or greater than, that used here. Our data show which subcortical asymmetries are heritable and suitable for detecting subtle modulatory effects and group differences. Taken together, our heritability- and meta-analyses indicate that asymmetries of the putamen, globus pallidus, hippocampus and thalamus are the most likely structures through which genetic variation may impact lateralization for human cognition, its variability, and susceptibility to brain disorders.

From a developmental perspective, some human CNS lateralizations change throughout life (Kovalev et al., 2003). Asymmetries are detectable during fetal gestation behaviorally (Hepper, 2013) and anatomically (Corballis, 2013), so differential development between the two human brain hemispheres must, at least in part, be genetically coded in utero (Francks, 2015). Three prior reports have suggested genetic contributions to variability in subcortical asymmetries based on twin-based heritability estimates. One found evidence for amygdala volumes being under strong genetic control, with higher heritability for the left than the right hemisphere ($h2 = 0.80$ and 0.55, respectively; (Hulshoff Pol et al., 2006)). Another found that genetic contributions to left and right volume variability were partly distinct for the nucleus accumbens and globus pallidus in particular (Eyler et al., 2014). A third found significant heritabilities of asymmetry indexes for the caudate nucleus and putamen, $h2 = 0.17$ and 0.32, respectively (Renteria, 2013).

In terms of developmental biology and molecular genetics, the best studied model organism for CNS lateralization is the zebrafish. During the zebrafish's development, there is a left-biased migration of a midline structure (the parapineal organ) that results in differential innervation of the bilateral epithalamus into the surrounding tissue, which later affects other brain regions (Concha et al., 2009). Specific molecular contributions to this process have been identified (Colombo et al., 2013). The relevance of this mechanism to humans is not clear, but a subcortical origin of lateralized development in the zebrafish brain suggests that similar or related mechanisms may be important in our species. Cerebral cortical lateralization may even be a downstream consequence of early subcortical lateralization.

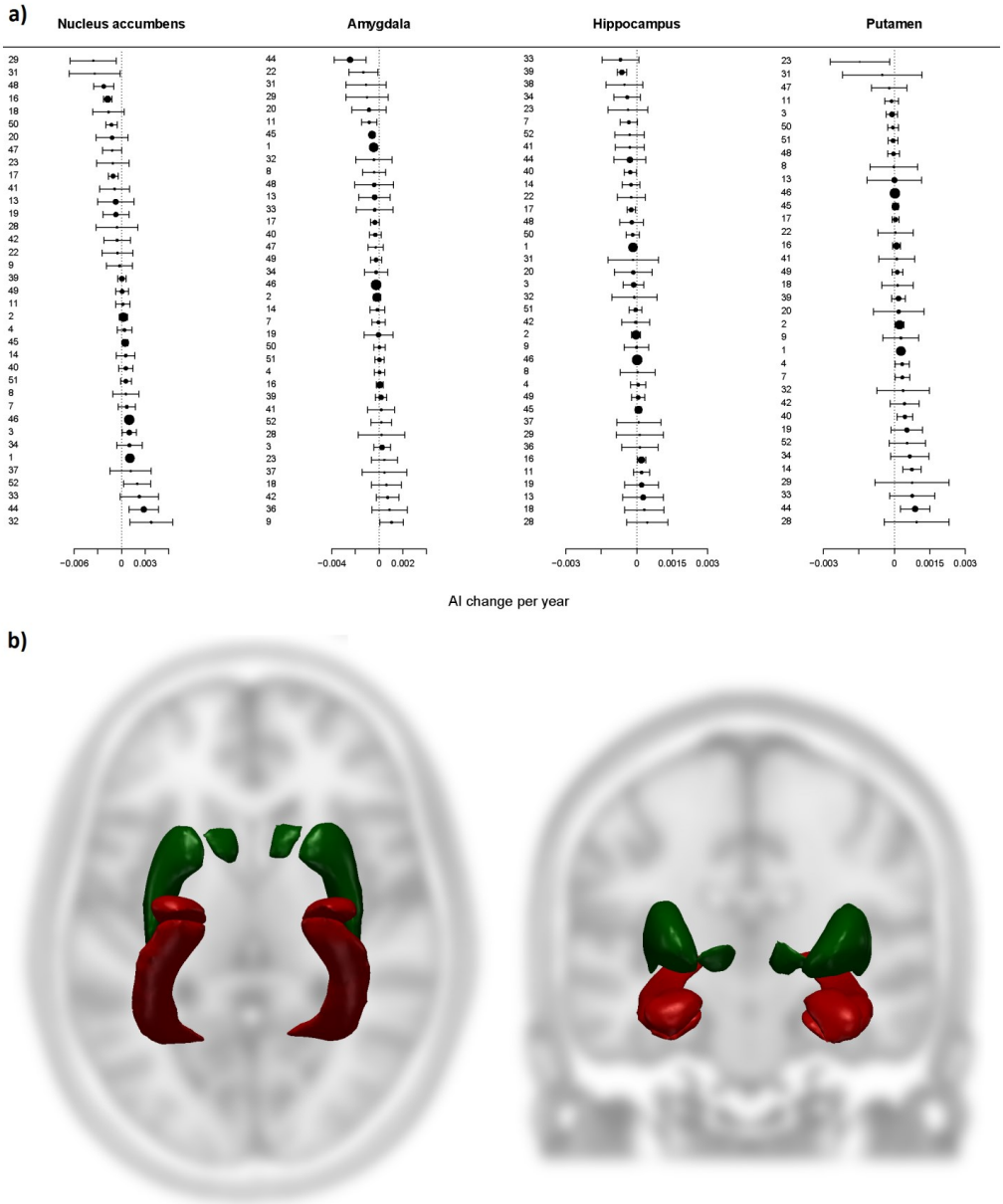

Figure 3. Results from meta-analysis of age effects. a) Forest plots of the age coefficients for each dataset on the AIs, for the four structures that showed significant age effects in meta-analysis. For each structure, the datasets are ordered top-to-bottom by their estimated age coefficient. The identities of the datasets are given by the numbers in the left-hand columns, with reference to Table 1. The size of a point is proportional to the square root of the dataset's sample size. The confidence intervals are also depicted, as well as dashed vertical lines to

indicate the point of an age coefficient with value zero. b) Visual representation of the 4 structures that showed significant age effects in meta-analysis, colored by the sign of the overall age effect, in either green (increasing leftward asymmetry with age) or red (increasing rightward asymmetry with age).

For the four structures that showed an age effect, asymmetry increased with age. This meant a more pronounced L>R asymmetry for the nucleus accumbens and putamen with increased age and a more pronounced R>L asymmetry for the amygdala and hippocampus with increased age. Environmental or age-dependent genetic factors may contribute to this increased lateralization over time. To our knowledge, these associations have not been reported before, except for an opposite age effect for the putamen in 120 healthy, young adults (Abedelahi et al., 2013). We tested only linear effects of age at the dataset level, and these coefficients were meta-analysed. Non-linear changes in AI with age might have gone undetected in our analysis, and may affect the measured linear effects. However, these meta-analyses were restricted to age effects observed in datasets with at least a 5-year age-range between the first and third quartile of participants. Most of our datasets had median ages between 20 and 60 years, so a linear regressor should have captured main effects of age on AIs, in these datasets, even if there were subtle non-linear effects.

Perhaps surprisingly, handedness had no detectable effect on subcortical asymmetries. However, as there are fewer left-handers than right-handers, the effective sample size was roughly one sixth for this analysis than for our analysis of sex differences. It remains possible, through even larger-scale meta-analysis, that handedness will relate to subcortical asymmetries. However, based on our present data, such effects must be very small.

Dataset heterogeneity

Studies of subcortical structure have been greatly advanced by in vivo imaging. Even so, findings of population-level mean lateralizations of subcortical structures have been inconsistently reported. For example, there have been reports of the putamen being leftward lateralized on average (i.e. the left volume larger than the right (Giedd et al., 1996; Kang et al., 2015), as well as rightward lateralized (Abedelahi et al., 2013). Likewise the globus pallidus has been reported as leftward lateralized (Kang et al., 2015), as well as rightward lateralized (Wyciszkiewicz and Pawlak, 2014). Similar discrepancies have also been found for the hippocampus (Kang et al., 2015; Niemann et al., 2000; Shi et al., 2009), amygdala (Makris et al., 2004; Niu et al., 2004; Szeszko et al., 1999) and the caudate nucleus (Abedelahi et al., 2013; Glenthoj et al., 2007; Raz et al., 1995; Vernaleken et al., 2007).

Here we used uniform image processing protocols, but our analysis showed substantial differences in mean AIs across datasets (see Table 2). Variability in image acquisition is likely a substantial source of dataset AI heterogeneity. The ability to distinguish different structures using MRI depends on the contrast achieved between different tissues. Subcortical structures and the surrounding tissue are often imperfectly contrasted, so that automated methods of image analysis must rely to some extent on atlas-derived information. These are often based on manual segmentations of existing datasets, which will reflect any mean asymmetries present in those datasets (Han and Fischl, 2007; Patenaude et al., 2011). In addition, any subtle but uncorrected scanner magnetic field inhomogeneities may lead to geometric distortions in segmentation of brain structures (Han and Fischl, 2007; Jovicich et al., 2009). These factors might bias segmentation, subtly affecting AI means. Manual segmentation does not avoid this problem, and can introduce asymmetric biases (Maltbie et al., 2012). In particular for assessing population variability (as opposed to as a diagnostic tool), automated methods clearly outperform manual segmentation in their reproducibility and feasibility for larger-scale studies (Guadalupe et al., 2014b; Morey et al., 2010).

In our study, all structures showed highly significant deviations from mean AI=0, i.e. zero population-level lateralization. Except for the hippocampus, the directions of significant mean AIs were in line with those reported in a recent study of 138 young adults, based also on subcortical volumes generated by FreeSurfer (Kang et al., 2015). However, given the caveats outlined above, we are cautious about interpreting the mean population AIs at face value. Different AI means across datasets may indicate which structures are more or less susceptible to methodological biases. The mean AIs for the hippocampus, amygdala, and putamen differed the least between datasets, the mean AI of the thalamus showed the highest heterogeneity across datasets, and at the same time showed one of the strongest population-level AI lateralizations. This pattern is in line with our previous report that the hippocampus AI showed the highest scan-rescan correlation of all structures quantified with FreeSurfer (among the seven structures studied here), while the thalamus showed the second lowest scan-rescan correlation, in subjects scanned twice using varying protocols, and sometimes using different scanners with different field strengths (Guadalupe et al., 2014b).

In contrast to the substantial heterogeneity across datasets in mean AIs for some structures, there was no evidence for dataset heterogeneity in the effects of sex on mean AIs. We detected stable sex differences in AIs regardless of differences in age or ICV between and within datasets, and the sex differences were highly significant in our meta-analyses. The three structures for which we detected sex

differences in AIs showed L>R population-level asymmetry. For the globus pallidus this was more pronounced in males, while the opposite was observed for the putamen and thalamus.

Implications for future studies

Our study underlines the utility, and indeed the necessity, of analyzing subtle subcortical asymmetries in vast samples. Regarding clinical studies, some brain disorders may be associated with larger alterations in subcortical asymmetries than variables such as sex, handedness, and age. Nonetheless future studies linking subcortical asymmetries to disorders should be better powered if they analyse larger samples than used previously. Such studies will be possible within the ENIGMA Consortium.

It is reassuring that consistent sex differences could be measured in our study, even when AI means varied across cohorts. Some AIs were also heritable, based on studying relative-pair similarities. It is therefore clear that automated segmentation methods can measure meaningful individual differences in subcortical and hippocampal volumetric asymmetries (Guadalupe et al., 2014b; Hibar et al., 2015). It follows that genome-wide association studies of subcortical and hippocampal AIs are supported by this methodology, which will require very large samples for their success (Hibar et al., 2015; Stein et al., 2012).

Acknowledgments

ENIGMA protocol development is supported by the NIH BD2K “Big Data to Knowledge” initiative (U54 020403; PI: Paul Thompson) which is funded by a cross-NIH partnership.

The **AMC OCD** dataset was supported by grants from ZonMW (grant numbers: 3160007, 91676084, 31160003, 31180002, 31000056, 2812412, 100001002, 100002034), NWO (grant numbers: 90461193, 40007080, 48004004, 40003330), and grants from the Amsterdam Brain Imaging Platform, Neuroscience Campus Amsterdam and the Dutch Brain foundation. The processing with FreeSurfer was performed on the Dutch e-Science Grid through BiG Grid project and COMMIT project “e-Biobanking with imaging for healthcare”, which are funded by the Netherlands Organization for Scientific Research (NWO).

The **Barcelona OCD** study was supported by project grants no. PI09/01331, PI10/01753, PI10/01003, CP10/00604, PI13/01958 and CIBER-CB06/03/0034 from the Carlos III Health Institute, grant no. 2014SGR1672 from the Agency for Administration of University and Research(AGAUR), and a ‘Miguel Servet’ contract (CP10/00604) from the Carlos III Health Institute to Dr. Soriano-Mas.

The Brain Imaging Genetics (**BIG**) database was established in Nijmegen in 2007. This resource is now part of Cognomics, a joint initiative by researchers of the Donders Centre for Cognitive Neuroimaging, the Human Genetics and Cognitive Neuroscience departments of the Radboud University Medical Center, and the Max Planck Institute for Psycholinguistics. The Cognomics Initiative is supported by the participating departments and centres and by external grants, i.e. the Biobanking and Biomolecular Resources Research Infrastructure (Netherlands) (BBMRI-NL), the Hersenstichting Nederland, and the Netherlands Organisation for Scientific Research (NWO). The research on BIG also receives funding from the European Community's Seventh Framework Programme (FP7/2007– 2013) under grant agreements #602450 (IMAGEMEND) and #602805 (Aggressotype) and from the National Institutes of Health (NIH) Consortium grant U54 EB020403, supported by a cross-NIH alliance that funds Big Data to Knowledge Centers of Excellence. We would also like to thank Hans van Bokhoven for his contributions to the Cognomics initiative and to all persons who kindly participated in this research. In addition, AF Marquand gratefully acknowledges support from the Language in Interaction project, funded by the NWO under the Gravitation Programme (grant 024.001.006)

The **CIAM** and **OCD-SU** datasets were supported by the Medical Research Council of South Africa**.**

CLiNG and **HMS** studies were partially supported by a research grant from the Competence Network Schizophrenia to Oliver Gruber.

The **FBIRN** study was supported by the National Center for Research Resources at the National Institutes of Health (grant numbers: NIH 1 U24 RR021992 (Function Biomedical Informatics Research Network) and NIH 1 U24 RR025736-01 (Biomedical Informatics Research Network Coordinating Center; http://www.birncommunity.org). FBIRN data was processed by the UCI High Performance Computing cluster supported by Joseph Farran, Harry Mangalam, and Adam Brenner and the National Center for Research Resources and the National Center for Advancing Translational Sciences, National Institutes of Health, through Grant UL1 TR000153. FBIRN thanks Mrs. Liv McMillan for overall study coordination.

The **HUBIN** study was supported by the Swedish Research Council (grant numbers K2009-62X-15077-06-3 and K2012-61X-15077-09-3), the Karolinska Institutet and the Knut and Alice Wallenberg Foundation.

The **IDIVAL-PAFIP** study was supported by Instituto de Salud Carlos III, FIS 00/3095, 01/3129, PI020499, PI060507, PI10/00183, PI14/00639, the SENY Fundació Research Grant CI 2005-0308007, and the Fundación Marqués de Valdecilla APIO7/011. We thank IDIVAL Neuroimaging Unit for its help in the technical execution of this work.

The **IMpACT** study was supported by a grant from the Brain & Cognition Excellence Program and a Vici grant (to Barbara Franke) of the Netherlands Organization for Scientific Research (NWO, grant numbers 433-09-229 and 016-130-669) and in part by the Netherlands Brain Foundation (grant number, 15F07[2]27)and the and BBMRI-NL (grant CP2010-33). The research leading to these results also received funding from the European Community's Seventh Framework Programme (FP7/2007–2013) under grant agreement no. 602805 (Aggressotype), no. 278948 (TACTICS), and no. 602450 (IMAGEMEND). In addition, the project received funding from the European Union's Horizon 2020 research and innovation programme under the Marie Sklodowska-Curie grant agreement no 643051 (MiND), the NIH BD2K U54 020403 grant for the ENIGMA Consortium, and from the ECNP Network ADHD across the lifespan.

IMAGEN received support from the following sources: the European Union-funded FP6 Integrated Project IMAGEN (Reinforcement-related behaviour in normal brain function and psychopathology) (LSHM-CT- 2007-037286), the FP7 projects IMAGEMEND(602450; IMAging GEnetics for MENtal Disorders), AGGRESSOTYPE (602805) and MATRICS (603016), the Innovative Medicine Initiative Project EU-AIMS (115300-2), a Medical Research Council Programme Grant ‘‘Developmental pathways into adolescent substance abuse’’ (93558), the Swedish funding agency FORMAS, the Medical Research Council and the Wellcome Trust (Behavioural and Clinical Neuroscience Institute, University of Cambridge), the National Institute for Health Research (NIHR) Biomedical Research Centre at South London and Maudsley NHS Foundation Trust and King’s College London, the Bundesministeriumfür Bildung und Forschung (BMBF grants 01GS08152; 01EV0711; eMED SysAlc01ZX1311A; Forschungsnetz AERIAL), the Deutsche Forschungsgemeinschaft (DFG grants SM 80/7-1, SM 80/7-2, SFB 940/1), the National Institutes of Health, U.S.A. (Axon, Testosterone and Mental Health during Adolescence; RO1 MH085772-01A1), and by NIH Consortium grant U54 EB020403, supported by a cross-NIH alliance that funds Big Data to Knowledge Centres of Excellence.

LBC1936: Data collection was supported by the Disconnected Mind project, funded by Age UK. J.M.W. is partly funded by the Scottish Funding Council as part of the SINAPSE Collaboration. The work was undertaken by The University of Edinburgh Centre for Cognitive Ageing and Cognitive Epidemiology, part of the cross-council Lifelong Health and Wellbeing Initiative (MR/K026992/1). Funding from the Biotechnology and Biological Sciences Research Council (BBSRC) and MRC is gratefully acknowledged. We thank the study participants. We also thank Catherine Murray for recruitment of the participants and the radiographers and other staff at the Brain Research Imaging Centre.

Sydney **MAS** and **OATS** were supported by a National Health and Medical Research Council (NHMRC)/Australian Research Council Strategic Award (Grant 401162); NHMRC Program Grants (350833, 568969) and a Project Grant (1045325). OATS was facilitated through access to the Australian Twin Registry, which is funded by the NHMRC Enabling Grant 310667. Karen Mather is supported by the NHMRC Capacity Building Grant 568940 and an Alzheimer's Australia Dementia Research Foundation Postdoctoral Fellowship. We would like to thank the Sydney MAS and OATS participants and their respective research teams.

The **MCIC** study was supported by the National Institutes of Health (NIH/NCRR P41RR14075 and R01EB005846 to Vince D. Calhoun), the Department of Energy (DE-FG02-99ER62764), the Mind Research Network, the Morphometry BIRN (1U24, RR021382A), the Function BIRN (U24RR021992-01, NIH.NCRR MO1 RR025758-01,1RC1MH089257 and 5P20RR021938/P20GM103472 to Vince D. Calhoun), the Deutsche Forschungsgemeinschaft (research fellowship to Stefan Ehrlich and Esther Walton), and a NARSAD Young Investigator Award (to Stefan Ehrlich).

The Münster Neuroimaging Cohort **(MüNC)** was supported by grants from the German Research Foundation (DFG; grant FOR 2107; DA1151/5-1 to UD) and Innovative Medizinische Forschung (IMF) of the Medical Faculty of Münster (DA120903 to UD, DA111107 to UD, and DA211012 to UD).

The **NCNG** study was supported by the Research Council of Norway (#154313, #177458, and #231286)

The infrastructure for the **NESDA** study (www.nesda.nl) is funded through the Geestkracht program of the Netherlands Organisation for Health Research and Development (Zon-Mw, grant number 10-000-1002) and is supported by participating universities (VU University Medical Center, GGZ inGeest, Arkin, Leiden University Medical Center, GGZ Rivierduinen, University Medical Center Groningen) and mental health care organizations, see www.nesda.nl. Lianne Schmaal is supported by The Netherlands Brain Foundation Grant number F2014(1)-24.

The **NeuroIMAGE** study was supported by NIH Grant R01MH62873, NWO Large Investment Grant 1750102007010, and grants from Radboud university medical center, University Medical Center Groningen and Accare, and VU University Amsterdam. This work was also supported by a grant from NWO Brain & Cognition (433-09-242). Further support was received from the European Union FP7 programmes TACTICS (278948) and IMAGEMEND (602450).

The **OCD-London** dataset was supported by project grant no. 064846 from the Wellcome Trust and a pilot R&D grant from the South London & Maudsley Trust, UK.

The **Osaka** study was partially supported by JSPS KAKENHI Grant Number 25293250 and 23659565, MEXT Grant-in-Aid for Scientific Research on Innovative Areas (Comprehensive Brain Science Network) Grant Number 221S0003, and Brain/MINDS, AMED. Part of computations were performed using Research Center for Computational Science, Okazaki, Japan.

QTIM: Australian National Health and Medical Research Council (Project Grants No. 496682 and 1009064 to MJ Wright and Fellowship No. 464914 to IB Hickie), US National Institute of Child Health and Human Development (RO1HD050735 to MJ Wright), and US National Institute on Drug Abuse (R00DA023549 to NA Gillespie). Baptiste Couvy-Duchesne is supported by a University of Queensland International PhD scholarship. We are grateful to the twins for their generosity of time and willingness to participate in our studies. We thank research assistants Marlene Grace, Ann Eldridge, Richard Parker, Lenore Sullivan, Lorelle Nunn, Kerrie Mcaloney, Kori Johnson, Aaron Quiggle, and Natalie Garden, radiographers Matthew Meredith, Peter Hobden, Kate Borg, Aiman Al Najjar, and Anita Burns for acquisition of the scans, and David Smyth, Anthony Conciotrorre, Daniel Park, and David Butler for IT support.

The Study of Health in Pomerania (**SHIP**) is supported by the German Federal Ministry of Education and Research (grants 01ZZ9603, 01ZZ0103 and 01ZZ0403) the Ministry of Cultural Affairs as well as the Social Ministry of the Federal State of Mecklenburg-West Pomerania. MRI scans were supported by Siemens Healthcare, Erlangen, Germany. SHIP-LEGEND was supported by the German Research Foundation (GR1912/5-1).

The **TCD|NUIG** sample was supported by grant funding from the Health Research Board (grant number HRA_POR/2011/100; HRA_POR/2012/54), Science Foundation Ireland (12/IP/1359; 08/IN.1/B1916), the Wellcome Trust (grant number 072894/2/03/Z) and the Brain and Behavior Research Foundation (grant number 17026), USA.

The **TOP** study was supported by the Research Council of Norway (#213837, #217776, #223273), the South-East Norway Health Authority (2013-123), and the KG Jebsen Foundation.

The **Zürich OCD** study was supported by the Swiss National Science Foundation (No. 320030_130237) and the Hartmann Müller Foundation (No. 1460). We thank Reto Iannaccone for supporting the data

collection. In the last 10 years, Prof. Dr. Susanne Walitza has received lecture honoraria from Janssen Cilag, AstraZeneca, Opopharma, and Eli Lilly.

Appendix

Supplementary Table S1: Dataset description and MR image acquisition details. On the left column are the reference numbers as used in Table 1, Figures 2 and 3.

Reference number	Dataset	Description	Scanner(s)	FreeSurfer version	T1 acquisition details
1	**BIG 1.5T**	The Brain Imaging Genetics database, split by scanner field strength. A population-based sample from Nijmegen, the Netherlands	1.5T (Sonata; Avanto) Siemens	5.3	MRI data in BIG were acquired with either a 1.5 Tesla Siemens Sonata or Avanto scanner or a 3 Tesla Siemens Trio or TimTrio scanner (Erlangen, Germany). Given that images were acquired during several smaller scale studies, the parameters used were slight variations of a standard T1-weighted three-dimensional magnetization prepared rapid gradient echo sequence (MPRAGE; 1.0×1.0×1.0 mm voxel size).
2	**BIG 3T**	The Brain Imaging Genetics database, split by scanner field strength. A population-based sample from Nijmegen, the Netherlands	3T (Trio; TimTrio) Siemens	5.3	MRI data in BIG were acquired with either a 1.5 Tesla Siemens Sonata or Avanto scanner or a 3 Tesla Siemens Trio or TimTrio scanner (Erlangen, Germany). Given that images were acquired during several smaller scale studies, the parameters used were slight variations of a standard T1-weighted three-dimensional magnetization prepared rapid gradient echo sequence (MPRAGE; 1.0×1.0×1.0 mm voxel size).
3	**BIL & GIN**	The Brain imaging of lateralization study at Groupe d'Imagerie Neurofonctionnelle, a sample of adult participants enriched in left-handers (45%), from Bordeaux, France (Mazoyer et al., 2015)	3T (Achieva) Philips	5.3	3D T1-weighted sequence: 3D-FFE-TFE; TR = 20ms; TE = 4.6ms; flip angle = 10°; inversion time = 800ms; turbo field echo factor = 65; sense factor = 2; matrix size = 256x256x180mm3; 1mm3 isotropic voxel size
4	**BP-Houston**	A subset of healthy controls from the Searching for Endophenotypes of Bipolar Disorders Study (BP)	a) 3T (Allegra) Siemens (1); b) 1.5 T (Gyroscan Intera) Philips & c) 1.5 T (Gyroscan Intera) Philips	5.3	a) T1-weighted MPRAGE scans: Flip angle = 8°, Echo time (TE)= 4.38ms, Repetition time (TR)= 1750ms, slice thickness = 1mm, matrix= 256x208, Number of slices =150. b) T1-weighted spoiled gradient recalled (SPGR) scans: Flip angle = 40°, Echo time (TE)= 5ms, Repetition time (TR)= 24ms, slice thickness = 1mm, matrix= 256x256, Number of slices =150. c) T1-weighted SENSE 3D scans: Flip angle = 6°, Echo time (TE)= 3.6ms, Repetition time (TR)= 8ms, slice thickness = 1mm, matrix= 256x256, Number of slices =150.
5	**CIAM**	A subset of healthy controls from Cortical Inhibition and Attentional Modulation: a study of psychosis (CIAM) - UCT.	3T (Allegra) Siemens	5.3	TR/TE, 2300/3.93 ms; flip angle, 12 degrees, FOV, 256 mm×240mm×160mm;andvoxelsize,1.3mm×1.0mm×1.0mm.
6	**CLiNG**	A sample of healthy controls from Clinical Neuroscience Göttingen	3 T (Trio Tim) Siemens	5.3	A T1-weighted, 3D magnetization prepared rapid gradient echo sequence (MPRAGE) (TR/TE/TI/FA=2250 ms/3.26 ms/900 ms/9°; image matrix = 256 x 256; duration 8 min and 26 sec) was acquired generating 192 sagittal slices with a voxel size of 1 mm3.
7	**FBIRN**	Healthy subjects from Function Biomedical Informatics Research Network (FBIRN)	a) 3T (TimTrio) Siemens & b) 3T (Discovery MR750) GE	5.1	a) MP-RAGE scan: scan plane=sagittal, TR/TE/TI=2300/2.94/1100ms, GRAPPA acceleration factor=2, flip angle=9°, resolution=256×256x160, FOV=220mm2, voxel size=0.86x0.86x1.2mm, and NEX=1. b) IR-SPGR scan: scan plane=sagittal, TR/TE/TI=5.95/1.99/450ms,

8	**HMS**	Healthy subjects from the Homburg Multidiagnosis Study	1.5T (Sonata) Siemens	5.3	ASSET acceleration factor=2, a flip angle=12°, resolution=256×256x166, FOV=220mm2, voxel size=0.86x0.86x1.2mm, and NEX=1.
9	**HUBIN**	A sample of healthy subjects from Human Brain Informatics	1.5T (Signa) GE	4.0	A T1-weighted, magnetization prepared rapid gradient echo sequence (MPRAGE) (TR/TE/TI/FA=1900 ms/4.0 ms/700 ms/15°; image matrix = 256 x 256) was acquired generating 176 consecutive sagittal slices with a voxel size of 1 mm3. ~5 min
10	**IMAGEN**	The Imaging-genetics consortium, an European international population-based sample (Schumann et al., 2010)	3T (Achieva) Philips; 3T Brucker; 3T (TrioTim) Siemens ; 3T (Verio) Siemens; 3T (Signa Excite) Brucker/GE & 3T (Signa HDx) GE	4.1	T1-weighted images, using a three-dimensional spoiled gradient recalled (SPGR) pulse sequence, were acquired with the following parameters; 1.5 mm coronal slices, no gap, 35° flip angle, repetition time (TR) = 24 ms, echo time (TE) = 6.0 ms, number of excitations (NEX) = 2, field of view (FOV) = 24 cm, acquisition matrix = 256 × 192. Magnetic resonance imaging data were acquired at 8 European centers, using a standardised 3 Tesla, T1-weighted gradient echo protocol (voxel size=1.1 mm isotropic) based on that from the ADNI initiative (http://adni.loni.usc.edu/methods/documents/mri-protocols/)
11	**IMpACT**	The International Multicentre persistent ADHD Genetics CollaboraTion: a subset Dutch healthy controls	1.5 T (Avanto) Siemens	5.3	All scans had a voxel size of 1×1×1 mm3, TR 2730 ms, TI=1000 ms, TE 2.95 ms, 176 sagittal slices, field of view 256 mm.
12	**LBC-1936**	Lothian birth cohort from 1936: Scotish sample of healthy older subjects (age~70) born on 1936, as part of a study on brain aging and cognition (Wardlaw et al., 2011)	1.5 T (Signa Horizon HDx) GE	4.3	3D IR-Prep T1-weighted whole brain FSPGR volumes were acquired in the coronal plane using a GE Signa Horizon HDxt 1.5 T clinical MRI scanner with manufacturer supplied eight-channel phased-array head coil; FOV = 256 x 256 mm, matrix = 192 x 192, 160 x 1.3 mm thick slices, 1 x 1 x 1.3 mm voxels, TR = 10 ms, TE = 4 ms and TI = 500 ms.
13	**MAS**	Sydney's Memory and Aging Study: an epidemiological sample of european subjects http://www.ncbi.nlm.nih.gov/pubmed/20637138	3T (Achieva Quasar Dual scanner) Phillips	5.3	3D T1-weighted structural (T1w TFE – turbo field echo) MRI, acquired coronally with repetition time TR = 6.39 ms, echo time TE = 2.9 ms, flip angle = 8°, matrix size = 256 × 256, field of view FOV = 256 × 256 × 190 mm3, and slice thickness = 1 mm with no gap between; yielding 1 × 1 × 1 mm3 isotropic voxels
14	**MCIC**	MIND Clinical Imaging Consortium formed by the Mental Illness and Neuroscience Discovery (MIND) Institute now the Mind Research Network (MRN; http//ww.mrn.org)	1.5T Siemens, 3T (Trio) Siemens & 3T (Signa) GE	4.0	TR = 2530 ms for 3 T, TR = 12 ms for 1.5 T; TE = 3.79 ms for 3 T, TE = 4.76 ms for 1.5 T; FA = 7 for 3 T, FA = 20 for 1.5 T; TI = 1100 for 3 T; Bandwidth = 181 for 3 T, Bandwidth = 110 for 1.5 T; 0.625×0.625 mm voxel size; slice thickness 1.5 mm; FOV 256×256×128 cm matrix
15	**Meth-CT**	Healthy controls from studies on methamphetamine use; University of Cape Town	3T (Magnetom Allegra) Siemens	5.3	T1-weighted, 3D-MEMPRAGE sequence: TR = 2530ms; graded TE = 1.53/2.21/4.89/6.57 m; flip angle = 7°; FOV = 256mm;slice thickness = 1mm
16	**MüNC**	The Münster Neuroimaging Cohort	3T (Gyroscan Intera), Philips	5.3	T1-weighted images were acquired using a fast gradient echo sequence (turbo field echo), repetition time 7.4 milliseconds, echo time 3.4 milliseconds, flip angle 9°, acquired over a field of view of 256 (feet-head [FH]) 204 (anterior-posterior [AP]) 160 (right-left) and reconstructed to cubic voxels of .5 mm .5 mm .5 mm [RL]) mm A Siemens Sonata 1.5 Tesla scanner (Siemens, Erlangen, Germany) with a conventional head coil was used. Two 3D MP-RAGE T1-weighted sequences (duration: 8 min 46 s) were run for all participants. Each volume consisted of 128 sagittal slices (1.33x1x1 mm3), with an in-plane voxel size of 1 mm3 (TR=2730 ms; TE=3.43 ms; TI=1000 ms; flip angle=7°; and 256×256 matrix). #2: A Siemens Avanto scanner was used to acquire two 3D MP-RAGE T1-weighted sequences (TR/TE/TI/FA=2400 ms/3.61 ms/1000 ms/8°; matrix=192×192; duration 7 min and 42 s per volume). Each volume consisted of 160 sagittal slices (1.25×1.25×1.20 mm3)
17	**NCNG**	The Norwegian Cognitive NeuroGenetics sample : a population-based sample of European subjects (Espeseth et al., 2012)	1.5 T (Sonata) Siemens & 1.5 T (Avanto) Siemens	4.5	

18	**NESDA**	A subset of healthy controls from the Netherlands Study of Depression and Anxiety.	3T (Achieva; Intera) Phillips	5.0	Imaging data were acquired at the Leiden University Medical Center, Amsterdam Medical Center, and University Medical Center Groningen, equipped with a SENSE-8 (Leiden University Medical Center and University Medical Center Groningen) or SENSE-6 (Amsterdam Medical Center) channel head coil. For each subject, anatomical images were obtained using a sagittal 3DI gradient-echo T1-weighted sequence (TR=9 ms, TE=3.5 ms; matrix=256x256; voxel size=1x1x1mm3; 170 slices; duration=4.5 minutes).
19	**NeuroIMAGE**	A sample of european healthy controls and healthy siblings of ADHD patients	1.5 T (Sonata), Siemens and 1.5 T (Avanto), Siemens	5.3	1.5T MRI scanners were employed (Siemens SONATA and Siemens AVANTO; Siemens, Erlangen, Germany), using identical head coils (8-channel Phase Array Head Coil). T1-weighted whole-brain scan (MP-RAGE, 176 slices, acquisition matrix 256x256, voxelsize:1.0x1.0x1.0mm; TE/TR=2.95/2730ms, TI=1000ms, FA=7°; GRAPPA-acceleration 2)
20	**OATS**	One individual per family of The Older Australian Twins Study	1.5 T (Gyroscan) Philips; 3T (Achieva Quasar Dual) Philips; 1.5 T (Magnetom Avanto) Siemens; 1.5 T (Sonata) Siemens	5.3	(1) Sequence name T1TFE. In-plane resolution 1×1 mm. 256 × 256 matrix. Slice thickness 1.5 mm without gap. Number of slices: 150. Orientation: cor TR/TE: 7.73/3.7 ms Flip angle: 8°. Scan duration: 385 sec. (2) Acquisition parameters for T1-weighted structural MRI scans were: TR = 6.39 ms, TE = 2.9 ms, flip angle = 8°, matrix size = 256x256, FOV = 256x256x190, and slice thickness = 1 mm with no gap between; yielding 1x1x1 mm3 isotropic voxels (3) in-plane resolution= 1×1 mm, slice thickness= 1.5 mm, slice number=144, TR (Repetition time) =1530 ms, TE (Echo time) = 3.24 ms, TI (Inversion time)= 780 ms, flip angle=8 and NEX (Number of Excitations) =1. (4) in-plane resolution= 1×1 mm, slice thickness= 1.5 mm, slice number=144, TR (Repetition time) =1530 ms, TE (Echo time) = 3.24 ms, TI (Inversion time) = 780 ms, flip angle=8 and NEX (Number of Excitations) =1.
21	**OCD-AMC**	Control subjects from studies on OCD (pedriatric)	3T (Intera) Philips	5.3	3T (Philips Intera MR) matrix 256x256, 182 slices, voxel size 1x1x1.2mm
22	**OCD-Barcelona**	Control subjects from studies on OCD	1.5T (Signa Excite) GE	5.3	matrix 256x256, 130 slices, voxel size 1.2x1.2x1.2mm
23	**OCD-Fukuoka**	Control subjects from studies on OCD	3T (Achieva TX) Philips	5.3	3T (Philips Achieva TX) matrix 240x240, TR 8.2ms, TE 3.8ms, TI(inversion time) 240 ms, Flip angle 8 degree, FOV 240x240, NSA 1, Slice tickness 1mm, number of slice 190, voxel size 1.8x1.8.1.8mm, scan time 320s
24	**OCD-India 1.5T**	Healthy controls, examined using a structured interview to rule out a psychiatric diagnosis or neurological disease	1.5T (Vison) Siemens	5.3	1.5T (Siemens Vision): matrix 256x256, 160 slices, 0.98x0.98x 1mm
25	**OCD-India 3T**	Healthy controls, examined using a structured interview to rule out a psychiatric diagnosis or neurological disease	3T (Skyra) Siemens	5.3	3T (Siemens Skyra): matrix 256X256, 192 slices, voxel size 1.0 X 1.0 X 1.0 mm;
26	**OCD-Kunming 1.5T**	Control subjects from studies on OCD	1.5T (Signa Excite) GE	5.3	1.5T (Signa Excite) GE: matrix 256x256, 172 slices, voxel size 0.93x0.93x0.9mm
27	**OCD-Kunming 3T**	Control subjects from studies on OCD	3T (Achieva) Philips	5.3	3T (Achieva) Philips : matrix 228x228, 230 slices, FOV=250, voxel size 1.1x1.1x0.6mm
28	**OCD-Kyoto 1.5T**	Control subjects from studies on OCD	1.5 T (Gyroscan Intera) Philips	5.3	Three-dimensional volumetric acquisition of a T1-weighted gradient echo sequence produced a gapless series of contiguous, thin sagittal sections with the following parameters: flip angle, 15°; acquisition matrix, 256 × 256; field of view, 25 cm; section thickness, 1.5 mm; voxel size, 0.98 mm × 0.98 mm × 1.5 mm; TR, 9.9 ms; TE, 5.8 ms.
29	**OCD-Kyoto 3T**	Control subjects from studies on OCD	3T (Achieva 3.0 TX) Philips	5.3	The scanning parameters of the T1-weighted three-dimensional magnetization-prepared rapid gradient-echo (3D-MPRAGE) sequences were as follows: flip angle, 10 degrees; acquisition matrix, 256x256x170; field of view, 25.6 cm; section thickness, 1.0 mm; voxel size, 1.0 mmx1.0 mmx1.0 mm; TR, 7.1 ms; and TE, 3.3 ms.

30	**OCD-London**	Control subjects from studies on OCD	1.5 T (Signa) GE and 1.5T (Signa HDx) GE	5.3	Sequence 1: 3D SPGR, TR: 14.8ms, TE: 1.7ms, FA: 20º, Orientation: Axial, Matrix size: 256 x 256 x 124, Voxel size: 0.94 x 0.94 x 1.50; Sequence 2: 3D SPGR, TR: 10.8ms, TE: 5.0ms, FA: 18º, Orientation: Axial, Matrix size: 256 x 256 x 146, Voxel size: 1.09 x 1.09 x 1.10
31	**OCD-Shanghai**	Control subjects from studies on OCD	3T (Verio) Siemens	5.3	3T (Siemens verio) matrix 256x256, 192 slices, slice tickness 1.0mm, voxel size 1x1x1mm, TR 2300ms, TE 2.96ms, FOV 256x240, flip angle 9 degree
32	**OCD-SNU A**	Control subjects from studies on OCD	1.5T (Signa) GE	5.3	MPRAGE sequence were acquired in 176 contiguous axial slices: TR/TE = 1160/4.76 ms, field of view = 23 cm, flip angle = 15°, matrix 416x512, voxel size 0.45x0.45x0.90 mm.
33	**OCD-SNU B**	Control subjects from studies on OCD	1.5T (Avanto) Siemens	5.3	Contiguous 1.5-mm sagittal images were obtained with a three-dimensional T1-weighted spoiled gradient-echo sequence (echo time=5.5 ms; repetition time=14.4 ms; flip angle=20°; field of view=21×21 cm; matrix 256x256; voxel size 0.82x0.82x1.50 mm).
34	**OCD-SNU C**	Control subjects from studies on OCD	3T (Magnetom Trio) SIemens	5.3	High-resolution T1-weighted, three-dimensional MPRAGE (TR = 670 ms; TE = 1.89 ms; FOV = 50 mm; FA = 9°; matrix 256x256; voxel size 1.000x0.977x0.977mm).
35	**OCD-SU**	Control subjects from studies on OCD	3T (Magnetom Allegra) Siemens	5.3	T1-weighted MPRAGE sagittal 3D volume (TR=2300ms ;TE=3.93ms; TI=1100ms; 160 slices; FOV=256 x 240 mm; voxel size=1.3x1.0x1.0 mm3; slice thickness= 1 mm, flip angle=12 degrees
36	**OCD-VUmc Amsterdam 1.5T**	Control subjects from studies on OCD	1.5T (Sonata) Siemens	5.3	1.5T (Siemens Sonata) matrix 256x256, 160 slices, voxel size 1x1x1.5mm
37	**OCD-VUmc Amsterdam 3T**	Control subjects from studies on OCD	3T (Signa HDxt) GE	5.3	3T (Signa HDxt) matrix 256x256, 172 slices, voxel size 1x0.977x0.977 mm
38	**OCD-Zurich**	Healthy control subjects (adolescents and adults)	3T (Achieva) Philips	5.3	3T (Philips Achieva) matrix 240x240, 160 slices, voxel size isotropic 1x1x1mm, TR 8.14ms, TE 3.7ms, Flip angle 8 degree
39	**Osaka 1.5T**	Control subjects from the Japanese Osaka case-control studies of schizophrenia	1.5 T (Signa) GE & 3T (Signa HDxt) GE	5.3	T1-weighted IR-FSPGR sagittal 3D volume (TR=12.6 ms; TE=4.2 ms; TI=400 ms; 124 slices, matrix size=256x256, FOV=24.0x24.0 cm2, voxel size=0.9375x0.9375x1.4 mm3, slice thickness = 1.4 mm, flip angle=15°) T1-weighted IR-FSPGR sagittal 3D volume (TR=7.2 ms; TE=2.9 ms; TI=400 ms; 172 slices, matrix size=256x256x172, FOV=24.0x24.0 cm2, voxel size=0.9375x0.9375x1.0 mm3, slice thickness = 1.0 mm, flip angle=11°)
40	**Osaka 3T**	Control subjects from the Japanese Osaka case-control studies of schizophrenia	1.5 T (Signa) GE & 3T (Signa HDxt) GE	5.3	T1-weighted IR-FSPGR sagittal 3D volume (TR=12.6 ms; TE=4.2 ms; TI=400 ms; 124 slices, matrix size=256x256, FOV=24.0x24.0 cm2, voxel size=0.9375x0.9375x1.4 mm3, slice thickness = 1.4 mm, flip angle=15°) T1-weighted IR-FSPGR sagittal 3D volume (TR=7.2 ms; TE=2.9 ms; TI=400 ms; 172 slices, matrix size=256x256x172, FOV=24.0x24.0 cm2, voxel size=0.9375x0.9375x1.0 mm3, slice thickness = 1.0 mm, flip angle=11°)
41	**PAFIP-IDIVAL1**	Healthy controls from studies on schizofrenia	1.5T (Signa) GE	5.0	T1-weighted images, using a spoiled grass (SPGR) sequence, were acquired in the coronal plane with the following parameters: TE = 5ms, TR =24ms, NEX =2, FA=45o , FOV =26x19.5cm, slice thickness=1.5mm and a matrix of 256x192
42	**PAFIP-IDIVAL2**	Healthy controls from studies on schizofrenia	3T (Achieva) Phillips	5.3	Sagittal T1,TR=3000ms; TE=4.6ms; FA=8o; Voxel size=1x1x1 mm; Slice thickness=1mm ; Matrix size=321x312
43	**PAFIP-IDIVAL3**	Healthy controls from studies on schizofrenia	1.5T (Signa) GE	5.0	T1-weighted images, using a spoiled grass (SPGR) sequence, were acquired in the coronal plane with the following parameters: TE = 5ms, TR =24ms, NEX =2, FA=45o , FOV =26x19.5cm, slice thickness=1.5mm and a matrix of 256x192
44	**QTIM**	An aselect subset of twin-singletons of european descent from The Queensland Twin Imaging study.	4T (Bruker) Medspec	5.3	Scans were collected on a 4 Tesla Bruker Medspec scanner (Bruker, Germany). T1-weighted structural scans were acquired with acquisition parameters: TR=1500ms, TE=3.35ms, TI=700ms, flip

					angle=8°, 256 or 240 (coronal or sagittal) slices, FOV=240mm, acquisition voxel size 1.1x0.9x0.9mm.
45	**SHIP-2**	Population based sample from The Study of health in Pomerania (north-eastern Germany)	1.5 T (Avanto) Siemens	5.1	3D T1-weighted MRI sequence with the following parameters: MP-RAGE/ axial plane, TR=1900 ms, TE=3.4 ms and Flip angle=15° and an original resolution of 1.0 x 1.0 x 1.0mm3
46	**SHIP-T**	Population based sample from The Study of health in Pomerania (north-eastern Germany)	1.5 T (Avanto) Siemens	5.1	3D T1-weighted MRI sequence with the following parameters: MP-RAGE/ axial plane, TR=1900 ms, TE=3.4 ms and Flip angle=15° and an original resolution of 1.0 x 1.0 x 1.0mm3
47	**STROKEMRI**	Healthy controls from an ongoing stroke study, Oslo	3T (HDxT) GE	5.3	Sagittal T1-weighted FSPGR sequence (TE: 2.956, TR: 7.8 ms, flip angle: 12 degrees, voxel sixe=1 x 1 x 1.2 millimeter, number of slices: 166)
48	**TCD|NUIG**	Healthy subjects from TCD (Dublin) and NUIG (Galway)	TCD : 3T (Intera) Philips; NUIG : 1.5T (Magnetom), Siemens	TCD : 5.3 NUIG : 5.1	TCD: T1-weighted TFE gradient echo (TE (ms) 3.8 ; TR (ms) 8.4 ; Flip angle (°) 8; FOV 230 ; Matrix 256 x 256; No. slices 180; slice thickness (mm) 0.9; Voxel-size (mm3) 0.9 x 0.9 x 0.9); NUIG: 1.5T: T1-weighted MP-RAGE (TE (ms) 4.38; TR (ms) 1140; Flip angle (°) 15; FOV 230 ; Matrix 512 x 512 (k-space interpolation from 256x256); No. slices 160; slice thickness (mm) 0.9; Voxel-size (mm3) 0.45 x 0.45 x 0.9)
49	**TOP**	Control subjects from Tematisk Område Psykoser (Thematically Organized Psychosis Research)	1.5T (Sonata) Siemens	5.3	Two sagittal T1-weighted magnetization prepared rapid gradient echo (MPRAGE) volumes were acquired with the Siemens tfl3d1_ns pulse sequence (TE = 3.93 ms, TR = 2730 ms, TI = 1000 ms, flip angle = 7°; FOV = 24 cm, voxel size= 1.33 x 0.94 x 1 mm3, number of partitions = 160)
50	**UCLA|NL BP**	Healthy controls from the Bipolar Genetics dataset. This NIMH-funded study is carried out at the University Medical Center Utrecht, the Netherlands, in a collaboration with the University of California Los Angeles	3T (Achieva) Philips	5.1	Three-dimensional T1-weighted images were acquired on a 3 Tesla Philips Achieva scanner (Philips Healthcare, Best, the Netherlands), equipped with an 8-channel SENSE-headcoil. Fast field echo scans with 200 contiguous sagittal slices (TE=4.6 ms, TR=10 ms, flip angle=8°, FOV=240 mm, 0.75 x 0.75 x 0.80 mm³ voxels) were obtained.
51	**UMCU**	Healthy controls from two independent schizophrenia cohorts recruited at the University Medical Centre Utrecht, the Netherlands	1.5T (Achieva) Philips	5.1	A Three-Dimensional-Fast Field Echo (3D-FFE) on a 1.5T Philips Achieva scanner: TE=4.6ms, TR=30ms, flip angle=30°, FOV=256x256mm2) with 160-180 contiguous coronal 1.2 mm slices
52	**Würzburg|Tübingen**	Data set of healthy controls from a study on ADHD	1.5T (Avanto) Siemens	5.3	A high-resolution T1-weighted magnetization-prepared rapid gradient-echo imaging (MP-RAGE) 3D MRI sequence was obtained from each participant (TR: 2250ms, TE: 3.93ms, 8° flip angle, FOV: 256mm, matrix: 256×256, voxel size: 1×1×1mm3

Supplementary Table S2. Meta-analysed results from testing population-level lateralization (mean AI's ≠ 0) separately by sex. A positive Z-score indicates leftward asymmetry in volume (L>R), while a negative Z-score reflects a rightward asymmetry (R>L).

Females	N	z-score
Nucleus accumbens	7957	-11.01
Amygdala	8049	-33.36
Caudate nucleus	7980	-34.92
Globus pallidus	7892	23.61
Hippocampus	7971	-22.67
Putamen	7920	59.86
Thalamus	8043	41.43

Males	N	z-score
Nucleus accumbens	7053	-4.80
Amygdala	7118	-32.72
Caudate nucleus	7125	-31.12
Globus pallidus	7040	31.16
Hippocampus	7075	-20.14
Putamen	7041	53.16
Thalamus	7115	33.44

Supplementary Table S3. List of datasets (arranged alphabetically) on which handedness analyses were performed, corresponding sample sizes and assessment methods.

Dataset	Left handed	Right handed	Assessment
BIG 1.5T	67	1205	Self-report
BIG 3T	56	1150	Self-report
BIL & GIN	205	248	Self-report
CLiNG	15	307	Self report confirmed by Edinburgh Handedness Inventory
FBIRN	5	173	Self-report
HMS	7	44	Self report confirmed by Edinburgh Handedness Inventory
HUBIN	6	90	Self-report
IMAGEN	160	1391	Self report confirmed by Purdue Pegboard test
IMpACT	15	126	Self-report
LBC-1936	34	522	Writing hand
MCIC	9	154	Annett Scale of Hand Preference
MüNC	14	729	Edinburgh Handedness Inventory: A threshold of 12 (out of 14) items was used to categorize as left- or right-handed.
NCNG	26	301	Self-report
NESDA	5	61	Self-report
NeuroIMAGE	45	333	Self-report
OCD-VUmc Amsterdam 1.5T	6	48	Self-report
OCD-VUmc Amsterdam 3T	7	31	Self-report
Osaka 1.5T	28	409	Self report confirmed by Edinburgh Handedness Inventory
Osaka 3T	11	226	Self report confirmed by Edinburgh Handedness Inventory
SHIP-2	57	1053	Self-report
SHIP-Trend	97	1943	Self-report
STROKEMRI	6	46	Self-report
TOP	22	279	Self-report
UCLA|NL BP	20	140	Self-report
UMCU	36	227	Self-report

Supplementary information S4 : Left-right flip checks

Of special importance was to assure the correct correspondence between the left/right orientation of the processed image data and the original subject space. In contrast to the other axes (antero-posterior or superior-inferior), the correct orientation on the left-right axis is not directly identifiable from visual features, making it difficult to readily detect any erroneous image flips during processing. Such problems are much more unlikely since the adoption of the nifti imaging standard (http://nifti.nimh.nih.gov/), but they can still be a potential source of artifact if the raw (often DICOM-formatted) data is processed with incorrect assumptions (SPM documentation, p. 157; http://www.fil.ion.ucl.ac.uk/spm/doc/manual.pdf).

Because the ENIGMA protocol starts after the raw (often DICOM-formatted) data has been converted into an imaging standard (or converted by FreeSurfer itself), this meant that conversion from the DICOM format was the most likely step where any error could have taken place. This was assessed using several strategies, depending on the available information at each site. The **BIL & GIN**, **FBIRN**, **MAS**, **NESDA** and **OATS** samples had made use of paramagnetic fiducial markers on a subset of their subjects, thus eliminating orientation ambiguity. In **QTIM** and **SHIP**, subjects with a known unilateral brain abnormality were used to check the correct orientation of the image after conversion. In **BIG**, **CLiNG**, **HMS** and **OCD-SU,** a few examples were manually checked for mismatches between the DICOM and nifti header information, i.e. a correct flip from 'radiological' to 'neurological' orientation. Finally, we checked the consistency between several, commonly used, DICOM to nifti conversion tools and DICOM images generated from different manufacturers/models (using examples downloaded from the manufacturer's websites). The convertors used in this step were: "mri_convert" (https://surfer.nmr.mgh.harvard.edu/pub/docs/html/mri_convert.help.xml.html), " MRIConvert" (http://lcni.uoregon.edu/downloads/mriconvert), "dcm2nii" (http://www.cabiatl.com/mricro/mricron/dcm2nii.html) and "spm_dicom_convert" (http://www.fil.ion.ucl.ac.uk/spm/).

Given that these checks yielded no problems, and that the datasets where no error was detected comprised 60% of the total meta-analysis sample, we were confident that such orientation errors must have been very unlikely.

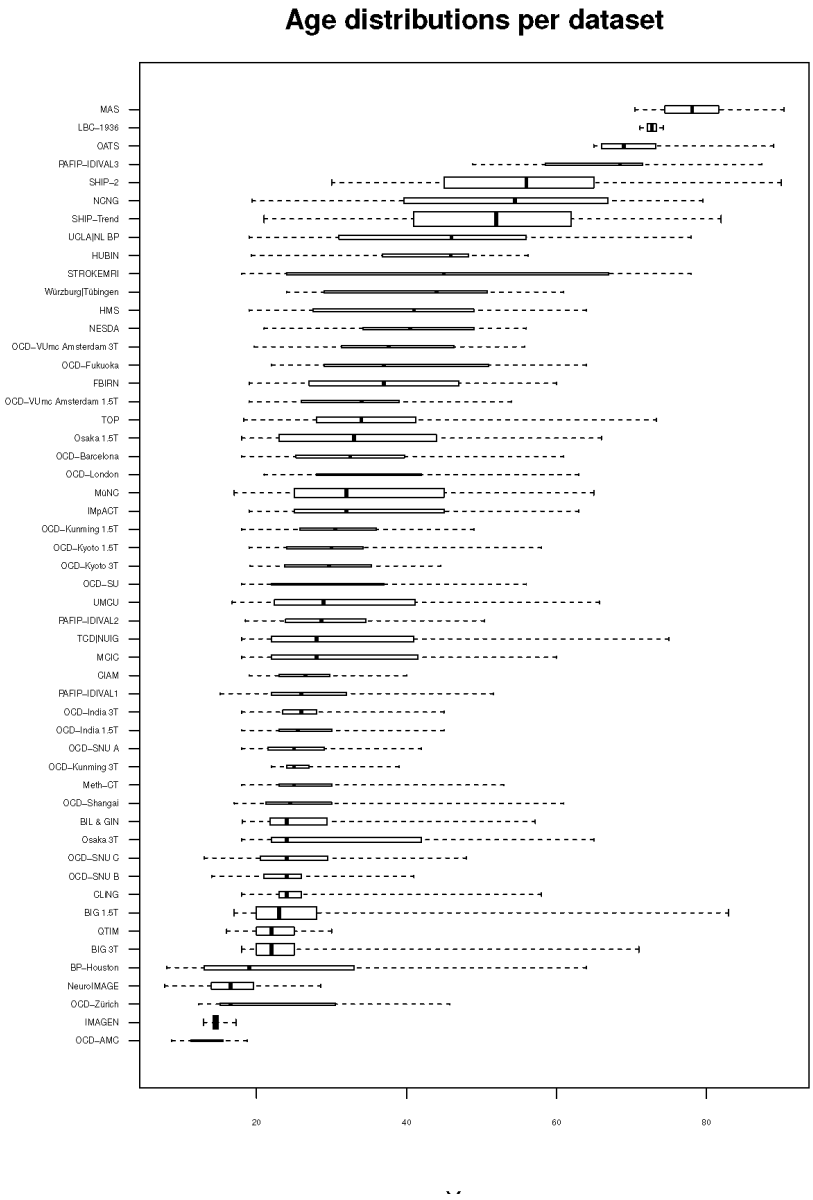

Supplementary Figure S1. Boxplots show the age distribution per cohort. The datasets are ordered vertically by median age, oldest at the top. On the x-axis are the age values (in years). The horizontal length of each boxplot represents the age at the 2nd and 3rd quartile of their distribution (thus containing half the respective dataset). The vertical width of the boxes is proportional to the square root of the dataset sample size. Boxes are split at the median age, and the whiskers reach to the minimum and maximum ages.

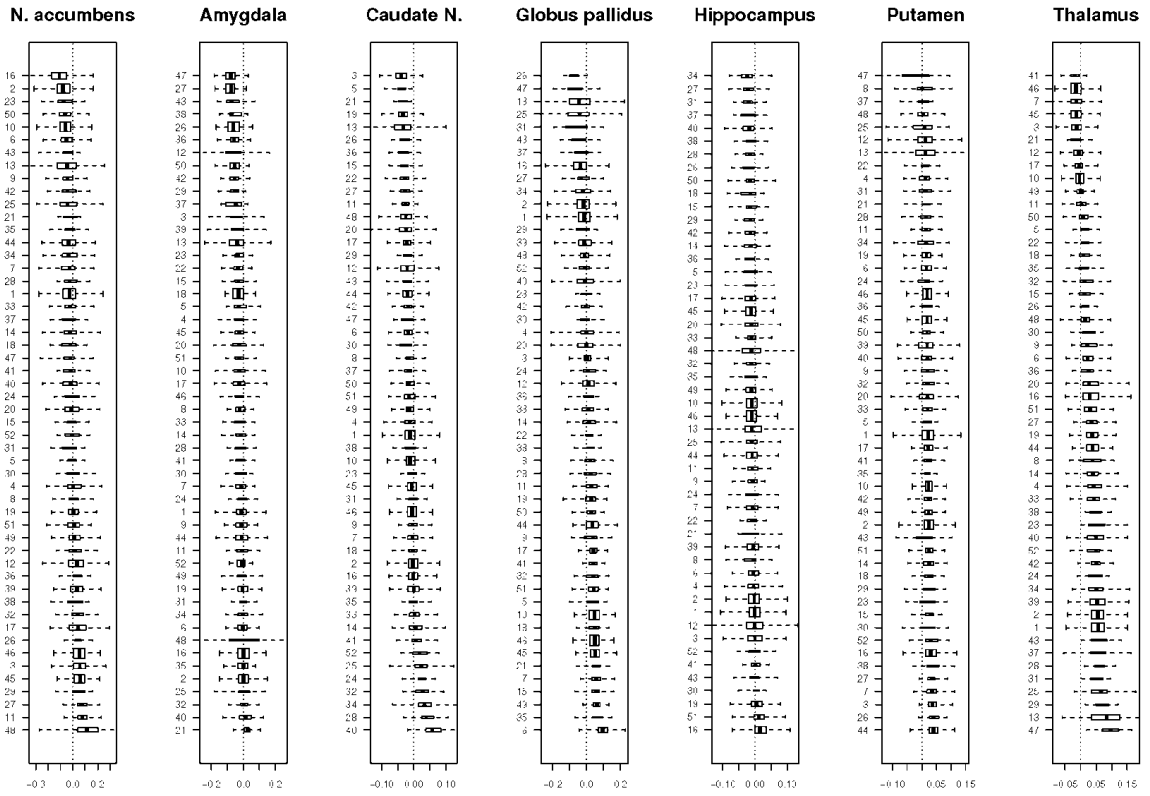

Supplementary Figure S2. Boxplots of AI distributions for each dataset and structure. For each structure, the datasets are ordered top-to-bottom by their median AIs. The identities of the datasets are given by the numbers in the lefthand columns, with reference to Table 1. The horizontal length of each box represents the 2nd to 3rd quartile of the AI distribution (i.e. containing half of subjects in each dataset) and split at the median AI. The vertical width of each dataset's box is proportional to the square root of its sample size. The whiskers show the minimum and maximum values (curtailed in cases where the outer box boundary was reached). The vertical dotted lines indicate the points of perfect symmetry, AI=0.

Chapter 6

General discussion

Brief summary of the background

Left-right asymmetry is an important aspect of brain organization, which is of relevance to human evolution, higher cognitive functions, and cognitive disorders. Key issues regarding the multifactorial nature and molecular/developmental basis of brain asymmetries remain virtually unexplored (Bishop, 2013; Francks, 2015; Ocklenburg et al., 2014). The present dissertation approached these open questions by assessing the effects of various biological factors on natural variability in brain morphological lateralization.

Contributions to brain asymmetry research

Sex and handedness are prominent factors in most theoretical accounts of cerebral lateralization. However, clear links between these factors and anatomical brain asymmetries in particular, remain elusive (see Chapter 1). A major source of uncertainty can be attributed to methodological heterogeneity between previous studies of these factors, which nonetheless have also suggested that they likely exert only subtle effects on the healthy variability in brain asymmetries. In order to achieve further progress, therefore, the set of investigations presented in this dissertation were based on the largest samples ever used to address these questions, in combination with uniform brain image analysis methods.

With regards to the effect of sex, I revealed subtle but statistically unambiguous links to anatomical brain asymmetries, in the cerebral cortex as well as subcortical structures (Chapter 3 & 5). In Chapter 3, for example, my survey of grey matter asymmetries over the entire cerebral cortex identified several regions showing subtle sexual dimorphisms. Of these, asymmetries corresponding to the planum temporale region were the most sexually dimorphic in the human brain. Although subtle, the observed effect of sex on planum temporale asymmetry was strongly significant in the BIG dataset (a sample of over 2,000 healthy subjects). Moreover, via a collaboration I replicated this finding in two independent datasets, thereby providing unambiguous evidence for sexual dimorphism of this particular brain asymmetry; prior to my study this was still debated issue (Sommer et al., 2008). In Chapter 5, in a meta-analysis that pooled results from several datasets from various populations, for a combined total sample of over 15,000 participants, I was able to discover even more subtle sex differences in the asymmetry of subcortical structures. My results strongly suggest that sex does have an effect, although subtle, on brain asymmetries, in addition to other aspects of brain morphology.

Conversely, my investigations of handedness did not establish any of its putative correlates with structural brain asymmetries, neither cortical nor subcortical (Chapter 2 & 5). In contrast to previous studies on this subject, my findings were less susceptible to an important limitation that usually affects handedness research, which has permeated the previous literature. This is the strongly unbalanced distribution of human handedness in the population, which often results in insufficient numbers of left-handers, within study samples of tens to low hundreds of individuals. The large samples that I used allowed, for the first time, adequate representations of the left-handed population, so that the null results which I obtained were based on sufficient statistical power to allow strong conclusions to be drawn. . A case in point, the null-findings described in Chapter 2 (where I studied handedness in relation to cerebral cortical grey matter asymmetries) strongly discourage the use of cortical anatomical features as endophenotypes to study the neural mechanisms of handedness in the adult brain, at least as defined by the image analysis method and brain atlas that I used. Together with previous reports of handedness being modestly heritable (Medland et al., 2009), my results further stress the need to investigate this trait as a complex and heterogeneous phenomenon.

It is important to note that, in contrast to experimentally designed studies, effect sizes observed from studies of natural variability do not directly serve as a proxy for the conceptual importance of an investigated factor. Rather, identifying a subtle effect can provide an entry point from which to further probe the complex biology underlying a human trait. This consideration is particularly relevant when investigating the genetic architecture of brain asymmetries through attributing some of their variability to genetic polymorphisms in the population. In chapter 3, for example, the initial finding of a subtle sex difference in asymmetry of the planum temporale informed the subsequent genetic analyses, eventually associating two specific gene networks involved in steroid hormone biology to individual differences in this asymmetry.

The investigations described in Chapter 3 & 4 constitute the first genome-wide, molecular genetic studies to have been performed in direct relation to human brain asymmetrical measures. In order to robustly identify the effects of individual genetic polymorphisms on brain morphology, each of which is likely to explain only a tiny fraction of phenotypic variability, statistical power will benefit from sample sizes in the order of tens of thousands (e.g. (Hibar et al., 2015; Stein et al., 2012). For this reason I now participate as the primary data analyst in the Lateralization working group within the ENIGMA (Enhancing Neuro Imaging Genetics through Meta-Analysis) consortium (Thompson et al., 2014). An international network of researchers, one of ENIGMA's main objectives is to identify genetic variants

which affect brain structure. My first investigation performed in this context is described in Chapter 5, a meta-analysis of sex, handedness and age effects on volumetric asymmetries of subcortical structures. While this investigation was not directly aimed at discovering genetic variants associated to brain asymmetry, I showed through this approach that we were able to detect very subtle group differences in brain asymmetry. Moreover, this study included analyses of heritability that indicated which of the subcortical structural asymmetries were under the strongest overall genetic control (heritability).

The series of studies composing this dissertation followed a common strategy. My investigations were done on large and complex datasets comprising both genetic and brain imaging data, each requiring several stages of processing prior to the experimental analyses. As a result, my dependence on automated methods for defining and measuring variables of interest from such rich datasets had to be evaluated in terms of reliability. Such careful assessments constituted central parts of all my empirical investigations, presented in Chapters 2 through 5.

To conclude, the investigations and findings presented in this dissertation have illustrated the utility of large-scale and meta-analytic approaches, as a means to reliably provide novel insights into the biological underpinnings of brain asymmetry.

Further scientific contributions

The studies performed for this dissertation also led to my involvement, as a co-author, in various other large-scale investigations of brain structure and genetics. Below are summaries of those most closely related to the main themes covered by this dissertation:

Brucato N, **Guadalupe T**, Franke B, Fisher SE, Francks C. (2015): A schizophrenia-associated HLA locus affects thalamus volume and asymmetry. Brain Behav Immun 46:311-8.

Certain genetic variants involved in the regulation of the human immune system have been found to convey a slight risk of developing schizophrenia. In addition, schizophrenia has also been linked to abnormal asymmetries of the thalamus and hippocampus. In this study, we found that common genetic variants linked to the immune system were related to changes in asymmetry of the thalamus in a sample of healthy adults. The genetic mechanisms underlying this association may relate to how these genetic variants influence susceptibility to schizophrenia.

Cai DC, Fonteijn H, **Guadalupe T**, Zwiers M, Wittfeld K, Teumer A, Hoogman M, AriasVasquez A, Yang Y, Buitelaar J, Fernandez G, Brunner HG, van Bokhoven H, Franke B, Hegenscheid K, Homuth G, Fisher SE, Grabe HJ, Francks C and Hagoort P. (2014): A genome-wide search for

quantitative trait loci affecting the cortical surface area and thickness of Heschl's gyrus. Genes Brain Behav 13(7):675-85.

The gyrus of Heschl, located bilaterally on the superior temporal gyrus, is a key region involved in auditory processing. Highly variable between individuals and hemispheres, its morphology has been linked to performance in specific auditory tasks. In this study, we performed a genome-wide screen for genetic polymorphisms associated to the morphology of this brain structure, in a total sample of 3,000 individuals.

Hoogman M, **Guadalupe T**, Zwiers MP, Klarenbeek P, Francks C, Fisher SE. (2014): Assessing the effects of common variation in the FOXP2 gene on human brain structure. Front Hum Neurosci 8:473.

Disrupting mutations of the FOXP2 gene have been shown to cause a severe form of language and speech impairment, including effects on brain structure and function. Subsequently, common genetic variants of FOXP2 have been investigated with regards to their effects on normal language processing in neuroimaging studies. In this study, based on a large sample of healthy individuals, we observed no association between common variants of the FOXP2 gene and brain morphology. We concluded by proposing more careful interpretations of previous neuroimaging genetics studies, which have often relied on experimental designs that did not provide adequate statistical power.

Gialluisi A, **Guadalupe T**, Francks C, Fisher SE.: Neuroimaging genetic analyses of novel candidate genes associated with reading and language. Brain and Language (in press).

Here we investigated the relationship between common genetic variants, which had been previously suggested to affect performance in language-related tasks, and structural changes of cortical regions of the language network. A suggestive association with a genetic variant of the RBFOX2 gene was discussed.

Becker M, **Guadalupe T**, Franke B, Hibar DP, Renteria ME, Stein JL, Thompson PM, Francks C, Vernes SC, Fisher SE. (2016): Early developmental gene enhancers affect subcortical volumes in the adult human brain. Hum Brain Mapp.

In this study we investigated whether genetic variants known to be located in genomic enhancer elements, which are active during forebrain development for regulating gene expression levels, showed association with changes in the volumes of subcortical structures. The analysis, based on the summary statistics from a large scale study of the ENIGMA consortium (Hibar et al., 2015), yielded an association

between genetic variability within these loci and variability in the volume of the hippocampus in the adult brain.

Future directions

Building upon the findings of this dissertation, and on the expertise gained from it, I am further pursuing this line of research on the biological underpinnings of brain asymmetry. As the hands-on leader of the ENIGMA-Lateralization working group, the focus of my next set of projects will be on cerebral cortical asymmetries, and the relevance of altered asymmetry to disorders including schizophrenia, major depression, and obsessive-compulsive disorder. Highly powered, large-scale investigations, which are possible within ENIGMA, will play a central role in detecting and measuring many of the relevant factors (genetic and non-genetic) which constitute the complex biology of brain asymmetry.

In parallel to my ENIGMA studies, which can be logistically intensive (relying on collaboration among many researchers located all over the world), I plan to perform other complementary projects, which will be based primarily on Nijmegen's Brain Imaging Genetics (BIG) dataset and the recently available genetic and brain MRI datasets from the UK-biobank. This complementary line of investigations will focus on the poorly understood link between anatomical and functional asymmetries (see Chapter 1). In other words, how and to what extent do anatomical brain asymmetries sub-serve the prominent functional lateralizations observed in humans (Ocklenburg et al., 2014; Willems et al., 2014). We will investigate these putative links using structural and resting-state (f)MRI scans from the UK-biobank resource. In close collaboration with partners in the University of Bordeaux, these investigations will include the development and application of newer imaging methodology, aimed at improving both the definition and measurement of brain asymmetrical features. The most popular automated tools to study brain morphology currently, for example, were not initially designed to allow comparisons between the left and right hemispheres. Various brain asymmetries, including brain torque or the several dimensions of peri-sylvian asymmetries, have not been able to be investigated at the scale that is now possible. In addition, we are now implementing a test of language lateralization that will be performed by the new participants of the BIG study, as part of an online test-battery. In time, this will allow us to assess the relevance of structural asymmetries directly on the performance of a language-related task.

References

Abedelahi A, Hasanzadeh H, Hadizadeh H, Joghataie MT. (2013): Morphometric and volumetric study of caudate and putamen nuclei in normal individuals by MRI: Effect of normal aging, gender and hemispheric differences. Pol J Radiol 78(3):7-14.

Abu-Rustum RS, Ziade MF, Abu-Rustum SE. (2013): Reference values for the right and left fetal choroid plexus at 11 to 13 weeks: an early sign of "developmental" laterality? J Ultrasound Med 32(9):1623-9.

Alkonyi B, Juhasz C, Muzik O, Behen ME, Jeong J-W, Chugani HT. (2010): Thalamocortical Connectivity in Healthy Children: Asymmetries and Robust Developmental Changes between Ages 8 and 17 Years. AJNR Am J Neuroradiol 32(5):962-969.

Almasy L, Blangero J. (1998): Multipoint quantitative-trait linkage analysis in general pedigrees. Am J Hum Genet 62(5):1198-211.

Altarelli I, Leroy F, Monzalvo K, Fluss J, Billard C, Dehaene-Lambertz G, Galaburda AM, Ramus F. (2014): Planum temporale asymmetry in developmental dyslexia: Revisiting an old question. Hum Brain Mapp 35(12):5717-35.

Amunts K, Schlaug G, Schleicher A, Steinmetz H, Dabringhaus A, Roland PE, Zilles K. (1996): Asymmetry in the Human Motor Cortex and Handedness. Neuroimage 4(3):216-222.

Annett M. (1967): The binomial distribution of right, mixed and left handedness. Q J Exp Psychol 19(4):327-33.

Annett M. (1972): The distribution of manual asymmetry. Br J Psychol 63(3):343-58.

Annett M. (1981): The Right Shift Theory of Handedness and Developmental Language Problems. Bulletin of the Orton Society 31:103-121.

Annett M. 1985. Left, Right, Hand and Brain: The Right Shift Theory. London: Laurence Erlbaum Associates.

Armour JA, Davison A, McManus IC. (2014): Genome-wide association study of handedness excludes simple genetic models. Heredity 112(3):221-225.

Arning L, Ocklenburg S, Schulz S, Ness V, Gerding WM, Hengstler JG, Falkenstein M, Epplen JT, Gunturkun O, Beste C. (2013): VNTR Polymorphism Is Associated with Degree of Handedness but Not Direction of Handedness. PLoS One 8(6).

Ashburner J. (2007): A fast diffeomorphic image registration algorithm. Neuroimage 38(1):95-113.

Ashburner J, Friston KJ. (2000): Voxel-based morphometry--the methods. Neuroimage 11(6 Pt 1):805-21.

Ashburner M, Ball CA, Blake JA, Botstein D, Butler H, Cherry JM, Davis AP, Dolinski K, Dwight SS, Eppig JT and others. (2000): Gene ontology: tool for the unification of biology. The Gene Ontology Consortium. Nat Genet 25(1):25-9.

Aylward EH, Reiss AL, Reader MJ, Singer HS, Brown JE, Denckla MB. (1996): Basal ganglia volumes in children with attention-deficit hyperactivity disorder. J Child Neurol 11(2):112-5.

Badzakova-Trajkov G, Häberling IS, Roberts RP, Corballis MC. (2010): Cerebral Asymmetries: Complementary and Independent Processes. PLoS One 5(3):e9682.

Balconi M, Finocchiaro R. (2015): Decisional impairments in cocaine addiction, reward bias, and cortical oscillation "unbalance". Neuropsychiatr Dis Treat 11:777-86.

Bastian HC. (1866): On the Specific Gravity of Different Parts of the Human Brain. The British Journal of Psychiatry 11(56):465-511.

Becker M, Guadalupe T, Franke B, Hibar DP, Renteria ME, Stein JL, Thompson PM, Francks C, Vernes SC, Fisher SE. (2016): Early developmental gene enhancers affect subcortical volumes in the adult human brain. Hum Brain Mapp.

Berker EA, Berker AH, Smith A. (1986): Translation of Broca's 1865 report. Localization of speech in the third left frontal convolution. Arch Neurol 43(10):1065-72.

Berlim MT, Mattevi BS, Belmonte-de-Abreu P, Crow TJ. (2003): The etiology of schizophrenia and the origin of language: Overview of a theory. Comprehensive Psychiatry 44(1):7-14.

Bichat X. 1809. Physiological researches upon life and death: Smith & Maxwell.
Bidula SP, Kroliczak G. (2015): Structural asymmetry of the insula is linked to the lateralization of gesture and language. Eur J Neurosci 41(11):1438-47.
Bis JC, DeCarli C, Smith AV, van der Lijn F, Crivello F, Fornage M, Debette S, Shulman JM, Schmidt H, Srikanth V and others. (2012): Common variants at 12q14 and 12q24 are associated with hippocampal volume. Nat Genet 44(5):545-51.
Bishop DVM. (1990a): Handedness, clumsiness and developmental language disorders. Neuropsychologia 28(7):681-690.
Bishop DVM. (1990b): How to increase your chances of obtaining a significant association between handedness and disorder. J Clin Exp Neuropsychol 12(5):812-6.
Bishop DVM. (2013): Cerebral Asymmetry and Language Development: Cause, Correlate, or Consequence? Science 340(6138).
Bloss CS, Delis DC, Salmon DP, Bondi MW. (2010): APOE genotype is associated with left-handedness and visuospatial skills in children. Neurobiol Aging 31(5):787-95.
Boles DB, Barth JM. (2011): "Does degree of asymmetry relate to performance?" A critical review. Brain and Cognition 76:1-4.
Bossy J, Godlewski G, Maurel JC. (1976): [Study of right-left asymmetry of the temporal planum in the fetus]. Bull Assoc Anat 60(169):253-8.
Boyd R. (1861): Tables of the Weights of the Human Body and Internal Organs in the Sane and Insane of Both Sexes at Various Ages, Arranged from 2614 Post-Mortem Examinations. Philosophical Transactions of the Royal Society of London 151:241-262.
Bramwell B. (1899): On "crossed" aphasia and the factors which go to determine whether the "leading" or "driving" speech-centres shall be located in the left or in the right hemisphere of the brain,: With notes of a case of "crossed" aphasia (aphasia with right-sided hemiplegia) in a left-handed man. The Lancet 153(3953):1473-1479.
Brandler WM, Morris AP, Evans DM, Scerri TS, Kemp JP, Timpson NJ, St Pourcain B, Smith GD, Ring SM, Stein J and others. (2013): Common variants in left/right asymmetry genes and pathways are associated with relative hand skill. PLoS Genet 9(9):12.
Broca P. (1865): Du siège de la faculté du langage articulé. Bulletins de la Société d'Anthropologie 6:377-393.
Brucato N, Guadalupe T, Franke B, Fisher SE, Francks C. (2015): A schizophrenia-associated HLA locus affects thalamus volume and asymmetry. Brain Behav Immun 46:311-8.
Bryden MP. 1982. Laterality : functional asymmetry in the intact brain. New York: Academic Press.
Bryden MP, McManus IC, Steenhuis RE. (1991): Handedness is not related to self-reported disease incidence. Cortex 27(4):605-11.
Bukowski H, Dricot L, Hanseeuw B, Rossion B. (2013): Cerebral lateralization of face-sensitive areas in left-handers: Only the FFA does not get it right. Cortex 49(9):2583-2589.
Byrd AL, Wright AGC, Sen S, Shedden K, Manuck SB. (2015): Reply To: The Liptak-Stouffer Test for Meta-Analyses. Biological Psychiatry 77(1):e3-e4.
Cai DC, Fonteijn H, Guadalupe T, Zwiers M, Wittfeld K, Teumer A, Hoogman M, Arias-Vasquez A, Yang Y, Buitelaar J and others. (2014): A genome-wide search for quantitative trait loci affecting the cortical surface area and thickness of Heschl's gyrus. Genes Brain Behav 13(7):675-85.
Castellanos FX, Giedd JN, Berquin PC, Walter JM, Sharp W, Tran T, Vaituzis AC, Blumenthal JD, Nelson J, Bastain TM and others. (2001): Quantitative brain magnetic resonance imaging in girls with attention-deficit/hyperactivity disorder. Arch Gen Psychiatry 58(3):289-95.
Castellanos FX, Giedd JN, Marsh WL, Hamburger SD, Vaituzis AC, Dickstein DP, Sarfatti SE, Vauss YC, Snell JW, Lange N and others. (1996): Quantitative brain magnetic resonance imaging in attention-deficit hyperactivity disorder. Arch Gen Psychiatry 53(7):607-16.

Caviness VS, Jr., Kennedy DN, Richelme C, Rademacher J, Filipek PA. (1996): The human brain age 7-11 years: a volumetric analysis based on magnetic resonance images. Cereb Cortex 6(5):726-36.
Cendes F, Leproux F, Melanson D, Ethier R, Evans A, Peters T, Andermann F. (1993): MRI of amygdala and hippocampus in temporal lobe epilepsy. J Comput Assist Tomogr 17(2):206-10.
Chakrabarti B, Dudbridge F, Kent L, Wheelwright S, Hill-Cawthorne G, Allison C, Banerjee-Basu S, Baron-Cohen S. (2009): Genes related to sex steroids, neural growth, and social–emotional behavior are associated with autistic traits, empathy, and Asperger syndrome. Autism Research 2(3):157-177.
Chance SA. (2014): The cortical microstructural basis of lateralized cognition: a review. Front Psychol 5:820.
Chouinard-Decorte F, McKay DR, Reid A, Khundrakpam B, Zhao L, Karama S, Rioux P, Sprooten E, Knowles E, Kent JW and others. (2014): Heritable changes in regional cortical thickness with age. Brain Imaging Behav 8(2):208-16.
Clark GM, Crow TJ, Barrick TR, Collinson SL, James AC, Roberts N, Mackay CE. (2010): Asymmetry loss is local rather than global in adolescent onset schizophrenia. Schizophrenia Research 120:84-86.
Clerke A, Clerke J. (2001): A literature review of the effect of handedness on isometric grip strength differences of the left and right hands. Am J Occup Ther 55(2):206-11.
Cloke B, Huhtinen K, Fusi L, Kajihara T, Yliheikkila M, Ho KK, Teklenburg G, Lavery S, Jones MC, Trew G and others. (2008): The androgen and progesterone receptors regulate distinct gene networks and cellular functions in decidualizing endometrium. Endocrinology 149(9):4462-74.
Colombo A, Palma K, Armijo L, Mione M, Signore IA, Morales C, Guerrero N, Meynard MM, Perez R, Suazo J and others. (2013): Daam1a mediates asymmetric habenular morphogenesis by regulating dendritic and axonal outgrowth. Development 140(19):3997-4007.
Concha ML, Burdine RD, Russell C, Schier AF, Wilson SW. (2000): A nodal signaling pathway regulates the laterality of neuroanatomical asymmetries in the zebrafish forebrain. Neuron 28(2):399-409.
Concha ML, Signore IA, Colombo A. (2009): Mechanisms of directional asymmetry in the zebrafish epithalamus. Seminars in Cell & Developmental Biology 20(4):498-509.
Consortium TGP. (2010): A map of human genome variation from population-scale sequencing. Nature 467(7319):1061-1073.
Corballis MC. (2013): Early signs of brain asymmetry. Trends Cogn Sci 17(11):554-5.
Corballis MC, Badzakova-Trajkov G, Haberling IS. (2012): Right hand, left brain: genetic and evolutionary bases of cerebral asymmetries for language and manual action. Wiley Interdisciplinary Reviews-Cognitive Science 3(1):1-17.
Coren S, Porac C. (1977): Fifty centuries of right-handedness: the historical record. Science 198(4317):631-2.
Crinion J, Turner R, Grogan A, Hanakawa T, Noppeney U, Devlin JT, Aso T, Urayama S, Fukuyama H, Stockton K and others. (2006): Language control in the bilingual brain. Science 312(5779):1537-40.
Crovitz HF, Zener K. (1962): A group-test for assessing hand- and eye-dominance. Am J Psychol 75:271-6.
Crow TJ. (2002): Handedness, language lateralisation and anatomical asymmetry: relevance of protocadherin XY to hominid speciation and the aetiology of psychosis. Point of view. Br J Psychiatry 181:295-7.
Cunningham DJ. (1892): Contribution to the Surface Anatomy of the Cerebral Hemispheres. Journal of Anatomy and Physiology 27(Pt 2):288-289.
Cunningham DJ. (1902): Right-Handedness and Left-Brainedness. The Journal of the Anthropological Institute of Great Britain and Ireland 32:273-296.
de Courten-Myers GM. (1999): The human cerebral cortex: gender differences in structure and function. J Neuropathol Exp Neurol 58(3):217-26.

de Guibert Cm, Maumet C, Jannin P, FerrÃ© J-C, TrÃ©guier C, Barillot C, Le Rumeur E, Allaire C, Biraben A. (2011): Abnormal functional lateralization and activity of language brain areas in typical specific language impairment (developmental dysphasia). Brain 134:3044-3058.

de Leon MJ, la Regina ME, Ferris SH, Gentes CI, Miller JD. (1986): Reduced incidence of left-handedness in clinically diagnosed dementia of the Alzheimer type. Neurobiol Aging 7(3):161-4.

Deep-Soboslay A, Hyde TM, Callicott JP, Lener MS, Verchinski BA, Apud JA, Weinberger DR, Elvevag B. (2010): Handedness, heritability, neurocognition and brain asymmetry in schizophrenia. Brain:awq160.

DeLisi LE, Sakuma M, Kushner M, Finer DL, Hoff AL, Crow TJ. (1997): Anomalous cerebral asymmetry and language processing in schizophrenia. Schizophr Bull 23(2):255-71.

DeLisi LE, Svetina C, Razi K, Shields G, Wellman N, Crow TJ. (2002): Hand preference and hand skill in families with schizophrenia. Laterality 7(4):321-32.

Destrieux C, Fischl B, Dale A, Halgren E. (2010): Automatic parcellation of human cortical gyri and sulci using standard anatomical nomenclature. Neuroimage 53(1):1-15.

Draganski B, Kherif F, Kloppel S, Cook PA, Alexander DC, Parker GJ, Deichmann R, Ashburner J, Frackowiak RS. (2008): Evidence for segregated and integrative connectivity patterns in the human Basal Ganglia. J Neurosci 28(28):7143-52.

Dubois J, Benders M, Lazeyras F, Borradori-Tolsa C, Leuchter RH, Mangin JF, Huppi PS. (2010): Structural asymmetries of perisylvian regions in the preterm newborn. Neuroimage 52(1):32-42.

Eberstaller O. (1884): Zur Oberflächenanatomie der Grosshirnhemisphären. Wien Med Bl 7:479–482.

Eckert MA, Lombardino LJ, Walczak AR, Bonihla L, Leonard CM, Binder JR. (2008): Manual and automated measures of superior temporal gyrus asymmetry: Concordant structural predictors of verbal ability in children. NeuroImage 41(3):813-822.

Eyler LT, Pierce K, Courchesne E. (2012): A failure of left temporal cortex to specialize for language is an early emerging and fundamental property of autism. Brain 135(3):949-960.

Eyler LT, Vuoksimaa E, Panizzon MS, Fennema-Notestine C, Neale MC, Chen CH, Jak A, Franz CE, Lyons MJ, Thompson WK and others. (2014): Conceptual and data-based investigation of genetic influences and brain asymmetry: a twin study of multiple structural phenotypes. J Cogn Neurosci 26(5):1100-17.

Faul F, Erdfelder E, Lang AG, Buchner A. (2007): G*Power 3: a flexible statistical power analysis program for the social, behavioral, and biomedical sciences. Behav Res Methods 39(2):175-91.

Faurie C, Raymond M. (2004): Handedness frequency over more than ten thousand years. Proc Biol Sci 7(271):S43-5.

Fearon P, O'Connell P, Frangou S, Aquino P, Nosarti C, Allin M, Taylor M, Stewart A, Rifkin L, Murray R. (2004): Brain volumes in adult survivors of very low birth weight: a sibling-controlled study. Pediatrics 114(2):367-71.

Fernandez G, Weis S, Stoffel-Wagner B, Tendolkar I, Reuber M, Beyenburg S, Klaver P, Fell J, de Greiff A, Ruhlmann J and others. (2003): Menstrual cycle-dependent neural plasticity in the adult human brain is hormone, task, and region specific. J Neurosci 23(9):3790-5.

Ferreira MA, Purcell SM. (2009): A multivariate test of association. Bioinformatics 25(1):132-3.

Filler AG. (2009): The history, development and impact of computed imaging in neurological diagnosis and neurosurgery: CT, MRI, and DTI. Nature Precedings 7(1):1-69.

Finger S, Roe D. (1999): Does Gustave Dax deserve to be forgotten? The temporal lobe theory and other contributions of an overlooked figure in the history of language and cerebral dominance. Brain Lang 69(1):16-30.

Fischl B, Salat DH, Busa E, Albert M, Dieterich M, Haselgrove C, van der Kouwe A, Killiany R, Kennedy D, Klaveness S and others. (2002): Whole brain segmentation: automated labeling of neuroanatomical structures in the human brain. Neuron 33(3):341-55.

Fischl B, van der Kouwe A, Destrieux C, Halgren E, Segonne F, Salat DH, Busa E, Seidman LJ, Goldstein J, Kennedy D and others. (2004): Automatically parcellating the human cerebral cortex. Cereb Cortex 14(1):11-22.

Floris DL, Lai MC, Auer T, Lombardo MV, Ecker C, Chakrabarti B, Wheelwright SJ, Bullmore ET, Murphy DG, Baron-Cohen S and others. (2016): Atypically rightward cerebral asymmetry in male adults with autism stratifies individuals with and without language delay. Hum Brain Mapp 37(1):230-53.

Foundas AL, Hong K, Leonard CM, Heilman KM. (1998): Hand preference and magnetic resonance imaging asymmetries of the central sulcus. Neuropsychiatry Neuropsychol Behav Neurol 11(2):65-71.

Foundas AL, Leonard CM, Heilman KM. (1995): Morphologic cerebral asymmetries and handedness. The pars triangularis and planum temporale. Arch Neurol 52(5):501-8.

Foundas AL, Mock JR, Cindass R, Jr., Corey DM. (2013): Atypical caudate anatomy in children who stutter. Percept Mot Skills 116(2):528-43.

Francks C. (2015): Exploring human brain lateralization with molecular genetics and genomics. Ann N Y Acad Sci.

Francks C, Maegawa S, Lauren J, Abrahams BS, Velayos-Baeza A, Medland SE, Colella S, Groszer M, McAuley EZ, Caffrey TM and others. (2007): LRRTM1 on chromosome 2p12 is a maternally suppressed gene that is associated paternally with handedness and schizophrenia. Mol Psychiatry 12(12):1129-39, 1057.

Frank Y, Pavlakis SG. (2001): Brain imaging in neurobehavioral disorders. Pediatr Neurol 25(4):278-87.

Franke B, Stein JL, Ripke S, Anttila V, Hibar DP, van Hulzen KJE, Arias-Vasquez A, Smoller JW, Nichols TE, Neale MC and others. (2016): Genetic influences on schizophrenia and subcortical brain volumes: large-scale proof of concept. Nat Neurosci 19(3):420-431.

Franke B, Vasquez AA, Veltman JA, Brunner HG, Rijpkema M, Fernandez G. (2010): Genetic variation in CACNA1C, a gene associated with bipolar disorder, influences brainstem rather than gray matter volume in healthy individuals. Biol Psychiatry 68(6):586-8.

Frasnelli E, Vallortigara G, Rogers LJ. (2012): Left-right asymmetries of behaviour and nervous system in invertebrates. Neuroscience and Biobehavioral Reviews 36(4):1273-1291.

Friederici AD. (2006): What's in control of language? Nat Neurosci 9(8):991-2.

Galaburda AM. (1993): The planum temporale. Arch Neurol 50(5):457.

Galaburda AM, Geschwind N. (1981): Anatomical asymmetries in the adult and developing brain and their implications for function. Adv Pediatr 28:271-92.

Gannon PJ, Holloway RL, Broadfield DC, Braun AR. (1998): Asymmetry of chimpanzee planum temporale: humanlike pattern of Wernicke's brain language area homolog. Science 279(5348):220-2.

Genovese CR, Lazar NA, Nichols T. (2002): Thresholding of statistical maps in functional neuroimaging using the false discovery rate. Neuroimage 15(4):870-8.

Geschwind N, Behan P. (1982): Left-handedness: association with immune disease, migraine, and developmental learning disorder. Proc Natl Acad Sci U S A 79(16):5097-100.

Geschwind N, Levitsky W. (1968): Human brain: left-right asymmetries in temporal speech region. Science 161(3837):186-7.

Giedd JN, Snell JW, Lange N, Rajapakse JC, Casey BJ, Kozuch PL, Vaituzis AC, Vauss YC, Hamburger SD, Kaysen D and others. (1996): Quantitative magnetic resonance imaging of human brain development: ages 4-18. Cereb Cortex 6(4):551-60.

Gil Robles S, Gatignol P, Capelle L, Mitchell MC, Duffau H. (2005): The role of dominant striatum in language: a study using intraoperative electrical stimulations. J Neurol Neurosurg Psychiatry 76(7):940-6.

Glenthoj A, Glenthoj BY, Mackeprang T, Pagsberg AK, Hemmingsen RP, Jernigan TL, Baare WF. (2007): Basal ganglia volumes in drug-naive first-episode schizophrenia patients before and after short-term treatment with either a typical or an atypical antipsychotic drug. Psychiatry Res 154(3):199-208.

Goldstein JM, Goodman JM, Seidman LJ, Kennedy DN, Makris N, Lee H, Tourville J, Caviness VS, Jr., Faraone SV, Tsuang MT. (1999): Cortical abnormalities in schizophrenia identified by structural magnetic resonance imaging. Arch Gen Psychiatry 56(6):537-47.

Goldstein JM, Seidman LJ, Makris N, Ahern T, O'Brien LM, Caviness VS, Jr., Kennedy DN, Faraone SV, Tsuang MT. (2007): Hypothalamic abnormalities in schizophrenia: sex effects and genetic vulnerability. Biol Psychiatry 61(8):935-45.

Good CD, Johnsrude I, Ashburner J, Henson RNA, Friston KJ, Frackowiak RSJ. (2001a): Cerebral asymmetry and the effects of sex and handedness on brain structure: A voxel-based morphometric analysis of 465 normal adult human brains. Neuroimage 14(3):685-700.

Good CD, Johnsrude IS, Ashburner J, Henson RN, Friston KJ, Frackowiak RS. (2001b): A voxel-based morphometric study of ageing in 465 normal adult human brains. Neuroimage 14(1 Pt 1):21-36.

Gordon HW, Kravetz S. (1991): The influence of gender, handedness, and performance level on specialized cognitive functioning. Brain and Cognition 15(1):37-61.

Grahn JA, Parkinson JA, Owen AM. (2008): The cognitive functions of the caudate nucleus. Prog Neurobiol 86(3):141-55.

Greve DN, Van der Haegen L, Cai Q, Stufflebeam S, Sabuncu MR, Fischl B, Brysbaert M. (2013): A surface-based analysis of language lateralization and cortical asymmetry. J Cogn Neurosci 25(9):1477-92.

Griffiths TD, Warren JD. (2002): The planum temporale as a computational hub. Trends Neurosci 25(7):348-53.

Guadalupe T, Mathias SR, van Erp TGM, Whelan CD, Zwiers MP, Abe Y, Abramovic L, Agartz I, Andreassen OA, Aribisala BS and others. Human brain asymmetries in 15,847 people worldwide reveal effects of age and sex.

Guadalupe T, Willems RM, Zwiers MP, Arias Vasquez A, Hoogman M, Hagoort P, Fernandez G, Buitelaar J, Franke B, Fisher SE and others. (2014a): Differences in cerebral cortical anatomy of left- and right-handers. Front Psychol 5(261).

Guadalupe T, Zwiers MP, Teumer A, Wittfeld K, Vasquez AA, Hoogman M, Hagoort P, Fernandez G, Buitelaar J, Hegenscheid K and others. (2014b): Measurement and genetics of human subcortical and hippocampal asymmetries in large datasets. Hum Brain Mapp 35(7):3277-89.

Guadalupe T, Zwiers MP, Wittfeld K, Teumer A, Vasquez AA, Hoogman M, Hagoort P, Fernandez G, Buitelaar J, van Bokhoven H and others. (2015): Asymmetry within and around the human planum temporale is sexually dimorphic and influenced by genes involved in steroid hormone receptor activity. Cortex 62:41-55.

Haaland KY, Harrington DL. (1996): Hemispheric asymmetry of movement. Curr Opin Neurobiol 6(6):796-800.

Habas PA, Scott JA, Roosta A, Rajagopalan V, Kim K, Rousseau F, Barkovich AJ, Glenn OA, Studholme C. (2012): Early folding patterns and asymmetries of the normal human brain detected from in utero MRI. Cereb Cortex 22(1):13-25.

Hadziselimovic H, Cus M. (1966): The appearance of internal structures of the brain in relation to configuration of the human skull. Acta Anat (Basel) 63(3):289-99.

Halpern DF, Haviland MG, Killian CD. (1998): Handedness and sex differences in intelligence: evidence from the medical college admission test. Brain Cogn 38(1):87-101.

Han X, Fischl B. (2007): Atlas renormalization for improved brain MR image segmentation across scanner platforms. IEEE Trans Med Imaging 26(4):479-86.

Hardyck C, Petrinovich LF. (1977): Left-handedness. Psychol Bull 84(3):385-404.

Harris LJ. (1980): Lateralized sex differences: substrates and significance. Behavioral and Brain Sciences 3(02):236-237.
Hasan A, Kremer L, Gruber O, Schneider-Axmann T, Guse B, Reith W, Falkai P, Wobrock T. (2011): Planum temporale asymmetry to the right hemisphere in first-episode schizophrenia. Psychiatry Research: Neuroimaging 193(1):56-59.
Hayashi Y, Nihonmatsu-Kikuchi N, Hisanaga S-i, Yu X-j, Tatebayashi Y. (2012): Neuropathological Similarities and Differences between Schizophrenia and Bipolar Disorder: A Flow Cytometric Postmortem Brain Study. PLoS ONE 7(3):e33019.
Hegenscheid K, Kuhn JP, Volzke H, Biffar R, Hosten N, Puls R. (2009): Whole-body magnetic resonance imaging of healthy volunteers: pilot study results from the population-based SHIP study. Rofo 181(8):748-59.
Hendren RL, De Backer I, Pandina GJ. (2000): Review of neuroimaging studies of child and adolescent psychiatric disorders from the past 10 years. J Am Acad Child Adolesc Psychiatry 39(7):815-28.
Hepper PG. (2013): The developmental origins of laterality: Fetal handedness. Developmental psychobiology 55(6):588-95.
Hepper PG, McCartney GR, Shannon EA. (1998): Lateralised behaviour in first trimester human foetuses. Neuropsychologia 36(6):531-4.
Hepper PG, Wells DL, Lynch C. (2005): Prenatal thumb sucking is related to postnatal handedness. Neuropsychologia 43(3):313-5.
Herbert MR, Ziegler DA, Deutsch CK, O'Brien LM, Kennedy DN, Filipek PA, Bakardjiev AI, Hodgson J, Takeoka M, Makris N and others. (2005): Brain asymmetries in autism and developmental language disorder: a nested whole-brain analysis. Brain 128(1):213-226.
Hering-Hanit R, Achiron R, Lipitz S, Achiron A. (2001): Asymmetry of fetal cerebral hemispheres: in utero ultrasound study. Arch Dis Child Fetal Neonatal Ed 85(3):F194-6.
Herve PV, Mazoyer B, Crivello F, Perchey G, Tzourio-Mazoyer N. (2005): Finger tapping, handedness and grey matter amount in the Rolando's genu area. Neuroimage 25(4):1133-1145.
Herve PY, Crivello F, Perchey G, Mazoyer B, Tzourio-Mazoyer N. (2006): Handedness and cerebral anatomical asymmetries in young adult males. Neuroimage 29(4):1066-1079.
Herve PY, Zago L, Petit L, Mazoyer B, Tzourio-Mazoyer N. (2013): Revisiting human hemispheric specialization with neuroimaging. Trends Cogn Sci 17(2):69-80.
Heschl RL. 1878. Über die vordere quere Schläfenwindung des menschlichen Grosshirns: Braumüller.
Hibar DP, Stein JL, Renteria ME, Arias-Vasquez A, Desrivieres S, Jahanshad N, Toro R, Wittfeld K, Abramovic L, Andersson M and others. (2015): Common genetic variants influence human subcortical brain structures. Nature 520(7546):224-9.
Hickok G, Poeppel D. (2007): The cortical organization of speech processing. Nat Rev Neurosci 8(5):393-402.
Higgins JP, Thompson SG. (2002): Quantifying heterogeneity in a meta-analysis. Stat Med 21(11):1539-58.
Hirnstein M, Westerhausen R, Hugdahl K. (2013): The right planum temporale is involved in stimulus-driven, auditory attention--evidence from transcranial magnetic stimulation. PLoS One 8(2):e57316.
Hoadley MF, Pearson K. (1929): On Measurement of the Internal Diameters of the Skull in Relation: (I) To the Prediction of its Capacity, (II) To the "Pre-Eminence" of the Left Hemisphere. Biometrika 21(1/4):85-123.
Hoogman M, Guadalupe T, Zwiers MP, Klarenbeek P, Francks C, Fisher SE. (2014): Assessing the effects of common variation in the FOXP2 gene on human brain structure. Front Hum Neurosci 8:473.

Hopkins WD, Phillips KA, Bania A, Calcutt SE, Gardner M, Russell J, Schaeffer J, Lonsdorf EV, Ross SR, Schapiro SJ. (2011): Hand preferences for coordinated bimanual actions in 777 great apes: implications for the evolution of handedness in hominins. J Hum Evol 60(5):605-11.

Hou G, Yang X, Yuan TF. (2013): Hippocampal asymmetry: differences in structures and functions. Neurochem Res 38(3):453-60.

Howie BN, Donnelly P, Marchini J. (2009): A flexible and accurate genotype imputation method for the next generation of genome-wide association studies. PLoS Genet 5(6):19.

Howie BN, Fuchsberger C, Stephens M, Marchini J, Abecasis GR. (2012): Fast and accurate genotype imputation in genome-wide association studies through pre-phasing. Nat Genet 44(8):955-9.

Hughlings-Jackson J. 1873a. Observations on the localisation of movements in the cerebral hemispheres, as revealed by cases of convulsion, chorea and 'aphasia'.

Hughlings-Jackson J. (1873b): On the anatomical & physiological localisation of movements in the brain. The Lancet 101(2581):232-235.

Hughlings-Jackson J. (1874): On the nature of the duality of the brain. Med Press Circ 1:41-44.

Hulshoff Pol HE, Schnack HG, Posthuma D, Mandl RCW, Baare WF, van Oel C, van Haren NE, Collins DL, Evans AC, Amunts K and others. (2006): Genetic Contributions to Human Brain Morphology and Intelligence. J. Neurosci. 26(40):10235-10242.

Hynd GW, Hern KL, Novey ES, Eliopulos D, Marshall R, Gonzalez JJ, Voeller KK. (1993): Attention deficit-hyperactivity disorder and asymmetry of the caudate nucleus. J Child Neurol 8(4):339-47.

Ikram MA, Fornage M, Smith AV, Seshadri S, Schmidt R, Debette S, Vrooman HA, Sigurdsson S, Ropele S, Taal HR and others. (2012): Common variants at 6q22 and 17q21 are associated with intracranial volume. Nat Genet 44(5):539-44.

Jahanshad N, Lee AD, Barysheva M, McMahon KL, de Zubicaray GI, Martin NG, Wright MJ, Toga AW, Thompson PM. (2010): Genetic influences on brain asymmetry: a DTI study of 374 twins and siblings. Neuroimage 52(2):455-69.

Jancke L, Schlaug G, Huang Y, Steinmetz H. (1994): Asymmetry of the planum parietale. Neuroreport 5(9):1161-3.

Jansen A, Liuzzi G, Deppe M, Kanowski M, Olschlager C, Albers JM, Schlaug G, Knecht S. (2010): Structural Correlates of Functional Language Dominance: A Voxel-Based Morphometry Study. Journal of Neuroimaging 20(2):148-156.

Jensen BH, Hougaard A, Amin FM, Larsson HB, Ashina M. (2015): Structural asymmetry of cortical visual areas is related to ocular dominance. Neuroreport 26(17):1071-6.

Johnson MB, Kawasawa YI, Mason CE, Krsnik Z, Coppola G, Bogdanovic D, Geschwind DH, Mane SM, State MW, Sestan N. (2009): Functional and evolutionary insights into human brain development through global transcriptome analysis. Neuron 62(4):494-509.

Josse G, Herve PY, Crivello F, Mazoyer B, Tzourio-Mazoyer N. (2006): Hemispheric specialization for language: Brain volume matters. Brain Res 12(1):184-93.

Josse G, Kherif F, Flandin G, Seghier ML, Price CJ. (2009): Predicting language lateralization from gray matter. J Neurosci 29(43):13516-23.

Jovicich J, Czanner S, Han X, Salat D, van der Kouwe A, Quinn B, Pacheco J, Albert M, Killiany R, Blacker D and others. (2009): MRI-derived measurements of human subcortical, ventricular and intracranial brain volumes: Reliability effects of scan sessions, acquisition sequences, data analyses, scanner upgrade, scanner vendors and field strengths. Neuroimage 46(1):177-92.

Kang X, Herron TJ, Ettlinger M, Woods DL. (2015): Hemispheric asymmetries in cortical and subcortical anatomy. Laterality:1-27.

Karlebach G, Francks C. (2015): Lateralization of gene expression in human language cortex. Cortex 67:30-6.

Kasprian G, Langs G, Brugger PC, Bittner M, Weber M, Arantes M, Prayer D. (2011): The prenatal origin of hemispheric asymmetry: an in utero neuroimaging study. Cereb Cortex 21(5):1076-83.

Kawakami R, Shinohara Y, Kato Y, Sugiyama H, Shigemoto R, Ito I. (2003): Asymmetrical allocation of NMDA receptor epsilon2 subunits in hippocampal circuitry. Science 300(5621):990-4.

Kawasaki Y, Suzuki M, Takahashi T, Nohara S, McGuire PK, Seto H, Kurachi M. (2008): Anomalous cerebral asymmetry in patients with schizophrenia demonstrated by voxel-based morphometry. Biol Psychiatry 63(8):793-800.

Kennedy DN, O'Craven KM, Ticho BS, Goldstein AM, Makris N, Henson JW. (1999): Structural and functional brain asymmetries in human situs inversus totalis. Neurology 53(6):1260-5.

Kloppel S, van Eimeren T, Glauche V, Vongerichten A, Munchau A, Frackowiak RS, Buchel C, Weiller C, Siebner HR. (2007): The effect of handedness on cortical motor activation during simple bilateral movements. Neuroimage 34(1):274-80.

Knecht S, Deppe M, Drager B, Bobe L, Lohmann H, Ringelstein EB, Henningsen H. (2000a): Language lateralization in healthy right-handers. Brain 123:74-81.

Knecht S, Drager B, Deppe M, Bobe L, Lohmann H, Floel A, Ringelstein EB, Henningsen H. (2000b): Handedness and hemispheric language dominance in healthy humans. Brain 123:2512-2518.

Knudsen PA. 1958. Ventriklernes storrelsesforhold i anatomisk normale Hjerner fra Voksne mennesker: Andesbogtrykkeriet.

Koran ME, Thornton-Wells TA, Jahanshad N, Glahn DC, Thompson PM, Blangero J, Nichols TE, Kochunov P, Landman BA. (2014): Impact of family structure and common environment on heritability estimation for neuroimaging genetics studies using Sequential Oligogenic Linkage Analysis Routines. J Med Imaging (Bellingham) 1(1):014005.

Kovalev VA, Kruggel F, von Cramon DY. (2003): Gender and age effects in structural brain asymmetry as measured by MRI texture analysis. Neuroimage 19(3):895-905.

Lambert N, Lambot MA, Bilheu A, Albert V, Englert Y, Libert F, Noel JC, Sotiriou C, Holloway AK, Pollard KS and others. (2011): Genes expressed in specific areas of the human fetal cerebral cortex display distinct patterns of evolution. PLoS One 6(3):e17753.

Last RJ, Tompsett DH. (1953): Casts of the cerebral ventricles. Br J Surg 40(164):525-43.

Lee JS, Yoo SS, Cho SY, Ock SM, Lim MK, Panych LP. (2006): Abnormal thalamic volume in treatment-naive boys with Tourette syndrome. Acta Psychiatr Scand 113(1):64-7.

Lee PH, O'Dushlaine C, Thomas B, Purcell SM. (2012): INRICH: interval-based enrichment analysis for genome-wide association studies. Bioinformatics 28(13):1797-9.

Lehericy S, Ducros M, Van de Moortele PF, Francois C, Thivard L, Poupon C, Swindale N, Ugurbil K, Kim DS. (2004): Diffusion tensor fiber tracking shows distinct corticostriatal circuits in humans. Ann Neurol 55(4):522-9.

LeMay M. (1976): Morphological cerebral asymmetries of modern man, fossil man, and nonhuman primate. Ann N Y Acad Sci 280:349-66.

Levy J, Nagylaki T. (1972): A model for the genetics of handedness. Genetics 72(1):117-28.

Li G, Nie J, Wang L, Shi F, Lyall AE, Lin W, Gilmore JH, Shen D. (2014): Mapping longitudinal hemispheric structural asymmetries of the human cerebral cortex from birth to 2 years of age. Cereb Cortex 24(5):1289-300.

Li Y, Willer CJ, Ding J, Scheet P, Abecasis GR. (2010): MaCH: using sequence and genotype data to estimate haplotypes and unobserved genotypes. Genet Epidemiol 34(8):816-34.

Liao YL, Sun YN, Hsieh JC, Su TP, Guo WY, Wu YT. (2008): Cortical complexity analysis of patients with bipolar disorder using three-dimensional gyrification index. Conf Proc IEEE Eng Med Biol Soc 2008:3933-6.

Liptak T. (1958): On the combination of independent tests. Magyar Tudomanyos Akademia Matematikai Kutato Intezetenek Kozlemenyei 3:171-197.

Lombardo MV, Ashwin E, Auyeung B, Chakrabarti B, Taylor K, Hackett G, Bullmore ET, Baron-Cohen S. (2012): Fetal testosterone influences sexually dimorphic gray matter in the human brain. J Neurosci 32(2):674-80.

London WP. (1989): Left-handedness and life expectancy. Percept Mot Skills 68(3 Pt 2):1040-2.

Lonsdorf EV, Hopkins WD. (2005): Wild chimpanzees show population-level handedness for tool use. Proceedings of the National Academy of Sciences of the United States of America 102(35):12634-12638.

Luh KE, Redl J, Levy J. (1994): Left- and right-handers see people differently: free-vision perceptual asymmetries for chimeric stimuli. Brain Cogn 25(2):141-60.

Lyn H, Pierre P, Bennett AJ, Fears S, Woods R, Hopkins WD. (2011): Planum temporale grey matter asymmetries in chimpanzees (Pan troglodytes), vervet (Chlorocebus aethiops sabaeus), rhesus (Macaca mulatta) and bonnet (Macaca radiata) monkeys. Neuropsychologia 49(7):2004-12.

Lyttelton OC, Karama S, Ad-Dab'bagh Y, Zatorre RJ, Carbonell F, Worsley K, Evans AC. (2009): Positional and surface area asymmetry of the human cerebral cortex. Neuroimage 46(4):895-903.

Makris N, Gasic GP, Seidman LJ, Goldstein JM, Gastfriend DR, Elman I, Albaugh MD, Hodge SM, Ziegler DA, Sheahan FS and others. (2004): Decreased absolute amygdala volume in cocaine addicts. Neuron 44(4):729-40.

Maltbie E, Bhatt K, Paniagua B, Smith RG, Graves MM, Mosconi MW, Peterson S, White S, Blocher J, El-Sayed M and others. (2012): Asymmetric bias in user guided segmentations of brain structures. Neuroimage 59(2):1315-23.

Marie D, Jobard G, Crivello F, Perchey G, Petit L, Mellet E, Joliot M, Zago L, Mazoyer B, Tzourio-Mazoyer N. (2015): Descriptive anatomy of Heschl's gyri in 430 healthy volunteers, including 198 left-handers. Brain structure & function 220(2):729-43.

Mazoyer B, Zago L, Jobard G, Crivello F, Joliot M, Perchey G, Mellet E, Petit L, Tzourio-Mazoyer N. (2014): Gaussian mixture modeling of hemispheric lateralization for language in a large sample of healthy individuals balanced for handedness. PLoS One 9(6):e101165.

McCarley RW, Salisbury DF, Hirayasu Y, Yurgelun-Todd DA, Tohen M, Zarate C, Kikinis R, Jolesz FA, Shenton ME. (2002): Association between smaller left posterior superior temporal gyrus volume on magnetic resonance imaging and smaller left temporal P300 amplitude in first-episode schizophrenia. Arch Gen Psychiatry 59(4):321-31.

McGraw KO, Wong SP. (1996): Forming inferences about some intraclass correlation coefficients. Psychological Methods 1(1):30-46.

McKay DR, Knowles EE, Winkler AA, Sprooten E, Kochunov P, Olvera RL, Curran JE, Kent JW, Jr., Carless MA, Goring HH and others. (2014): Influence of age, sex and genetic factors on the human brain. Brain Imaging Behav 8(2):143-52.

McKeever WF, Rich DA. (1990): Left handedness and immune disorders. Cortex 26(1):33-40.

McManus IC. (1985): Right- and left-hand skill: failure of the right shift model. Br J Psychol 76(Pt 1):1-34.

McManus IC. (1991): The inheritance of left-handedness. Ciba Found Symp 162:251-67.

McManus IC. (2009): The history and geography of human handedness. In "Language lateralisation and psychosis", Edited by: Sommer, IE and Kahn R. p 37–57. Cambridge, UK: Cambridge University Press.

McManus IC, Davison A, Armour JA. (2013): Multilocus genetic models of handedness closely resemble single-locus models in explaining family data and are compatible with genome-wide association studies. Ann N Y Acad Sci:30.

Medland SE. (2009): Meta-analysis of GWAS for Handedness: results from the ENGAGE consortium. Meeting Abstract.

Medland SE, Duffy DL, Spurdle AB, Wright MJ, Geffen GM, Montgomery GW, Martin NG. (2005): Opposite effects of androgen receptor CAG repeat length on increased risk of left-handedness in males and females. Behav Genet 35(6):735-44.

Medland SE, Duffy DL, Wright MJ, Geffen GM, Hay DA, Levy F, van-Beijsterveldt CEM, Willemsen G, Townsend GC, White V and others. (2009): Genetic influences on handedness: Data from 25,732 Australian and Dutch twin families. Neuropsychologia 47(2):330-337.

Mellet E, Jobard G, Zago L, Crivello F, Petit L, Joliot M, Mazoyer B, Tzourio-Mazoyer N. (2014): Relationships between hand laterality and verbal and spatial skills in 436 healthy adults balanced for handedness. Laterality 7:7.

Meunier H, Fizet J, Vauclair J. (2013): Tonkean macaques communicate with their right hand. Brain and Language 126(2):181-7.

Mitchell BD, Kammerer CM, Blangero J, Mahaney MC, Rainwater DL, Dyke B, Hixson JE, Henkel RD, Sharp RM, Comuzzie AG and others. (1996): Genetic and environmental contributions to cardiovascular risk factors in Mexican Americans. The San Antonio Family Heart Study. Circulation 94(9):2159-70.

Morey RA, Petty CM, Xu Y, Hayes JP, Wagner HR, Lewis DV, Labar KS, Styner M, McCarthy G. (2009): A comparison of automated segmentation and manual tracing for quantifying hippocampal and amygdala volumes. Neuroimage 45(3):855-866.

Morey RA, Selgrade ES, Wagner HR, Huettel SA, Wang LH, McCarthy G. (2010): Scan-Rescan Reliability of Subcortical Brain Volumes Derived From Automated Segmentation. Human Brain Mapping 31(11):1751-1762.

Narr KL, Bilder RM, Luders E, Thompson PM, Woods RP, Robinson D, Szeszko PR, Dimtcheva T, Gurbani M, Toga AW. (2007): Asymmetries of cortical shape: Effects of handedness, sex and schizophrenia. Neuroimage 34(3):939-948.

Niemann K, Hammers A, Coenen VA, Thron A, Klosterkotter J. (2000): Evidence of a smaller left hippocampus and left temporal horn in both patients with first episode schizophrenia and normal control subjects. Psychiatry Res 99(2):93-110.

Niu L, Matsui M, Zhou SY, Hagino H, Takahashi T, Yoneyama E, Kawasaki Y, Suzuki M, Seto H, Ono T and others. (2004): Volume reduction of the amygdala in patients with schizophrenia: a magnetic resonance imaging study. Psychiatry Res 132(1):41-51.

Nugent AC, Luckenbaugh DA, Wood SE, Bogers W, Zarate CA, Jr., Drevets WC. (2012): Automated subcortical segmentation using FIRST: Test-retest reliability, interscanner reliability, and comparison to manual segmentation. Hum Brain Mapp 19(10):22068.

Ocklenburg S, Beste C, Arning L, Peterburs J, Gunturkun O. (2014): The ontogenesis of language lateralization and its relation to handedness. Neurosci Biobehav Rev 43:191-8.

Ocklenburg S, Beste C, Gunturkun O. (2013): Handedness: a neurogenetic shift of perspective. Neurosci Biobehav Rev 37(10 Pt 2):2788-93.

Ocklenburg S, Gunturkun O. (2012): Hemispheric asymmetries: the comparative view. Front Psychol 3:5.

Ocklenburg S, Gunturkun O, Beste C. (2011): Lateralized neural mechanisms underlying the modulation of response inhibition processes. Neuroimage 55(4):1771-8.

Ocklenburg S, Gunturkun O, Hugdahl K, Hirnstein M. (2015): Laterality and mental disorders in the postgenomic age - A closer look at schizophrenia and language lateralization. Neurosci Biobehav Rev 59:100-110.

Oertel-Knochel V, Knochel C, Stablein M, Linden DE. (2012): Abnormal functional and structural asymmetry as biomarker for schizophrenia. Curr Top Med Chem 12(21):2434-51.

Oertel-Knochel V, Linden DE. (2011): Cerebral asymmetry in schizophrenia. Neuroscientist 17(5):456-67.

Oertel V, Knochel C, Rotarska-Jagiela A, Schonmeyer R, Lindner M, van de Ven V, Haenschel C, Uhlhaas P, Maurer K, Linden DE. (2010): Reduced laterality as a trait marker of schizophrenia--evidence from structural and functional neuroimaging. J Neurosci 30(6):2289-99.

Oldfield RC. (1971): The assessment and analysis of handedness: the Edinburgh inventory. Neuropsychologia 9(1):97-113.

Ooki S. (2014): An overview of human handedness in twins. Front Psychol 5:10.

Ossewaarde L, van Wingen GA, Rijpkema M, Backstrom T, Hermans EJ, Fernandez G. (2011): Menstrual cycle-related changes in amygdala morphology are associated with changes in stress sensitivity. Hum Brain Mapp 34(5):1187-93.

Panizzon MS, Fennema-Notestine C, Eyler LT, Jernigan TL, Prom-Wormley E, Neale M, Jacobson K, Lyons MJ, Grant MD, Franz CE and others. (2009): Distinct genetic influences on cortical surface area and cortical thickness. Cereb Cortex 19(11):2728-35.

Patenaude B, Smith SM, Kennedy DN, Jenkinson M. (2011): A Bayesian model of shape and appearance for subcortical brain segmentation. Neuroimage 56(3):907-922.

Pearson TA, Manolio TA. (2008): How to interpret a genome-wide association study. Jama-Journal of the American Medical Association 299(11):1335-1344.

Peng Z, Li G, Shi F, Shi C, Yang Q, Chan RC, Shen D. (2015): Cortical asymmetries in unaffected siblings of patients with obsessive-compulsive disorder. Psychiatry Res 234(3):346-51.

Peters M, Reimers S, Manning JT. (2006): Hand preference for writing and associations with selected demographic and behavioral variables in 255,100 subjects: the BBC internet study. Brain Cogn 62(2):177-89.

Plessen KJ, Hugdahl K, Bansal R, Hao X, Peterson BS. (2014): Sex, age, and cognitive correlates of asymmetries in thickness of the cortical mantle across the life span. J Neurosci 34(18):6294-302.

Pletikos M, Sousa AM, Sedmak G, Meyer KA, Zhu Y, Cheng F, Li M, Kawasawa YI, Sestan N. (2014): Temporal specification and bilaterality of human neocortical topographic gene expression. Neuron 81(2):321-32.

Powell JL, Kemp GJ, Roberts N, Garcia-Finana M. (2012): Sulcal morphology and volume of Broca's area linked to handedness and sex. Brain and Language 121(3):206-218.

Purcell S, Neale B, Todd-Brown K, Thomas L, Ferreira MA, Bender D, Maller J, Sklar P, de Bakker PI, Daly MJ and others. (2007): PLINK: a tool set for whole-genome association and population-based linkage analyses. Am J Hum Genet 81(3):559-575.

Qiu A, Wang L, Younes L, Harms MP, Ratnanather JT, Miller MI, Csernansky JG. (2009): Neuroanatomical asymmetry patterns in individuals with schizophrenia and their non-psychotic siblings. Neuroimage 47(4):1221-9.

Rabbee N, Speed TP. (2006): A genotype calling algorithm for affymetrix SNP arrays. Bioinformatics 22(1):7-12.

Ransil BJ, Schachter SC. (1994): Test-retest reliability of the Edinburgh Handedness Inventory and Global Handedness preference measurements, and their correlation. Percept Mot Skills 79(3 Pt 1):1355-72.

Raz N, Torres IJ, Acker JD. (1995): Age, gender, and hemispheric differences in human striatum: a quantitative review and new data from in vivo MRI morphometry. Neurobiol Learn Mem 63(2):133-42.

Renteria ME. (2012): Cerebral asymmetry: a quantitative, multifactorial, and plastic brain phenotype. Twin Res Hum Genet 15(3):401-13.

Renteria ME. (2013): Mapping the genetic architecture of subcortical brain anatomy. PhD Thesis (http://espace.library.uq.edu.au/view/UQ:320790).

Renteria ME, Stein JL, Johnson K, Medland SE, McMahon KL, De Zubicaray GI, Montgomery GW, Thompson PM, Martin NG, Wright MJ. (2011): Genetics of cerebral asymmetry in the caudate nucleus. Poster presentation ASHG 2011 - October 2011.

Renteria ME, Wallace A, Strike L, Johnson K, Hibar DP, Stein JL, De Zubicaray G, McMahon KL, Montgomery GW, Thompson PM and others. (2012): Genetics of left- and right-hemisphere subcortical structures in the human brain. . Poster presentation ASHG 2012 - November 2012.

Richlan F, Kronbichler M, Wimmer H. (2013): Structural abnormalities in the dyslexic brain: a meta-analysis of voxel-based morphometry studies. Hum Brain Mapp 34(11):3055-65.

Roos A, Jones G, Howells FM, Stein DJ, Donald KA. (2014): Structural brain changes in prenatal methamphetamine-exposed children. Metab Brain Dis 29(2):341-9.

Ruigrok AN, Salimi-Khorshidi G, Lai MC, Baron-Cohen S, Lombardo MV, Tait RJ, Suckling J. (2014): A meta-analysis of sex differences in human brain structure. Neurosci Biobehav Rev 39:34-50.

Ruxton GD. (2006): The unequal variance t-test is an underused alternative to Student's t-test and the Mann–Whitney U test. Behavioral Ecology 17(4):688-690.

Savitz J, van der Merwe L, Solms M, Ramesar R. (2007): Lateralization of hand skill in bipolar affective disorder. Genes Brain Behav 6(8):698-705.

Scerri TS, Brandler WM, Paracchini S, Morris AP, Ring SM, Richardson AJ, Talcott JB, Stein J, Monaco AP. (2011): PCSK6 is associated with handedness in individuals with dyslexia. Hum Mol Genet 20(3):608-14.

Schrimsher GW, Billingsley RL, Jackson EF, Moore BD. (2002): Caudate nucleus volume asymmetry predicts attention-deficit hyperactivity disorder (ADHD) symptomatology in children. Journal of Child Neurology 17(12):877-884.

Shapleske J, Rossell SL, Woodruff PW, David AS. (1999): The planum temporale: a systematic, quantitative review of its structural, functional and clinical significance. Brain Res Brain Res Rev 29(1):26-49.

Shaw P, Lalonde F, Lepage C, Rabin C, Eckstrand K, Sharp W, Greenstein D, Evans A, Giedd JN, Rapoport J. (2009): Development of cortical asymmetry in typically developing children and its disruption in attention-deficit/hyperactivity disorder. Arch Gen Psychiatry 66(8):888-96.

Sherwood CC, Gordon AD, Allen JS, Phillips KA, Erwin JM, Hof PR, Hopkins WD. (2011): Aging of the cerebral cortex differs between humans and chimpanzees. Proc Natl Acad Sci U S A 108(32):13029-34.

Shi F, Liu B, Zhou Y, Yu C, Jiang T. (2009): Hippocampal volume and asymmetry in mild cognitive impairment and Alzheimer's disease: Meta-analyses of MRI studies. Hippocampus 19(11):1055-64.

Shinohara K, Kawasumi A, Takamatsu A, Yoshiba S, Botilde Y, Motoyama N, Reith W, Durand B, Shiratori H, Hamada H. (2012): Two rotating cilia in the node cavity are sufficient to break left-right symmetry in the mouse embryo. Nat Commun 3:622.

Shrout PE, Fleiss JL. (1979): Intraclass correlations: uses in assessing rater reliability. Psychol Bull 86(2):420-8.

Singer HS, Reiss AL, Brown JE, Aylward EH, Shih B, Chee E, Harris EL, Reader MJ, Chase GA, Bryan RN and others. (1993): Volumetric MRI changes in basal ganglia of children with Tourette's syndrome. Neurology 43(5):950-6.

Singleton AB, Hardy J, Traynor BJ, Houlden H. (2010): Towards a complete resolution of the genetic architecture of disease. Trends Genet 26(10):438-42.

Sleiman PMA, Satterthwaite T, Ruparel K, Kim C, Chiavacci R, Calkins ME, Gur RC, Gur RE, Hakonarson H. (2012): Genome-wide association of structural MRI data in a large, normally developing, pediatric population. . Poster presentation ASHG 2012 - November 2012.

Smith GE. (1925): RIGHT- AND LEFT-HANDEDNESS IN PRIMITIVE MEN. BMJ 2(3389):1107-1108.

Snedecor GW. (1950): THE STATISTICAL PART OF THE SCIENTIFIC METHOD. Annals of the New York Academy of Sciences 52(6):792-799.

Soininen HS, Partanen K, Pitkanen A, Vainio P, Hanninen T, Hallikainen M, Koivisto K, Riekkinen PJ, Sr. (1994): Volumetric MRI analysis of the amygdala and the hippocampus in subjects with age-associated memory impairment: correlation to visual and verbal memory. Neurology 44(9):1660-8.

Sommer I, Ramsey N, Kahn R, Aleman A, Bouma A. (2001): Handedness, language lateralisation and anatomical asymmetry in schizophrenia: meta-analysis. Br J Psychiatry 178:344-51.

Sommer IE, Aleman A, Somers M, Boks MP, Kahn RS. (2008): Sex differences in handedness, asymmetry of the Planum Temporale and functional language lateralization. Brain Research 1206:76-88.

Steenhuis RE, Bryden MP. (1989): Different dimensions of hand preference that relate to skilled and unskilled activities. Cortex 25(2):289-304.

Stein JL, Medland SE, Vasquez AA, Hibar DP, Senstad RE, Winkler AM, Toro R, Appel K, Bartecek R, Bergmann O and others. (2012): Identification of common variants associated with human hippocampal and intracranial volumes. Nat Genet 44(5):552-61.

Steinmetz H. (1996): Structure, Function and Cerebral Asymmetry: In Vivo Morphometry of the Planum Temporale. Neuroscience & Biobehavioral Reviews 20(4):587-591.

Steinmetz H, Volkmann J, Jancke L, Freund HJ. (1991): Anatomical left-right asymmetry of language-related temporal cortex is different in left- and right-handers. Ann Neurol 29(3):315-9.

Stiles J, Jernigan TL. (2010): The basics of brain development. Neuropsychol Rev 20(4):327-48.

Sun T, Patoine C, Abu-Khalil A, Visvader J, Sum E, Cherry TJ, Orkin SH, Geschwind DH, Walsh CA. (2005): Early Asymmetry of Gene Transcription in Embryonic Human Left and Right Cerebral Cortex. Science 308(5729):1794-1798.

Sun T, Walsh CA. (2006): Molecular approaches to brain asymmetry and handedness. Nat Rev Neurosci 7(8):655-662.

Szabo CA, Xiong J, Lancaster JL, Rainey L, Fox P. (2001): Amygdalar and hippocampal volumetry in control participants: differences regarding handedness. AJNR Am J Neuroradiol 22(7):1342-5.

Szeszko PR, Robinson D, Alvir JM, Bilder RM, Lencz T, Ashtari M, Wu H, Bogerts B. (1999): Orbital frontal and amygdala volume reductions in obsessive-compulsive disorder. Arch Gen Psychiatry 56(10):913-9.

Takaoka K, Yamamoto M, Hamada H. (2007): Origin of body axes in the mouse embryo. Current Opinion in Genetics & Development 17(4):344-350.

Tamura K, Yonei-Tamura S, Izpisua Belmonte JC. (1999): Molecular basis of left-right asymmetry. Dev Growth Differ 41(6):645-56.

Tan U. (1993): Normal distribution of hand preference and its bimodality. Int J Neurosci 68(1-2):61-5.

Tanaka S, Kanzaki R, Yoshibayashi M, Kamiya T, Sugishita M. (1999): Dichotic listening in patients with situs inversus: brain asymmetry and situs asymmetry. Neuropsychologia 37(7):869-74.

Tau GZ, Peterson BS. (2010): Normal development of brain circuits. Neuropsychopharmacology 35(1):147-68.

Taylor RW, Hsieh YW, Gamse JT, Chuang CF. (2010): Making a difference together: reciprocal interactions in C. elegans and zebrafish asymmetric neural development. Development 137(5):681-91.

Thompson P, Stein J, Medland S, Hibar D, Vasquez A, Renteria M, Toro R, Jahanshad N, Schumann G, Franke B and others. (2014): The ENIGMA Consortium: large-scale collaborative analyses of neuroimaging and genetic data. Brain Imaging and Behavior:1-30.

Titova OE, Hjorth OC, Schioth HB, Brooks SJ. (2013): Anorexia nervosa is linked to reduced brain structure in reward and somatosensory regions: a meta-analysis of VBM studies. BMC Psychiatry 13:110.

Toga AW, Thompson PM. (2003): Mapping brain asymmetry. Nature Reviews Neuroscience 4(1):37-48.
Tzourio-Mazoyer N, Marie D, Zago L, Jobard G, Perchey G, Leroux G, Mellet E, Joliot M, Crivello F, Petit L and others. (2015): Heschl's gyrification pattern is related to speech-listening hemispheric lateralization: FMRI investigation in 281 healthy volunteers. Brain structure & function 220(3):1585-99.
Tzourio-Mazoyer N, Petit L, Razafimandimby A, Crivello F, Zago L, Jobard G, Joliot M, Mellet E, Mazoyer B. (2010a): Left hemisphere lateralization for language in right-handers is controlled in part by familial sinistrality, manual preference strength, and head size. J Neurosci 30(40):13314-8.
Tzourio-Mazoyer N, Simon G, Crivello F, Jobard G, Zago L, Perchey G, Herve PY, Joliot M, Petit L, Mellet E and others. (2010b): Effect of Familial Sinistrality on Planum Temporale Surface and Brain Tissue Asymmetries. Cerebral Cortex 20(6):1476-1485.
Tzourio N, Crivello F, Mellet E, Nkanga-Ngila B, Mazoyer B. (1998): Functional anatomy of dominance for speech comprehension in left handers vs right handers. Neuroimage 8(1):1-16.
Uhlikova P, Paclt I, Vaneckova M, Morcinek T, Seidel Z, Krasensky J, Danes J. (2007): Asymmetry of basal ganglia in children with attention deficit hyperactivity disorder. Neuro Endocrinol Lett 28(5):604-9.
Vallortigara G, Chiandetti C, Sovrano VA. (2011): Brain asymmetry (animal). Wiley Interdisciplinary Reviews-Cognitive Science 2(2):146-157.
van Erp TG, Hibar DP, Rasmussen JM, Glahn DC, Pearlson GD, Andreassen OA, Agartz I, Westlye LT, Haukvik UK, Dale AM and others. (2016): Subcortical brain volume abnormalities in 2028 individuals with schizophrenia and 2540 healthy controls via the ENIGMA consortium. Mol Psychiatry 21(4):547-53.
Vernaleken I, Weibrich C, Siessmeier T, Buchholz HG, Rosch F, Heinz A, Cumming P, Stoeter P, Bartenstein P, Grunder G. (2007): Asymmetry in dopamine D(2/3) receptors of caudate nucleus is lost with age. Neuroimage 34(3):870-8.
Visscher PM, Brown MA, McCarthy MI, Yang J. (2012): Five Years of GWAS Discovery. American Journal of Human Genetics 90(1):7-24.
Volzke H, Alte D, Schmidt CO, Radke D, Lorbeer R, Friedrich N, Aumann N, Lau K, Piontek M, Born G and others. (2011): Cohort profile: the study of health in Pomerania. Int J Epidemiol 40(2):294-307.
Vuoksimaa E, Koskenvuo M, Rose RJ, Kaprio J. (2009): Origins of handedness: A nationwide study of 30 161 adults. Neuropsychologia 47(5):1294-1301.
Wallentin M. (2009): Putative sex differences in verbal abilities and language cortex: a critical review. Brain Lang 108(3):175-83.
Watkins KE, Paus T, Lerch JP, Zijdenbos A, Collins DL, Neelin P, Taylor J, Worsley KJ, Evans AC. (2001): Structural asymmetries in the human brain: a voxel-based statistical analysis of 142 MRI scans. Cerebral Cortex 11(9):868-877.
Weiner KX, Ciesla J, Jaffe AB, Ketring R, Maley F, Maley GF. (1995): Chromosomal location and structural organization of the human deoxycytidylate deaminase gene. J Biol Chem 270(32):18727-9.
Wernicke C. 1874. Der Aphasische Symtomenkomplex. Eine Psychologische Studie auf Anatomischer Basis. Breslau: M. Cohn und Weigart.
Whitehouse AJ, Bishop DV. (2009): Hemispheric division of function is the result of independent probabilistic biases. Neuropsychologia 47(8-9):1938-43.
Whitehouse AJO, Mattes E, Maybery MT, Sawyer MG, Jacoby P, Keelan JA, Hickey M. (2012): Sex-specific associations between umbilical cord blood testosterone levels and language delay in early childhood. Journal of Child Psychology and Psychiatry 53(7):726-734.
Willems RM, Hagoort P. (2009): Hand preference influences neural correlates of action observation. Brain Res 7:90-104.

Willems RM, Peelen MV, Hagoort P. (2010): Cerebral lateralization of face-selective and body-selective visual areas depends on handedness. Cereb Cortex 20(7):1719-25.
Willems RM, Van der Haegen L, Fisher SE, Francks C. (2014): On the other hand: including left-handers in cognitive neuroscience and neurogenetics. Nat Rev Neurosci 15(3):193-201.
Willer CJ, Li Y, Abecasis GR. (2010): METAL: fast and efficient meta-analysis of genomewide association scans. Bioinformatics 26(17):2190-2191.
Willford J, Day R, Aizenstein H, Day N. (2010): Caudate asymmetry: a neurobiological marker of moderate prenatal alcohol exposure in young adults. Neurotoxicol Teratol 32(6):589-94.
Witelson SF, Kigar DL. (1992): Sylvian fissure morphology and asymmetry in men and women: bilateral differences in relation to handedness in men. J Comp Neurol 323(3):326-40.
Wonderlick JS, Ziegler DA, Hosseini-Varnamkhasti P, Locascio JJ, Bakkour A, van der Kouwe A, Triantafyllou C, Corkin S, Dickerson BC. (2009): Reliability of MRI-derived cortical and subcortical morphometric measures: effects of pulse sequence, voxel geometry, and parallel imaging. Neuroimage 44(4):1324-33.
Woo YJ, Wang T, Guadalupe T, Nebel RA, Vino A, Del Bene VA, Molholm S, Ross LA, Zwiers MP, Fisher SE and others. (2016): A Common CYFIP1 Variant at the 15q11.2 Disease Locus Is Associated with Structural Variation at the Language-Related Left Supramarginal Gyrus. PLoS One 11(6):e0158036.
Woolard AA, Heckers S. (2012): Anatomical and functional correlates of human hippocampal volume asymmetry. Psychiatry Res 201(1):48-53.
Wyciszkiewicz A, Pawlak MA. (2014): Basal Ganglia Volumes: MR-Derived Reference Ranges and Lateralization Indices for Children and Young Adults. Neuroradiol J 27(5):595-612.
Xia J, Chen J, Zhou Y, Zhang J, Yang B, Xia L, Wang C. (2004): Volumetric MRI analysis of the amygdala and hippocampus in subjects with major depression. J Huazhong Univ Sci Technolog Med Sci 24(5):500-2, 506.
Yamashita K, Yoshiura T, Hiwatashi A, Noguchi T, Togao O, Takayama Y, Nagao E, Kamano H, Hatakenaka M, Honda H. (2011): Volumetric asymmetry and differential aging effect of the human caudate nucleus in normal individuals: a prospective MR imaging study. J Neuroimaging 21(1):34-7.
Yoshiba S, Shiratori H, Kuo IY, Kawasumi A, Shinohara K, Nonaka S, Asai Y, Sasaki G, Belo JA, Sasaki H and others. (2012): Cilia at the node of mouse embryos sense fluid flow for left-right determination via Pkd2. Science 338(6104):226-31.
Zatorre RJ, Evans AC, Meyer E, Gjedde A. (1992): Lateralization of phonetic and pitch discrimination in speech processing. Science 256(5058):846-849.
Zhou SY, Suzuki M, Hagino H, Takahashi T, Kawasaki Y, Nohara S, Yamashita I, Seto H, Kurachi M. (2003): Decreased volume and increased asymmetry of the anterior limb of the internal capsule in patients with schizophrenia. Biol Psychiatry 54(4):427-36.
Zimmerman AM, Abrams MT, Giuliano JD, Denckla MB, Singer HS. (2000): Subcortical volumes in girls with tourette syndrome: support for a gender effect. Neurology 54(12):2224-9.

Samenvatting

Links-rechts vershillen zijn een belangrijk aspect van de organisatie van de hersenen, die van belang zijn voor hogere cognitieve functies en cognitieve stoornissen. Belangrijke kwesties met betrekking tot de multifactoriële aard, moleculaire- en ontwikkelingsbasis van deze asymmetrieën van de hersenen blijven vrijwel onbekend. Dit proefschrift benaderde deze open vragen door te kijken naar de effecten van verschillende biologische factoren op de natuurlijke variabiliteit in morfologische lateralisatie van de hersenen.

In hoofdstuk 2 onderzoek ik de mogelijke relaties tussen de anatomie van de cerebrale cortex en *handedness* in de grootste studie dat tot op heden is uitgevoerd hierover (1960 rechtshandige en 106 linkshandige proefpersonen). Het identificeren van anatomische hersencorrelaten van *handedness* zou aanwijzingen kunnen geven over de orsprong ervan. Verder, door specifieke ontogenetische mechanismen te vooronderstellen, kunnen deze richting geven aan verder onderzoek naar de algemene genetische architectuur. Daarnaast kunnen de relaties tussen *handedness* en andere vormen van gelateraliseerde cognitie worden verduidelijkt, inclusief de relatie tussen de structuur van de hersenen en functie.

Er wordt vaak verondersteld dat seks een van de drijvende factoren is achter verschillen in asymmetrieën van de hersenen. Echter, er is momenteel geen sterke consensus met betrekking tot de morfologische specificiteit van seks effecten of hun functionele gevolgen. In Hoofdstuk 3 heb ik sekseverschillen in asymetrie van grijze stof over de gehele cerebrale cortex in kaart gebracht, in eerste instantie in meer dan 2.000 gezonde volwassenen. Dit werd gevolgd door een replicatie-analyse, in samenwerking met de Universiteit van Greifswald, waarmee onze conclusies met betrekking tot sekse effecten in de hersenen van volwassenen werden bevestigd. Met deze samenwerking werd het tegelijkertijd mogelijk om gedetailleerd onderzoek te doen naar de genetische basis van de meest seks-bepaalde asymmetrie in de hersenen, waardoor de eerste genoom-brede analyse van een corticale asymmetrie tot op heden is uitgevoerd. Bovendien werden verdere analyses uitgevoerd met de intentie om gen-netwerken te identificeren die relevant zijn voor asymmetrie bepalende processen. Door deze benadering was het mogelijk om genetische mechanismen en specifieke kandidaatgenen uit te lichten die verder kunnen worden onderzocht met betrekking tot menselijke cognitieve variatie, in het bijzonder gerelateerd aan gelateraliseerde functies.

In lijn met de aanwijzingen voor een mogelijke subcorticale oorsprong van de ontwikkeling van asymetrie van de hersenen (zoals hierboven beschreven), in Hoofdstuk 4 onderzoek ik volume-gerelateerde asymmetrie in 6 subcorticale structuren en de hippocampus. Door de overal sterke gelijkenis tussen de linker- en rechterkant van deze bilaterale structuren, de initiële focus van deze studie was om de haalbaarheid van geautomatiseerde metingen van subtiele verschillen in volume-gerelateerde asymmetrie, toegepast op grote datasets, te beoordelen. De metingen werden gedaan door twee geautomatiseerde methoden van segmentatie (FSL | FIRST en FreeSurfer). Door gebruik te maken van de gegevens van 235 patiënten die MRI twee keer hadden ondergaan, was ik in staat om zowel de interindividuele overeenkomsten tussen metingen verkregen op verschillende tijdstippen, alsook de overeenkomst tussen beide geautomatiseerde methoden te beoordelen. Daarnaast kon ik ook systematische asymetrische fouten in de geautomatiseerde processen evalueren. Dergelijke fouten zouden onjuiste bevindingen ten aanzien van directionele asymmetrie op populatieniveau kunnen

introduceren. Dit werd gedaan door dezelfde hersenbeelden opnieuw te analyseren, nadat ze waren gedraaid om de links/rechts-as. De meest betrouwbare meting werd verder meta-geanalyseerd in een genoom-brede associatie scan, in een gecombineerde steekproef van 3.028 volwassen proefpersonen. Nogmaals, dit was de eerste uitgebreide genetische associatie studie naar een menselijk subcorticale brein asymmetrie.

Hoofdstuk 5 presenteert het eerste werk van de Lateralisatie werkgroep binnen de ENIGMA consortium (Enhancing Neuro Imaging Genetics through Meta-Analysis). ENIGMA is een internationaal samenwerkingsverband met het doel om grootschalige analyses van hersen morfologie, gemeten met MRI, uit te voeren, en om genetische varianten te identificeren die van invloed zijn hierop. Eerder onderzoek over subcorticale asymmetrie was niet concluderend met betrekking tot de rol van leeftijd, handedness en geslacht in het beïnvloeden van subcorticale hersenen asymmetrie. In een meta-analyse van meer dan 15.000 proefpersonen in de ENIGMA consortium, hebben we duidelijke effecten van sekse en leeftijd op de asymmetrie van enkele subcorticale structuren vastgesteld. Dit werd gedaan door gegevens uit 52 verschillende datasets die wereldwijd werden gerekruteerd samen te voegen. Dit was een van de grootste studies ooit te zijn verricht naar enig aspect van variabiliteit in het menselijk brein. Verder is de erfelijkheid van subcorticale volume-gerelateerde asymmetrieën geschat. Deze informatie zal waardevol zijn om verdere genetische studies naar deze asymmetrieën van de hersenen te ondersteunen.

Tenslotte worden in Hoofdstuk 6 mijn resultaten besproken in de context van de bijdragen aan ons begrip van asymmetrie van de hersenen en de orsprong hiervan. In Hoofdstuk 6 worden ook de nieuwe onderzoeksrichtingen die nu binnen de ENIGMA-Lateralisatie werkgroep kunnen worden voortgezet bediscussieerd. Zulke uitgebreide studies zijn nodig om de zeer complexe biologie onderliggend aan asymmetrie van de hersenen, met name de genetica, te ontrafelen.

Biographical note

Tulio Manuel Guadalupe Estrada was born on November 3, 1982. He was raised in Lima, Peru, where he completed his highschool education, as well as following several undergraduate courses at the Pontifical Catholic University of Peru. In 2004 he moved to the Netherlands to study Psychology at the Erasmus University Rotterdam. He obtained his Master's degree with a specialization in Biological and Cognitive Psychology in 2009. He continued this work as a research assistant and also worked as teaching staff at Erasmus' Institute for Psychology. In 2011, Tulio began work for his PhD at the Max Planck Institute for Psycholinguistics in Nijmegen, the Netherlands. He became part of the recently established department on Language and Genetics, led by Prof. Simon Fisher. He worked within Dr. Clyde Franks' group, investigating the genetic and biological factors related to brain asymmetries.

Acknowledgments

This dissertation would not have been possible without the contribution, help and guidance from many people. I would like to give my thanks to Simon, for the opportunity to learn from and be part of an excellent scientific environment. I am also deeply grateful to Clyde, whose dedicated mentoring and outstanding expertise have been both educational and inspiring. Thank you to the reading committee for your effort and willingness to take part this doctoral process. I would also like to thank the BIG hands-on team, in particular Marcel, Martine, Barbara, Janita, Elena, Hubert, Martin and Alejandro. Your help and contributions have been central to this work.

Thank you to the wonderful people at the MPI and DCCN, in particular Amaia, Gabriela, Dan, to my former office mates Alessandro, Jasper, Sarah and Nicolas. I've enjoyed our discussions as well as your friendship. Thank you to my friends and family for your continuous support.

Finally, special thanks to Brittany (Silas y Juniper)...and to my old M11604481

MPI series in Psycholinguistics

1. The electrophysiology of speaking: Investigations on the time course of semantic, syntactic, and phonological processing. *Miranda van Turennout*
2. The role of the syllable in speech production: Evidence from lexical statistics, metalinguistics, masked priming, and electromagnetic midsagittal articulography. *Niels O. Schiller*
3. Lexical access in the production of ellipsis and pronouns. *Bernadette M. Schmitt*
4. The open-/closed-class distinction in spoken-word recognition. *Alette Haveman*
5. The acquisition of phonetic categories in young infants: A self-organising artificial neural network approach. *Kay Behnke*
6. Gesture and speech production. *Jan-Peter de Ruiter*
7. Comparative intonational phonology: English and German. *Esther Grabe*
8. Finiteness in adult and child German. *Ingeborg Lasser*
9. Language input for word discovery. *Joost van de Weijer*
10. Inherent complement verbs revisited: Towards an understanding of argument structure in Ewe. *James Essegbey*
11. Producing past and plural inflections. *Dirk Janssen*
12. Valence and transitivity in Saliba: An Oceanic language of Papua New Guinea. *Anna Margetts*
13. From speech to words. *Arie van der Lugt*
14. Simple and complex verbs in Jaminjung: A study of event categorisation in an Australian language. *Eva Schultze-Berndt*
15. Interpreting indefinites: An experimental study of children's language comprehension. *Irene Krämer*
16. Language-specific listening: The case of phonetic sequences. *Andrea Weber*
17. Moving eyes and naming objects. *Femke van der Meulen*
18. Analogy in morphology: The selection of linking elements in Dutch compounds. *Andrea Krott*
19. Morphology in speech comprehension. *Kerstin Mauth*
20. Morphological families in the mental lexicon. *Nivja H. de Jong*
21. Fixed expressions and the production of idioms. *Simone A. Sprenger*
22. The grammatical coding of postural semantics in Goemai (a West Chadic language of Nigeria). *Birgit Hellwig*
23. Paradigmatic structures in morphological processing: Computational and cross-linguistic experimental studies. *Fermín Moscoso del Prado Martín*
24. Contextual influences on spoken-word processing: An electrophysiological approach. *Daniëlle van den Brink*
25. Perceptual relevance of prevoicing in Dutch. *Petra M. van Alphen*
26. Syllables in speech production: Effects of syllable preparation and syllable frequency. *Joana Cholin*
27. Producing complex spoken numerals for time and space. *Marjolein Meeuwissen*

28. Morphology in auditory lexical processing: Sensitivity to fine phonetic detail and insensitivity to suffix reduction. *Rachèl J. J. K. Kemps*
29. At the same time...: The expression of simultaneity in learner varieties. *Barbara Schmiedtová*
30. A grammar of Jalonke argument structure. *Friederike Lüpke*
31. Agrammatic comprehension: An electrophysiological approach. *Marlies Wassenaar*
32. The structure and use of shape-based noun classes in Miraña (North West Amazon). *Frank Seifart*
33. Prosodically-conditioned detail in the recognition of spoken words. *Anne Pier Salverda*
34. Phonetic and lexical processing in a second language. *Mirjam Broersma*
35. Retrieving semantic and syntactic word properties. *Oliver Müller*
36. Lexically-guided perceptual learning in speech processing. *Frank Eisner*
37. Sensitivity to detailed acoustic information in word recognition. *Keren B. Shatzman*
38. The relationship between spoken word production and comprehension. *Rebecca Özdemir*
39. Disfluency: Interrupting speech and gesture. *Mandana Seyfeddinipur*
40. The acquisition of phonological structure: Distinguishing contrastive from non-contrastive variation. *Christiane Dietrich*
41. Cognitive cladistics and the relativity of spatial cognition. *Daniel B.M. Haun*
42. The acquisition of auditory categories. *Martijn Goudbeek*
43. Affix reduction in spoken Dutch. *Mark Pluymaekers*
44. Continuous-speech segmentation at the beginning of language acquisition: Electrophysiological evidence. *Valesca Kooijman*
45. Space and iconicity in German Sign Language (DGS). *Pamela Perniss*
46. On the production of morphologically complex words with special attention to effects of frequency. *Heidrun Bien*
47. Crosslinguistic influence in first and second languages: Convergence in speech and gesture. *Amanda Brown*
48. The acquisition of verb compounding in Mandarin Chinese. *Jidong Chen*
49. Phoneme inventories and patterns of speech sound perception. *Anita Wagner*
50. Lexical processing of morphologically complex words: An information-theoretical perspective. *Victor Kuperman*
51. A grammar of Savosavo, a Papuan language of the Solomon Islands. *Claudia Wegener*
52. Prosodic structure in speech production and perception. *Claudia Kuzla*
53. The acquisition of finiteness by Turkish learners of German and Turkish learners of French: Investigating knowledge of forms and functions in production and comprehension. *Sarah Schimke*
54. Studies on intonation and information structure in child and adult German. *Laura de Ruiter*
55. Processing the fine temporal structure of spoken words. *Eva Reinisch*
56. Semantics and (ir)regular inflection in morphological processing. *Wieke Tabak*
57. Processing strongly reduced forms in casual speech. *Susanne Brouwer*
58. Ambiguous pronoun resolution in L1 and L2 German and Dutch. *Miriam Ellert*
59. Lexical interactions in non-native speech comprehension: Evidence from electro-encephalography, eye-tracking, and functional magnetic resonance imaging. *Ian FitzPatrick*
60. Processing casual speech in native and non-native language. *Annelie Tuinman*

61. *Split intransitivity in Rotokas, a Papuan language of Bougainville. Stuart Robinson*
62. Evidentiality and intersubjectivity in Yurakaré: An interactional account. *Sonja Gipper*
63. The influence of information structure on language comprehension: A neurocognitive perspective. *Lin Wang*
64. The meaning and use of ideophones in Siwu. *Mark Dingemanse*
65. The role of acoustic detail and context in the comprehension of reduced pronunciation variants. *Marco van de Ven*
66. Speech reduction in spontaneous French and Spanish. *Francisco Torreira*
67. The relevance of early word recognition: Insights from the infant brain. *Caroline Junge*
68. Adjusting to different speakers: Extrinsic normalization in vowel perception. *Matthias J. Sjerps*
69. Structuring language. Contributions to the neurocognition of syntax. *Katrien R. Segaert*
70. Infants' appreciation of others' mental states in prelinguistic communication: A second person approach to mindreading. *Birgit Knudsen*
71. Gaze behavior in face-to-face interaction. *Federico Rossano*
72. Sign-spatiality in Kata Kolok: how a village sign language of Bali inscribes its signing space. *Conny de Vos*
73. Who is talking? Behavioural and neural evidence for norm-based coding in voice identity learning. *Attila Andics*
74. Lexical processing of foreign-accented speech: Rapid and flexible adaptation. *Marijt Witteman*
75. The use of deictic versus representational gestures in infancy. *Daniel Puccini*
76. Territories of knowledge in Japanese conversation. *Kaoru Hayano*
77. Family and neighbourhood relations in the mental lexicon: A cross-language perspective. *Kimberley Mulder*
78. Contributions of executive control to individual differences in word production. *Zeshu Shao*
79. Hearing speech and seeing speech: Perceptual adjustments in auditory-visual processing. *Patrick van der Zande*
80. High pitches and thick voices: The role of language in space-pitch associations. *Sarah Dolscheid*
81. Seeing what's next: Processing and anticipating language referring to objects. *Joost Rommers*
82. Mental representation and processing of reduced words in casual speech. *Iris Hanique*
83. The many ways listeners adapt to reductions in casual speech. *Katja Poellmann*
84. Contrasting opposite polarity in Germanic and Romance languages: Verum Focus and affirmative particles in native speakers and advanced L2 learners. *Giuseppina Turco*
85. Morphological processing in younger and older people: Evidence for flexible dual-route access. *Jana Reifegerste*
86. Semantic and syntactic constraints on the production of subject-verb agreement. *Alma Veenstra*
87. The acquisition of morphophonological alternations across languages. *Helen Buckler*
88. The evolutionary dynamics of motion event encoding. *Annemarie Verkerk*
89. Rediscovering a forgotten language. *Jiyoun Choi*
90. The road to native listening: Language-general perception, language-specific input. *Sho Tsuji*
91. Infants'understanding of communication as participants and observers. *Gudmundur Bjarki Thorgrímsson*
92. Information structure in Avatime. *Saskia van Putten*
93. Switch reference in Whitesands. *Jeremy Hammond*
94. Machine learning for gesture recognition from videos. *Binyam Gebrekidan Gebre*

95. Acquisition of spatial language by signing and speaking children: a comparison of Turkish sign language (TID) and Turkish. *Beyza Sümer*

96. An ear for pitch: on the effects of experience and aptitude in processing pitch in language and music. *Salomi Savvatia Asaridou*

97. Incrementality and Flexibility in Sentence Production. *Maartje van de Velde*

98. Social learning dynamics in chimpanzees: Reflections on (nonhuman) animal culture. *Edwin van Leeuwen*

99. The request system in Italian interaction. *Giovanni Rossi*

100. Timing turns in conversation: A temporal preparation account. *Lilla Magyari*

101. Assessing birth language memory in young adoptees*. Wencui Zhou*

102. A social and neurobiological approach to pointing in speech and gesture*. David Peeters*

103. Investigating the genetic basis of reading and language skills. *Alessandro Gialluisi*

104. Conversation Electrified: The Electrophysiology of Spoken Speech Act Recognition. *Rósa Signý Gisladottir*

105. Modelling Multimodal Language Processing*. Alastair Smith*

106. Predicting language in different contexts: The nature and limits of mechanisms in anticipatory language processing*. Florian Hintz*

107. Situational variation in non-native communication. *Huib Kouwenhoven*

108. Sustained attention in language production. *Suzanne Jongman*

109. Acoustic reduction in spoken-word processing: Distributional, syntactic, morphosyntatic, and orthographic effects. *Malte Viebahn*

110. Nativeness, dominance, and the flexibility of listening to spoken language. *Laurence Bruggeman*

111. Semantic specificity of perception verbs in Maniq. *Ewelina Wnuk*

112. *On the identification of FOXP2 gene enhancers and their role in brain development. Martin* Becker

113. Events in language and thought: The case of serial verb constructions in Avatime. *Rebecca Defina*

114. Deciphering common and rare genetic effects on reading ability. *Amaia Carrión Castillo*

115. Music and language comprehension in the brain*. Richard Kunert*

116. Comprehending Comprehension: Insights from neuronal oscillations on the neuronal basis of language. *Nietzsche H.L. Lam*

117. The biology of variation in anatomical brain asymmetries. *Tulio Guadalupe*